

**THE ROLE OF THE INTRINSIC CARDIAC
NERVOUS SYSTEM IN CARDIAC
ELECTROPHYSIOLOGY AND DISEASE**

Thesis submitted for the degree of Doctor of Philosophy
at the University of Leicester

by

Emily Wake BSc (Hons)

Department of Cardiovascular Sciences
University of Leicester

May 2017

Abstract

The role of the intrinsic cardiac nervous system in cardiac physiology and disease

Emily Wake

It is well recognised that the complex neuronal hierarchy of the autonomic nervous system is important in the pathology of heart disease. In addition to the peripheral autonomic nerves, there is a dense network of intrinsic cardiac ganglia located at the level of the heart and acting as the final stage in the autonomic regulation of cardiac function. Understanding the role of this network in cardiac function could prove vital in understanding heart disease.

The aims of this study were to characterise the topography and neurochemical phenotype of the rabbit intrinsic cardiac nervous system (ICNS) as well as to investigate the functional effects of electrical stimulation of intrinsic cardiac ganglia on the sinus and AV nodes. A coronary artery ligation heart failure model was used to examine the effects of myocardial infarction (MI) and heart failure (HF) on both the topography of the ICNS and the functional role of the ICNS.

Histochemical staining revealed an intricate network of nerves and ganglia located primarily on the heart hilum. Significant neuronal remodelling was evident following MI, with the enlargement of somata within ganglia that are known to preferentially innervate the ventricles. Heart rate changes occurred primarily as a result of stimulation of ganglia within the right atrial (RA) and right neuronal cluster (RNC) regions. MI resulted in exaggerated bradycardic responses during stimulation of the RA and RNC regions, accompanied by a significant increase in tachycardia responses during stimulation of ganglia within the RA and RNC.

In conclusion, it is becoming increasingly evident that the ICNS is a key network in the cardiac neuronal hierarchy. The ability of the ICNS to function both in normal physiology and also to adapt following MI and HF suggests that the ICNS could be a significant potential therapeutic target for the prevention and treatment of cardiac disease.

Acknowledgements

First and foremost, I would like to thank my supervisors Professor G André Ng and Dr Richard Rainbow for their continued support and for their expertise, advice and guidance throughout. My thanks also go to Dr Kieran Brack for providing me with the opportunity to undertake this PhD and for his expertise and insight in guiding the direction of my PhD and for teaching me invaluable laboratory skills.

I would also like to extend my appreciation to all of the staff at the Division of Biomedical Services and in particular to Deborah Bursnall and Lucy Onions for all of their help with surgical procedures and for their advice and support ensuring the best possible care for the animals involved. Many thanks also go to Dr Michael Kelly and Justyna Janus for their assistance and perseverance with preclinical imaging and also to the Department of Cardiovascular Sciences at the University of Leicester and to the British Heart Foundation for providing me the foundation and funding to complete this PhD.

Many thanks go to Professor Blair Grubb for all of his advice at the beginning of this project and in particular for his assistance in teaching me the techniques required for immunohistochemistry. I would also like to thank past and present members of Professor Ng's research group, without whom this project would not have been possible. Thanks go to Pott Pongpaopattanakul, Reshma Chauhan and also Dr Gabriella Kocsis-Fodor for their invaluable help and advice during experiments, for their assistance in surgical procedures and for being a great support throughout my PhD.

Lastly, my warmest thanks go to my family for their love and support and to Luke, for his constant encouragement and for always believing in me.

Contents

| | |
|-----------------|-----|
| Title | i |
| Abstract | ii |
| Acknowledgments | iii |
| Contents | iv |
| Publications | ix |
| Abbreviations | x |

Chapter 1: Introduction

| | | |
|-----------|---|----|
| 1.1 | Cardiac function | 1 |
| 1.2 | Cardiac electrophysiology | 1 |
| 1.2.1 | The sinoatrial node action potential | 2 |
| 1.2.2 | The ventricular cardiac action potential | 4 |
| 1.2.3 | Excitation-contraction coupling | 8 |
| 1.3 | Neuronal control of the heart | 10 |
| 1.3.1 | Autonomic control of the heart | 13 |
| 1.3.1.1 | Autonomic cardiac neurons | 13 |
| 1.3.1.2 | Mechanisms of autonomic modulation | 15 |
| 1.3.1.2.1 | Acetylcholine | 15 |
| 1.3.1.2.2 | The physiological effects of acetylcholine acting on M ₂ muscarinic receptors | 16 |
| 1.3.1.2.3 | Noradrenaline | 17 |
| 1.3.1.2.4 | The physiological effects of adrenergic receptor activation | 18 |
| 1.3.1.3 | Cardiac neuromodulators and neuropeptides | 21 |
| 1.3.1.3.1 | Nitric oxide and neuronal nitric oxide synthase | 21 |
| 1.3.1.3.2 | Additional neuronal modulators | 25 |
| 1.4 | The intrinsic cardiac nervous system | 27 |
| 1.4.1 | The human intrinsic cardiac nervous system | 29 |
| 1.4.2 | The intrinsic cardiac nervous system in experimental mammalian species | 35 |
| 1.4.3 | The morphology of the rabbit intrinsic cardiac nervous system | 39 |

| | | |
|--|---|----|
| 1.4.4 | Neurochemical phenotype of the ICNS | 42 |
| 1.5 | Autonomic control of cardiac electrophysiology: from peripheral control to the intrinsic cardiac nervous system | 47 |
| 1.5.1 | Peripheral neuronal inputs to the heart | 47 |
| 1.5.2 | The role of the ICNS in cardiac electrophysiology | 49 |
| 1.6 | The clinical relevance of studying the autonomic nervous control of the heart | 53 |
| 1.6.1 | Myocardial infarction and heart failure | 53 |
| 1.6.2 | The effects of myocardial infarction and heart failure on the ICNS | 54 |
| 1.6.2 | Cardiac arrhythmia and the ICNS | 58 |
| 1.7 | Aims | 61 |
| <u>Chapter 2: Materials and Methods</u> | | |
| 2.1 | Experimental animals | 63 |
| 2.1.1 | Ethical statement | 63 |
| 2.2 | Coronary artery ligation in the rabbit: a model of heart failure | 65 |
| 2.2.1 | Echocardiography and <i>ex-vivo</i> MRI | 67 |
| 2.2.2 | MRI and imaging processing | 68 |
| 2.2.3 | Organ retrieval and cardiac remodelling | 69 |
| 2.3 | The anatomy and morphology of the rabbit intrinsic cardiac nervous system | 70 |
| 2.3.1. | Non-sectioned pressure-distended heart preparation | 70 |
| 2.3.2 | Whole mount preparation | 71 |
| 2.3.3 | Brightfield microscopy | 74 |
| 2.4 | Whole-mount preparation for immunohistochemistry | 74 |
| 2.4.1 | Fluorescence microscopy | 75 |
| 2.5 | Statistical analysis | 75 |
| 2.6 | Investigating the role of the intrinsic cardiac nervous system on cardiac electrophysiology | 77 |
| 2.6.1 | Isolation of the Langendorff heart preparation | 77 |
| 2.6.2 | Langendorff perfusion | 77 |
| 2.6.3 | Electrical stimulation of intrinsic cardiac ganglionic plexuses | 80 |
| 2.6.3.1 | Experimental protocols for the electrical stimulation of intrinsic cardiac ganglia | 82 |

| | | |
|---------|---|----|
| 2.6.3.2 | Cardiac constant pacing | 82 |
| 2.6.4 | Pharmacological agents | 82 |
| 2.6.5 | Signal measurements and data analysis | 82 |
| 2.7 | Investigating the interaction between the rabbit ICNS and peripheral autonomic nerves | 84 |
| 2.7.1 | Isolated innervated heart preparation | 84 |
| 2.7.2 | Perfusion and mounting of the preparation | 86 |
| 2.7.3 | Signal measurements | 89 |
| 2.7.4 | Nerve stimulation protocols | 89 |
| 2.7.4.1 | Electrical stimulation protocols | 89 |
| 2.7.5 | Data analysis | 90 |

Chapter 3: Heart failure in the rabbit

| | | |
|-------|---|-----|
| 3.1 | Introduction | 91 |
| 3.2 | Results | 92 |
| 3.2.1 | Cardiac Dysfunction | 92 |
| 3.2.2 | Organ Congestion | 92 |
| 3.2.3 | Cardiac Remodelling | 96 |
| 3.2.4 | MRI and lesion volume in the intact excised heart | 98 |
| 3.3 | Discussion | 101 |

Chapter 4: The effects of heart failure on the anatomy and morphology of the rabbit intrinsic cardiac nervous system

| | | |
|---------|---|-----|
| 4.1 | Introduction | 102 |
| 4.2 | Results | 104 |
| 4.2.1 | Distribution of intrinsic cardiac neurons in the whole rabbit heart | 104 |
| 4.2.2 | Heart failure and the overall distribution of intrinsic cardiac neurons in the whole rabbit heart | 107 |
| 4.2.2.1 | Quantification of rabbit intrinsic cardiac ganglia and the effect of heart failure | 108 |
| 4.2.3 | Distribution of immunohistochemically distinct intrinsic cardiac ganglia and neurons | 117 |
| 4.3 | Discussion | 123 |
| 4.3.1 | Distribution of intrinsic cardiac neurons in the whole rabbit heart | 123 |
| 4.3.2 | The effects of heart failure on the morphology of the rabbit ICNS | 125 |

| | | |
|-------|---|-----|
| 4.3.3 | The immunohistochemical profile of the rabbit ICNS in healthy rabbits | 128 |
|-------|---|-----|

Chapter 5: The functional role of intrinsic cardiac ganglia in the rabbit

| | | |
|---------|--|-----|
| 5.1 | Introduction | 132 |
| 5.2 | Results | 134 |
| 5.2.1 | The effects of electrical stimulation of cardiac intrinsic ganglionated plexuses | 134 |
| 5.2.1.1 | Chronotropic responses to electrical stimulation of intrinsic cardiac ganglia | 135 |
| 5.2.1.2 | Left ventricular pressure and monophasic action potential duration changes | 140 |
| 5.3 | The functional role of the ICNS following MI | 142 |
| 5.3.1 | Chronotropic responses to electrical stimulation of intrinsic cardiac ganglia following MI | 142 |
| 5.3.2 | Left ventricular pressure and monophasic action potential duration changes in the heart failure and sham operated groups | 147 |
| 5.4 | Dromotropic responses to electrical stimulation of intrinsic cardiac ganglia | 150 |
| 5.5 | The effects of heart failure on dromotropic responses to electrical stimulation of intrinsic cardiac ganglia | 153 |
| 5.6 | The effects of pharmacological agents on cardiac responses of electrical stimulation of intrinsic cardiac ganglia | 157 |
| 5.7 | Discussion | 159 |
| 5.7.1 | The effects of electrical stimulation of intrinsic cardiac ganglia on cardiac function | 159 |
| 5.7.2 | The effects of heart failure on the functional role of the ICNS | 163 |

Chapter 6: The interaction between peripheral neuronal inputs and the ICNS

| | | |
|-------|--|-----|
| 6.1 | Introduction | 167 |
| 6.2 | Results | 169 |
| 6.2.1 | Heart rate response characteristics of vagal nerve stimulation | 169 |
| 6.2.2 | The effects of peripheral and intrinsic cardiac stimulation on cardiac chronotropy | 172 |
| 6.2.3 | The effects of peripheral and intrinsic cardiac stimulation on cardiac dromotropy | 175 |

| | | |
|-------|--|-----|
| 6.2.4 | Pharmacological blockade of vagal and ICNS responses to electrical stimulation | 177 |
| 6.3 | Discussion | 180 |
| | <u>Chapter 7: Concluding remarks</u> | 185 |
| | <u>Chapter 8: Bibliography</u> | 190 |

Publications

In addition to the work presented in this thesis, I have been first author in a publication reviewing the anatomical and physiological characteristics that define the intrinsic cardiac nervous system.

Wake E, Brack KE. Characterization of the intrinsic cardiac nervous system. *Auton Neurosci*. 2016 S1566-0702 (16); 30129-1. doi: 10.1016/j.autneu.2016.08.006.

Abstracts

Physiological Society Meeting, Dublin, Ireland, July 2016

Wake E, Chin SH, Brack KE, Ng GA. The neurocardiological effects of autonomic nerve stimulation in a rabbit model of heart failure. *Physiology 2016*; Poster communication.

Chauhan RA, Coote JH, **Wake E**, Brack KE, Ng GA. Differential effects from left and right sympathetic nerve stimulation on ventricular electrophysiology and arrhythmia inducibility. *Physiology 2016*; Poster communication.

Pongpaopattanakul P, **Wake E**, Kocsis-Fodor GO, Brack KE, Ng GA. Low-level vagus nerve stimulation protects against ventricular arrhythmias in the isolated innervated rabbit heart. *Physiology 2016*; Poster communication.

3Rs Seminar: Promoting the 3Rs initiatives at University of Leicester, March 2016

Brack KE, **Wake E**, Chin SH, Ng GA. Refinements in the coronary artery ligation model of heart failure (HF) in the rabbit. *University of Leicester*.

European Society of Cardiology Meeting, Europace, Milan, Italy, June 2015

Chin SH, **Wake E**, Brack KE, Ng GA. The Effect of Sympatho-vagal Interaction and Beta-blocker on Heart Rate and Ventricular Refractoriness in Isolated Rabbit Hearts. *Europace 2015*; 17(suppl 3): iii30-iii55 (doi:<http://dx.doi.org/10.1093/europace/euv156>)

Chin SH, **Wake E**, Brack KE, Ng GA. The Effect of Beta-blocker in Modulating Ventricular Fibrillation Inducibility and Electrical Restitution during Sympatho-vagal Interaction in Isolated Rabbit Hearts. *Europace 2015*; 17(suppl 3): iii237-iii259 (doi:<http://dx.doi.org/10.1093/europace/euv182>)

Chin SH, **Wake E**, Brack KE, Ng GA. Modulation of Ventricular Fibrillation Inducibility and Electrical Restitution during Sympatho-vagal Interaction by Beta-Blocker in Isolated Rabbit Hearts. *Heart Rhythm 2015*; 12(5): S409(doi:<http://dx.doi.org/10.1016/j.hrthm.2015.03.052>)

Physiological Society Meeting, London, UK, July 2014

Monaghan A, Brack KE, Mitcheson J, **Wake E**, Ng GA. Electrophysiological effects of pharmacologically induced Long QT Syndrome 1 & 2. *Physiology 2014* (London, UK) (2014) Proc Physiol Soc 31, PCA023.

Zhang C, Brack KE, **Wake E**, Ng GA. Effects of ivabradine on the ventricle in isolated guinea pig hearts. *Physiology 2014* (London, UK) (2014) Proc Physiol Soc 31, PCA026.

Abbreviations

| | |
|--------------------------------|--|
| AC | Adenylyl cyclase |
| ACh | Acetylcholine |
| AChE | Acetylcholinesterase |
| AF | Atrial fibrillation |
| Ao | Aortic root |
| AP | Action potential |
| APD | Action potential duration |
| ARGP | Anterior right ganglionic plexus |
| ATP | Adenosine triphosphate |
| AV node | Atrioventricular node |
| BRS | Baroreceptor stimulation |
| CA | Conus arteriosus |
| Ca ²⁺ | Calcium ion |
| cAMP | Cyclic adenosine monophosphate |
| cGMP | Cyclic guanosine monophosphate |
| CGRP | Calcitonin gene-related peptide |
| ChAT | Choline acetyltransferase |
| CICR | Calcium-induced calcium release |
| CS | Coronary sinus |
| CV | Caudal vein |
| DMV | Dorsal motor nucleus of the vagus |
| DRA | Dorsal right atrial subplexus |
| DRG | Dorsal root ganglia |
| ECC | Excitation-contraction coupling |
| ECG | Electrocardiogram |
| EDV | End diastolic volume |
| EF | Ejection fraction |
| ERP | Effective refractory period |
| ES | Electrical stimulation |
| ESV | End systolic volume |
| GalR ₁ | Galanin receptor |
| GC | Guanylate cyclase |
| GDP | Guanosine diphosphate |
| G _i /G _o | Inhibitory pertussis toxin sensitive G-protein |
| GP | Ganglionic plexus |
| G _s | Stimulatory G-protein |
| GTP | Guanosine triphosphate |
| HF | Heart failure |
| HR | Heart rate |
| I _{Ca} | Calcium current |
| ICG | Intrinsic cardiac ganglia |
| ICN | Intrinsic cardiac neuron |
| ICNS | Intrinsic cardiac nervous system |
| I _{K1} | Inward rectifier potassium current |
| I _{KACH} | Inwardly rectifying ACh sensitive potassium channels |
| I _{KR} | Delayed outward rectifier potassium current, rapid |

| | |
|--------------------|---|
| I _{KS} | Delayed outward rectifier potassium current, slow |
| I _{Na} | Inward sodium current |
| IR | Immunoreactivity |
| IRGP | Inferior right ganglionic plexus |
| I _{To} | Transient outward potassium current |
| IVC | Inferior vena cava |
| IVC-ILA GP | Inferior vena cava-inferior left atrial ganglionic plexus |
| K ⁺ | Potassium ion |
| LA | Left atrium |
| LAu | Left auricle |
| LC | Left coronary subplexus |
| LCV | Left cranial vein |
| LD | Left dorsal subplexus |
| LNC | Left neuronal cluster |
| LPV | Left pulmonary vein |
| LTCC | L-type calcium channel |
| LV | Left ventricle |
| LVS | Left vagus stimulation |
| LVEF | Left ventricular ejection fraction |
| mAChR | Muscarinic acetylcholine receptor |
| MAP | Monophasic action potential |
| MAPD | MAP duration |
| MD | Middle dorsal subplexus |
| MI | Myocardial infarction |
| MPV | Middle pulmonary vein |
| NA | Noradrenaline |
| Na ⁺ | Sodium ion |
| [Na ⁺] | Sodium ion concentration |
| nAChR | Nicotinic acetylcholine receptor |
| NCX | Sodium/calcium exchanger |
| NGF | Nerve growth factor |
| NO | Nitric oxide |
| NOS | Nitric oxide synthase |
| NPY | Neuropeptide Y |
| PA | Pulmonary artery |
| PAGP | Posterior atrial ganglionic plexus |
| PB | Phosphate buffer |
| PBS | Phosphate buffered saline |
| PDE | Phosphodiesterase |
| PFA | Paraformaldehyde |
| PGP9.5 | Protein gene product 9.5 |
| PKA | Protein kinase A |
| PKC | Protein kinase C |
| PKG | Protein kinase G |
| PLB | Phospholamban |
| PS | Parasympathetic |
| PT | Pulmonary trunk |

| | |
|---------|---|
| PV | Pulmonary vein |
| PVCV | Pulmonary vein-caudal vein |
| PVI | Pulmonary vein isolation |
| RA | Right atrium |
| RAGP | Right atrial ganglionic plexus |
| RAu | Right auricle |
| RC | Right coronary subplexus |
| RCV | Right cranial vein |
| RNC | Right neuronal cluster |
| RPV | Right pulmonary vein |
| RSPV | Right superior pulmonary vein |
| RV | Right ventricle |
| RVS | Right vagus stimulation |
| RyR | Ryanodine receptor |
| SA Node | Sinoatrial node |
| SERCA | Sarcoplasmic/endoplasmic reticulum calcium ATPase |
| sGC | Soluble guanylate cyclase |
| SLGP | Superior left ganglionic plexus |
| SNS | Sympathetic nervous system |
| SR | Sarcoplasmic reticulum |
| SCD | Sudden cardiac death |
| SIF | Small intensely fluorescent |
| SVC | Superior vena cava |
| TH | Tyrosine hydroxylase |
| TnC | Troponin C |
| TnI | Troponin I |
| TnT | Troponin T |
| VF | Ventricular fibrillation |
| VFT | Ventricular fibrillation threshold |
| VIP | Vasoactive intestinal peptide |
| VIV-GP | Ventral interventricular ganglionic plexus |
| VLA | Ventral left atrial subplexus |
| VNS | Vagus nerve stimulation |
| VRA | Ventral right atrial subplexus |

Chapter 1: Introduction

Cardiovascular disease remains an unresolved clinical problem, with increasing pressure being put on the research community to provide prophylactic treatments to control disease. It is well recognised that dysfunction in the autonomic neuronal control of the heart is associated with the development of cardiac disease pathology. Abnormalities in the activity of the autonomic nervous system can have significant repercussions in the development of congestive heart failure and life-threatening arrhythmias, which can ultimately result in sudden cardiac death (SCD).

1.1 Cardiac function

The heart is a major organ responsible for the continuous circulation of blood around the body. It is separated into two functional components; the pulmonary and the systemic circulation, with the heart being the pump through which blood passes. The systemic circulatory system collects deoxygenated blood from around the body and drives it to the heart. The deoxygenated blood is then pumped to the lungs by the pulmonary circulatory system for gaseous exchange of carbon dioxide and oxygen. The systemic circulatory system carries the oxygenated blood around the body and on return to the heart, the now deoxygenated blood is propelled back to the lungs.

The heart is separated into left and right sides, which control the systemic and pulmonary circulation respectively, with both sides having a thinner walled atrial chamber acting as a reservoir and a ventricular unit. Blood pumped from the atria into the muscular ventricles is forcefully ejected to either the lungs or the rest of the body, with valves throughout preventing bidirectional flow. The heart generates its mechanistic actions via an electrical conduction system with the co-ordinated propagation of electrical activity in the form of action potentials (AP) enabling the efficient contraction of the heart.

1.2 Cardiac electrophysiology

The cardiac cycle is initiated by electrical signals produced at the sinoatrial node (SA node); a small area located in the right atrium known as the intrinsic cardiac pacemaker, and is transmitted as a precise wave of excitation through specific routes. This wave of electricity is propagated across the right, then the left atrium to initiate atrial

contraction and ultimately reaches the atrioventricular node (AV node). Following a short delay period to allow the atria to contract, this wave is transmitted down the ventricles along the Bundle of His, further diverging along the Purkinje fibres to stimulate a synchronous contraction of both ventricles. Any disruption to any part of the conduction system can result in cardiac arrhythmia.

1.2.1 The sinoatrial node action potential

In the adult human heart under normal physiological conditions, the SA node is the dominant structure of the cardiac conduction system due to having the highest rate of spontaneous depolarisation and is therefore responsible for generating pacemaker activity. The SA node is a heterogeneous collection of specialised myocytes that collectively act as the pacemaker for the initiation of the normal heart beat during sinus rhythm. The automaticity with which cells within the SA node act depends on a specific electrophysiological profile and the movement of particular ions. In order for a SA nodal cell to generate an electrical signal, the membrane potential of the cell needs to slowly depolarise until a specific threshold voltage is reached. SA nodal cells are characterised as lacking a true stable resting potential, primarily due to the lack of the inward rectifier K^+ channel, I_{K1} . In addition, the depolarising current in SA nodal cells occurs due to the movement of Ca^{2+} as opposed to Na^+ , which is the primary ion involved in depolarisation in other non-pacemaker action potentials produced by atrial and ventricular cells which will be described later.

The action potential of SA nodal cells is divided into three phases; phases 4, 0 and 3 (figure 1.1).

Phase 4: spontaneous membrane depolarisation that triggers the action potential when the threshold voltage is reached (between -40 and -30mV).

Phase 0: the depolarisation phase of the SA node action potential.

Phase 3: the repolarisation phase brought about by the movement of K^+ .

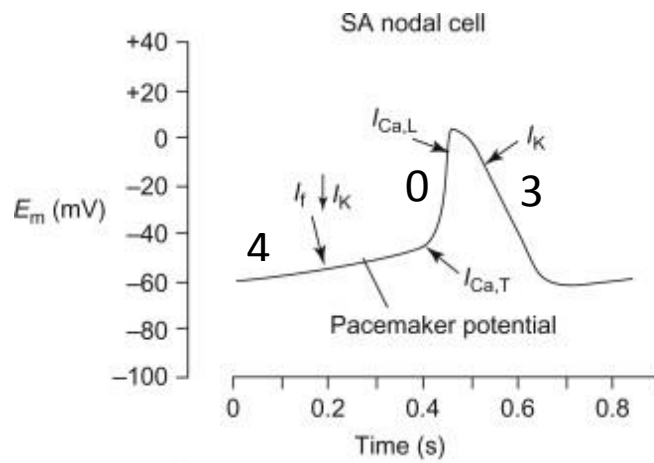


Figure 1.1. The sinoatrial node action potential. An example trace of the action potential of a SA nodal cell. Spontaneous membrane depolarisation occurs during phase 4, with further rapid depolarisation due to movement of Ca^{2+} being initiated once the threshold voltage is reached. Phase 3 or the repolarisation phase ensues due to the movement of K^+ . Image modified from Feher (2012).

At very negative membrane potentials (approximately -60mV) ion channels open allowing the conductance of slow depolarising Na^+ currents. During this diastolic depolarisation, one of the most important currents is the “funny current” or I_f . This current, first discovered in 1979 (Brown *et al.*, 1979), allows the influx of Na^+ via hyperpolarisation-activated and cyclic nucleotide-gated channels (HCN channels), which open in response to membrane hyperpolarisation hence why this current is referred to as the “funny current”. The influx of Na^+ causes the membrane to spontaneous depolarisation and the initiation of phase 4. Subsequently, the membrane potential increases to reach -50mV, triggering the opening of transient of T-type Ca^{2+} channels and the movement of Ca^{2+} into the cell, causing further depolarisation. As the membrane potential reaches around -40mV, long lasting or L-type Ca^{2+} channels including $\text{Ca}_v1.3$ open, resulting in depolarisation. In addition to the opening of Na^+ and Ca^{2+} channels, there is a slow decline in the outward movement of K^+ following on from phase 3. Upon reaching the membrane potential threshold, rapid depolarisation occurs primarily because of the increased movement of Ca^{2+} through the L-type Ca^{2+} channels seen as the upstroke of phase 0. The slope of this upstroke is less steep in comparison to that of other cardiac cells due to the relatively slower movement of Ca^{2+} and the lack of large Na^+ currents, which will be described later. Repolarisation of the membrane (phase 3 of the action potential) occurs due to an increase in K^+ permeability and the opening of voltage-gated K^+ channels. This increase in K^+ movement, accompanied by the inactivation and closure of the L-type Ca^{2+} channels and therefore a reduction in the inward depolarising currents, leads to hyperpolarisation of the cell.

1.2.2 The ventricular cardiac action potential

In order for the heart to mechanically contract, electrical activation is required. This comes in the form of the cardiac action potential, which once generated indicates the start of the excitation-contraction coupling (ECC) process. In order for the heart to contract in a synchronous manner, the rapid conduction of action potentials is required. As mentioned, action potentials originate in the pacemaker cells of the SA node, propagating excitation from myocyte to myocyte through the heart to the ventricles. The structure of the AP differs depending on the location of the cell across the heart. The shape of an AP implies a distinct and separate function of the cell propagating it.

The AP produced by the cells of the SA and AV nodes is the foundation for a spontaneous impulse generation compared to the APs seen with atrial and ventricular cells, whose purpose are to enable contraction. The more prominent plateau phase evident with the ventricular AP is caused by a delay in repolarisation and a maintained depolarisation, with this longer action potential duration (APD) preventing re-excitation of the cell and allowing for relaxation before the next stimuli (figure 1.2).

ECC is the cellular process by which a heartbeat occurs, enabling synchrony between electrical and mechanical function of the heart (Bers, 2006). APs that are passed via the conduction system, propagate excitation between myocytes via the selective permeability of sodium ion (Na^+), potassium ion (K^+) and calcium ion (Ca^{2+}) channels that are distributed on the cell membrane. The configuration of the ventricular action potential is divided in to 5 phases; phase 0-4 (figure 1.2).

Phase 4: the membrane potential is in the 'rest' phase prior to the generation of an AP. This phase is maintained by the inward rectifier current, I_{K1} , and in this phase the cardiomyocyte membrane is preferentially permeable to K^+ .

Phase 0: membrane depolarisation initiated by an AP triggers the opening of rapidly activating voltage-gated Na^+ channels, NaV1.5 , increasing the cells permeability to Na^+ and a rapid inward Na^+ current (I_{Na}) resulting in the upward stroke of the AP.

Phase 1: the early repolarisation phase governed by the closure of the Na^+ channels and activation of the transient outward potassium current (I_{To}).

Phase 2: during the plateau phase, where there is little change in the membrane potential, an influx of Ca^{2+} through voltage gated L-type Ca^{2+} channels (LTCC) occurs. This entry of calcium plays a crucial role in ECC and the initiation of contraction.

Phase 3: a decline in LTCC activation and an increase in K^+ conductance governed by repolarising K^+ currents (the rapid delayed rectifier potassium current (I_{KR}) and slow delayed rectifier potassium current (I_{KS})), which leads to the late/rapid depolarisation phase.

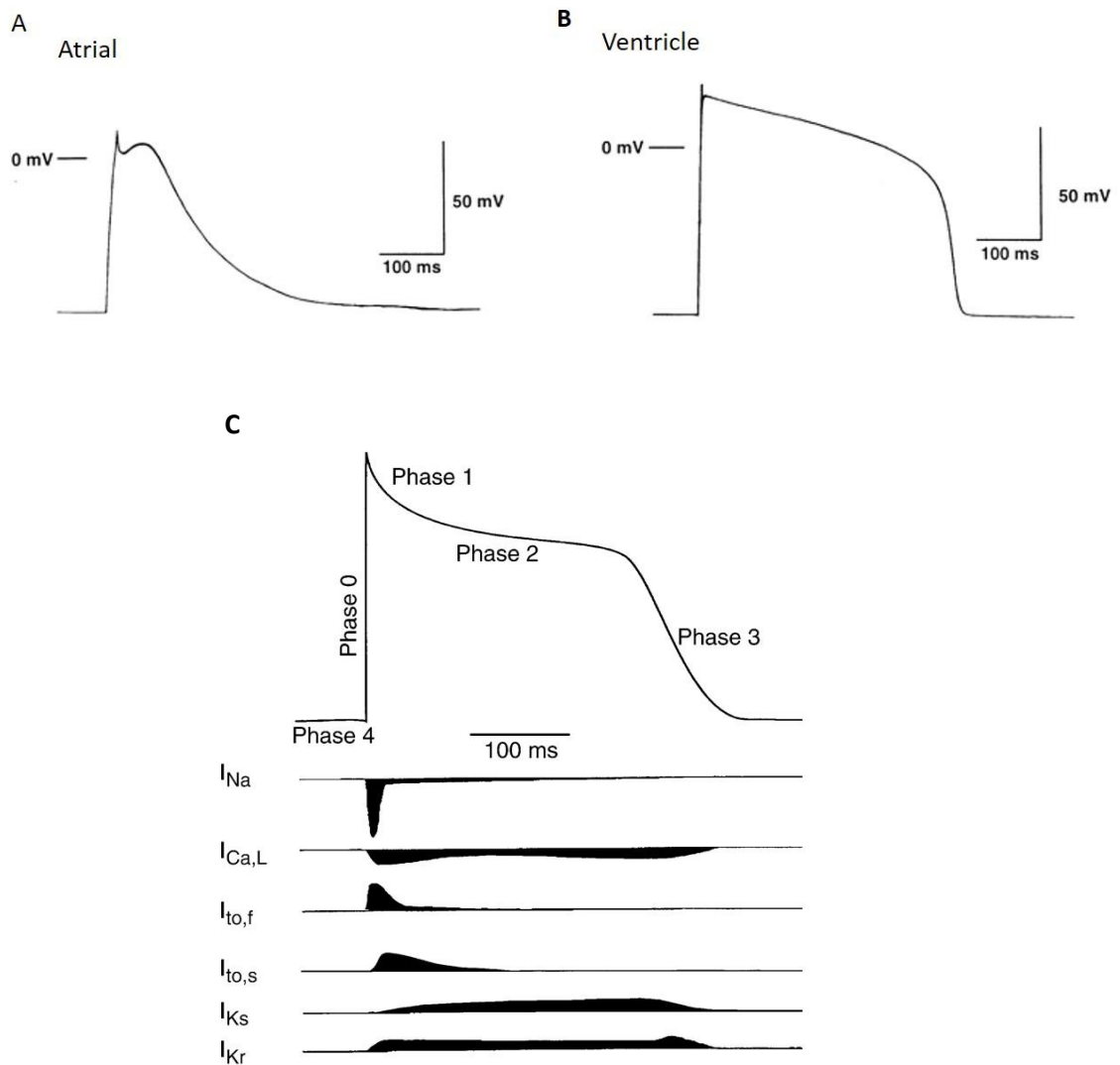


Figure 1.2. The human atrial and ventricular action potentials. Example tracings of action potentials in human atrial (A) and ventricular myocytes (B). Image C shows a schematic representation of a human ventricular AP and the ionic currents underlying each of the 5 phases (phases 0,1,2,3 and 4). Modified from Koumi *et al.* (1995) and Nerbonne and Kass (2005).

The ventricular AP (figure 1.2) is characteristically represented by a steady state resting membrane potential of around -90mV, termed phase 4. The current responsible for establishing the resting membrane potential is the inward rectifier potassium current, I_{K1} . Following cellular excitation an influx of Na^+ (phase 0) is triggered. Membrane depolarisation results in the opening of fast Na^+ channels, generating a large inward Na^+ current and the rapid upstroke of the AP. During this phase, the outward movement of K^+ remains constant and with the fast Na^+ channels inactivating as rapidly as they activated, the K^+ current becomes dominant and repolarisation of the AP begins (phase 1). During phase 1, the closure of fast Na^+ channels and the activation of the transient outward K^+ current (I_{TO}) results in a rapid, but short and incomplete phase of repolarisation. This however is not sufficient enough to return the membrane potential to that seen during the resting state.

This early period of partial repolarisation through I_{TO} in addition to the L-type Ca^{2+} current ($I_{Ca,L}$) activated by membrane depolarisation, enables the transfer into the prolonged plateau phase of the ventricular AP (phase 2). During this plateau phase, a steady prolonged inward influx of Ca^{2+} through voltage gated LTCC is balanced by the potassium efflux by the outward delayed rectifier K^+ currents; the rapid delayed rectifier current (I_{KR}) and the slow delayed rectifier current (I_{KS}) (Bers, 2001). Calcium entry through LTCCs during this phase is a key player in the ECC (discussed later). During this period, the sodium calcium exchange current (NCX) also plays a role, albeit much smaller than the LTCC, in contributing to the entry of Ca^{2+} into the cell. As LTCCs begin to inactivate, repolarisation begins to accelerate leading into the final late and rapid repolarisation phase (phase 3). This repolarisation comes as a result of the reduction of Ca^{2+} entry into the cell due to inactivation of the LTCC. As repolarisation progresses, there is a further increase in I_{K1} as the depolarisation-induced block is released, leading to the restoration of the resting membrane potential.

Species variation in ventricular AP morphology due to differences in cardiac ion channel expression is a vital factor when investigating cardiac electrophysiology in animal models, in order to enable translation into clinical human studies. The larger plateau phase and presence of the I_{TO} current, both important factors in repolarisation (Wang *et al.*, 1999), occur in the rabbit ventricular AP. This is in comparison for example to the

guinea pig, where I_{TO} currents are absent therefore making this species a less competent model to compare to human electrophysiology. The rabbit is commonly used as a model to study cardiac electrophysiology both in whole heart procedures and when studying single cardiac cells due to the ventricular electrophysiology being comparatively similar to that seen in humans, as opposed to smaller experimental animals. Recordings of ventricular action potentials show significant species variation in terms of morphology and duration, primarily due to differences in the relative contributions of certain repolarising currents and the variation in the expression of potassium ion channels. In intermediate and larger animals such as guinea pigs, rabbits and canines, the delayed repolarisation which occurs as a result of the slowly activating delayed rectifier currents leads to the dome shaped action potential morphology. In contrast, the ventricular action potential in small mammals such as mice and rats exhibits a triangular morphology due to rapid repolarisation via a prominent transient outward current and therefore a shorter APD. These known factors in cardiac electrophysiology therefore make the rabbit the preferred animal model to investigate ventricular cardiac electrophysiology.

1.2.3 Excitation-contraction coupling

The conversion of electrical impulses into myocardial contraction occurs via ECC. For ECC to take place, a number of key contractile proteins need to be involved. The sarcomere is the structural unit within cardiomyocytes and is responsible for contraction. It is composed of a thick myofilament called myosin and a thin myofilament called actin (figure 1.3). Contraction occurs through a sliding filament mechanism with an interaction between myosin heads on the myosin filament forming cross bridges with the actin filament.

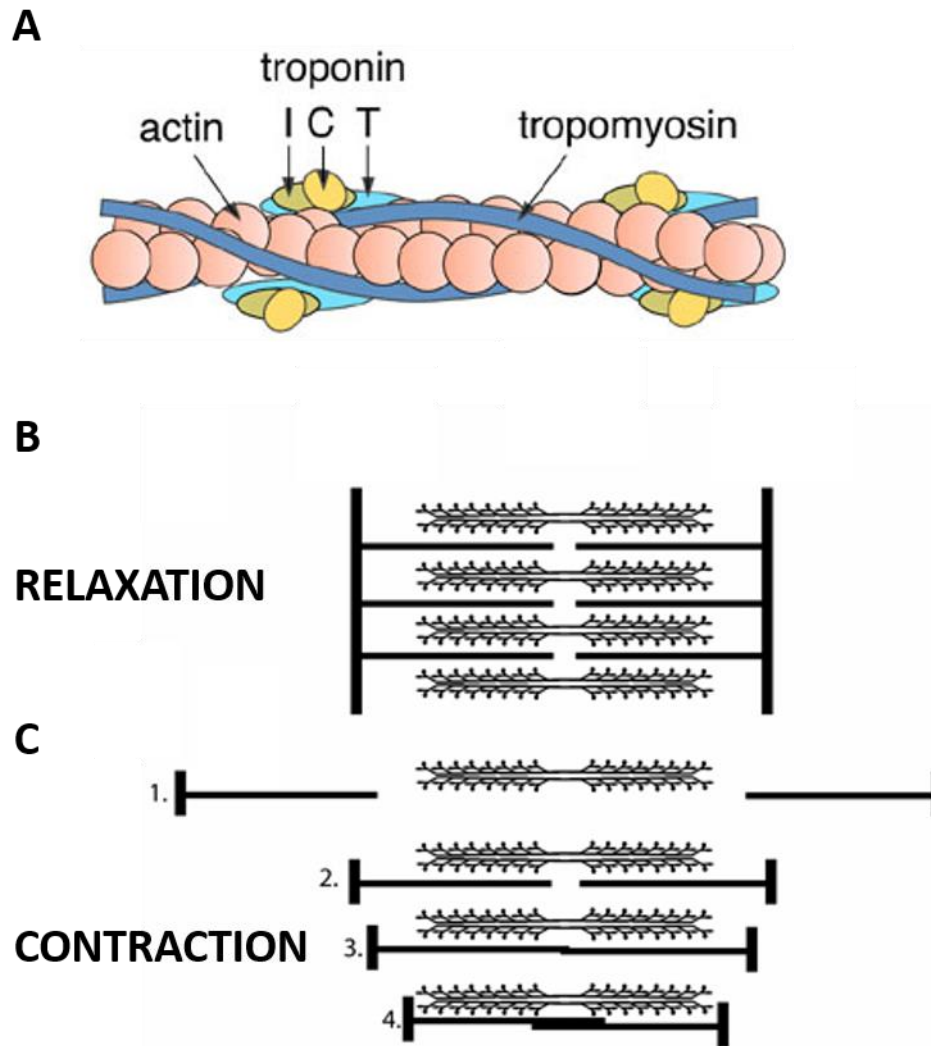


Figure 1.3. An illustration of the interaction between the actin myofilament, the troponin complex, which consists of 3 proteins, troponin I (TnI), troponin C (TnC) and troponin T (TnT) and tropomyosin (A). The sufficient binding of calcium to TnC results in a conformational change and enabling the binding of the myosin head. The actin and myosin filaments are unable to bind during diastole (B) due to the inhibitory interaction between TnI and actin. During systole and as a result of an increase in intracellular calcium however, active sites on the actin molecule are uncovered, allowing the binding of myosin and leading to contraction (C). Images modified from (Opie, 2004) and (Batter *et al.*, 2014).

The troponin complex, consisting of 3 proteins, troponin I (TnI), troponin C (TnC) and troponin T (TnT) interacts with tropomyosin, a contractile protein coupled to the actin myofilament. TnI acts as an inhibitory protein by preventing the interaction between the actin and myosin filaments. During diastole i.e. the rest period between contractions, intracellular $[Ca^{2+}]_i$ is low and contraction is inhibited due to the strong interaction between TnI and actin. As such the troponin-myosin complex covers the actin-myosin binding sites and prevents TnC-TnI interaction.

The influx of calcium ions carried by LTCCs and NCX during the plateau phase of the AP is generally insufficient to activate contraction but acts as the trigger (Lederer *et al.*, 1990) for the release of internal Ca^{2+} from the sarcoplasmic reticulum (SR) in a process known as calcium-induced calcium release (CICR). SR- Ca^{2+} release occurs through ryanodine receptors (RyR) allowing $[Ca^{2+}]_i$ to rise. Following this increase in $[Ca^{2+}]_i$ during systole, cytosolic Ca^{2+} binds to the TnC protein resulting in a conformational change in the troponin-tropomyosin complex. This change strengthens the interaction of the troponin complex with TnI and uncovers an active site on the actin molecule to which myosin can bind, promoting cross bridge-formation and therefore contraction (figure 1.3).

Following contraction it is crucial for cardiomyocyte relaxation to occur in order for the heart to function. During AP repolarisation $[Ca^{2+}]_i$ falls and results in the dissociation of Ca^{2+} from the low affinity binding site of TnC, which must be removed from the cytosol. This process is completed by a number of mechanisms including the sarcoendoplasmic reticulum Ca^{2+} ATPase transport pump (SERCA) and NCX. SERCA sequesters calcium back into the SR in an ATP-dependent manner and is regulated by phospholamban (PLB), which in its unphosphorylated state acts to inhibit Ca^{2+} transport and sequestration.

1.3 Neuronal control of the heart

The nervous system is a highly complex and extensive system responsible for the control of the human body. It is divided into two sections: the central and peripheral nervous systems, with cardiac activity being modulated by centrally derived parasympathetic and sympathetic branches of the autonomic nervous system (figure 1.4). It is well known that the sympathetic nervous system (SNS) has a strong augmentative effect on the

heart increasing heart rate (chronotropy), conduction velocity (dromotropy), myocardial contraction (inotropy) and relaxation (lusitropy). The sympathetic branch innervates the heart primarily via specific intrathoracic ganglia. Cardiac preganglionic cell bodies are located within the grey matter of the intermediolateral column of the first six segments (T1 – T6) of the upper thoracic spinal cord. Axons exit the spinal cord by the ventral roots where they join the sympathetic chain via the white rami (Coote and Chauhan, 2016). Cardiac preganglionic efferent nerves project to postganglionic neurons in the stellate ganglia (the main supply of postganglionic efferent sympathetic nerves to the heart) (Kawashima, 2005) and the caudal cervical ganglia (Norris *et al.*, 1977, Kawashima, 2005, Armour and Hopkins, 1981). Sympathetic postganglionic nerves extending from the stellate and caudal cervical ganglia enter the heart and extensively branch to all four chambers of the heart with limited overlap of the left and right spatially diverse neuronal inputs (Randall, 1977).

In contrast, the parasympathetic branch of the autonomic nervous system exerts an antagonistic effect to the sympathetic branch, with tonic levels of vagal activity present during rest, at a more pronounced level than that of the sympathetic branch (Yang and Levy, 1984). Myelinated parasympathetic preganglionic fibres originate from columns of cells in the medulla oblongata i.e. the dorsal motor nucleus of the vagus (DMV) (Hopkins and Armour, 1984) and the nucleus ambiguus (Hopkins and Armour, 1984) in the midbrain. These fibres are conveyed within the left and right vagus nerves where they synapse with parasympathetic postganglionic fibres in and around the heart and great vessels. Direct effects of vagal activation result in the attenuation of both heart rate and conduction velocity through the hyperpolarization of nodal tissue (Imaizumi *et al.*, 1990).

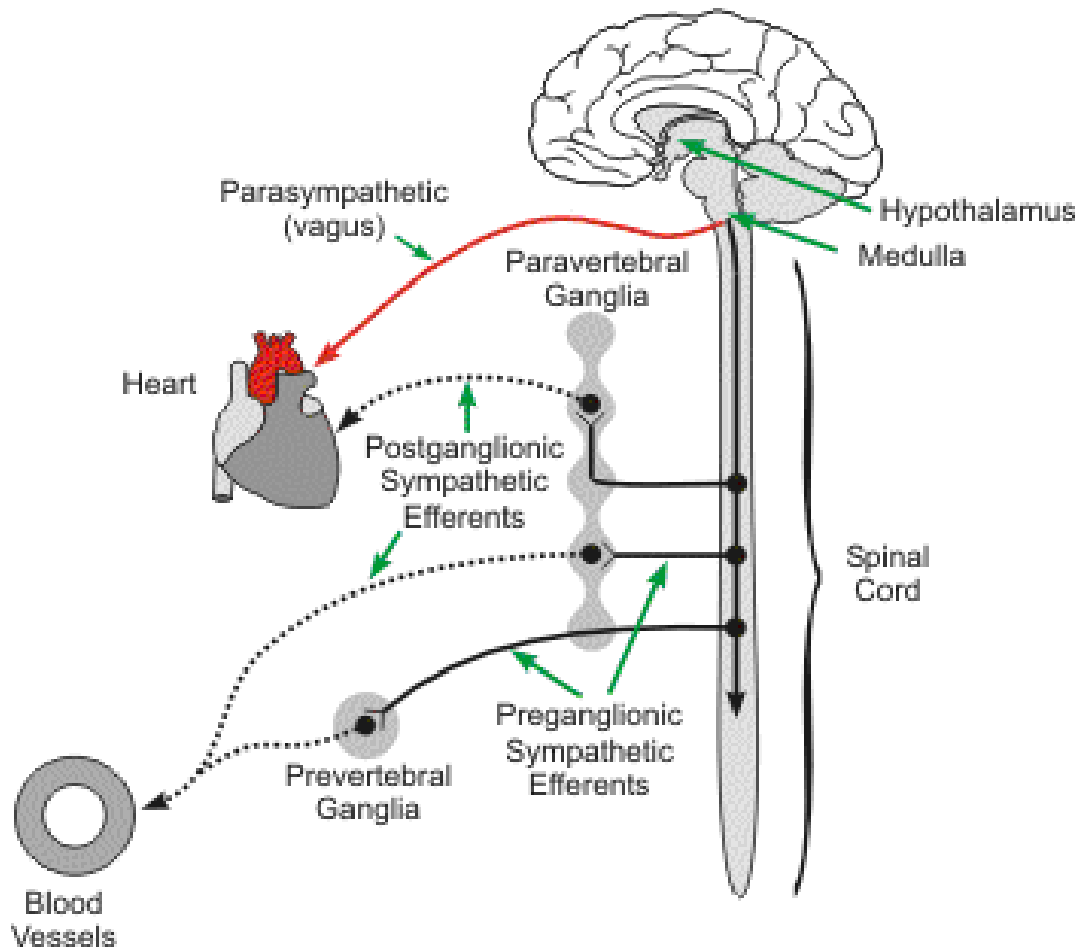


Figure 1.4. A basic representation of the interactions of extrinsic preganglionic and postganglionic autonomic nerves and the routes of innervation of the heart. The parasympathetic input to the heart comes from the left and right vagal nerves whilst sympathetic innervation is brought about via specific intrathoracic ganglia. Image taken from http://www.cvpharmacology.com/autonomic_ganglia on 09/02/16.

Autonomic modulation is the result of direct and indirect actions of specific neurotransmitters released from efferent nerve fibres. As a result of the interaction between these neurotransmitters and their corresponding receptors, a variety of signalling cascades come into play, ultimately leading to alterations in cardiac chronotropy and dromotropy. Complex interactions exist between the two divisions of the autonomic nervous system and contribute to heart health, with disturbances to this interaction leading to disease (Bibeovski and Dunlap, 2011).

1.3.1 Autonomic control of the heart

Neuronal signalling in the control of cardiac function is a complex phenomenon involving a series of reflex control networks (Ardell and Armour, 2016). The overall network can be divided into three tiers; 1) the higher control centre encompassing the spinal cord and medulla, 2) the intrathoracic extracardiac ganglia and 3) the intrinsic cardiac ganglia. These networks contain afferent, efferent and local circuit neurons, which interact both locally and also act independently to fine tune the final influence on the heart.

1.3.1.1 Autonomic cardiac neurons

The complex neuronal hierarchy requires a significant level of communication between all levels of the cardiac innervation, involving a variety of different neuronal subtypes; namely peripheral sympathetic and parasympathetic pre- and post- ganglionic efferent neurons, afferent neurons, and local circuit neurons found at the level of the heart itself termed intrinsic cardiac neurons.

Cardiac motor or efferent neurons carry finely tuned information from the central nervous system, providing constant feedback in the control of cardiac function. As mentioned, the sympathetic preganglionic efferent neurons that reside within the intermediolateral column of the spinal cord, synapse with sympathetic postganglionic neurons both within intrathoracic and intrinsic cardiac ganglia. The majority of sympathetic efferent postganglionic neuronal somata located in intrinsic and intrathoracic ganglia express a phenotype implying the presence of catecholamines such as noradrenaline (NA) (Baluk and Gabella, 1990). Immunoreactivity (IR) for tyrosine hydroxylase (TH) was historically believed to be present in populations of small intensely fluorescent (SIF) cells; however, it is becoming increasingly apparent that larger

populations of somata also demonstrate TH-IR and these cells are possibly even principal neurons (long axoned cells capable of transmitting information over relatively longer distances) (Rysevaite *et al.*, 2011b, Hoover *et al.*, 2009).

Cardiac afferent nerves are generally associated with neurons that have their cell bodies in extracardiac ganglia such as the nodose and dorsal root ganglia (DRG) and relay sensory information to the brain and spinal cord (Hopkins and Armour, 1989). Alterations in the chemical and mechanical milieu around afferent nerves are detected by receptors on axons within the myocardium and allow the transduction of sensory information about blood pressure, blood volume, perfusion and metabolic status (Ardell, 1994). There are many types of afferent nerves which possess a unique transduction capability allowing for different sensory information to be relayed to the central nervous system. The constant feedback provided by afferent neurons residing within intrinsic cardiac ganglia at the level of the heart provides the precedence for beat-to-beat control (Fukuda *et al.*, 2015).

A separate population of neurons capable of processing these afferent and efferent neuronal inputs exists in both intrathoracic and intrinsic cardiac ganglia (Armour, 2007, Armour, 1991), termed local circuit neurons. These neurons demonstrate the ability to communicate with neurons within the same ganglia as well with neurons within spatially diverse ganglia. Intrinsic cardiac local circuit neurons have been shown to receive inputs from both sympathetic and parasympathetic efferent preganglionic neurons (Armour, 1991) therefore suggesting a significant role of such neuronal subtype in the processing of sensory and motor information and the eventual influence of cardiodynamics. Excessive activation of local circuit neurons involved in the transduction of afferent signals into mechanical efferent effects plays a role in the induction of atrial fibrillation (AF) (Beaumont *et al.*, 2013). This implication of local circuit neurons involved in cardiac arrhythmias accompanied by the fact that such arrhythmia susceptibility can be altered during vagal nerve stimulation (Beaumont *et al.*, 2013) suggests that this population of neurons may represent a novel therapeutic target.

1.3.1.2 Mechanisms of autonomic modulation

Autonomic modulation of the heart relies on the release of specific neurotransmitters including catecholamines and acetylcholine from sympathetic and parasympathetic nerves respectively. These bind to specific postsynaptic receptors on the cell membrane and trigger a variety of signal transduction pathways. The main mechanism of modulation occurs via the activation of a secondary messenger system. Such pathways involve sarcolemmal located receptors coupled to guanosine triphosphate (GTP) regulated proteins, known as G-proteins, which have three subunits (α , β and γ). In resting conditions the α subunit is bound with guanosine diphosphate (GDP) and so is closely associated with the β and γ subunit. Upon receptor activation, the exchange of GTP for GDP is catalysed resulting in the $G\alpha$ -GTP subunit dissociating from the membrane bound $G\beta\gamma$ subunit. The activated $G\alpha$ -GTP subunit initiates the physiological downstream effects depending upon which cardiac G-protein subtype is involved (figure 1.5).

1.3.1.2.1 Acetylcholine

Cholinergic modulation is predominantly mediated by the release of acetylcholine not only at the nerve terminals of parasympathetic postganglionic neurons but also at the preganglionic level, playing a role in both sympathetic and parasympathetic innervation. Acetylcholine is therefore not only involved at the synaptic junction of vagal (parasympathetic) neurons, but is also the neurotransmitter released at all cardiac autonomic ganglia. Cholinergic modulation classically involves 2 receptors; muscarinic-acetylcholine receptors (mAChRs) of which there are 5 subtypes (M_1 - M_5) and nicotinic-acetylcholine receptors (nAChRs). Nicotinic receptors can be divided into ganglionic or somatic muscle nicotinic receptors. Somatic muscle (N_1) nicotinic receptors are located at the neuromuscular junction and allow for the transmission of nerve impulses from motor nerves to muscle fibres. Ganglionic nicotinic receptors, which play a key role in the transmission of cholinergic signals in the autonomic nervous system and are important when understanding the role of acetylcholine in cardiac autonomic ganglia, are found on the cell bodies of both sympathetic and parasympathetic postganglionic neurons. When activated by the binding of acetylcholine, the receptors, which are ligand gated ion channels, undergo a conformational change allowing for the opening of the

channel. The nAChR is a non-selective cation channel, meaning a number of ions including Na^+ , K^+ and Ca^{2+} can pass through. The movement of cations causes a depolarisation of the plasma membrane and results in an excitatory postsynaptic potential in neurons and the transmission of neuronal signals, with such responses being blocked by the antagonist hexamethonium.

Of the 5 subtypes of mAChRs, the M_2 subtype predominates in the heart (Brodde and Michel, 1999). Cholinergic modulation occurs in 3 ways; 1) the principal mechanism via activation of mAChRs coupled to an inhibitory pertussis toxin sensitive G-protein (G_i/G_o). The dissociation of this α -subunit complex results in the inhibition of adenylyl cyclase (AC) which in turn causes a reduction in intracellular cyclic adenosine monophosphate (cAMP) levels, so leading to a reduced activity of protein kinase A (PKA), (2) direct activation and opening of inwardly rectifying acetylcholine sensitive potassium channels, K_{ACh} , by the $G\beta\gamma$ subunit, leading to an efflux of K^+ and cell hyperpolarization, and/or (3) via activation of guanylate cyclase (GC) resulting in an increase in cyclic guanosine monophosphate (cGMP), which in turn activates protein kinase G (PKG), phosphorylates and modulating the action of various intracellular proteins. Cholinergic modulation can be regulated at the pre- and post- ganglionic level, with the signalling molecule nitric oxide (NO) known to play a role in modulating the effect of acetylcholine at nerve terminals (Herring *et al.*, 2001).

1.3.1.2.2 The physiological effects of acetylcholine acting on M_2 muscarinic receptors

The binding of acetylcholine to M_2 receptors and subsequent activation of a G_i mechanism by inhibiting adenylyl cyclase and therefore decreasing cAMP levels. The resultant reduction in PKA activity prevents the phosphorylation of a number of key proteins involved in ECC including LTCCs and RyR2. This leads to a decrease in depolarising currents carried by LTCCs and a decrease in Ca^{2+} entry into the cell.

Acetylcholine also has a strong inhibitory action on the I_f current, producing a negative chronotropic effect. Reduced cAMP causes a consequential shift of the current activation curve to more negative values and slowing the spontaneous rate of firing of the pacemaker cells and slowing heart rate. Neurotransmitters such as acetylcholine specifically act to alter the steepness of diastolic depolarisation rather than to modify

the action potential threshold (Bucchi *et al.*, 2007). The spontaneous activity of SA node pacemaker cells is also slowed down in the presence of ryanodine, suggesting that Ca^{2+} cycling may also be a mechanism for heart rate regulation (DiFrancesco, 2010).

The rate of depolarisation is also influenced by the modulation of specific K^+ channels. Upon dissociation of the α and $\beta\gamma$ subunits, the $\text{G}\beta\gamma$ heterodimers directly activate G-protein-coupled inward rectifying potassium (GIRK) channels, resulting in membrane hyperpolarisation of cells within the SA and AV nodes. Similarly, the activation of K_{ACH} channels through the G_i pathway leads to membrane hyperpolarisation via a potassium efflux. Hyperpolarisation of cells means an increase in the cellular threshold for triggering rapid depolarisation (phase 0 of the SA nodal action potential) and therefore a reduction in the firing rate.

The physiological effects of M_2 receptors are very effectively blocked by muscarinic receptor antagonists such as atropine, which prevent the binding of acetylcholine and therefore, the activation of the receptor. Clinically, atropine is used to prevent sinus bradycardia and AV nodal block caused by the excessive activation of the vagus nerves innervating the heart. A decrease in vagal tone is known to occur relatively early on in the development of heart failure. Studies have recorded an attenuation in the activity of acetylcholinesterase and altered muscarinic receptor densities (Dunlap *et al.*, 2003) in heart failure, with evidence of blunting of the parasympathetic influence on sympathetic activity (Azevedo and Parker, 1999).

1.3.1.2.3 Noradrenaline

Sympathetic effects are elicited by the binding of catecholamines such as adrenaline and noradrenaline to adrenergic receptors. Adrenergic receptors exist in multiple subtypes and isoforms; the α subtype, of which there are 2 isoforms, and the β subtype, of which there are 3 ($\beta 1$ -3), with the $\beta 1$ -isoform being the primary cardiac isoform (Brodde and Michel, 1999). β -adrenoreceptors are also G-protein coupled receptors located on the cardiomyocyte surface consisting of G_α , G_β and G_γ subunits. The $\beta 1$ -adrenoreceptor is coupled to the stimulatory G-protein (G_s), which upon activation stimulates the dissociation of the G_α subunit to activate the membrane bound protein adenylyl cyclase, which in turn catalyses the conversion of adenosine triphosphate (ATP) into cAMP. This

amplification step triggers several downstream effector processes. The primary target of cAMP is PKA although cAMP can also alter ion channel function by directly acting on the channel protein. PKA, a cAMP-dependent phosphorylation enzyme, phosphorylates multiple downstream effector proteins including the LTCC, PLB, RyR2 and TnI (Bers, 2001), delayed rectifier type K⁺ channels and voltage-dependent Na⁺ channels. The G_α subunit has intrinsic GTPase activity that acts to convert the GTP to GDP, which allows the re-association of the 3 subunits for further adrenergic activation when required.

1.3.1.2.4 The physiological effects of adrenergic receptor activation

The primary mechanisms thought to underlie sympathetic-induced increases in heart rate include the effect of cAMP on cardiac pacemaker channels that give rise to the “funny current” seen in SA and AV nodal cells (Accili *et al.*, 2002) and the effect of PKA phosphorylation of Ca²⁺ channels. The direct activation of I_f by cAMP causes an increase in the slope of the pacemaker potential, reducing the time required for SA nodal cells to reach the threshold voltage needed to initiate an action potential and therefore increasing the frequency at which action potentials are produced. Beta-adrenergic receptor stimulation also increases I_f by shifting the activation curve of the current to more positive voltages through the direct binding of cAMP to channels (DiFrancesco and Tromba, 1988), the opposite mechanism to parasympathetic stimulation.

The phosphorylation of the LTCC results in a several-fold increase in I_{Ca} and a larger Ca²⁺ influx. The increase in I_{Ca} provides a larger trigger for CICR and enhances the amplitude of the Ca²⁺ transient. PKA also phosphorylates PLB resulting in a reduction in the inhibitory effect of PLB on SERCA. This causes an increase in SERCA activity, therefore an increase in Ca²⁺ uptake into the sarcoplasmic reticulum and a faster decline in intracellular calcium concentration (Bers, 2001). Over time, this also results in an increase in the level of the SR calcium store. The combination of the phosphorylation of the LTCC, RyR2 and PLB leads to an increase in the firing rate of the SA node and gives rise to the chronotropic and inotropic effects seen with β₁ adrenoreceptor stimulation.

Heart failure results in alterations in this signal transduction mechanism that affect cardiac chronotropy. Hyperactivity of sympathetic nerves during HF causes an increase in the release of neurotransmitters such as noradrenaline. This causes a resultant

activation of β 1-receptor activation enabling the heart to utilise its remaining chronotropic reserve and hence the clinical use of β -blockers such as metoprolol; used with the intent of reducing the effects of sympathetic over-activation. Evidence of hyperphosphorylation of both the LTCCs and RyR2 has been observed in heart failure (Marx *et al.*, 2000, Schroder *et al.*, 1998), implying HF leads to an increased propensity for SR Ca^{2+} release during diastole and therefore an increased susceptibility to arrhythmia.

Conversely, it is also thought that despite hyperinnervation of the sympathetic nervous system, mechanisms exist with the aim of providing a protective effect during heart failure. Studies identifying β -adrenergic desensitisation and a site specific reduction in β -adrenergic receptor density can lead to uncoupling of G_s from the receptors and result in the hypophosphorylation of PKA substrates such as PLB and Troponin. This further confirms the complexity of the involvement of the autonomic nervous system in cardiac disease and heart failure.

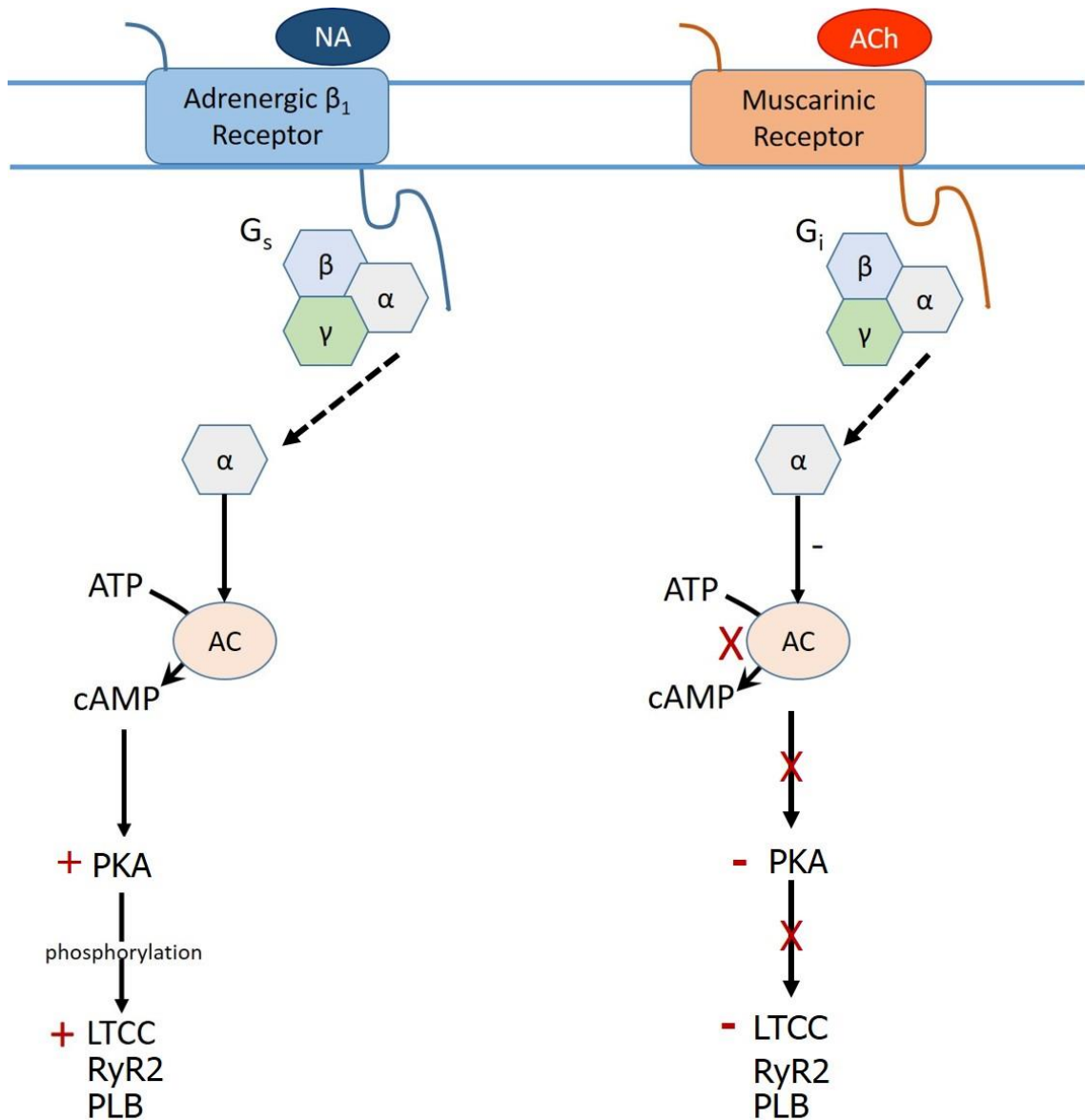


Figure 1.5. Schematic representation of the mechanisms involved in sympathetic (adrenergic) and parasympathetic (muscarinic) receptor activation. Binding of noradrenaline to adrenergic receptors and acetylcholine to muscarinic receptors leads to the dissociation of the α -subunit complex and the regulation of cAMP. Abbreviations: AC, adenylyl cyclase; ACh, acetylcholine; ATP, adenosine triphosphate; cAMP, cyclic adenosine monophosphate; LTCC, L-type calcium channel; NA, noradrenaline; PKA, protein kinase A; PLB, phospholamban; RyR2, ryanodine receptor.

1.3.1.3 Cardiac neuromodulators and neuropeptides

Signal transduction in both the sympathetic and parasympathetic autonomic pathways is complex and alongside the binding of 'standard' neurotransmitters (noradrenaline and acetylcholine) to receptors to initiate signalling cascades, numerous neuromodulators and co-transmitters are involved. Emerging research suggests that these factors influence sympathovagal innervation at the level of the heart, requiring an intricate interplay between all aspects. Such modulators include NO, neuropeptide Y (NPY) (Herring *et al.*, 2008, Herring *et al.*, 2002), substance P, calcitonin gene-related peptide (CGRP) (Rysevaite *et al.*, 2011b) and vasoactive intestinal peptide (VIP) (Parsons *et al.*, 2006), along with other neuronally released natriuretic peptides that act in a paracrine manner. Alterations in the presence and involvement of these neurotransmitters and modulators occur during cardiac disease (Rajendran *et al.*, 2016) and result in a dysregulation in the autonomic responsiveness of the heart.

1.3.1.3.1 Nitric oxide and neuronal nitric oxide synthase

Nitric oxide, a free radical gaseous signalling molecule, is synthesised by the enzyme nitric oxide synthase. Of the three cardiac isoforms; neuronal (nNOS), inducible (iNOS) and endothelial (eNOS), this study will focus primarily of nNOS. nNOS, which is constitutively expressed in autonomic nerves and intracardiac ganglia (Choate and Paterson, 1999), plays a significant role in producing physiological changes due to its co-localisation with a number of cholinergic intracardiac neurons (Choate *et al.*, 2001). Neuronal NO is an important modulator of neuronal function (Herring and Paterson, 2009) acting both postsynaptically (as a co-transmitter) or presynaptically in the modulation of vagal neurotransmission. The presence of nNOS within the intrinsic cardiac nervous system (which will be described in detail further on) therefore implies the intrinsic cardiac ganglia play a role in the modulation and fine tuning of peripheral vagal inputs.

Nitric oxide acts within both cholinergic and sympathetic ganglia and neurons (figure 1.6). The majority of physiological changes by NO, specifically in terms of cholinergic control, are considered to be site specific (Herring *et al.*, 2002). NO generated by nNOS can facilitate the release of acetylcholine with parasympathetic innervation via vagus

nerve stimulation (Brack *et al.*, 2007). Within cholinergic neurons, nerve depolarisation and NO release results in the promotion of vesicular fusion to the neuronal membrane and Ca^{2+} induced exocytotic acetylcholine release. NO primarily binds to soluble guanylate cyclase (sGC) and alters cardiac physiology in both a cGMP dependent and independent manner. NO binding to sGC results in its activation and an increase in the conversion of GTP into cGMP so allowing sGC to transmit an NO dependent signal to the downstream elements of the signalling cascade (Denninger and Marletta, 1999). Increased levels of cGMP lead to modulation and activation of PKG. PKG is capable of the direct phosphorylation of components of ECC including the LTCC, causing inhibition of the LTCC and a reduction in the intracellular Ca^{2+} concentration, the RyR2, facilitating Ca^{2+} leak and PLB, therefore enhancing Ca^{2+} sequestration. In addition, PKG can lead to the indirect regulation of PKA via specific phosphodiesterases (PDEs), in particular via the inhibition of PDE3. The inhibition of PDE3 results in a local increase in cAMP and therefore an increase in LTCC (Loscalzo and Vita, 2000). The resultant increase in cAMP-PKA-dependent phosphorylation of N-type calcium channels ultimately leads to a calcium-induced exocytotic release of acetylcholine.

Vagus nerve stimulation has been implicated in the protection of the heart against ventricular fibrillation via cholinergic receptor stimulation. It has been demonstrated that the anti-fibrillatory action of cholinergic signalling via muscarinic receptors involves the release of NO, whilst a reduction of NO using NOS inhibitors (Brack *et al.*, 2011) significantly alters the protective effect of the vagus (Herring and Paterson, 2001, Kalla *et al.*, 2016).

Conversely, it has been determined that NO, which is also present in the cardiomyocyte, inhibits the positive chronotropic and inotropic responses evoked by the sympathetic branch of cardiac control, presumably through stimulation of PDE2 (Choate and Paterson, 1999, Herring and Paterson, 2009), resulting in a reduction in noradrenaline release via a cGMP-PDE2-dependent pathway. In terms of cardiac function, cGMP-mediated PDE2 activation causes a decrease in cAMP. In addition, PDE2 is influential in pacemaker cells by causing the inhibition of the L-type Ca^{2+} current, I_{Ca} . A recent review by Herring and Paterson (2009) highlighted the emerging evidence regarding the involvement of NO and nNOS within sympathetic ganglia, where they illustrated work

by Wang *et al.* (2006) (see figure 1.5). Using the gene transfer of nNOS with non-specific adenoviral vectors, Wang *et al.* (2006) provided direct evidence that the targeting of nNOS to cardiac sympathetic neurons resulted in a decrease in sympathetic transmission. This correlates with a study by Mongillo *et al.* (2006) where a functional coupling between PDE2 and adenylyl cyclase activated by β -adrenoreceptor stimulation was suggested.

Despite evidence that NO plays a significant role in the modulation of both cholinergic and adrenergic innervation, the complete mechanism of NO downstream signalling in regards to neuronal control and modulation is still not completely understood and with increasing numbers of nNOS positive neuronal somata evident during heart failure (Nakamura *et al.*, 2016) presumably in the aim of reducing the release of noradrenaline and dampening down the sympathetic overdrive.

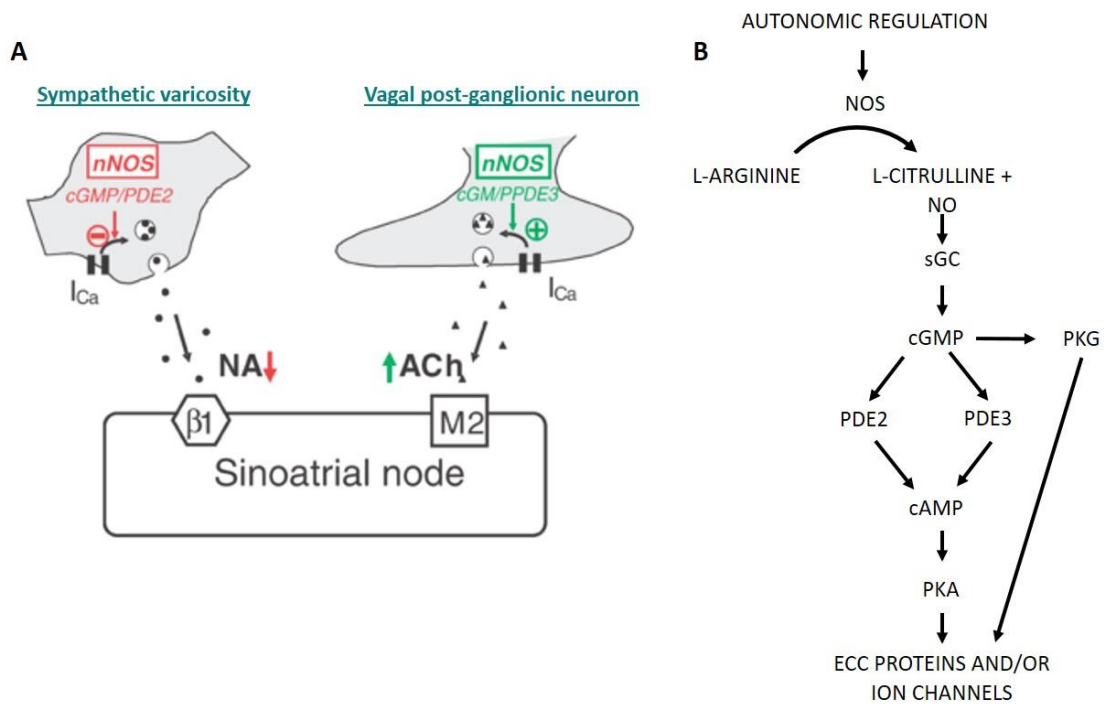


Figure 1.6. The actions of NO within both the sympathetic and parasympathetic branches of the autonomic nervous system. Nitric oxide augments the bradycardic response to vagal nerve stimulation with an increase in acetylcholine release via a cGMP and phosphodiesterase 3 pathway. Conversely, NO reduces the release of noradrenaline via a cGMP-PDE2-dependent pathway. Image A modified from Herring and Paterson (2009). The cGMP-dependent NO signalling pathway involved is shown in more detail in B. Abbreviations: ACh, acetylcholine; cAMP, cyclic adenosine monophosphate; cGMP, cyclic guanosine monophosphate; ECC, excitation-contraction coupling; NA, noradrenaline; NO, nitric oxide; NOS, nitric oxide synthase; PDE, phosphodiesterase; PKA, protein kinase A; PKG, protein kinase G.

1.3.1.3.2 Additional neuronal modulators

NPY is a neurotransmitter that is primarily synthesised and released by sympathetic neurons (Lundberg *et al.*, 1991) throughout the autonomic nervous system. It is abundant within the cardiovascular system and is also known to be present in a variety of intrinsic cardiac neurons including sensory, sympathetic and interneurons (Herring, 2015). NPY has been described as a major modulator of sympathetic-parasympathetic interaction and mediates the inhibition of vagal-acetylcholine release during longer periods of sympathetic stimulation (Yang and Levy, 1992). The varying functions of NPY are mediated by NPY receptors of which there are five distinct subtypes: Y₁, Y₂, Y₄, Y₅ and Y₆. These receptors are members of the GPCR receptor family, all of which couple to pertussis toxin-sensitive G_{i/o} proteins. Activation of NPY receptors leads to the release of the G_i subunit and the inhibition of the production of cAMP. The majority of effects of NPY in the cardiovascular system are mediated through Y₁, Y₂ and Y₅ receptors, with (Herring *et al.*, 2012) showing that Y₂ receptor antagonists can prevent the inhibition of vagal bradycardia during sympathetic stimulation.

The ability of NPY to act as a prejunctional inhibitor of vagally mediated negative inotropic responses (Serone and Angus, 1999) is brought about by the modulation of acetylcholine release at parasympathetic nerve terminals, independent of PKA, but instead dependent on PKC (Herring *et al.*, 2008). In addition to modulating vagal tone via the depression of acetylcholine release at parasympathetic nerve terminals, NPY is also capable of exerting a direct effect on parasympathetic intracardiac neurons leading to decreased parasympathetic tone via the modulation of calcium channels involved in myocyte electrophysiology.

Patients with conditions such as myocardial infarction (MI) and congestive heart failure (HF), where sympathetic drive is high, have an increased plasma level of NPY suggesting it is necessary to further investigate the role of NPY in cardiac control. It has been questioned whether this increased level could be due to NPY acting as a sympathetic co-transmitter reducing vagal activity (Herring and Paterson, 2009). Targeting NPY receptors pharmacologically may therefore provide a therapeutic target following myocardial infarction.

Recently, markers for vasoactive intestinal peptide, which is known to be co-released alongside acetylcholine (Kuncova *et al.*, 2003), have been illustrated within the ICNS (Steele *et al.*, 1994, Parsons *et al.*, 2006). VIP is present in the peripheral and central nervous systems, with VIP containing neurons being believed to be either intrinsic neurons involved in local reflexes or postganglionic neurons under nicotinic control. (Henning and Sawmiller, 2001). The majority of neural structures positive for VIP in cardiac tissues have been identified in atria with much smaller amounts described in ventricular myocardium (Weihe and Reinecke, 1981). The effects of VIP are mediated through VIP receptors of which there are two subtypes; VPAC₁ and VPAC₂. As with NPY receptors, VIP receptors are GPCR, which are coupled to the G_s subunit. Binding of VIP to these receptors results in the activation of adenylyl cyclase and a VIP induced increase in cAMP concentration. As with the action of acetylcholine and M₂ receptors, this increase in cAMP can activate PKA which goes on to phosphorylate PLB and therefore increases the sequestration of Ca²⁺ by the sarcoplasmic reticulum (Murray, 1990). VIP is thought to contribute to the regulation of coronary vasomotor tone and alter coronary artery blood flow, which correlates with the increase in VIP following myocardial infarction in an attempt to increase coronary blood flow (Hershberger *et al.*, 1988). Despite the evidence of VIP-positive fibres existing within the ICNS, which will be discussed, the origin and precise function of these fibres is unclear in relation to cardiac control.

The final neuropeptide to be discussed herein, but by no means the final neurotransmitter known to play a role in the autonomic control of the heart, is the tachykinin, substance P. Substance P is a key target in identifying sensory nerve fibres (Wake and Brack, 2016) and is widely distributed throughout the central and peripheral nervous systems. It is primarily produced by C-fibre sensory nerves and is involved in the regulation of heart rate and blood pressure (Dehlin and Levick, 2014). Substance P acts primarily by binding to the neurokinin (NK)₁ receptor. The NK₁ receptor is distributed in the plasma membrane of cell bodies and dendrites of unstimulated neurons. Following the binding of substance P to NK₁ receptors, the receptor undergoes rapid internalisation and rapid recycling to the membrane. In the heart, Hoover and Hancock (1988) described substance P receptors in the parasympathetic ganglia within the

epicardium adjacent to the pulmonary trunk, ascending aorta and right atrium. Substance P-positive fibres are characteristic of afferent nerves and are well known to have negative inotropic and chronotropic effects (Hoover, 1990). The release of Substance-P from sensory nerves directly and indirectly modifies neuronal activity and following the release of the peptide, it is believed to act on nearby vasculature and endothelial cells triggering the release of substances such as ATP and serotonin. This corresponds with the distribution of Substance P-positive fibres around coronary vessels, however they are also present in the atria and ventricles although this appears to be species dependent (Papka and Urban, 1987). Substance P-positive nerves also play a role in a multitude of cardiac diseases including HF and AF (Yu *et al.*, 2012).

1.4 The intrinsic cardiac nervous system

Dogma previously stipulated that neurocardiac control originated solely from extrinsic innervation, however increasing evidence now suggests the contrary, with Randall *et al.* (1996) describing the heart's 'little brain'. The ICNS, which resides at the level of the heart, is the final co-ordinator of cardiac function; modulating inputs from higher neuronal networks including intrathoracic ganglia and peripheral autonomic nerves.

The degree in which the ICNS acts independently of peripheral nerves is poorly understood, as is the full capability of this highly complex network of neurons in terms of cardiac function. Neurocardiological control within the ICNS involves a variety of different neuronal subtypes; namely peripheral sympathetic and parasympathetic pre- and post- ganglionic efferent neurons, afferent neurons, and neurons found at the level of the heart itself termed intrinsic cardiac neurons (figure 1.7).

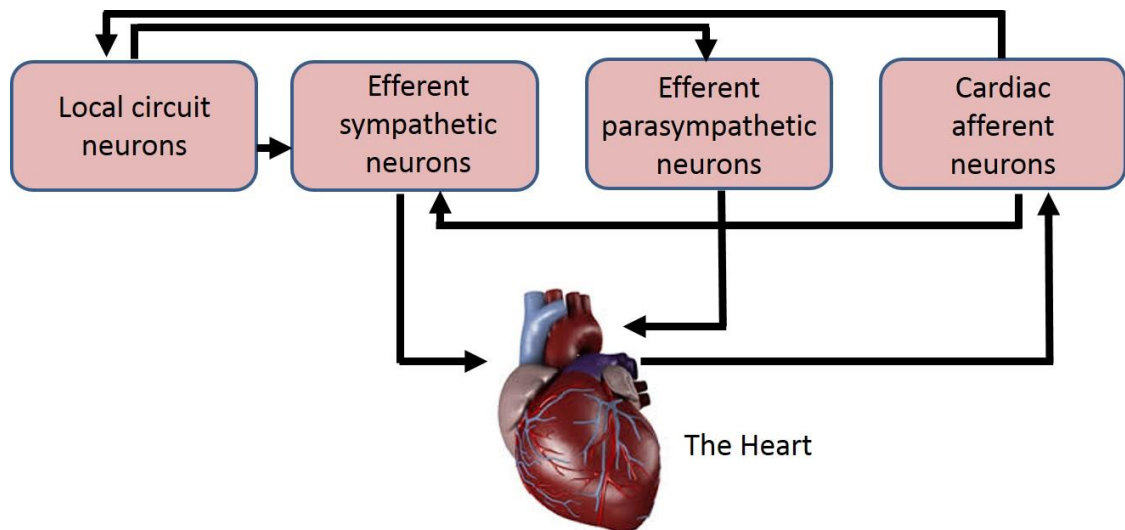


Figure 1.7. A simplified model for the intrinsic cardiac neuronal hierarchy. The complex interactions enabling fine-tuned cardiac feedback to the heart are shown. The ICNS (consisting of numerous neural subtypes shown in red boxes) is a rich network of cardiac nerves that converge to form distinct ganglia and extend across the heart. The neural structures demonstrate complex interactions to modulate cardiac function.

The ICNS comprises of collections of neuronal stomata and connecting nerve fibres known as ganglionic plexuses (GPs) or intrinsic cardiac ganglia (ICG). These plexuses are known to reside primarily on the surface of the heart on supraventricular tissues. Traditionally, it was considered that the intrinsic ganglia contained the terminal portion of postganglionic parasympathetic efferents and that only cholinergic neurotransmitters and markers such as acetylcholine and choline acetyltransferase (ChAT) would be present (Langley, 1921). This is not the case and more recent physiological data produced by Beaumont *et al.* (2013) demonstrates that the ICNS is not merely a relay station between effector sites and the central nervous system.

1.4.1 The human intrinsic cardiac nervous system

Despite the knowledge that the autonomic nervous system modulates cardiac dynamics and electrophysiology, data regarding the involvement of the ICNS remains limited and only a handful of studies have investigated the gross morphology of the human ICNS.

Clinical studies demonstrate that dysfunction of the ICNS is associated with cardiac diseases, including atrial and ventricular arrhythmias (Scherlag and Po, 2006, He *et al.*, 2013), so understanding the gross anatomy and function of the human ICNS is of increasing importance. Early studies by Worobiew (1925, 1928, 1958 cited by (Pauza *et al.*, 2000)) examining neuronal cardiac inputs, identified intrinsic cardiac ganglia localised at fixed regions on the human heart as shown in table 1.1.

| Neural Ganglionated Plexus | Origin | Effector Site |
|-----------------------------------|-------------------------------|------------------------------|
| Left anterior coronary | Roots of Ao and PT | Left ventricle |
| Right anterior coronary | Roots of Ao and PT | Right ventricle |
| Right posterior longitudinal | Between SVC and RSPV | Posterior LA, LV, RV and RA |
| Left posterior longitudinal | Left atria | Posterior LA, LV and RV |
| Anterior atrial | Anterior left and right atria | Transverse pericardial sinus |
| Haller's Sinus | Superior left atrium | Right and left superior PVs |

Table 1.1. The location of ganglionated plexi in the human heart according to Worobiew (1925). Abbreviations: Ao, aortic root; LA, left atria; LV, left ventricle; PT, pulmonary trunk; PV, pulmonary veins; RA, right atria; RSPV, right superior pulmonary vein; RV, right ventricle; SVC, superior vena cava.

These original studies demonstrated that ganglia are present at specific localities, yet despite this basic knowledge, a better understanding and gross morphological map was still needed. Decades later in 1997, Armour *et al* determined the full extent and relationship of the human ICNS by examining the gross and microscopic anatomy using a methylene blue histological stain. The study detailed intrinsic cardiac ganglia linked via interconnecting nerves to form GPs and which were consistently present at five atrial (the superior right atrial, superior left atrial, posterior right atrial, posteromedial left atrial and posterolateral left atrial GPs) and five ventricular locations (the aortic root, the anterior descending, posterior descending, right acute marginal and obtuse marginal GPs), illustrated in figure 1.8.

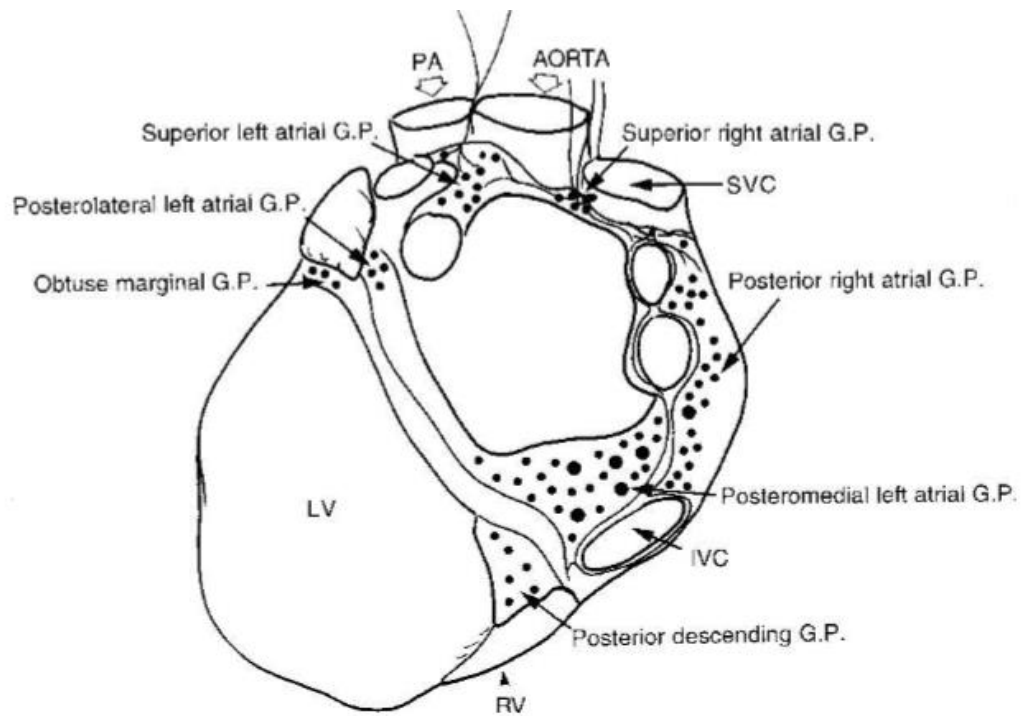


Figure 1.8. An illustration taken from Armour *et al.* (1997) of the posterior angle of the human heart. Detailed are the atrial and ventricular ganglionated plexi. Abbreviations: IVC, inferior vena cava; PA, pulmonary artery; RV, right ventricle; SVC, superior vena cava

An estimated 14,000 or more neurons reside on the human heart, subdivided into over 550 individual cardiac ganglia, approximately 450 of which are present on the atria compared to less than 100 on ventricular tissue (Armour *et al.*, 1997). The extensive distribution of the human ICNS was further characterised by Pauza *et al.* (2000). Regardless of differences in the classification and subdivision of ganglia present on specific regions of the epicardium amongst groups, the general anatomical concept displays similarities.

Neuronal cell bodies on the heart hilum are either grouped into smaller localised ganglia or gathered into larger, more dispersed clusters with ganglia sizes ranging from just a few neurons to a few hundred (Pauza *et al.*, 2000, Armour *et al.*, 1997, Singh *et al.*, 1996). More recently, fields of ganglionated plexuses present on the epicardial regions have been split into 7 defined locations (table 1.2), identifying routes of neural input and outflow from ganglia and incorporating previous anatomical findings.

As is seen in many experimental mammalian species, extrinsic cardiac nerves access the heart arterially, around the roots of the pulmonary artery (PA) and aortic root (Ao) and at the venous portion of the heart hilum around the roots of the pulmonary veins (PVs) and SVC (Batulevicius *et al.*, 2008, Saburkina *et al.*, 2010, Pauza *et al.*, 2002b, Richardson *et al.*, 2003, Batulevicius *et al.*, 2003). The majority of ganglia across species are found on the dorsal atrial regions, namely at the superior aspect of the right atrium and posteromedial aspect of the left atrium, with fewer and comparably smaller ganglia being found at ventricular regions.

| Ganglionic Subplexus | Origin | Effector site |
|-----------------------------|--|-----------------------------|
| Ventral Right Atrial | Superior interatrial sulcus | Root of SVC |
| Ventral Left Atrial | Between superior interatrial sulcus and left atrial nerve fold | Ventral inferior left atria |
| Left Dorsal | Left atrial nerve fold | Middle left atria |
| Middle Dorsal | Between right and left superior PVs | Middle left atria |
| Dorsal Right Atrial | Between SVC and RSPV | Interatrial septum |
| Left Coronary | Ao/PT | Left ventricle |
| Right coronary | Ao/PT | Right ventricle |

Table 1.2. An overview of the organisation of the ICNS according to Pauza *et al.* (2000).
Abbreviations: Ao, aorta; PT, pulmonary trunk; PV, pulmonary vein; SVC, superior vena cava.

As will be discussed later, neural modulation from the ICNS, including from ganglia around the roots of the pulmonary veins, is implicated in the generation of AF. Targeting such ganglia could therefore provide a method of modifying fibrillation. Human pulmonary veins are supplied by 3 epicardial subplexuses; the dorsal right atrial, middle dorsal and left dorsal subplexuses, with an estimated 2000 neurons residing at the base of each pulmonary vein (Vaitkevicius *et al.*, 2009). Histochemical characterisation shows a direct neural connection linking pulmonary vein ganglia to the SA node, a finding that would concur with clinical data suggesting that stimulation or ablation of such ganglia could trigger bradycardia, asystole and increased AF susceptibility (Kurotobi *et al.*, 2015). PV ganglia are therefore speculated to modulate cardiac function and factors such as heart rate variability.

Mammalian ventricles were historically believed to be devoid of ganglia and any innervation from the ICNS until Gagliardi *et al.* (1988) described ganglia of human ventricular myocardium at locations ventral to the coronary groove and around the region of the conus arteriosus (CA). The ventricles are now known to be innervated by ganglia located adjacent to the aortic root and the root of the pulmonary trunk as well as the cranial aspect of the ventral interventricular groove and a smaller one around the region of the left atrioventricular sulcus (Armour *et al.*, 1997, Pauza *et al.*, 2000). Electrical stimulation of such ganglia alters ventricular indices supporting a functional role of the ICNS (Thompson *et al.*, 2000). Understanding the anatomy of the ICNS has allowed functional studies to explore the roles of specific ganglia. Previous beliefs that GPs innervate one specific effector site are no longer supported, with studies demonstrating an interaction between several plexuses to influence cardiodynamics.

1.4.2 The intrinsic cardiac nervous system in experimental mammalian species

As study of the human intrinsic cardiac nervous system is not always viable, scientists have examined the anatomical and physiological capabilities of this network in several experimental mammalian species including but not exclusive to mice, rats, dogs, sheep and pigs (Batulevicius *et al.*, 2008, Saburkina *et al.*, 2010, Pauza *et al.*, 2002b, Richardson *et al.*, 2003, Batulevicius *et al.*, 2003). In order to develop a topographical map of the ICNS a moderated Karnovsky Roots medium (Saburkina *et al.*, 2014) that provides the visualisation of acetylcholinesterase (AChE) activity is commonly used. AChE is a

hydrolysing enzyme found within cholinergic synapses and is responsible for the breakdown of acetylcholine. It is therefore considered a pan neuronal marker.

In general, the complexity of ganglionic plexuses on the hearts of smaller mammals such as mice and rats (Batulevicius *et al.*, 2003, Rysevaite *et al.*, 2011a) is comparatively similar to that of larger mammals including sheep (Saburkina *et al.*, 2010) and pigs (Batulevicius *et al.*, 2008). There is a reduced density of innervation by neuronal cellbodies in smaller mammals when compared to larger mammals, where cardiac neuronal innervation is much more complex and more liberally distributed across the hilum of the heart. In larger mammalian species such as sheep, pigs and dogs, extrinsic mediastinal nerves access the heart at multiple sites, primarily around the root of the superior vena cava, the origin of the left azygos vein, at the roots of the pulmonary veins and in some instances between the roots of the aorta and pulmonary trunk (Saburkina *et al.*, 2010, Batulevicius *et al.*, 2008, Pauza *et al.*, 2002b). The neural sources of these nerves are the cervicothoracic and thoracic sympathetic ganglia (T2-T6) and the cervical vagus nerves, with these extracardiac nerves connecting to intrinsic cardiac ganglia and subplexus routes (Saburkina *et al.*, 2010).

The nerves accessing the arterial region of the heart hilum (i.e around the roots of the pulmonary trunk and the aorta) extend principally towards the ventricles. In contrast to humans, dogs and sheep (Saburkina *et al.*, 2010), the extracardiac nerves that access at the aorta are not visible in the pig, with porcine ventricles receiving innervation from nerves accessing the atria (Batulevicius *et al.*, 2008). Extrinsic nerves synapse with specific intrinsic ganglia, although in all species substantial variability between the location, size and number of ganglia has been noted (Saburkina *et al.*, 2014, Pauza *et al.*, 2002b).

For example, the total number of ganglia in a sheep heart is on average 769 ± 52 compared to 363 ± 52 and up to 2000 in pig and canine hearts respectively (Pauza *et al.*, 2002a). The total numbers of neurons per heart also varies between mammalian species as well as compared to the number thought to be present on the human heart (table 1.3).

| Species | Average number of intrinsic neurons per heart | Average number of intrinsic ganglia per heart | Investigators |
|-------------------|--|--|--|
| Mice | 1082 ± 160 | 19 ± 3 | (Rysevaite <i>et al.</i> , 2011a) |
| Rat | 6576 ± 317 | Not documented | (Batulevicius <i>et al.</i> , 2003) |
| Guinea Pig | 2321 ± 215 | 262 ± 28 | (Batulevicius <i>et al.</i> , 2005) |
| Rabbit | 2200 ± 262 | Unknown | (Saburkina <i>et al.</i> , 2014) |
| Dog | Estimated 80000 | Approx. 2000 | (Pauza <i>et al.</i> , 2002b), (Yuan <i>et al.</i> , 1994) |
| Sheep | Estimated 17000 | 769 ± 52 | (Saburkina <i>et al.</i> , 2010) |
| Pig | Approximately 12000 | 362 ± 52 | (Batulevicius <i>et al.</i> , 2008) |
| Human | 43000-94000 | 836 ± 76 | (Armour <i>et al.</i> , 1997), (Pauza <i>et al.</i> , 2000) |

Table 1.3. A comparison of the average numbers of intrinsic neurons and ganglia present on individual hearts from a variety of species. N.B. these numbers are taken from one study per species and numbers do vary between studies.

In all species, ganglia are linked via small interconnecting commissural nerves. The presence of such nerves reiterates the notion that ganglia and even individual neurons within ganglia can communicate with each other in order to provide autonomic feedback and ensure the heart as a whole is physiologically functioning efficiently.

The clusters of intrinsic ganglia and neurons that are located on the heart hilum link to form definitive ganglionated subplexus routes. As seen in humans, individual subplexus routes extend epicardially to specific effector sites. Even amongst larger mammals, differences in these routes have been identified with 7 subplexuses noted in canine and ovine hearts compared to 5 in pigs, because of the absence of innervation of the arterial portion of the heart hilum.

As is observed in larger mammals, the extracardiac neural sources for nerves entering the hearts of small mammals are the sympathetic ganglia at the cervicothoracic and thoracic levels of the spinal cord and the vagus nerves (Rysevaite *et al.*, 2011a). Preganglionic sympathetic axons originating from neurons in the T1-T5 spinal region project to sympathetic efferent postganglionic cardiac neurons located in the sympathetic chain and throughout the superior and middle cervical ganglia (Norris *et al.*, 1977).

In mice, rats and guinea pigs, accessing nerves from the venous portion of the heart hilum at the bifurcation of the pulmonary trunk extend epicardially and form two large ganglionated clusters; the left and right neuronal clusters. Unlike larger mammals where left and right extrinsic nerves overlap in front of the heart to access the same locations (Saburkina *et al.*, 2010), in smaller mammals, there is a complete symmetry of sympathetic and vagal inputs to the heart. In both mice and rats, right sympathetic and vagal nerves enter the heart hilum at the root of the right cranial vein and the left nerves enter at the left cranial vein where they form a GP containing two clusters. As in larger mammals, epicardial nerves extend from both clusters of ganglia to innervate specific regions of the heart, namely the right and left ventral and dorsal regions of the atria (Rysevaite *et al.*, 2011a, Batulevicius *et al.*, 2003). In comparison to humans, dogs and other larger mammals the size and ganglia are much smaller in smaller mammals. The total number of neurons found within the ICNS varies from 1000 in the mouse to 5500 in the rat (Batulevicius *et al.*, 2005, Batulevicius *et al.*, 2003, Rysevaite *et al.*, 2011a).

Despite these numerical differences, the location of such ganglia are analogous with that seen in the human making smaller mammals such as mice and rats useable as experimental cardiac research models.

In contrast to the data regarding cardiac innervation of the atria, that of the ventricles still remains relatively unknown. The pattern of innervation originates as described previously via the accessing mediastinal nerves entering arterially around the Ao and PT or venously around the roots of the PVs on the heart hilum. The numbers of ganglia present around the region of the CA varies dramatically between hearts, ranging from 11-220 or being absent (Pauziene *et al.*, 2016). A marked difference between different species is the innervation of the ventricles. Unlike in larger species where ganglia are evident around the arterial access root of the heart, smaller species appear to lack the presence of such ganglia. In rats, nerve supply to the ventricles extends from nerves accessing the heart at the roots of the PT and Ao, with the ventral surface of the ventricles in the mouse being principally supplied by the subplexus route originating from the right ventral atrial region (Batulevicius *et al.*, 2003). This is a stark contrast compared to larger species, where the left and right coronary subplexuses originating from the ganglia at the PT/Ao are responsible for the majority of ventricular innervation. These data further reiterate the increasing level of neuronal complexity with alternative models.

1.4.3 The morphology of the rabbit intrinsic cardiac nervous system

Despite the rabbit being used as a preferred small animal experimental model for some cardiac research, very little is known with regards to the full functional capability and anatomical architecture of the ICNS. To date, only one study has looked into the gross morphology of the ICNS, which identified a complex and intricate network of nerves and ganglia, primarily present on the heart hilum and around the roots of the PVs (Saburkina *et al.*, 2014). As is seen in other mammalian species, Saburkina *et al.* (2014) described intrinsic cardiac neurons grouped into clusters called GPs. Singular, thin extrinsic cardiac autonomic nerves accessed the heart via arterial and venous routes around the bifurcation of the pulmonary trunk; the hilum at the base of the heart and along the root of the superior vena cava respectively (figure 1.9). The accessing nerves synapse with neuronal cell bodies of GPs. These cell bodies are thought to reside within a single layer

over the epicardium, however, further research involving deeper tissues is warranted. Data produced by Saburkina *et al.* (2014) indicated variability between hearts in terms of the presence of certain ganglia, yet despite this occasional variability, two large clusters were identified:

- 1) The left neuronal cluster (LNC), at the roots of the left and middle PV
- 2) The right neuronal cluster (RNC), at the cranial aspect of the interatrial groove.

Overall the LNC consists of a larger number of cell bodies with approximately 1200 cells compared to approximately 700 in the RNC. These differences in number of cells per region could be indicative of the innervation pattern of specific regions of myocardium. It is estimated that approximately 2000 intrinsic cardiac neurons reside on the hilum of the rabbit heart (Saburkina *et al.*, 2014), although this number varies between animals. The majority of these neurons form ganglia ranging from 3 to over 700 cells, the largest located beneath the PVs. The majority of these neurons show ChAT-IR suggesting postganglionic cholinergic dominance. Throughout the rabbit intrinsic network, a lack of Substance P-IR cell bodies is evident, implying a reduced level of neuronal control via this specific peptide. These data are not in accord with the extensive peptidergic network found in the rat (Richardson *et al.*, 2003, Rysevaite *et al.*, 2011b). Peptidergic neuronal structures in the rabbit heart are only present in varicose fibres passing close to intrinsic neurons. The lack of investigation into the neurotransmitter profile of the rabbit ICNS is clear and if future physiological data is to be interpreted accurately, it is vital that investigation into neuronal populations is systematically undertaken.

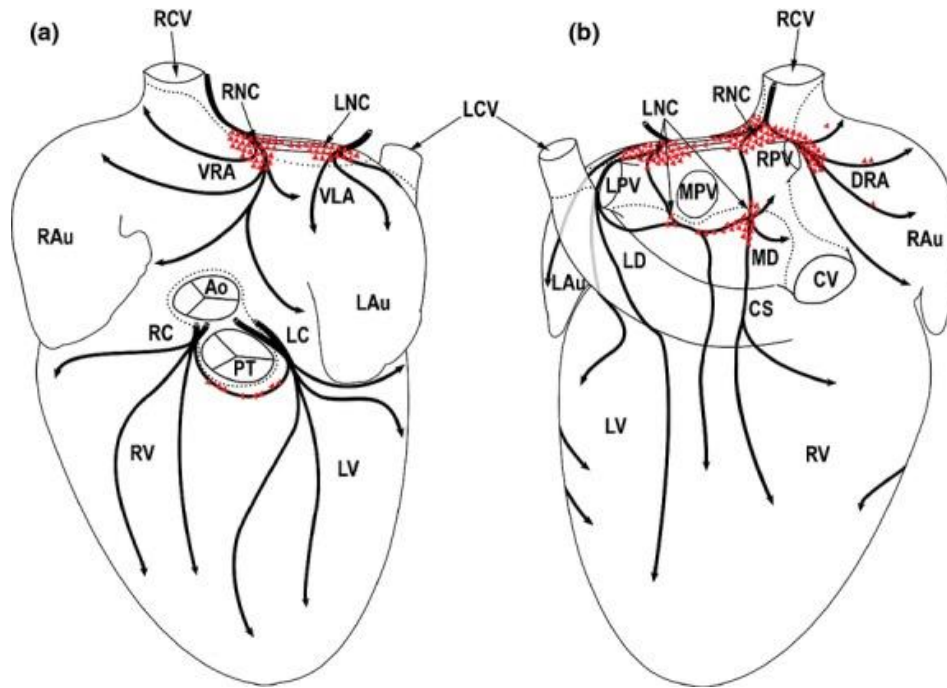


Figure 1.9. A topographical map of the rabbit ICNS taken from Saburkina *et al.*, (2014).

Clusters of intrinsic cardiac ganglia are shown in red on the heart hilum, with subplexus routes being shown with black arrowed lines. The presence of ganglia consistently around the roots of the pulmonary veins is shown. Ao, ascending aorta; CS, coronary sinus; CV, caudal vein; DRA, dorsal right atrial subplexus; ICNs, intrinsic cardiac neurons; LAu, left auricle; LC, left coronary subplexus; LCV, left cranial vein; LD, left dorsal subplexus; LNC, left neuronal cluster; LPV, left pulmonary vein; LV, left ventricle; MD, middle dorsal subplexus; MPV, middle pulmonary vein; PT, pulmonary trunk; RAu, right auricle; RC, right coronary subplexus; RCV, right cranial vein (superior caval vein); RNC, right neuronal cluster; RPV, right pulmonary vein; RV, right ventricle; VLA, ventral left atrial subplexus; VRA, ventral right atrial subplexus.

Intrinsic cardiac nerves extend from GPs on the heart epicardially to innervate the atria, interatrial septum and the ventricles (Pauza *et al.*, 2000, Saburkina *et al.*, 2014). Two subplexus routes extend from the arterial region of the hilum between the pulmonary trunk and the aorta, to effector sites on the left and right ventricles: the left and right coronary subplexuses respectively. Another five subplexuses originate from the venous region on the heart hilum around the PVs. In general, 1) the dorsal right atrial subplexus originates from either the right cranial vein (RCV) or the superior vena cava branching out to supply the SA node and the dorsal region of the right atrium. 2) The middle dorsal subplexus branching from amongst the pulmonary veins in the direction of the dorsal coronary groove with neuronal connections with 3) the left dorsal subplexus, terminating on dorsal left atrial and ventricular regions. Two ventral subplexuses also exist with the sparse nerves of 4) the ventral left atrial subplexus, beginning ventrally to the left PV and joining ganglia on the ventral left atrial region and finally, connecting the ventral right atrium to the ventro-medial region around the superior vena cava, 5) the right ventral subplexus. These defined routes noted in the rabbit are comparatively similar to those previously identified in several other mammalian species demonstrating a common trait for heterogeneous neurocardiac control by the ICNS.

The fact that subplexus neuronal projections branch onto the ventricles, emphasises the role of the ICNS in ventricular control. Anatomical study of cardiac innervation in the rabbit shows that small numbers of somata and by definition ganglionic plexuses are present on sub-atrial and ventricular regions. Nerve fibres extending from ventricular ganglia, identified at the region of the conus arteriosus extensively distribute across the ventricular epicardium and endocardium. The widespread innervation by subplexal neural routes from ventricular ganglia, which are mostly adrenergic (Pauziene *et al.*, 2016), along with the known ventricular innervation by subplexal nerves extending from atrial ganglia (Saburkina *et al.*, 2014) suggests a physiological role in the control of ventricular electrophysiology.

1.4.4 Neurochemical phenotype of the ICNS

Recently, a number of studies have partially determined the neurotransmitter content of intrinsic cardiac nerves. As mentioned previously, the ICNS was historically believed to be a simple parasympathetic relay station, investigated using histological staining for

AChE. In order to fully understand the neuronal hierarchy within the ICNS, the development of a complete neurochemical profile between species and different ganglia within the same species is vital. Several studies have now confirmed the presence of not only ChAT-IR neurons, indicative of postganglionic parasympathetic neurons, but also; TH, NPY, SP, nNOS, CGRP, VIP, galanin and protein gene product 9.5 (PGP9.5). Until recently very little research looked into the neurochemical profile of the rabbit intrinsic cardiac ganglia.

The neuromodulation of cells within cardiac ganglia is brought about by a variety of neurotransmitters and neuromodulators including those mentioned above, with such neurotransmitter expression showing possible species dependent expression. Intrinsic cardiac neurons predominantly manifest as IR for ChAT i.e cholinergic with between 60-100% of neurons ChAT-IR (Horackova *et al.*, 2000, Hoard *et al.*, 2007, Rysevaite *et al.*, 2011b, Richardson *et al.*, 2003). Smaller percentages of neurons IR for TH (and therefore adrenergic) are present within the ICNS however there is currently some debate as to the actual level of adrenergic innervation (figure 1.10). Within the ICNS there are numerous cell types including principal neurons and SIF cells (Rysevaite *et al.*, 2011b). SIF cells display very strong immunoreactivity for TH (figure 1.10) and are generally located within larger ganglia, grouped into small clusters or dispersed on the walls of the atria and ventricles (Rysevaite *et al.*, 2011b).

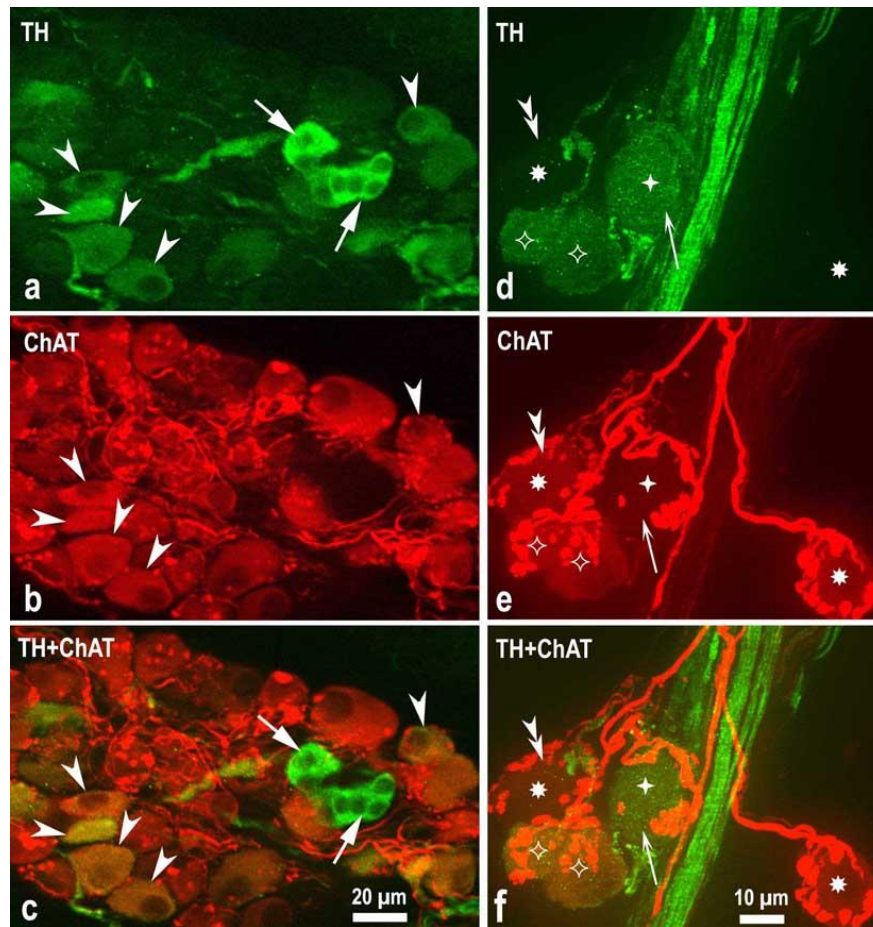


Figure 1.10. Microphotographs illustrating the presence of both cholinergic and adrenergic nerve fibres and neurons. Image taken from (Rysevaite *et al.*, 2011b) showing the predominance of ChAT-IR within the intrinsic cardiac ganglia. The ganglion imaged (a-c) also contains biphenotypic cells (arrowheads) reactive for both ChAT and TH. Small intensely fluorescent cells (white arrows) display very strong TH-IR and were smaller than TH-IR nerve cells. Baskets of ChAT positive neural terminals surround neurons (d-f). Neurons exclusively positive to TH are indicated by white crosses, positive to ChAT only by asterisks and biphenotypic cells by white diamonds.

Despite the significant cholinergic dominance within intrinsic cardiac neurons, the phenotype of the nerve fibres appears to be regionally specific. Nerves accessing the heart are predominantly adrenergic (TH-IR), with fewer ChAT-IR nerves evident. Within the intrinsic neural plexus at the level of the heart hilum, the majority of nerve fibres are cholinergic, including those interconnecting individual intrinsic ganglia. This cholinergic dominance is particularly evident within the dense meshwork of ChAT-IR nerve fibres at the SA and AV nodal regions (Richardson *et al.*, 2003, Rysevaite *et al.*, 2011b). Such dense cholinergic input to the regions around the SA and AV nodes shows a correlation with vagal nerve stimulation activating the SA node through cholinergic ganglia and interconnecting nerve fibres and causing a decrease in heart rate as a result (Randall *et al.*, 1985). In contrast to the cholinergic dominance at regions innervating the SA and AV nodes, adrenergic fibres are more abundant within the left and right coronary subplexuses (the neural supply of innervation to the ventricles) (Pauziene *et al.*, 2016).

Despite studies demonstrating ICNS-cholinergic dominance, it is also evident that there is a high level of neurochemical variability throughout the ICNS. The neuromodulator nNOS is localized in a smaller subpopulation of cells within cardiac ganglia and nerve fibres (Klimaschewski *et al.*, 1992) and commonly co-localised with ChAT-IR neurons (Richardson *et al.*, 2003, Hoover *et al.*, 2009, Herring *et al.*, 2002). This data is in accord with functional studies where it has been shown that nNOS acts as a co-transmitter either postsynaptically or presynaptically to modulate vagal effects (Herring *et al.*, 2002, Herring and Paterson, 2001, Herring *et al.*, 2001). Neurons expressing nNOS exhibit morphological differences allowing for the possibility that nNOS neurons may serve different physiological functions dependent upon location and morphology. As well as the axons from specific nNOS – IR neurons projecting to and from specific ganglia, fibres from neurons are also distributed within specific ganglia and acting as interneurons, suggesting the existence of possible crosstalk between neurons within specific ganglia (Hoover *et al.*, 2009).

The presence of populations of adrenergic neurons, shown using IR for TH, suggests the possibility of selective GP involvement in the functional effects from sympathetic activation. The overall proportion of TH-IR neurons in experimental models is under

debate with numbers varying greatly between studies (Richardson *et al.*, 2003, Hoover *et al.*, 2009, Rysevaite *et al.*, 2011b). Currently, data is not in accord regarding the presence of principal cells IR for TH with some studies reporting a complete lack of principal cells with a catecholaminergic phenotype (Richardson *et al.*, 2003) compared to others indicating catecholaminergic ganglionic neurons of larger diameter (20-40µm) (Horackova *et al.*, 2000, Slavikova *et al.*, 2003) There are also reports of small populations of biphenotypic GP neurons e.g. neurons showing both ChAT-IR and TH-IR, which represent between 10-20% of all neurons. These data are in accord with the electrophysiology of isolated intrinsic cardiac neurons responsive to the application of noradrenaline in vitro (Xu and Adams, 1993) and implies that the role of an adrenergic input to cholinergic neurons needs further investigation.

There is increasing evidence for the presence of a diverse range of neuropeptides and neurotransmitters within the ICNS, raising questions to the extent and functional roles of these chemicals. Recently markers for VIP have been identified in the ICNS. VIP, which is now known to be co-released alongside acetylcholine (Kuncova *et al.*, 2003), has been shown to be present in fibres and cells distributed across the hilum of the heart in several mammalian species (Steele *et al.*, 1994, Parsons *et al.*, 2006). As much as 100% of the nerve fibres within a ganglia can be immunoreactive for VIP (Parsons *et al.*, 2006, Hoover *et al.*, 2009, Steele *et al.*, 1996), whilst the presence of VIP in neuronal somata remains inconclusive. The origin of these fibres is unclear but it has been suggested that such fibres originate from sources extrinsic to the heart i.e. the central nervous system.

CGRP and Substance P, peptidergic nociceptive afferent cardiac substances, enable the detection of chemical signals and sensory information. In several mammalian species, CGRP and Substance P nerve fibres are most abundant adjacent to the heart hilum. (Rysevaite *et al.*, 2011b). The pattern of innervation of CGRP is similar to that seen with Substance P, although in a lesser abundance (Rysevaite *et al.*, 2011b), with studies showing that the majority of nerves positive for Substance P are also positive for CGRP. The absence of ganglia demonstrating somata that are immunoreactive for either CGRP or Substance P implies the source of these sensory nerves is external to the intrinsic cardiac ganglia and that these nerve fibres extend from extrinsic sensory ganglia and form varicosities around principal neurons within the ICNS (Li *et al.*, 2014).

A study by Herring *et al.* (2012) investigated the role of the sympathetic co-transmitter, galanin; released during high frequency sympathetic stimulation. The presence of galanin has not been studied in depth in relation to the ICNS but the galanin receptor, GalR₁ has been localised on intrinsic cholinergic neurons at the level of the SA node, suggesting a putative role in the ICNS. This is made furthermore intriguing by the ability of galanin to alter vagal control of heart rate via a presynaptic pathway involving AChE, in a way similar to NPY (Herring *et al.*, 2012).

1.5 Autonomic control of cardiac electrophysiology: from peripheral control to the intrinsic cardiac nervous system

As mentioned previously, the heart generates its mechanistic actions via an electrical conduction system. The sympathetic and parasympathetic nervous systems play a crucial role in the control of cardiac function, ultimately determining cardiac chronotropy, dromotropy, inotropy and lusitropy.

1.5.1 Peripheral neuronal inputs to the heart

Extrinsic cardiac innervation involves postganglionic sympathetic nerve fibres and vagal efferent fibres. These fibres are now known to interact with ganglia on the ICNS to modulate cardiac function, however the precise extrinsic-intrinsic interaction is currently unclear.

The interactions between sympathetic and vagal stimulation are complex, with stimulation of both branches resulting in a heart rate change different from the algebraic sum of stimulation of each branch individually (Brack *et al.* 2003). Background vagal stimulation reduces the positive chronotropic effect of sympathetic stimulation and background sympathetic stimulation enhances the negative chronotropic effect of vagal stimulation (Brack *et al.* 2003). This relationship demonstrates the complex underlying mechanisms involving sympatho-vagal interaction in the modulation of cardiac control.

Parasympathetic nerves densely innervate the atria, SA and AV nodes and conducting tissue (Randall, 1984). The cervical vagi, which contain a mixture of both afferent and efferent axons (Hoover *et al.*, 2008, Seki *et al.*, 2014) impact multiple cardiac electrical and mechanical functions when stimulated including decreased heart rate and systemic pressure (Ardell *et al.*, 2015). The vagus nerves are thought to be diverse in their roles

in cardiac control. Greater innervation of the SA node comes from the right vagus nerve in comparison to the left, with the left vagus being shown to produce a more significant change in cardiac dromotropy when compared to the right (Ardell and Randall, 1986, Brack et al. 2003), demonstrating the functional importance of vagal innervation of the heart. Furthermore, reduced activity of the vagus is a key factor in sudden cardiac death and life threatening arrhythmias, with therapy involving the stimulation of the vagus recently being translated into a novel treatment for heart failure; INOVATE-HF (Hauptman *et al.*, 2012). Despite this, the precise mechanism by which patient outcome could be improved using vagal stimulation is yet to be fully understood.

Vagus nerve stimulation (VNS) provides protection against induced VF, demonstrated by an increase in VF threshold (VFT) (Ng *et al.*, 2007). Dogma states that this protection occurs via ACh and muscarinic receptors but the discovery that this increase in VFT was maintained during muscarinic receptor blockade (Brack *et al.*, 2011) showed that the anti-fibrillatory effects were mediated via alternative mechanisms. In a recent review of the cardiac vagus nerve, three mechanisms of influencing the myocardium were described (Coote, 2013). The first mechanism involves direct interaction with sympathetic nerves, the second: an independent vagal action and third and most relevant for this work, through an interaction with neurons of the intrinsic cardiac nerve plexus.

The involvement of the peripheral autonomic nervous system in the control of certain cardiodynamics including action potential duration restitution, VFT and heart rate has been shown *in vitro* using an isolated innervated Langendorff rabbit model (Brack *et al.*, 2013), in turn providing a significant insight into mechanisms of cardiac regulation.

Similar to that seen with vagal nerve stimulation, functional heterogeneity between the left and right sympathetic paravertebral chains is well documented and quantification in the comparison between the outputs of both nerve supplies, confirms functional and electrophysiological differences in response to nerve stimulation and denervation (Winter *et al.*, 2012). Nerves arising from the left sympathetic chain influence left ventricular contractility and electrical conduction via the atrioventricular node to a greater degree than the right, whilst the nerves arising from the right hand side have a more significant effect on sinus rate via the SA node (Winter *et al.*, 2012). It is now a

possibility that the nature of such cardiac innervation could be redefined by the presence of sympathetic neurons and nerve fibres within the ICNS and that the heterogeneity evident could be due to these ganglia.

1.5.2 The role of the ICNS in cardiac electrophysiology

Investigation into the neuronal control of the heart has evolved from concentrating on the role of extrinsic nerves to include the ICNS. This includes studying both the interaction between intrinsic cardiac ganglia and peripheral nerves, as well as the solely independent influence of intrinsic cardiac ganglia on cardiac function, with a suggestion that vagal activity may even tonically inhibit the activity of the ICNS (Lo *et al.*, 2013). The precise connections between synapsing afferent postganglionic and efferent postganglionic neurons has remained somewhat elusive, yet it is possible that the ICNS acts as the final stage in the control and co-ordination of regional cardiac indices.

Classically it was thought that efferent vagal innervation was concentrated at both the sinoatrial and atrioventricular nodes (Herring and Paterson, 2009) and that the ICNS acted purely as a parasympathetic relay station. Study in larger mammals shows that ablation of the ganglia located between the superior vena cava and the aorta, results in acute elimination of the effects of vagal stimulation (Chiou *et al.*, 1997), suggesting the ICNS, which is capable of acting as an independent neuronal circuit (Murphy *et al.*, 2000), acts to co-ordinate peripheral inputs.

Previous investigation by Cheng, Powley and colleagues (Cheng *et al.*, 1999, Cheng and Powley, 2000) using anterograde fluorescent tracing protocols, demonstrated the innervation of major cardiac ganglionated plexuses by fibres originating in either the nucleus ambiguus or the dorsal motor nucleus of the vagus in the midbrain. Efferent nerves projecting from the DMV go on to innervate both principal neurons and SIF cells within intrinsic cardiac ganglia. In addition, substantial numbers of nerves originating in the nucleus ambiguus were shown to terminate on principal neurons in all ganglia investigated. Interestingly, these studies demonstrated evidence of vagal afferent neurons projecting exclusively to SIF cells from the DMV only, with Cheng and Powley suggesting the two distinct motor neuron pools derived from the nucleus ambiguus and DMV are specially functionalised in modulating vagal control of cardiac functions.

Previous beliefs surfaced around the idea that individual GPs were solely responsible for the innervation of a specific adjacent region of the heart, e.g. the right atrial GP (RAGP) to innervate and affect the SA node and the inferior vena cava-inferior left atrial GP (IVC-ILA GP) regulating the atrioventricular node (Lazzara *et al.*, 1973). It is now well documented that GPs innervate adjacent regions but can also alter cardiac outputs further afield, via intra- and interganglionic communication (Hou *et al.*, 2007a, Liao *et al.*, 2015). The co-ordination of neuronal inputs and outputs within the ICNS depends upon the nature of the afferent nerve supply, the efferent neuronal inputs received from the central / peripheral sympathetic and parasympathetic nerves and the intrinsic connections within the ICNS via local circuit neurons.

Using both electrical and chemical stimulation of ganglia and neurons, possible intra-ganglionic interactions have been identified. The principal excitatory neurotransmitter in intracardiac ganglionic synapses (Priola *et al.*, 1977) is acetylcholine, with responses evoked through nicotinic receptors (Smith, 1999). Chemical stimulation of specific GPs through an injection of nicotine to simulate activation, elicits 3 typical responses: 1) bradycardia alone, 2) tachycardia alone and 3) a biphasic response of bradycardia followed by tachycardia (Cardinal *et al.*, 2009). This functional data implies the presence of both catecholaminergic and adrenergic neurons within the same loci to produce such a biphenotypic response that corresponds with anatomical and neurochemical data previously discussed (section 1.4.4).

Whilst the role of the right atrial and inferior vena cava-inferior left atrial ganglionic plexuses in chronotropy and AV node conduction has been confirmed by multiple studies of the same group (Ardell and Randall, 1986, Cardinal *et al.*, 2009, Randall *et al.*, 2003), it is now evident that intrinsic cardiac neurons from all GPs at the atrial level of the heart are involved in some sort of cardiac regulation (figure 1.11). Selective ablation of specific ganglia within the ICNS leads to a disruption in neuronal modulation of the heart (Randall *et al.*, 2003, Randall *et al.*, 1992). Under normal circumstances, stress leads to a biphasic increase in heart rate (Randall *et al.*, 1998) with an initial rapid acceleration followed by a prolonged further increase. Original hypotheses led to the idea that such a heart rate response would be diminished or even abolished when the right atrial GP were ablated. This however is not the case, with ablation of this GP only

blunting the initial acceleration phase and being ineffective at impacting on the prolonged phase (Randall *et al.*, 1998). Multiple intrinsic ganglia therefore innervate the same region i.e. the RAGP and the posterior atrial GP (PAGP) innervating the sinoatrial node. As a result of this complex interaction between individual ganglia within the ICNS as well as with central neuronal networks (Armour, 2011), it is important that all ganglia are examined in concert in order to develop a comprehensive understanding of the functional role of the ICNS in cardiac control. This is further reiterated by anatomical data demonstrated by (Gray *et al.*, 2004) showing the complex level of interaction not only between functional cardiac regions but also between individual ganglia.

Although the functional role of the ICNS is of increasing interest as the final stage of control of cardiac function (Armour, 2004), gaps are still evident in the information and data available demonstrating the need for further study of the ICNS as a whole. All regions of the ICNS are capable of producing changes in cardiac chronotropy and dromotropy when stimulated, with the ICNS recently being attributed to preventing further damage during central neuronal dysregulation in disease and protecting the heart against the central predisposition to increased susceptibility of cardiac arrhythmias.

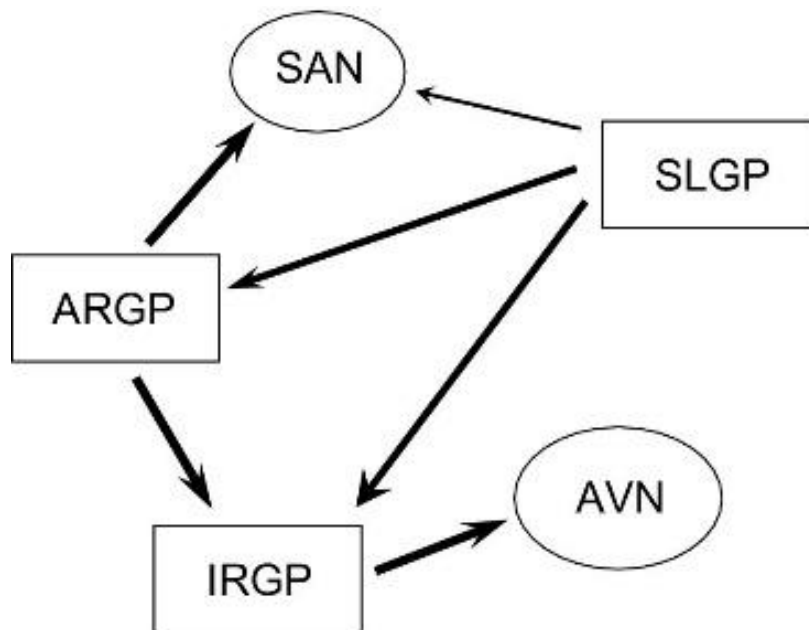


Figure 1.11. The functional interactions of the ICNS. A summary of the proposed functional interconnections between the anterior right GP (ARGP), the inferior right GP (IRGP) and the superior left GP (SLGP) during control of sinoatrial and atrioventricular nodal function in a canine model (Hou *et al.*, 2007a).

1.6 The clinical relevance of studying the autonomic nervous control of the heart

The high burden of cardiovascular disease means it is vital that potential and relevant treatments are constantly being investigated. It is well recognised that the ANS plays a role in the development of cardiac diseases including cardiac arrhythmias, MI and HF (La Rovere *et al.*, 1998, Ng, 2016, Nolan *et al.*, 1998). The potential involvement of the ICNS could provide putative links to develop prophylactic treatments.

1.6.1 Myocardial Infarction and heart failure

'Normal' cardiac function implies a certain level of co-ordination of the heart in order to provide a significant enough hydraulic power for it to fulfil its purpose of sufficiently maintaining circulation and cardiac output. Following myocardial infarction, 'normal' cardiac function begins to fail. Myocardial infarction, often caused by disease of the coronary artery, results in significant deleterious effects on cardiac function including a reduction in the number of functional myocytes in the heart and abnormal regional wall motion. To try and compensate for reduced pump efficiency and in an aim to maintain cardiac output and blood pressure (Poole-Wilson, 1993), structural and functional remodelling of the heart and also systemic remodelling occurs. Increased wall tension due to abnormal contraction of the ventricle produces local changes to the heart including significant cardiac and in particular, left ventricular hypertrophy. Pressure overload due to obstruction of outflow and reduced ventricular contraction causes increased back pressure from the left ventricle. In turn this leads to pulmonary congestion, right ventricular overload and hepatic congestion (Ng *et al.*, 1998).

In concert with and often preceding these structural and functional changes at the organ level, is a dysregulation in the cardiac autonomic control of the heart. Heart failure sees an increased level of sympathetic drive to preserve cardiac output (Triposkiadis *et al.*, 2009a) alongside a withdrawal of parasympathetic tone. The primary mechanism involved in increased sympathoexcitation is the reduced sensitivity of reflexes including the arterial baroreflex and cardiopulmonary reflexes (Zucker *et al.*, 2009) accompanied by alterations in circulating and local hormonal factors e.g. nitric oxide.

Despite these changes in autonomic function being of initial benefit in overcoming the developing effects of heart failure, they can in fact cause more harm than good and lead to an increased susceptibility to cardiac arrhythmia and sudden cardiac death.

1.6.2 The effects of myocardial infarction and heart failure on the ICNS

The tight regulation of cardiac neuronal innervation is disrupted throughout all levels following myocardial infarction, yet the extent of this dysregulation at the level of the ICNS is relatively unknown. Ischemic insult results in alterations of neurohumoral control including alterations in cardiac neuronal hierarchy and altered functional capability of the GP neurons (Huang *et al.*, 1993). It is now evident that not only does neuronal remodelling occur at the intrathoracic and central neural levels, but also within intrinsic cardiac neurons (Hopkins *et al.*, 2000). The overall effect of ischemia and the ICNS is dependent upon the location of the cell damage and modified sensory signals. Following ischemic insult, centrally derived cardiac sympathetic tone is increased to overcome the reduced cardiac output caused by a loss of adrenergic tone within damaged and dead regions of myocardium. The reflex induced increased in sympathetic drive partly due to changes in the local feedback loops within the ICNS are accompanied by a reduced central parasympathetic output to the heart (Armour, 2008) often resulting in a poor clinical outcome.

The neuronal remodelling that occurs within the ICNS during heart failure is spatially diverse and dependent upon the region of myocardium that becomes infarcted. Neuronal denervation occurs within the infarcted region as well as regions adjacent to this area (Lorentz *et al.*, 2013), with apparent hyperinnervation of the remaining functional ventricular myocardium. The ischemic insult, along with hyperinnervation of surrounding tissue results in chronic neuronal signalling and an increase in the transduction of afferent signals. This excessive activation of specific ganglia is in part, responsible for the neuronal enlargement and remodelling that has been illustrated following myocardial infarction (Nakamura *et al.*, 2016, Rajendran *et al.*, 2016).

Following compromised regional coronary artery blood supply to intrinsic cardiac neurons, pathological and degenerative changes to ganglia occur, in addition to those mentioned previously. Studies have shown that populations of neurons demonstrate

abnormal appearance compared to those seen in control conditions, with neurons becoming enlarged (Hopkins *et al.*, 2000, Rajendran *et al.*, 2016), degenerative changes to dendrites and axons and frequently with an increased presence of cytoplasmic inclusions, a resemblance of results commonly seen in patients with neuronal degeneration disorders (Singh *et al.*, 2013). The pathological changes to and hypertrophy of intrinsic cardiac neurons caused by HF (figure 1.12), leads to an increased possibility of neurons failing to reach their excitability threshold and is potentially a cause of parasympathetic withdrawal (Singh *et al.*, 2013).

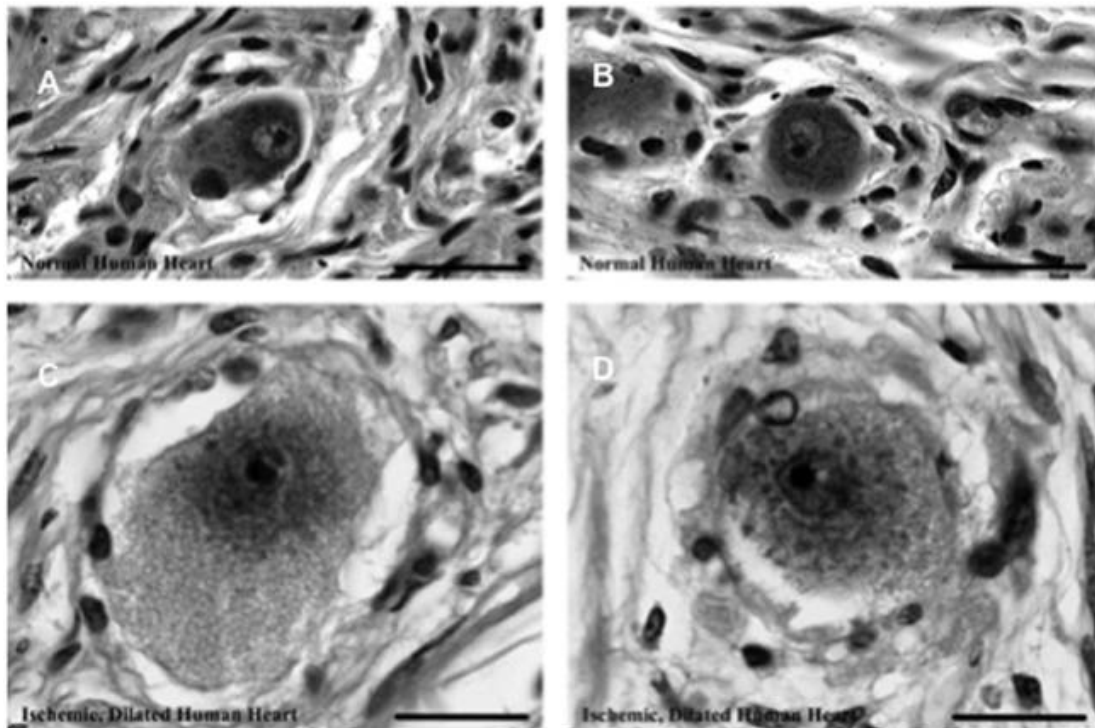


Figure 1.12. Micrographs showing examples of representative neurons taken from ganglia in human hearts. A and B show neurons of normal hearts and C and D are taken from a heart where ischemic heart failure was evident. Neurons in ischaemic human hearts demonstrate significant enlargement with evidence of oedema compared to those seen in normal hearts. Neurons examined in the failing heart also appeared much paler than those in normal hearts with a notably lighter cytoplasm. Image taken from Singh *et al.* (2013). Scale bars = 20 μ m.

MI is known to alter the ability of afferent intrinsic cardiac neurons to transduce mechanosensitive inputs. Afferent nerve activity from infarcted regions of tissue are generally reduced, whilst intracardiac local circuit neurons become hyperactive to transduce both afferent and efferent inputs from the remaining healthy myocardium (Rajendran *et al.*, 2016).

Significant phenotypic change is evident throughout the ICNS as a result of heart failure. The reorganisation and remodelling of the ICNS, demonstrated in part to be triggered by spinal cord neurons, is linked to the increased intrinsic cardiac neuronal excitability. Neuronal remodelling is thought to be most dynamic within the first 7 days following an MI and is accompanied by increased adrenergic sensitivity and increased nNOS expression within parasympathetic postganglionic intrinsic cardiac neurons (Hardwick *et al.*, 2014). Neuronal remodelling occurs primarily within regions of non-infarcted myocardium, presumably enabling the ICNS to cope with the damage caused and allowing cardiac function to be maintained. It has been hypothesised that this increase in nNOS expression has evolved in order to provide a protective purpose, reducing the initial increase in sympathetic drive and increasing the capabilities of the parasympathetic neuronal inputs (Hardwick *et al.*, 2014). Ganglia known to innervate the ventricles (including the ventral interventricular GP (VIV-GP) in the dog), with a likely connection to infarcted and damaged myocardium, show an MI-induced decrease in cholinergic phenotype (Huang *et al.*, 1993), correlating with the central withdrawal of parasympathetic tone.

Overall the functional connectivity within the ICNS is significantly altered, potentially decreasing the capacity of the neuronal control of the heart to maintain cardiac stability. One important question remains relatively unanswered: does the remodelling seen following MI affect the communication between extrinsic and intrinsic cardiac neurons therefore altering the ability of the heart to cope with reduced function and leading to further injury? Evidence so far suggests that following damage and cardiac insult, adaptation of the neurons and neuronal connections within the ICNS occurs in an attempt to maintain the sympathovagal balance (Singh *et al.*, 2013, Rajendran *et al.*, 2016), with the aim of a reduction in the destabilising factors that arise from such events.

1.6.3 Cardiac arrhythmia and the ICNS

There is increasingly strong evidence that impairment in cardiac autonomic control leads to an increased susceptibility to lethal arrhythmias (Shen and Zipes, 2014). Due to an incomplete understanding of these complex multifactorial diseases, atrial and ventricular arrhythmias and the resultant SCD have a high mortality rate to which there is currently no effective prophylactic treatment.

An increase in sympathetic drive, accompanied by a withdrawal of parasympathetic tone significantly increases the susceptibility of the heart to cardiac arrhythmias. Previous study by Verrier *et al.* (1974) demonstrated that an increase in sympathetic stimulation via the stellate ganglion increased the vulnerability of the heart to ventricular fibrillation. Conversely, it was demonstrated by Einbrodt (1859) more than 100 years ago with the aid of an inductorium (a means of delivering repetitive stimuli), that stimulation of vagal nerves can lead to an increase in the threshold to ventricular fibrillation, therefore implying a reduced susceptibility to VF.

Current treatment of autonomic dysfunction in clinical patients includes the administration of beta-blockers in order to reduce the increasing sympathetic drive. Treatment of arrhythmia with beta-blockers however is crude and is not always successful due to the lack of understanding of the underlying mechanisms resulting in arrhythmia.

Atrial fibrillation is the most common cardiac arrhythmia, with preventative measures currently including cardiac ablation. Cardiac ablation is continually evolving in the aim of improving patient outcome, however this technique is not without its limitations. The role of the intrinsic cardiac ganglia in the initiation and maintenance of atrial fibrillation has become increasingly apparent with the continual development in the understanding of the anatomy and functional capabilities of such ganglia. In spite of ablation therapy commonly being used to try and prevent recurrent AF, such therapy doesn't account for the significant level of remodelling that can occur within the nerves and ganglia of the ICNS (Yu *et al.*, 2012). Changes following ablation therapy which include increased levels of adrenergic/sympathetic neurons in atrial ganglionic plexuses and an increased density of acetylcholine positively labelled neurons (notably in the ventral left atrial

region) could alter the effects of ablation therapy and render it inadequate in controlling the initiation of AF.

The ability of the ICNS to function independently to extrinsic neural inputs provides the basis for the intrinsic cardiac ganglia playing a possible role in the initiation of arrhythmogenesis. This independent function and the ability of the ICNS to remodel also lead us to ask the question as to what the role of the ICNS is in the transplanted heart. Unfortunately to date, little is known with regards to answering the question, although the fact that the peripheral neural inputs are no longer 'connected' suggests that the ICNS is key to enable the continuing functioning of the heart.

With a widening appreciation of the role of ICNS in cardiac control, questions have emerged as to whether it is possible to utilise this system for prophylactic measures in terms of cardiac fibrillation? Liao *et al.* (2015) investigated the role of the ICNS in AF suppression and found that during low level baroreceptor BRS, ganglia in the superior right and anterior right regions of the heart showed reduced neural activity. Despite this, only two regions of ganglia were investigated and it is likely that when targeting clusters of neuronal somata, selective targeting may not be possible. It is known from the anatomical studies individual cells and ganglia are linked via thinner commissural nerves and local circuit neurons (Saburkina *et al.*, 2014, Armour, 2007). Therefore, it is possible that a direct correlation between functional neural activities is not a direct outcome of the stimulation of specific ganglia.

Despite the knowledge that hot spots of electrical activity or "nest sites" (Chang *et al.*, 2014) are primarily located around atrial/PV junctions and that selective ablation significantly reduces AF inducibility, ablation does not completely abolish AF in all cases. There is also potential to denervate the ventricles. In addition, although GP ablation substantially increases the success rate in freedom from AF, isolation of a specific GP i.e. without PVI or circumferential isolation, can lead to early recurrence of AF. Subsequent and additive PVI is often required to reduce recurrence, indicating that understanding the precise locations and functionality of individual GP are crucial in helping to develop a prophylactic treatment. Despite ablation becoming increasingly common, it is not without its pitfalls. This was demonstrated by both Osman *et al.* (2010), who reported that patients undergoing pulmonary vein isolation for treatment of AF have gone on to

develop VF and by He *et al.* (2013) who showed that ablation of GPs during PVI in patients with structural heart disease actually increase the likelihood of lethal cardiac arrhythmias. This therefore emphasises further the multiple underlying mechanisms of cardiac arrhythmia that still require investigation and the complexity of treating such diseases.

The majority of studies to date have concentrated on the role of the ICNS in atrial fibrillation, with limited study investigating the influence of the ICNS on ventricular electrophysiological properties (He *et al.*, 2013). Activation of GPs by electrical stimulation results in a prolongation of the ventricular effective refractory period (ERP) i.e. the period following on from a previous action potential where there is an insufficient magnitude of depolarisation to reach the threshold for the generation of the following action potential. However, GP ablation in the same mammalian model in healthy hearts also leads to a prolongation in ventricular ERP, with no corresponding change in the VFT (He *et al.*, 2013). In comparison, GP ablation of corresponding regions of ganglia in a model of acute myocardial infarction significantly promotes ventricular arrhythmia, presumably as a result of the reduction of intrinsic parasympathetic neurons adding to the central reduction in parasympathetic tone.

1.7 Aims

The ICNS, a heterogeneous collection of nerves and ganglionic plexuses is the final stage of cardiac neuronal control, playing a vital role in the regulation of cardiac chronotropy and dromotropy. Despite this and the fact that the rabbit is commonly used to investigate cardiac electrophysiology, there is very little knowledge regarding the anatomy and topography of the ICNS and also the functional role of the intrinsic cardiac ganglia in cardiac control in the rabbit.

The aims and objectives of this study were therefore:

1) To characterise the coronary artery ligation model of heart failure in the rabbit

This model, which was first developed and characterised by Pye *et al.* (1996), has recently been used to assess the autonomic modulation on various aspects of cardiac electrophysiology in a rabbit heart failure model. To ensure the development of comparable degrees of heart failure and dysfunction similar to those described previously, this coronary artery model of heart failure will firstly be characterised.

2) To examine the anatomy and topography of the ICNS and investigate the effects of heart failure

The main aim of this study will be to determine the gross anatomy of the rabbit ICNS. To date, only one study has investigated the anatomy of the rabbit ICNS (Saburkina *et al.*, 2014). To ensure further investigation done within this project correlated with previous publication and therefore advancing current knowledge of the ICNS, histological staining for acetylcholinesterase in a pressure distended whole heart preparation will be carried out.

It is proposed that the ICNS undergoes structural and functional remodelling as a result of myocardial infarction and heart failure (Rajendran *et al.*, 2016, Nakamura *et al.*, 2016). Furthermore, dysregulation of the central autonomic nervous system is known to occur following MI. Despite this, the information regarding the involvement of the ICNS in HF is lacking. The next stage of this study will therefore be to extend pre-existing knowledge of the rabbit ICNS by

investigating the effects of MI and HF on the gross anatomy of the rabbit ICNS in the coronary artery ligation model of heart failure initially characterised.

Current literature demonstrates that the ICNS is not merely a parasympathetic relay station with numerous studies in several mammalian species showing that not only sympathetic and parasympathetic neurons are present, but the ICNS also consists of numerous other neuromodulators and neuropeptides. In order to understand the functional role of the ICNS in cardiac control, a more comprehensive and detailed map of the intricate nerve plexuses is needed. The next part of this study will therefore be to characterize the neurochemical phenotype of the rabbit ICNS using immunofluorescent markers for ChAT, TH and nNOS.

3) To determine the functional role of the ICNS

The final part of this study will be designed to determine the functional role of the rabbit ICNS in controlling specific cardiac indices including heart rate and atrioventricular conduction and in particular, investigating alterations in such control during HF.

Chapter 2: Materials and Methods

2.1 Experimental animals

Adult male New Zealand white rabbits were used throughout this study. Animals used solely for terminal procedures were obtained directly from Envigo (Harlan Laboratories, Loughborough, UK) whilst those used as part of the study of heart failure in a rabbit model were originally obtained from Charles River Laboratories, France and housed in environmentally controlled rooms (lights on from 06:00 to 18:00) within the University of Leicester Preclinical Research Facility (PRF) for a minimum of three weeks prior to surgery (figure 2.1). Food and water were provided *ad libitum*.

2.1.1 Ethical statement

All procedures were undertaken in accordance with the UK Animals (Scientific Procedures) Act 1985 and the Guide for the Care of Use of Laboratory Animals Published by the US National Institutes of Health (NIH Publication No. 85-23, revised 1985) and the European Union directive on the protection of animals for scientific research (2010/63/EU). Local ethics approval was obtained from the University of Leicester animal welfare review board (AWERB) under the Home Office Project Licence PPL 70/8501.

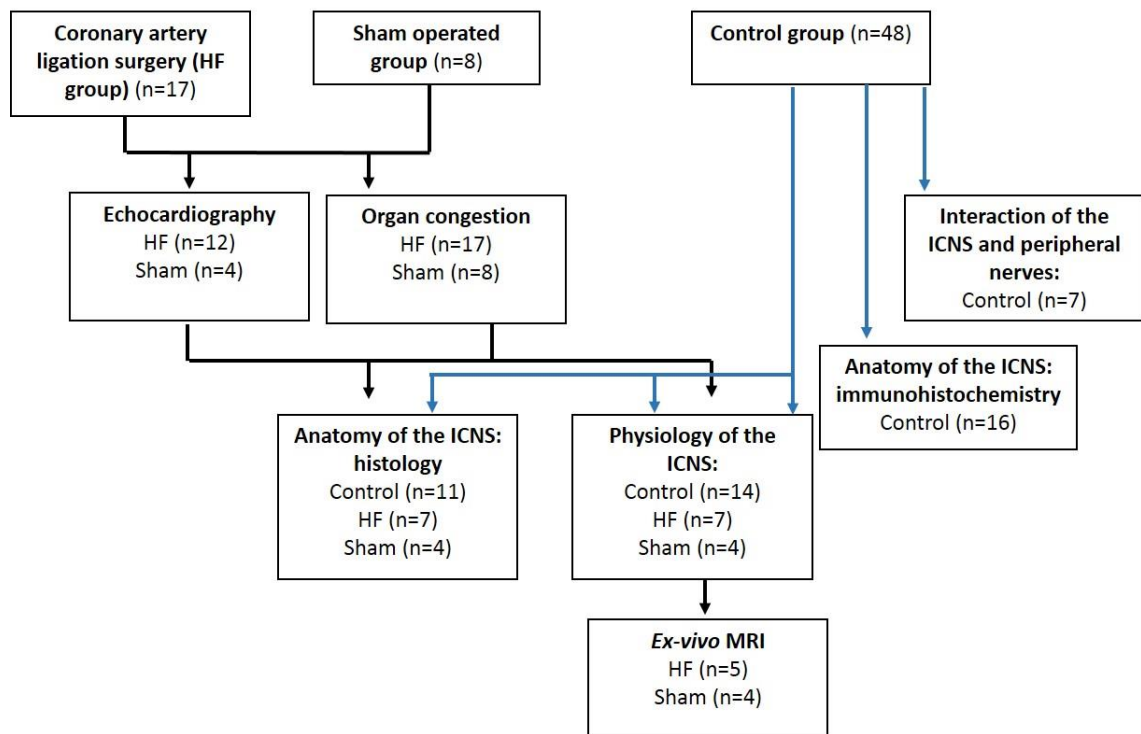


Figure 2.1. The process of experimental protocols used within this study. The order in which various parts of this study were conducted are illustrated in the above flow chart. Animals used in the control group, where no surgery was carried out prior to terminal experiments, are illustrated with blue lines. Those used in the HF and sham operated groups are illustrated using black lines.

2.2 Coronary artery ligation in the rabbit: a model of heart failure

Numerous animal models have been used previously with the aim of studying heart failure (Dawson *et al.*, 2008, Hardwick *et al.*, 2014, Ng *et al.*, 1998, Olivas *et al.*, 2016) all resulting in varying final states of heart failure. With the aim of providing a potential insight into clinical heart failure in humans and determining the level of involvement of the intrinsic cardiac nervous system, a suitable and comparable animal model is necessary. A rabbit coronary artery ligation model of heart failure previously established in the Department of Cardiology, Glasgow Royal Infirmary by Dr Maurice Pye and Prof. Stuart Cobbe (Pye *et al.*, 1996) and further developed and modified by Prof G Andre Ng and Dr S H Chin (Chin, 2017) in the department of Cardiovascular Sciences, University of Leicester was used throughout this study.

The animal model described in this study induces heart failure through the induction of an apical infarct. The use of complete coronary artery ligation to induce myocardial infarction results in a variable loss of myocardial function dependent upon the initial size of the infarct. Accompanied by the development of left ventricular dilatation, increased filling pressures and a reduction in systolic function (Pye *et al.*, 1996, Sabbah *et al.*, 1991), characteristics echoing those seen in heart failure patients (Cohn *et al.*, 2000) make this model clinically relevant.

Adult male New Zealand White rabbits (2.9-3.5kg) were premedicated with Ketaset (ketamine, 0.15ml/kg, Fort Dodge, UK), Sedator (medetomidine hydrochloride, 0.2 ml/kg, Dechra, UK) and Torbugesic (butorphanol, 0.01 ml/kg, Fort Dodge, UK) via subcutaneous injection. Following stable sedation, the marginal ear vein was cannulated with a 1F-butterfly infusion needle and 5ml saline administered. Perioperative prophylactic antibiotics were given via subcutaneous injection of Baytril (enrofloxacin, 0.2ml/kg) along with an injection of Metacam (meloxicam, 0.2mg/kg, 2mg/ml) subcutaneously for the relief of pain and inflammation. The rabbit was ventilated with 4% oxygen through a small animal mask whilst the anterior chest wall was shaved and further sedation was administered subcutaneously containing Ketaset (ketamine, 75µl/kg, Fort Dodge, UK) and Sedator (medetomidine hydrochloride, 0.1ml/kg, Dechra, UK).

Rabbits were intubated with a size 2.5 – 3.0 cuffed endotracheal tube inserted over a soft-tipped wire introducer with the aid of a laryngoscope. The endotracheal tube was inserted to approximately 14 – 15cm to the level of the incisors and the cuff fully inflated to secure the tube and prevent movement and irritation of the trachea. Following transfer of the rabbit to the operating table the endotracheal tube was connected to a Harvard small animal ventilator. The rabbit was ventilated with a mixture of oxygen and 1-2% isoflurane at a tidal volume of 15ml at a rate of 30 breaths per minute.

Body temperature was monitored and maintained throughout by means of a thermostatically controlled heated table. Heart rate and levels of oxygen saturation were monitored using an animal pulse oximeter and heart rate monitor attached to the ear of the rabbit.

The shaved anterior region of the chest wall was cleaned and sterilised using a chlorhexidine scrub, followed by a final wash with iodine solution. Following local analgesia injection (Marcain, (bupivacaine), 0.1ml at each injection site) at ribs 2-5, a left thoracotomy was performed through the 4th intercostal space. Upon entry of the pleural cavity, the deflated left lung was gently retracted and the cavity packed with swabs to prevent damage to the lungs. An incision was made into the pericardium at the level of AV groove and extended laterally. Following excision, a clamp was placed at the apical region of the pericardium and used to evert the heart. A tie placed through the apex of the ventricle for control of heart manipulation. The large marginal branch of the left circumflex coronary artery which supplies the left ventricular apex and the majority of the left ventricular free wall was identified and ligated using 4/0 Monocryl suture. Ligation was carried out midway between the left atrial appendage and the cardiac apex, resulting in a homogeneous transmural apical infarct occupying approximately 30- 40% of the LV myocardium. Following occlusion, a period of 20 minutes observation was carried out in order to monitor the occurrence of cardiac arrhythmia. Ventricular fibrillation occurred in 4% of cases at approximately 16 minutes following coronary artery occlusion and defibrillation undertaken with a 3J DC shock via small sterilised paddles applied directly on the epicardial surface of the heart.

Once the animal was deemed to be stable, the collapsed left lung was reinflated by occluding the ventilator outlet and the chest closed using 3 x 1/0 interrupted sutures in

the deep muscle layer bringing the ribs together. The remaining muscle layers were closed using 3/0 interrupted sutures and finally 6/0 Vicryl suture was used to close the skin with a continuous subcuticular mattress suture. A total of 20ml saline was administered intravenously throughout surgery with 5ml being given at approximately 30 minute intervals to replace perioperative fluid losses.

Following wound closure, reversal of sedation was achieved using a subcutaneous injection of Atipam (atipamezole hydrochloride, 0.2ml/kg) along with the subcutaneous administration of analgesia; 0.05mg/kg Vetergesic (buprenorphine hydrochloride 0.3mg/ml). Once stable, the animals were allowed to recover in a warm, clean, quiet environment with necessary monitoring for any signs of distress.

The animals were monitored closely for a 5 days with a further 4 doses (morning and evening) of Vetergesic being given subcutaneously alongside morning oral doses of Metacam for 5 days following surgery. Heart failure was allowed to develop and the animals allowed to recover for up to 8 weeks, at which time terminal experimental studies were carried out.

Sham operated animals underwent comparable surgery including thoracotomy, pericardium incision and the same manipulation of the heart to position a tie at the apex of the left ventricle but without the ligation of the coronary artery. These animals were used as controls for age and weight and the overall impact of the surgical procedure however without the development of coronary ligation induced heart failure. As with the animals that underwent coronary artery ligation, the terminal experimental studies were carried out 8 weeks following recovery.

2.2.1 Echocardiography and ex-vivo MRI

Ultrasound and echocardiography were first recorded in the 1950's, with Swedish investigators Edler and Hertz (1954) being the first to record cardiac structure movements. Echocardiography is commonly used in clinical situations as a method for non-invasive imaging and as a diagnostic tool to assess the structural, functional and haemodynamic status of the cardiovascular system. Using echocardiography, clinicians are able to assess sizes of cardiac chambers, evaluate the performance of the ventricles and to investigate valvular function. Data produced using echocardiography can provide

a reasonable visual estimate of ventricular performance and using two-dimensional measurements of left ventricular end diastolic and systolic volume, left ventricular ejection fraction (LVEF) can be calculated. LVEF is commonly used as an indicator of heart failure with an ejection fraction of 40% or less indicating moderate or severe ventricular dysfunction. The correlation between heart failure development and a depression in ejection fraction has previously been characterised in a rabbit model using coronary artery ligation, with a close association between the infarct size and level of ventricular dysfunction being shown (Pye *et al.*, 1996).

Echocardiography was performed by Pott Pongpaupattanakul, 8 weeks following coronary ligation surgery, prior to sacrifice for the experimental studies, in order to assess *in vivo* cardiac performance. This was performed using a L125 array 50nm probe with a Philips HDI 5000 sonograph. Animals were pre-medicated with Ketaset (ketamine, 0.15ml/kg, Fort Dodge, UK), Sedator (medetomidine hydrochloride, 0.2 ml/kg, Dechra, UK) and Torbugesic (butorphanol, 0.01 ml/kg, Fort Dodge, UK) via subcutaneous injection. The anterior chest wall was shaved to provide a reasonable echo window and the animal positioned in a left lateral position. Ejection fraction (EF) was assessed using a parasternal short axis view at a level just below the tips of the mitral valve leaflets. The endocardial border was outlined in frames captured during the end-diastolic and end-systolic phases and the enclosed area automatically computed.

EF was calculated as:

$$EF = \text{stroke volume (end-diastolic volume (EDV) – end systolic volume (ESV))} / EDV$$

This calculation was based upon the assumption that the LV is ellipsoid and therefore the estimation of the area calculated was translated into the ejection fraction; a measurement of volume.

2.2.2 MRI and image processing

Ex-vivo MRI was carried out at the state-of-the-art University of Leicester Central Research Facility by Dr Michael Kelly, Preclinical Imaging Manager. Hearts were retrieved following Langendorff perfusion following on from terminal functional experimental procedures and were fixed and stored in PFA (4%) until imaging. Prior to imaging, intact excised rabbit hearts were placed in test tubes filled with a proton-free

fluid, Fomblin-Y (Sigma-Aldrich), which has no MRI signal and is susceptibility matched to tissue.

MRI scanning was performed on a 9.4T Agilent scanner (Agilent Technologies, Santa Clara, CA, USA) with a 310mm bore diameter and 6cm inner-diameter gradient coil (1000 mT/m maximum gradient strength), interfaced with a DirectDrive Console. Radio frequency transmission and reception was achieved with a 40mm millipede transmit/receive RF coil. The rabbit hearts were positioned at the isocenter of the magnet and located with fast gradient echo scan. 3D gradient echo shimming of first and second order shims was performed over the entire heart and shim quality was confirmed using point resolved spectroscopy (PRESS) of the water peak. T2-weighted images were acquired using a fast spin echo (FSE) sequence with TR/TE = 3000/40ms, 30 x 30mm field of view (256 x 256 matrix), 36 x 1mm coronal slices and 3 signal averages (scan duration = 9mins 42sec). The resultant images were used to generate 2D slice montage representations of the heart.

For accurate quantification of scar volume, T1-weighted images were acquired using a 3-dimensional magnetization prepared rapid gradient-echo (MP-RAGE) sequence with TR/TE = 6.5/3.3ms, 40 x 30 x 30mm field of view (256 x 192 x 192 matrix) and 2 signal averages (scan duration = 57mins 39sec). Scar volume was calculated using semi-automated ROI analysis tools in 3D Slicer (<http://www.slicer.org>).

2.2.3 Organ retrieval and cardiac remodelling

It has been demonstrated both in humans and animals that following myocardial infarction and heart failure, significant structural changes occur to the heart. Myocardial infarction leads to contractile dysfunction and a reduced ability of the heart to sufficiently pump blood around the body. In order to compensate for this functional incapacitation, the heart undergoes structural remodelling including a significant degree of cardiac hypertrophy. Contractile dysfunction due to ventricular failure also leads to an increase in back-pressure within the heart as well as the proximal organs resulting in pulmonary and hepatic congestion.

Following the 8 week recovery period and at the time of sacrifice during the terminal experiment, both the left and right lungs and the liver were excised from the animals.

Excess blood and fluid was blotted from the organs and the wet weights were measured. After each experiment in which the heart was used for the isolated Langendorff perfused method (see section 2.6), the heart was also blotted of excess fluid and the wet weight measured. Hearts were weighed free from excess fat and pulmonary vessels. All organs were then dried in an oven heated to 50°C and the weight measured every 7 days until the weight of the organ plateaued and the dry weight was obtained.

2.3 The anatomy and morphology of the rabbit intrinsic cardiac nervous system

The following protocols describe the methods used to further describe the anatomy and morphology of the rabbit intrinsic cardiac nervous system and to understand what happens to these ganglia during heart disease.

2.3.1 Non-sectioned pressure-distended heart preparation

In order to expose the heart for histological examination, animals were pre-medicated with Ketaset (ketamine, 0.15ml/kg, Fort Dodge, UK), Sedator (medetomidine hydrochloride, 0.2 ml/kg, Dechra, UK) and Torbugesic (butorphanol, 0.01 ml/kg, Fort Dodge, UK) via subcutaneous injection. Following stable sedation demonstrated by the absence of corneal and pedal reflexes, the marginal ear vein was cannulated with an IF-butterfly infusion needle to administer intravenous pre-operative Heparin (1000 IU, Wockhardt UK Ltd, UK) in order to prevent coagulation and thromboembolism. Euthanasia was established via the same cannular using Pentoject (pentobarbitone sodium, 111ml/kg, Animalcare Ltd, UK). Death was confirmed with the absence of respiration as well as the cessation of circulation.

A midline incision was made through the skin, at the level of the clavicle and extended mid-way down the abdomen to expose the chest. A second horizontal incision extending the width of the torso was then made at the base of the chest (approximately at the level of the 10th rib) to allow for the retraction of the skin, allowing exposure of the ribcage and the superior forelimbs. A bilateral thoracotomy was performed and the anterior portion of the ribcage removed to expose the lungs and the heart. The pericardium was cut for access to the heart. The caudal vena cava (vena cava caudalis; 'inferior vena cava') was identified and cannulated and tied off using silk sutures (Size 0, Harvard Apparatus, UK) therefore providing perfusate to the right side of the heart. A

small incision was subsequently made at the superior edge of the left atrium and a cannula inserted and secured, thereby perfusing the left side of the heart. To prevent the continuation of blood flow from the body and head back into the heart, the right cranial vena cava (vena cava cranialis dextra; superior vena cava) and left cranial vein (vena cava cranialis sinistra) were clamped.

The heart was perfused using ice-cold (4 °C) phosphate buffered saline (PBS; pH 7.4) via both the left atrial and caudal vena cava cannulae until flushed of blood, followed by *in situ* pressure inflation of the atria and ventricles with a 20% gelatin solution. Once the gelatin solution was set, the heart was removed from the chest and immediately immersed into ice cold PBS. Any remaining excessive pulmonary vessels, mediastinal fat and pericardium were then dissected away from the heart using a Leica M80 microscope at x5 magnification (Leica Microsystems, Germany). Following dissection, the heart was fixed using a solution of 4% paraformaldehyde (PFA) in 0.01M phosphate buffer (PB, pH7.4, 4°C, 30 minutes) and to increase tissue permeability, immersed into a hyaluronidase solution in PBS (0.5mg/100ml, 4°C, 60 minutes).

To provide insight into the location of nerve fibres and plexuses within the intrinsic cardiac nervous system, the heart was histochemically stained for AChE (Saburkina *et al.*, 2014). Hearts were immersed in a modified medium first described by Karnovsky and Roots (1964) and containing the following (in mM): Sodium Acetate 60, Acetylthiocholine Iodide 2, Sodium Citrate 15, CuSO₄ 3, K₃Fe(CN)₆ 0.5, iso-OMPA 0.5, Triton-X 1% and Hyaluronidase 0.5mg/100ml to further increase tissue permeability, for 4 hours at 4°C (pH5.6). Following staining, whole hearts were post-fixed for long-term storage until imaging, using PFA (4%).

2.3.2 Whole mount preparation

Neural structures were visualised from flattened atrial tissue prepared from pressure distended whole hearts; a technique commonly used in similar study's by Danius Pauza's group in Lithuania (Saburkina *et al.*, 2014, Batulevicius *et al.*, 2008, Rysevaite *et al.*, 2011a). The whole heart was illuminated by a fibre optic light guide system (KL1500 LCD, Schott UK) and imaged using a Leica M80 microscope at magnifications ranging from x0.75 to x6 (Leica Microsystems, Germany).

The heart was microdissected into several atrial regions (figure 2.2): the precise anatomy of each being dependent upon the topography of the intrinsic cardiac neurons demonstrated by the AChE staining. In general these regions were;

1. The heart hilum (the region above the base of the heart around the pulmonary vessels)
2. The region at the base of the pulmonary trunk and aortic root known as the conus arteriosus
3. The region ventral to the roots of the left, middle and right pulmonary veins
4. The root of the right cranial vein

Each section was removed from adjacent tissue and placed into glass dishes. Sections were dehydrated through a series of graded ethanol solutions (70%, 90% and 100%) and then submerged in xylene (Fisher, UK) for between 30 mins and 2 hours dependent upon the thickness of the section. Each section was flattened, mounted onto a microscope slide using Histomount mounting medium (National Diagnostics, UK) and covered with a thin coverslip for microscopic analysis.

2.3.3 Brightfield microscopy

Cardiac sections were examined and imaged using an upright microscope (Axio, Carl Zeiss Microscopy, UK) and images were captured using a digital camera (AxioCam, Carl Zeiss Microscopy, UK). Stereoscopic examination was achieved between x20-40 magnification by transiently directing fibre optic illuminators at the section of tissue. Overall topography was constructed offline and image examination and analysis was completed using ZEN software (Carl Zeiss Microscopy, UK) and Image J 1.49v software. Neurons were identified, counted and individually measured using x20 magnification images with Image J 1.49v software.

2.4 Whole-mount preparation for immunohistochemistry

To investigate the neurotransmitter profile of the ICNS, hearts were examined immunohistochemically using antibodies specific for various neuronal indicators following brief staining for AChE (a method adapted from those previously used by Pauza's and Grubb's groups (Pauza *et al.*, 2014, Fryatt *et al.*, 2009). Whole hearts were perfused with PBS (pH7.4) as mentioned previously for whole heart non-sectioned preparations and pressure inflated *in situ* using a 20% gelatin solution. Hearts were removed from the chest, placed into ice-cold PBS (pH 7.4, 4 °C) and the surrounding pericardium, mediastinal fat and excessive pulmonary vessels were removed. As described above, hearts were prefixed using 4% PFA (0.01M PB, pH7.4) for 30 minutes, followed by incubation in Hyaluronidase solution (PBS, 0.5mg/100ml) for 60 minutes. In order to optimally visualise and dissect the atrial regions where intrinsic cardiac neurons reside, whole hearts were pre-treated in the modified Karnovsky-Roots medium (described above) for a maximum of 30 minutes to provide a faint stain and guide micro-dissection.

The heart was dissected into several atrial regions as described previously (section 2.3.2). Each section was removed from the adjacent tissue and pinned flat into a custom made silicone based dissecting dish to allow for subsequent washes (3 x 10 minutes) in ice cold PB (0.01M, pH.4, 4°C). In order to prevent non-specific protein binding, each section was incubated in a blocking buffer of 0.01M PB containing 10% normal horse serum (Vector Laboratories, UK) and 0.5% Triton X-100 (Sigma Aldrich, UK) for 30

minutes. Preparations were then incubated in a double primary antibody mixture (Table 2.1) (antibodies were diluted in a solution of 0.01M PB containing 10% normal horse serum and 0.5% Triton X-100) for 48 hours at 4°C in a humidity chamber.

After a washing step (3 x 10 minute washes in 0.01M PB), all sections were incubated in the correct combination of corresponding secondary antibodies (Table 2.1) for 2 hours in a dark humid chamber at room temperature. After a final wash step (3 x 10 minute washes in 0.01M PB) each atrial region was mounted using Vectashield Hardset Mounting Medium (Vector Laboratories), covered with a coverslip and sealed using clear nail varnish ready for microscopic analysis.

2.4.1 Fluorescence microscopy

Immunohistochemically stained neural structures were visualised and imaged using an upright fluorescence microscope (Axio, Carl Zeiss Microscopy, UK). Images were captured using a digital camera (Axiocam, Carl Zeiss Microscopy, UK). Stereoscopic examination was achieved between x10-40 magnification. Sections were examined using 2 fluorescence filters; 1) Alexa Fluor 594- conjugated antibodies absorb light at around 591nm and fluoresce with light emitted with a peak around 614nm and 2) FITC (fluorescein isothiocyanate) conjugated antibodies which absorb light maximally at 492nm and fluoresce maximally at 520nm. Overall topography was constructed offline and image examination and analysis was completed using ZEN software (Carl Zeiss Microscopy, UK) and Image J 1.49v software.

2.5 Statistical analysis

Data analysis was performed using both Origin Lab software (v.2015; OriginLab, Northampton, MA, USA) and GraphPad Prism 6 software (v6.04, GraphPad, CA, USA). Data are expressed as mean \pm standard error of mean (SEM). Statistical analysis was performed using an unpaired t test with differences being considered statistically significant at $P < 0.05$.

| Primary Antibody | Host Species | Dilution | Catalogue Number and Supplier |
|----------------------------|--------------|----------|-------------------------------|
| ChAT | Goat | 1:100 | AB144P Merck Millipore |
| TH | Mouse | 1:2000 | 22941 Immunostar |
| nNOS | Mouse | 1:300 | SC-5302 Santa Cruz |
| nNOS | Sheep | 1:1000 | Gift from Prof Trevor Batten |
| Secondary Antibody | | | |
| Anti-goat (AlexaFluor594) | Donkey | 1:300 | Jackson Immunoresearch |
| Anti-goat (FITC) | Donkey | 1:100 | Jackson Immunoresearch |
| Anti-mouse (AlexaFluor594) | Donkey | 1:300 | Jackson Immunoresearch |
| Anti-mouse (FITC) | Donkey | 1:100 | Jackson Immunoresearch |

Table 2.1. Antibodies used during whole-mount immunohistochemistry.

2.6 Investigating the role of the intrinsic cardiac nervous system on cardiac electrophysiology

2.6.1 Isolation of the Langendorff heart preparation

Animals from each of the three groups (control, heart failure and sham-operated) were pre-medicated with Ketaset, Sedator and Torbugesic as in section 2.3.1 with a subcutaneous injection. Following stable sedation demonstrated by the absence of corneal and pedal reflexes, the marginal ear vein was cannulated with an IF- butterfly infusion needle to administer intravenous pre-operative Heparin (1000 IU, Wockhardt UK Ltd, UK). Euthanasia was established via the same cannular using Pentoject (pentobarbitone sodium, 111ml/kg, Animalcare Ltd, UK). Death was confirmed with the absence of respiration as well as the cessation of circulation.

After confirmation of death in accordance with the UK ASPA 1985, the thoracic cavity was opened with a transverse incision anterior to the diaphragm. Lateral incisions were made along both sides of the rib cage and the chest wall was removed in order to expose the mediastinal contents. The heart was rapidly removed following incisions made at the great vessels, both lung hila and the inferior vena cava, with care being taken to ensure the length of the ascending aorta was adequate for cannulating. The excised heart was submerged into ice cold Tyrode's solution containing (in mM): Na⁺ 138.0; K⁺ 4.0; Ca²⁺ 1.8; Mg²⁺ 1.0; HCO₃⁻ 24.0; H₂PO₄⁻ 0.4; Cl⁻ 124.0; Glucose 11.0, (chilled to 4°C) to reduce metabolic rate.

The heart was cannulated onto the perfusion apparatus via the ascending aorta and held in place using a bulldog clip. The aorta was secured using silk sutures in order to ensure the retrograde free flow of perfusate and the bulldog clip removed. A small incision was made in the pulmonary artery to allow the flow of coronary effluent following the resumption of contraction.

2.6.2 Langendorff perfusion

Hearts were retrogradely perfused through the ascending aorta in conditions of constant flow Langendorff mode (40 ml/min) using a Gilson Minipulse 3 peristaltic pump (Anachem, Luton, UK), with care being taken to ensure no air bubbles were present within the perfusion system to prevent embolism in the heart. Retrograde perfusion of

the heart involves the forced closing of the aortic valve, redirecting perfusate into the coronary vasculature and supplying cardiac tissue with the necessary components to continue to function (figure 2.3). Tyrode's solution was maintained at a constant temperature of 37°C and pH of 7.4 by continuous bubbling with Carbogen [95% O₂/5% CO₂] and the use of water baths for heating the solution as well as continuously supplying warm water to the water jackets in the perfusion glassware to reduce loss of heat.

A 1mm ID, 2mm OD polypropylene catheter (Porlex, Kent, UK) was inserted through the left ventricular apex for Thebesian venous effluent drainage. Left intraventricular pressure was monitored using a fluid-filled latex balloon inserted and secured at the left atrial appendage and connected with a 3F cannula to a pressure transducer (MLT0380/D ADInstruments Ltd, UK). LV end diastolic pressure was maintained between 0 and 5 mmHg. Aortic perfusion pressure was recorded with a second solid state pressure transducer connected in series to the aortic cannula. Both pressure transducers were calibrated using a sphygmomanometer to a 2-point calibration prior to each experiment.

Prior to further instrumentation, the dissection of any remaining pulmonary vessels, mediastinal fat or pericardium was completed down to the plane at which the intrinsic cardiac ganglia are known to be located. A pair of platinum pacing hook electrodes (Grass Instruments, USA) were inserted into the right atrial appendage for constant atrial pacing. Monophasic action potentials (MAPs) were measured at regions of the apex and base using contact electrodes (73-0150, Harvard Apparatus, Kent, UK) applied to the epicardial surface of the heart and the signal was amplified using a custom made DC-coupled high input impedance differential amplifier (Joint Biomedical Workshop, University of Leicester, UK).

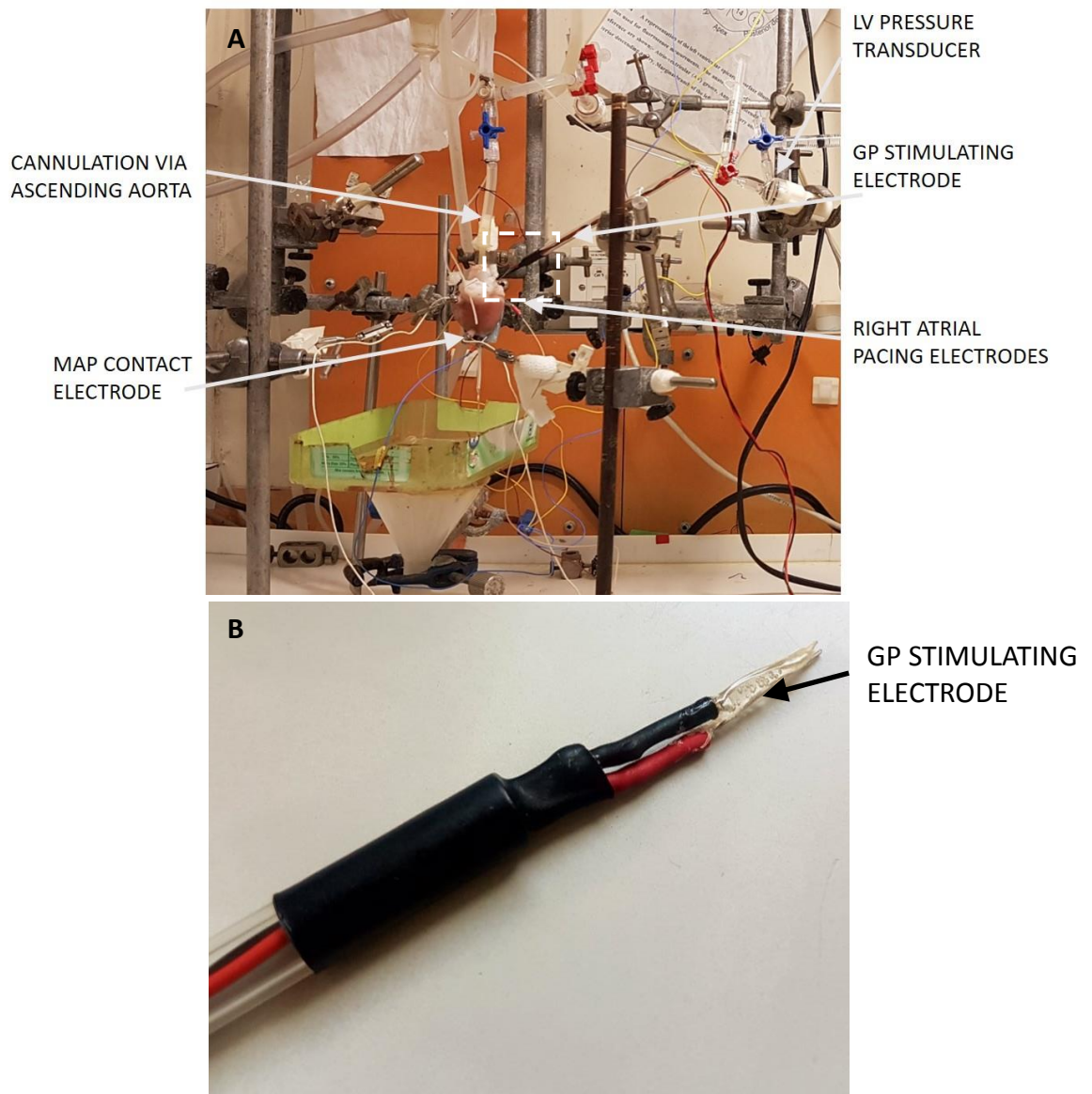


Figure 2.3. Langendorff heart preparation for investigating the role of the ICNS on cardiac electrophysiology. Electrical stimulation of intrinsic cardiac ganglia was performed on Langendorff perfused hearts **(A)** using a custom made bipolar silver electrode with an insulated tip **(B)**.

2.6.3 Electrical stimulation of intrinsic cardiac ganglionic plexuses

Stimulation of epicardial ganglia was performed at four sites (figure 2.4). These sites were determined using the topographical map previously produced by Saburkina *et al.* (2014) along with the data represented in chapter 4 and included; 1) the left neuronal complex (LNC), 2) the right neuronal complex (RNC), 3) the right atrial ganglia region (RAGP) and 4) the region between the middle pulmonary veins and the caudal vena cava (vena cava caudialis; 'inferior vena cava') (PVCV).

Regions known to contain intrinsic cardiac neurons were stimulated epicardially using a custom-made bipolar silver electrode (0.5mm diameter, Advent research materials, Oxford, UK). The tip of the electrode was insulated in order to prevent unwanted electrical spread and to allow a more precise application of stimulation (figure 2.3).

Electrical stimulation of intrinsic cardiac ganglia was achieved using a single-channel constant voltage square-pulse stimulator (SD9, Grass Instruments, Astro-Med), connected in sequence to a constant current stimulator (DS7A Constant Current Stimulator, Digitimer Ltd, UK). The stimulating electrode was placed on the heart at locations known to contain ganglia and the cardiac pacing threshold was determined at 3V, 4Hz and with a 0.1ms pulse (He *et al.* 2013), in an attempt to limit the stimulus to neuronal somata. Responses of intrinsic cardiac ganglia to electrical stimulation both during sinus rhythm and during constant atrial pacing were recorded between 10 and 50Hz stimulation frequencies at 50% of the cardiac pacing threshold. When the change in HR reached a plateau or the change in atrioventricular delay stabilised, stimulation was stopped and the heart was allowed to recover to baseline.

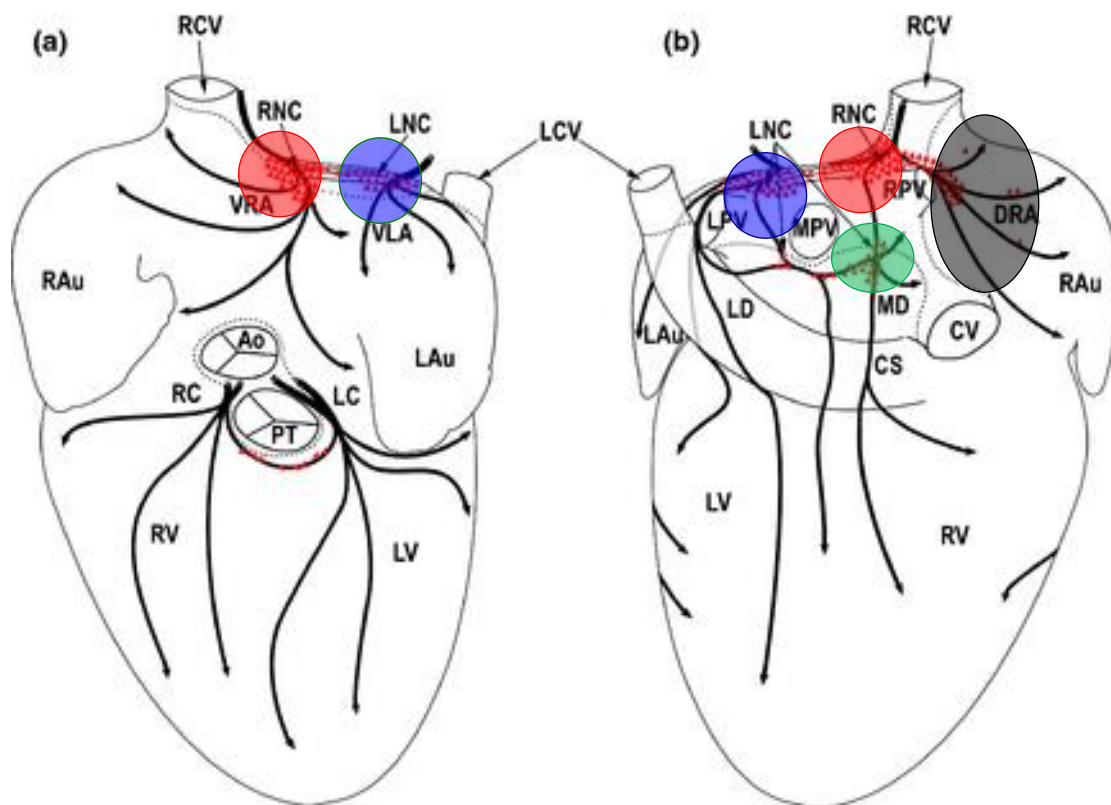


Figure 2.4: Ventral (a) and dorsal (b) view of the heart indicating the regions for electrical stimulation of the intrinsic cardiac ganglia. Abbreviations: Ao, aorta; CS, coronary sinus; CV, caudal vein; DRA, dorsal right atrial subplexus; LAu, left auricle; LC, left coronary subplexus; LCV, left cranial vein; LD, left dorsal subplexus; LNC, left neuronal cluster; LPV, left pulmonary vein; LV, left ventricle; MD, middle dorsal subplexus; MPV, middle pulmonary vein; PT; pulmonary trunk; RAu, right auricle; RC, right coronary subplexus; RCV, right cranial vein; RNC, right neuronal cluster; RPV, right pulmonary vein; RV, right ventricle; VLA, ventral left atrial subplexus; VRA, ventral right atrial subplexus.

2.6.3.1 Experimental Protocols for the electrical stimulation of intrinsic cardiac ganglia

2.6.3.2 Cardiac Constant Pacing

A pair of platinum pacing electrodes positioned at the right atrial appendage were used to pace the heart at a predetermined and fixed heart rate. Throughout all experiments, hearts were paced at a cycle length of 240ms resulting in a constant heart rate of 250bpm. A cycle length of 240ms was chosen to account for the maximum anticipated increase in heart rate (HR) observed during preliminary investigations. The diastolic pacing threshold was determined prior to each protocol and then doubled to ensure constant cardiac pacing was maintained throughout.

2.6.4 Pharmacological agents

At each site of the ICNS investigated, the cardiac response in control conditions (normal Tyrode's solution only) was determined at 20Hz and at half the cardiac pacing threshold. To determine which specific autonomic receptors were involved in the cardiac responses produced by electrical stimulation, protocols were repeated in the presence of the muscarinic (M2) receptor antagonist, atropine (0.1 μ M (Ng *et al.*, 2001)), a β -adrenergic receptor blocker, metoprolol (1.8 μ M (Ng *et al.*, 2001)) and the autonomic ganglionic blocker, hexamethonium (0.5 mM (Brack *et al.*, 2011, Winter *et al.*, 2012)). Each pharmacological blocker was dissolved into a small volume of Tyrode's solution. The preparation was perfused with each agent for 5-10 minutes until a stable response was recorded. Measurements were recorded during sinus rhythm and constant atrial pacing followed by a period of washout using normal Tyrode's solution. Washout periods of a minimum of 15 minutes ensured the confirmation that any diminished/eliminated response was a result of the application of a pharmacological agent.

2.6.5 Signal measurements and data analysis

Functional parameters including LV pressure, perfusion pressure and ECG were recorded using a Powerlab 16 channel system (ADInstruments Ltd, Chalgrove, UK) and digitised at 2kHz using LabChart software version 7 and Scope software (ADInstruments Ltd). Data analysis was completed using LabChart software version 8. MAP duration was measured at 90% repolarisation (MAPD₉₀) using custom-made NewMap analysis software (Dr F Burton, University of Glasgow). To determine atrioventricular delay

during constant atrial pacing data parameters were measured from averaged data using Scope software (ADInstruments Ltd). Atrioventricular delay, measured in milliseconds, was calculated as the time from the cardiac pacing stimuli to the activation of the ventricular electrical signal. HR and LV pressure were measured and calculated from an average of 10 cardiac cycles during baseline and subsequently during the steady state response.

2.7 Investigating the interaction between the rabbit ICNS and peripheral autonomic nerves

As part of the continuing research aimed at determining the overall role and involvement of the intrinsic cardiac nervous system in the control and influence of specific cardiodynamics, it is crucial not only to understand what the ICNS is capable of independent of peripheral neuronal input, but also how it can modulate extrinsic neuronal stimulation. A number of preliminary experiments were conducted in order to evaluate this interaction using a modified version of a novel neurocardiological preparation; the dual innervated Langendorff perfused heart preparation. This preparation, originally developed and reported in 2001 (Ng *et al.*, 2001) allows the study of the effects of either direct sympathetic or vagal nerve stimulation on whole heart electrophysiology and mechanical performance without the confounding effects of circulating hormones and *in vivo* reflexes.

2.7.1 Isolated innervated heart preparation

Animals were pre-medicated with Ketaset, Sedator and Torbugesic as in section 2.3.1 via subcutaneous injection. Following stable sedation demonstrated by the absence of corneal and pedal reflexes, the marginal ear vein was cannulated with an IF- butterfly infusion needle for the intravenous introduction of pre-operative Heparin (1000 IU, Wockhardt UK Ltd, UK) and for the injection of Propofol (10mg/ml, Zoetis, London,UK) for the maintenance of surgical anaesthesia . The limbs of the animal were restrained and the anterior torso of the rabbit was shaved from the mandible to the abdomen. The depth of anaesthesia and pain threshold was tested by checking the pedal reflex and a subsequent cervical midline incision was made. The superficial muscle layers were dissected and the trachea identified. Further blunt dissection allowed the trachea to be isolated and the cannulated with a 5mm diameter plastic tube and secured using silk suture (size 0-0, Harvard apparatus, UK) to enable ventilation. Ventilation was sustained with positive pressure via a small animal ventilator (Harvard Apparatus Ltd, Edenbridge, Kent, UK; 50-60 breaths/min). Following ventilation, general anaesthesia was maintained with bolus injections of Propofol, taking care not to affect cardiac function. The common carotid arteries were identified and isolated using silk sutures with

attention being given to avoid damaging the delicate vagus nerves lying in close proximity.

The midline incision was extended along the chest wall and subsequent lateral incisions at the level of the lower intercostal spaces resulted in exposure of the ribcage. Further incision was made through the pectoral muscles down to the surgical plane just below the pectoralis minor. Prior to the ligation of the larger subclavian vessels, a bolus injection of Propofol was administered to eliminate pain. Ties were placed around the neurovascular bundle which was ligated and the plane between the pectoral muscles and the portion of the sternocleidomastoid muscles nearest the clavicular head was identified and the jugular vein also ligated. Although the intercostal vascular bundle which is located below the trapezius muscle only has a small artery running through it, numerous smaller vessels are present and if left can result in an unwanted decrease in perfusion pressure and hence was also ligated.

Just prior to sacrifice of the animal both vagus nerves were carefully dissected in order to prevent damage during the final portion of surgery. Both vagi were identified, running parallel to the previously tied carotid arteries. The sternomastoid muscles were cut and separated from the underlying tissues. The vagus nerves were isolated from the carotid arteries using careful blunt dissection and in a way that the nerves were not directly handled with forceps. The nerves were then transected proximally as close to the nodose ganglia as possible.

Another 1000IU heparin was administered prior to animal sacrifice, which was accomplished with an overdose of pentobarbitone sodium (111ml/kg, Animalcare Ltd, UK). Ventilation was stopped and the tracheal tube removed. The thoracic cavity was exposed and the anterior portion of the ribcage removed. Immediately after exposure of the mediastinal contents, ice-cold Tyrode was applied and the thorax packed with ice in order to lower the temperature of the preparation and therefore the metabolic rate. The internal mammary vessels were isolated as proximally as possible and tied off with suture. The lower thoracic portion of the descending aorta was isolated from surrounding tissues and cannulated level with the apex of the heart with a custom made flanged 5mm diameter plastic tube. The distal portion of the descending aorta was also

closed to minimise blood loss. An incision was made in the pericardium which was peeled back from the heart. The pulmonary artery was cut to allow the flow of perfusate out of the right of the heart. A dual vertebral osteotomy was performed at the level of the 12th thoracic vertebra and the 1st cervical vertebra and the preparation was dissected from surrounding tissue and excised from the neck to the thorax, ready for mounting. All of the preceding steps were taken rapidly in the aim of reducing ischemia.

2.7.2 Perfusion and mounting of the preparation

Prior to surgery the perfusion system was primed with Tyrode's solution as outlined for preparation of the Langendorff system described in section 2.6.2. The preparation was transferred to the perfusion rig and positioned on the mounting platform and pinned in place. The descending aorta cannula was connected to the perfusion system and being careful to ensure no air bubbles were present the preparation was perfused in conditions of constant flow (100ml/min). Both lungs were tied off and removed to prevent air being sucked back into the heart and following a very short period of perfusion with warm Tyrode's solution, the heart would begin to beat steadily.

Perfusion flow rate was reduced to 50% and the preparation cooled down in order to reduce heart rate and contraction and therefore damage during the insertion of a catheter and balloon into the left ventricle. A small incision was made in the left atrium and a 1mm ID, 2mm OD polypropylene catheter (Porlex, Kent, UK) was inserted through the LV apex for Thebesian venous effluent drainage. Left intraventricular pressure was monitored using a fluid-filled latex balloon connected with a 3F cannula to a pressure transducer (MLT0380/D ADInstruments Ltd, UK). LV end diastolic pressure was maintained between 0 and 5 mmHg. The flow rate was returned to 100ml/min and aortic perfusion pressure was recorded with a second solid state pressure transducer connected in series to the aortic cannula. Both pressure transducers were calibrated using a sphygmomanometer to a 2-point calibration prior to each experiment (figure 2.5C).

Once the preparation had stabilised, further dissection was done in order to gain access to the region of the heart where the ganglia of the right neuronal cluster are known to

reside. The pericardium was dissected and as much of the ribcage removed as possible without interrupting the ties previously made around the internal mammary vessels. The thymus was bluntly dissected from any remaining pericardium and carefully pinned back to expose the ascending aorta and pulmonary artery.

The pulmonary artery was fully transected and the left and right branches dissected away from the region at the base of the heart known as the heart hilum. The right cranial vena cava was identified and a loose loop of suture placed around it in order to ease manipulation during the placement of the stimulation electrode. All manipulation and blunt dissection was done with great care to avoid damage to any peripheral neural connections and intrinsic cardiac ganglia (figure 2.5).

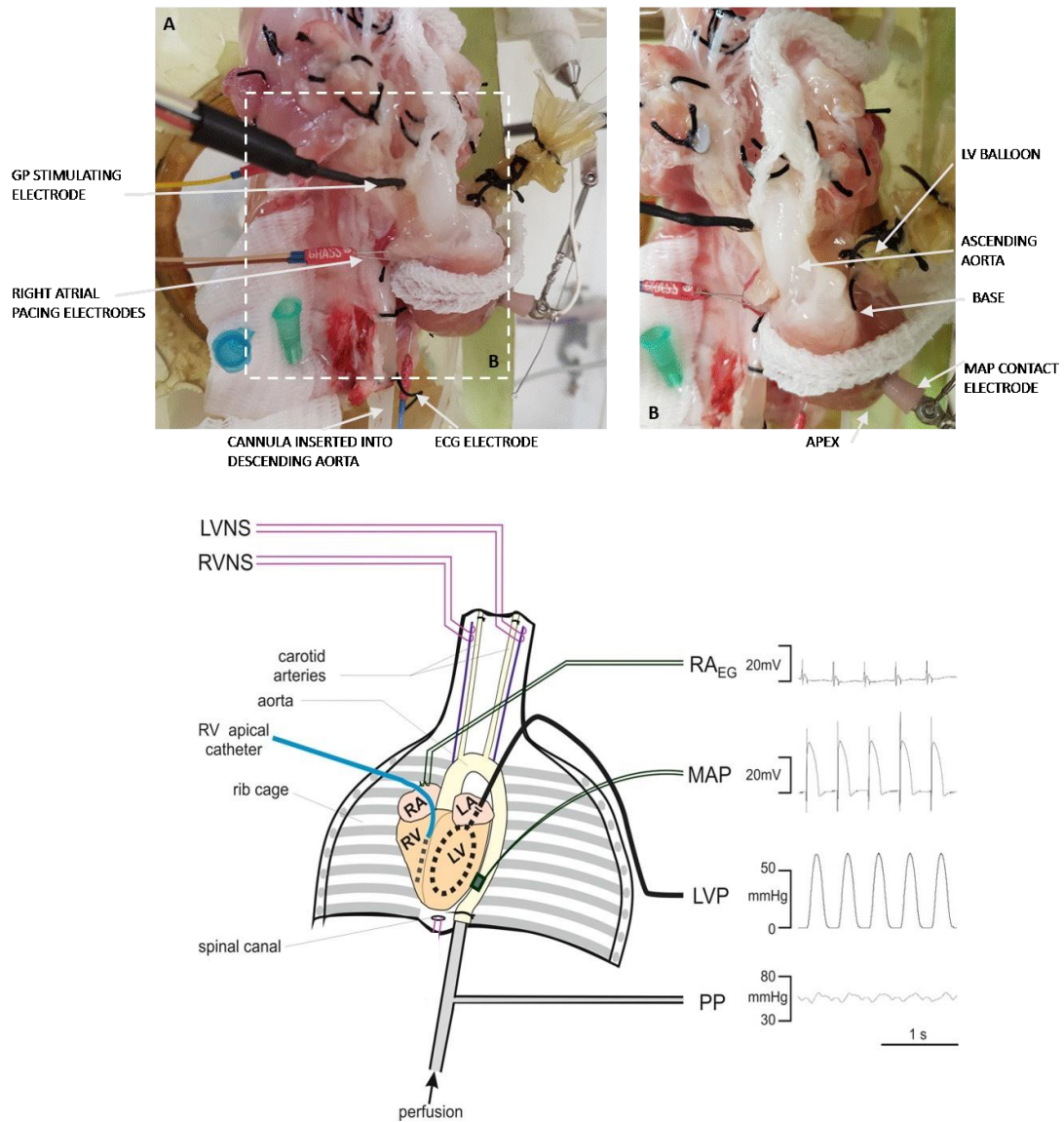


Figure 2.5. Representation (adapted from Ng et al 2001) of the dual innervated heart preparation. A illustrates the innervated preparation with GP stimulating electrode position with the boxed region representing the area magnified in B. The innervated preparation was used to investigate the interaction between the intrinsic cardiac nervous system and the vagus nerves along with sample experimental recordings of LVP, PP and monophasic action potentials (C). Abbreviations: LA, left atrium; LV, left ventricle; RA, right atrium; RV, right ventricle; LVNS, left vagus nerve stimulation; RA_{EG}, right atrial electrogram; MAP, monophasic action potential; LVP, left ventricular pressure; PP, aortic perfusion pressure).

2.7.3 Signal measurements

As was described previously (section 2.6.3.2) a pair of platinum pacing electrodes (Grass Instruments, USA) were inserted into the right atrial appendage for constant atrial pacing. Monophasic action potentials were measured at regions of the apex and base (see figure 2.5) using contact electrodes. Similar to the Langendorff preparation, functional parameters including LV pressure, perfusion pressure and ECG were recorded using a Powerlab 16 channel system (ADInstruments Ltd, Chalgrove, UK) and digitised at 2kHz using LabChart software version 7 and Scope software (ADInstruments Ltd).

2.7.4 Nerve stimulation protocols

Vagus nerves were stimulated individually (left or right) using a custom made silver chloride bipolar electrode. To determine the stimulation parameters to be used during each experiment, the effect of nerve stimulation was examined using a 2ms pulse width at a fixed frequency (5Hz) and a changing stimulus strength. HR reductions were recorded at incremental voltages ranging from 1V to 20V. The stimulus strength that produced a heart rate equivalent to 80% of the maximal response was used throughout the study. Using this stimulus strength (voltage), the effect of changing the frequency of stimulation was examined at 5, 7 and 10Hz. The frequency that produced a reduction in HR to between 70 and 100bpm was used throughout the remainder of the study. When the reduction in HR during vagal stimulation reached a stable plateau, stimulation was stopped and the heart rate allowed to return to baseline.

2.7.4.1 Electrical stimulation protocols

Regions within the right neuronal cluster of the ICNS were stimulated epicardially using a custom-made bipolar silver electrode (0.5mm diameter, Advent research materials, Oxford, UK). Electrical stimulation was achieved using the previously described method (section 2.6.3.1). In brief, the cardiac pacing threshold at each site was determined at 3V, 4Hz and with a 0.1ms pulse. At sites where changes in HR were recorded, the ganglia were stimulated at 50% of the cardiac pacing threshold at a frequency of 20Hz.

At each site responses to the following were recorded:

- 1) Vagus nerve stimulation
- 2) RNC GP electrical stimulation (GP ES)
- 3) GP ES followed by vagus nerve stimulation
- 4) Vagus nerve stimulation followed by GP ES

Stimulation was applied until a stable plateaued response was observed before either ending stimulation or adding the second level of stimulation.

2.7.5 Data analysis

As in section 2.6.5, data analysis was completed using LabChart software version 8. MAP duration was measured at 90% repolarisation (MAPD₉₀) using custom-made NewMap analysis software (Dr F Burton, University of Glasgow). To determine atrioventricular delay during constant atrial pacing data parameters were measured from averaged data using Scope software (ADInstruments Ltd). HR and LV pressure were measured and calculated from an average of 10 cardiac cycles during baseline and subsequently during the steady state response.

Chapter 3: Heart failure in the rabbit

3.1 Introduction

Myocardial infarction leads to contractile dysfunction and a reduced ability of the heart to sufficiently pump blood around the body. Clinically, the majority of pathology that occurs with heart failure, develops as a result of the body trying to counteract the functional incapacitation. Various animal models have been used to investigate the effect of heart failure including models of chronic pressure overload (Beaumont *et al.*, 2016), acute myocardial infarction (He *et al.*, 2013) and chronic myocardial infarction (Ng *et al.*, 1998). It has been shown that following surgically induced MI in an animal model, significant structural changes occur to the heart including remodelling and a significant degree of cardiac hypertrophy (Ng *et al.*, 1998). Contractile dysfunction due to ventricular failure resulted in an increase in back-pressure within the heart along with an increase in left ventricular end-diastolic pressure. The increased back pressure in the pulmonary vasculature resulted in pulmonary congestion and oedema; well recognised features in the clinical syndrome of heart failure.

The most commonly used diagnostic tool for assessing the severity and progression of heart failure is echocardiography and the measurement of ejection fraction. Clinically, an ejection fraction of between 50 and 75% is characterised as normal and an ejection fraction of lower than 50% is an early sign of heart failure and left ventricular dysfunction.

In order to determine the mechanisms responsible for this decline in cardiac function, the use of animal models is imperative and of particular importance are models of cardiac failure due to MI. It has been demonstrated that ligation of the coronary artery in the rabbit results in both local and systemic changes, similar to those seen clinically in heart failure (Ng *et al.*, 1998, Pye *et al.*, 1996).

Therefore, the aim of this chapter was to validate the animal model of coronary artery ligation in order to ensure comparable data with previous work and to ensure differences in parameters examined at a later date were solely due to the development of heart failure and not due to the surgical procedure itself.

3.2 Results

3.2.1 Cardiac Dysfunction

Coronary artery ligation surgery, where the large marginal branch of the left circumflex coronary artery was ligated (see chapter 2 section 2.2) was performed in a total of 17 animals. In addition, sham surgical procedures (where similar surgery was conducted minus the ligation of the left coronary artery) were done in a total of 8 animals. Approximately 8 weeks following surgery, *in vivo* echocardiography was performed using a parasternal short axis view in order to compute ejection fraction. Due to the availability of technical support, echocardiography was only completed in a total of 12 animals from the heart failure group compared to 4 rabbits in the sham operated group. Echocardiographic data demonstrated evidence of significant cardiac dysfunction with the measured ejection fraction being significantly lower in rabbits in the heart failure group compared to the sham operated group, 34.9 ± 1.1 vs 62.2 ± 1.2 respectively (see table 3.1).

3.2.2 Organ congestion

Clinically, heart failure originating from damage to the left ventricle, can lead to pulmonary congestion and oedema, with instances of right ventricular failure and therefore hepatic congestion developing. For that reason and to determine the systemic effects of myocardial infarction and heart failure, liver and lung weights were measured in a total of 25 rabbits (17 from the HF group and 8 from the sham operated group). Both liver and lung weights from rabbits in the heart failure group were significantly increased in comparison to sham operated animals (table 3.1).

The wet weights of hearts from both the HF and sham operated groups were compared. Dry heart weights were unavailable during this study due to the hearts being used for imaging studies. Hearts from the HF group were significantly enlarged when compared to those from the sham operated group (14.6 ± 0.2 vs 11.9 ± 0.1 , $p < 0.0001$). When the weights of the RV and LV free wall were examined between both groups, there was evidence of a significant increase in weight in the HF group (table 3.1). Increased lung weights when corrected for overall body weight and compared with EF showed a negatively correlated trend, however this was not significant. In comparison, liver

weights (when corrected for body weight) were significantly correlated with ejection fraction, as were corrected RV weights (figures 3.1A, B and C) further reiterating the presence of ventricular hypertrophy. Clinically, RV dysfunction leads to hepatic congestion. To determine whether this was the case in the rabbit model, right ventricular weights and liver weights were examined. When values were corrected for body weight, RV and liver weights were significantly correlated (figure 3.1D) ($r = 0.60$, $p < 0.01$).

| | Heart Failure | Sham | P Value |
|------------------------------------|----------------------|--------------|----------------|
| | n = 17 | n = 8 | |
| Body weight (kg) | 3.8 ± 0.1 | 3.9 ± 0.1 | Ns |
| Ejection fraction (%) | 34.9 ± 1.1 | 62.2 ± 1.2 | <0.0001 |
| Liver wet weight (g) | 116.3 ± 3.6 | 94.4 ± 4.5 | 0.0013 |
| Lung wet weight (g) | 25.4 ± 1.9 | 20.0 ± 1.6 | 0.0429 |
| Heart wet weight (g) | 14.6 ± 0.2 | 11.9 ± 0.1 | <0.0001 |
| RA wet weight (g) | 0.6 ± 0.0 | 0.4 ± 0.0 | 0.0004 |
| LA wet weight (g) | 0.8 ± 0.1 | 0.4 ± 0.0 | 0.0079 |
| Ventricle wet weight (g) | 11.4 ± 0.2 | 9.8 ± 0.1 | 0.0003 |
| RV free wall wet weight (g) | 2.7 ± 0.2 | 2.3 ± 0.1 | 0.0412 |
| LV free wall wet weight (g) | 5.2 ± 0.2 | 4.3 ± 0.0 | 0.0146 |
| Liver dry weight (g) | 32.5 ± 0.8 | 27.4 ± 1.8 | 0.0068 |
| Lung dry weight (g) | 2.7 ± 0.1 | 2.6 ± 0.2 | ns |

Table 3.1: Comparison of organ weights and *in vivo* functional parameters (ejection fraction) between animals from the heart failure and sham operated groups. Data is presented as mean ± SEM, statistical significance determined using unpaired t-test. (LA – left atrium, LV-left ventricle, RA- right atrium, RV-right ventricle).

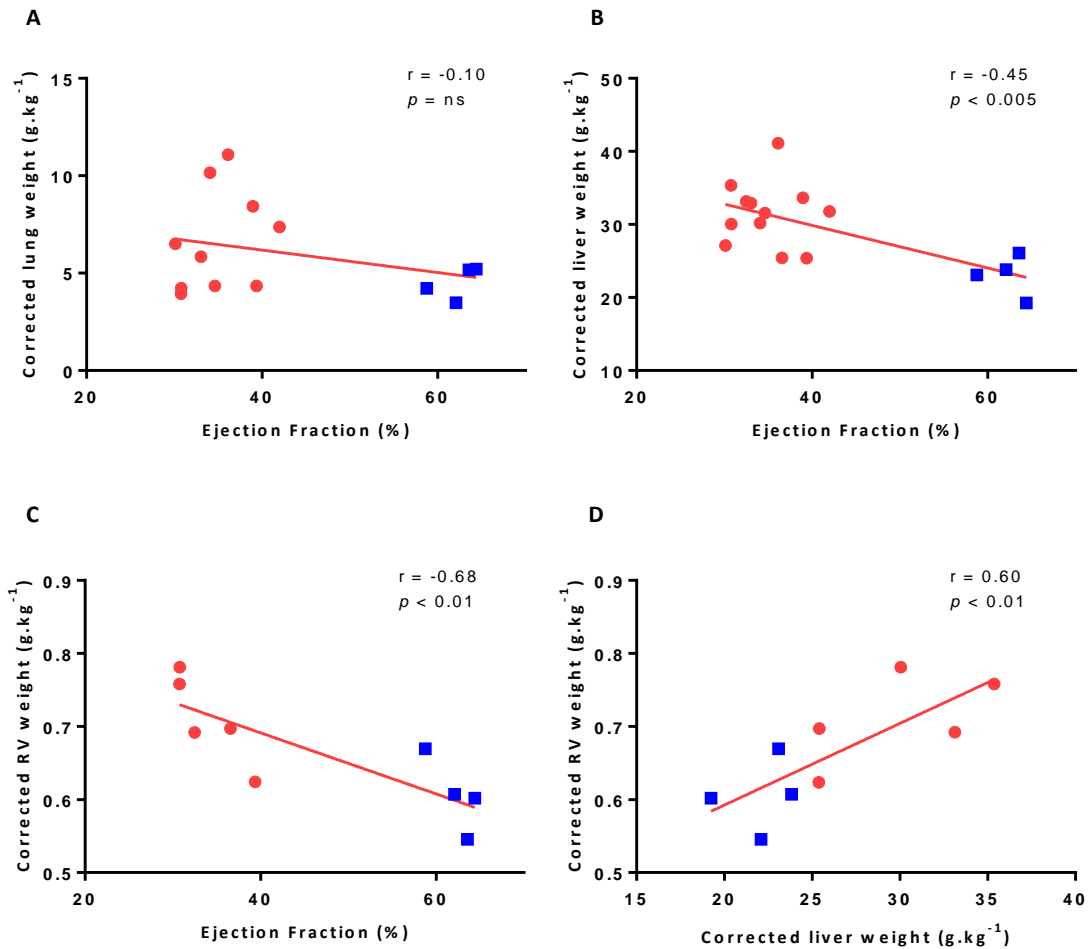


Figure 3.1: The relationship between organ weights and ventricular function measured as ejection fraction. Plots of lung (A), liver (B) and right ventricular weights (C) corrected for body weight against ejection fraction in heart failure (●) and sham operated (■) groups. The relationship between ventricular dysfunction and hepatic congestion was examined (D) by plotting right ventricular weight and liver weight, both corrected for body weight. Solid red lines represent the linear regression when the correlation between both parameters was determined with correlation coefficients (r) and slope significance values (p) shown.

3.2.3 Cardiac remodelling

As mentioned, the wet weight of the left ventricular free wall was significantly increased in animals from the heart failure group when compared to sham operated animals. In addition, there was also a significant correlation ($r = -0.59$, $p < 0.01$) between left ventricular weight and ejection fraction (when LV weight was corrected for body weight) (figure 3.2), suggesting myocardial infarction initiates significant compensatory mechanisms including hypertrophy in an attempt to counteract left ventricular dysfunction.

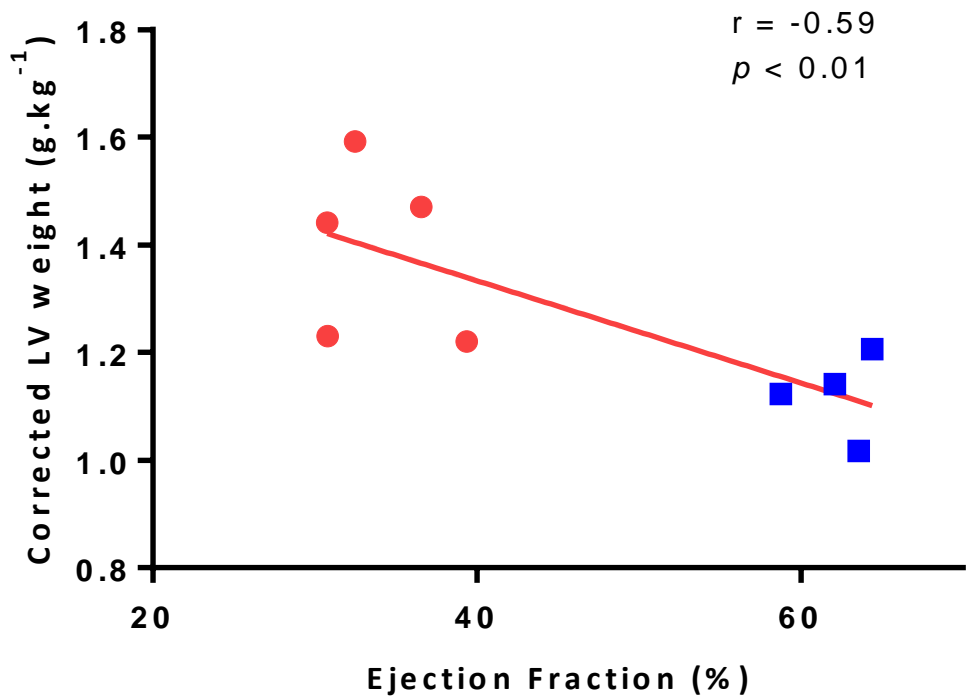


Figure 3.2: A plot showing the negative correlation between the weight of left ventricular tissue (corrected for bodyweight) and ejection fraction in the heart failure (●) and sham operated (■) groups. The solid red line represents the linear regression when correlation between the two parameters was determined with the correlation coefficient (r) and slope significance value (p) shown.

3.2.4 MRI and lesion volume in the intact excised heart

Following terminal experiments involving the use of the non-innervated heart preparation to investigate the role of the intrinsic cardiac ganglia on cardiac electrophysiology, hearts were rapidly removed from the Langendorff setup and fixed. A total of 9 intact excised hearts (5 from the HF group and 4 from the sham operated group) were then transferred to a proton-free fluid, Fomblin-Y (see chapter 2 section 2.2.2) and imaged using MRI. *Ex vivo* whole heart imaging enabled the accurate quantification of scar formation and the determination of the effects of myocardial infarction and heart failure on viable myocardium.

All sham operated hearts that were imaged using MRI demonstrated no lesion formation (see figures 3.3 and 3.4B), suggesting the use of an apical tie for manipulation of the heart during sham coronary artery ligation surgery resulted in no significant damage to the myocardium. An illustration comparing scar visibility in a heart from the HF group with the lack of scar in a sham operated animal is shown in figure 3.3. All hearts within the heart failure group showed significantly increased lesion volumes when compared to those from the sham operated group ($627 \pm 122\text{mm}^3$ vs $0 \pm 0\text{mm}^3$ respectively, $p < 0.01$ (unpaired two-tailed t-test). Lesion volume in hearts from the heart failure group ranged from 209mm^3 to 967mm^3 suggesting coronary artery ligation in a rabbit model results in differing degrees of myocardial damage, as seen clinically.

To determine the effects of myocardial damage and lesion volume on cardiac dysfunction, the relationship between lesion volume and ejection fraction was determined (figure 3.4). The increased lesion volume associated with coronary artery ligation was significantly correlated with a reduced ejection fraction when compared to the sham operated group (figure 3.4B). Ventricular scarring caused by myocardial infarction, demonstrated by cardiac MRI, results in the impairment of myocardial contractility shown by a lower ejection fraction, corresponding to that seen clinically (Hamrell and Alpert, 1986).

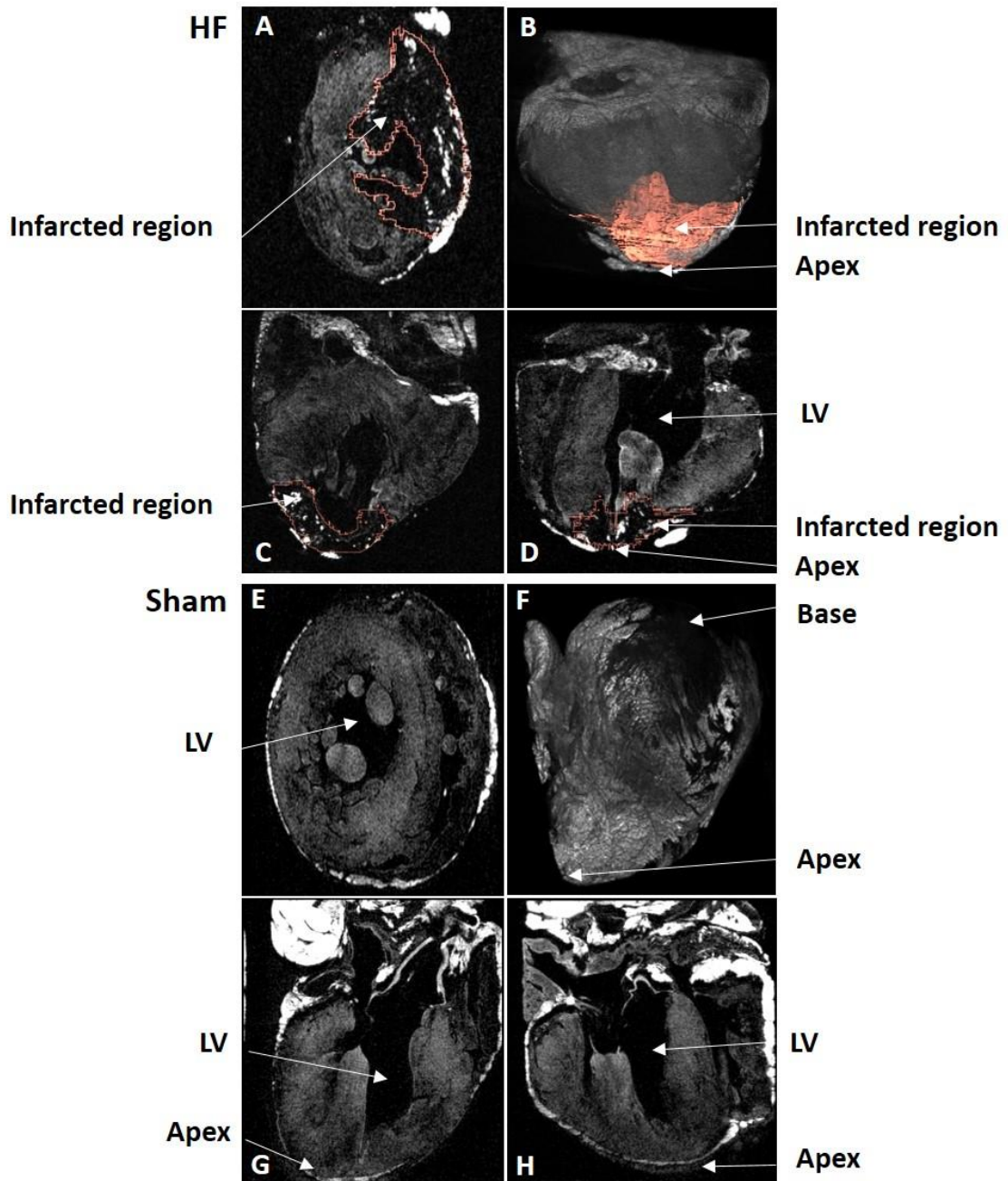


Figure 3.3. Comparison of lesion formation between hearts from the heart failure and sham operated groups using MRI. Two individual hearts analysed using MRI (HF (A-D) and Sham (E-H)). Two-dimensional MRI images of different orientations showing lesion development in a heart from the HF group (A, C and D) (black region at the apex of hearts in images C and D illustrates infarcted tissue). Image B represents a 3D reconstruction of an infarcted heart with the pink region indicating the lesion area analysed. E, G and H represent a sham operated heart with no evidence of infarct and F illustrates a three-dimensional reconstruction of a sham operated heart.

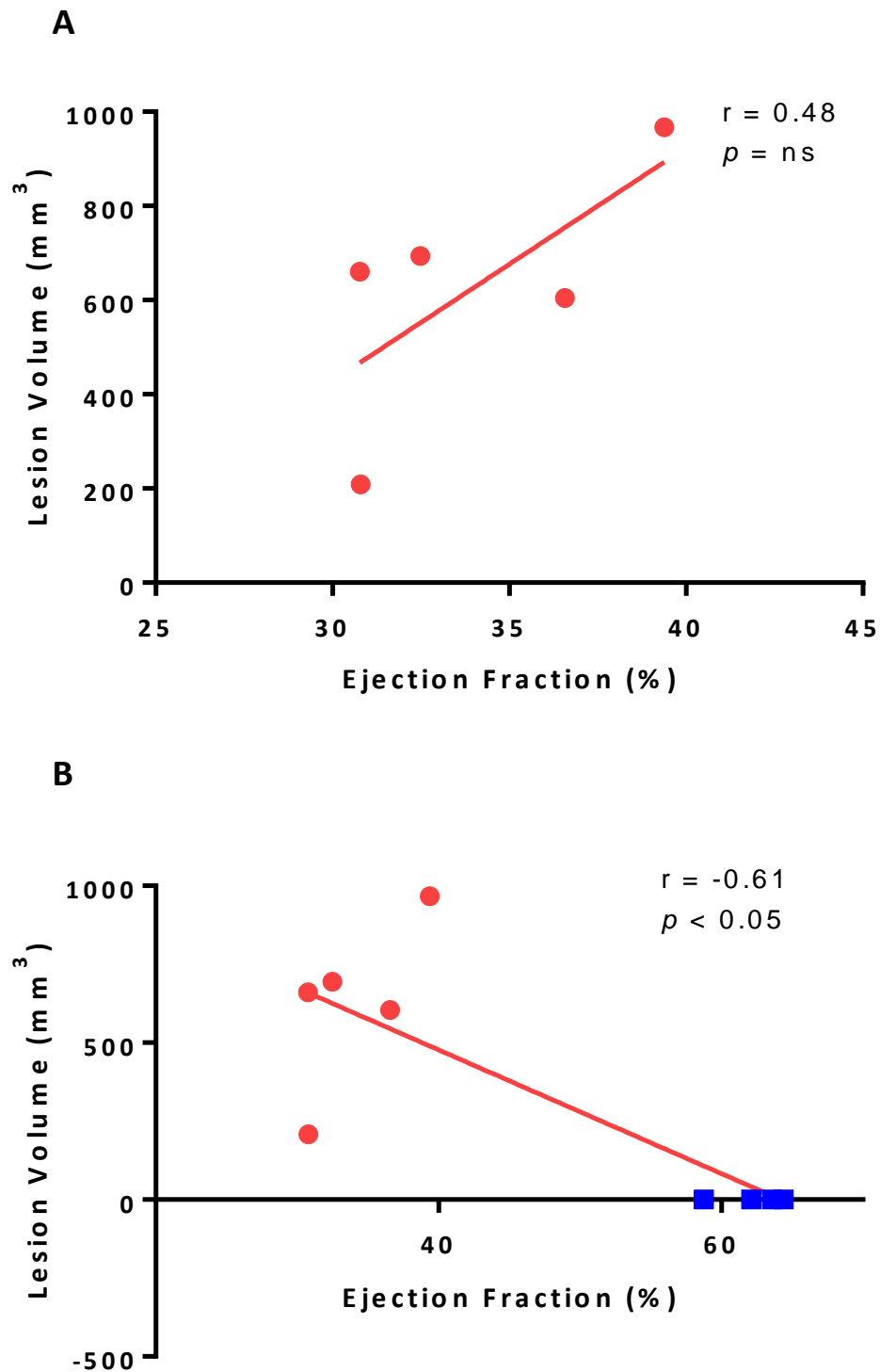


Figure 3.4: The correlation between lesion volume and ejection fraction. A. Plot comparing lesion volume (mm^3) with cardiac dysfunction measured as ejection fraction (%) within the heart failure group only ($n=5$). **B.** Plot of lesion volume against ejection fraction in heart failure (●) and sham operated groups (■). Both solid red lines represent the linear regression when correlation between the two parameters was determined with the correlation coefficient (r) and slope significance value (p) shown.

3.3 Discussion

The evidence of local and systemic changes in relation to heart failure as a result of coronary artery ligation were investigated in the rabbit. Changes in the structure of the heart as a result of coronary artery ligation were demonstrated, with an overall increase in weight and more specifically hypertrophy of the left ventricle being evident. This structural change was also accompanied by an increase in systolic dysfunction as a result of the inability of the left ventricle to contract sufficiently enough to maintain cardiac output demonstrated by a significant reduction in ejection fraction. Coronary artery ligation leads to deleterious effects on myocardial tissue, illustrated by the significant lesion formation and evidence of infarcted myocardium. In order to compensate for the reduced ability of the damaged heart to maintain cardiac output and blood pressure (Poole-Wilson, 1993), significant ventricular hypertrophy develops, again shown in this study.

Following on from the initial cardiac insult and despite local changes to the heart in order to continue functioning at full capacity, the continued development of heart failure results in further downstream systemic changes. These changes include pulmonary oedema and hepatic congestion. As a result of increased back pressure in the left ventricle due to left ventricular dysfunction, pulmonary congestion develops. If left to develop, heart failure leads to further ventricular failure and right ventricular overload, which in turn results in hepatic congestion. Previous studies investigating the effects of myocardial ischemia and heart failure in similar animal models, including the rabbit (Pye *et al.*, 1996, Ng *et al.*, 1998), have shown the production of these systemic changes equivalent to those seen in humans. Data presented here also correlates with this research showing both increased lung weights as well as significantly increased liver weights suggesting the development of pulmonary oedema and hepatic congestion.

The data presented in this chapter further reiterates the use of the rabbit coronary artery ligation model as a clinically relevant model of myocardial infarction and heart failure. The changes in cardiac function as well as the organ congestion observed as a downstream effect suggest the use of this model should deliver structural and functional changes reflecting those expected in the equivalent clinical and human scenario.

Chapter 4: The effects of heart failure on the anatomy and morphology of the rabbit intrinsic cardiac nervous system

4.1 Introduction

Despite previous hypotheses that neurocardiac control originated solely from sources of extrinsic innervation, it is becoming increasingly apparent that the ICNS plays a significant role in the control of cardiac function. In order to fully understand the functional importance of the ICNS, the overall anatomy and morphology firstly need to be determined in detail. The rabbit is commonly used as a preferred small animal experimental model, yet despite this, to date only one study has investigated the gross morphology of the rabbit ICNS (Saburkina *et al.*, 2014) to date.

These data showed comparable topography with both smaller rodent models including mice (Pauza *et al.*, 2013, Rysevaite *et al.*, 2011a) and rats (Batulevicius *et al.*, 2003), as well as larger mammals such as sheep (Saburkina *et al.*, 2010) and pigs (Batulevicius *et al.*, 2008): albeit simpler in structure. In general, the ICNS is described as a complex and intricate network of nerves and ganglia, primarily present at the level of the atria on the heart hilum and around the roots of the pulmonary veins (Saburkina *et al.*, 2014, Yuan *et al.*, 1994). Numerous studies have investigated the neurochemical profile of the ICNS of multiple mammalian models and confirmed the presence of not only choline acetyltransferase (ChAT) IR neurons, indicative of postganglionic parasympathetic neurons, but also; tyrosine hydroxylase (TH), neuropeptide Y (NPY), substance P (subP), nNOS and calcitonin gene related peptide (CGRP) and the generic neuronal marker protein gene product 9.5 (PGP9.5) (Richardson *et al.*, 2003, Rysevaite *et al.*, 2011b, Steele *et al.*, 1994, Hoover *et al.*, 2009).

Understanding the overall morphology of the ICNS prior to any disease provides a foundation for investigating the role, if any, that this collection of nerves and ganglia has during cardiac diseases such as heart failure. It is well known that autonomic imbalances following myocardial infarction increase the potential for sudden cardiac death (Ng, 2016, Fukuda *et al.*, 2015). Following MI, the ICNS undergoes neuronal remodelling including spatially diverse intrinsic cardiac neuronal enlargement, in particular within ganglia which exert preferential influence over the ventricles (Rajendran *et al.*, 2016,

Nakamura *et al.*, 2016). This along with neuronal degeneration, the development of inclusions and vacuoles (Hopkins *et al.*, 2000) within neuronal somata and adaptive changes in the neurochemical profile (Hardwick *et al.*, 2014) indicates a pathological involvement of the ICNS following cardiac insult.

The aims of this chapter were two-fold;

- Firstly, to further describe the overall topology of the rabbit ICNS, advancing on work previously done in the rabbit (Saburkina *et al.*, 2014) by including investigation of the neurochemical profile.
- Secondly, to investigate the effects of myocardial infarction and heart failure on the structure of the rabbit ICNS, of which there is currently very limited information.

4.2 Results

4.2.1 Distribution of intrinsic cardiac neurons in the whole rabbit heart

To determine the distribution of intrinsic cardiac neurons present in the rabbit heart, 11 hearts were examined from control rabbits i.e. no prior surgery had been undertaken. This was done using the pan neuronal AChE stain described previously (chapter 2).

The majority of neurons were found to lie on supraventricular tissues, particularly on the venous part of the heart hilum and the epicardial surface of the heart. Intrinsic cardiac ganglia were also identified at the region of the conus arteriosus at the root of the pulmonary trunk, termed ventricular neurons (figure 4.1). The distribution of nerves and intrinsic cardiac neuronal somata as well as the size and shape of the intrinsic cardiac ganglia showed variation between hearts, however in all hearts somata existed either grouped into ganglia (defined as a collection of 3 or more neurons), as single cells or as pairs of cells (figure 4.2).

Extrinsic cardiac nerves accessed the heart at both the arterial and venous portions of the heart. Nerves extended from the root of the bifurcation of the pulmonary trunk across the heart to the region of the heart hilum. Nerves also accessed the ICNS at the venous portion of the heart hilum, particularly around the roots of the pulmonary veins, the right inferior and the right superior caval veins and extended to numerous ganglia both on the heart hilum and around the roots of the middle and right pulmonary veins.

Extrinsic nerves extended to numerous ganglia, the distribution of which varied between all hearts making direct comparisons difficult. However, in all hearts, 2 large clusters of neurons were identified as the left and right neuronal clusters (LNC and RNC) (figure 4.2). In general, the RNC was located at the cranial aspect of the interatrial groove at the anterior region of the root of the right cranial vein (superior vena cava) and dorsal to the root of the right pulmonary vein. The location of the LNC was more diverse in comparison but was commonly found dorsal to the roots of the left and middle pulmonary veins (figure 4.2).

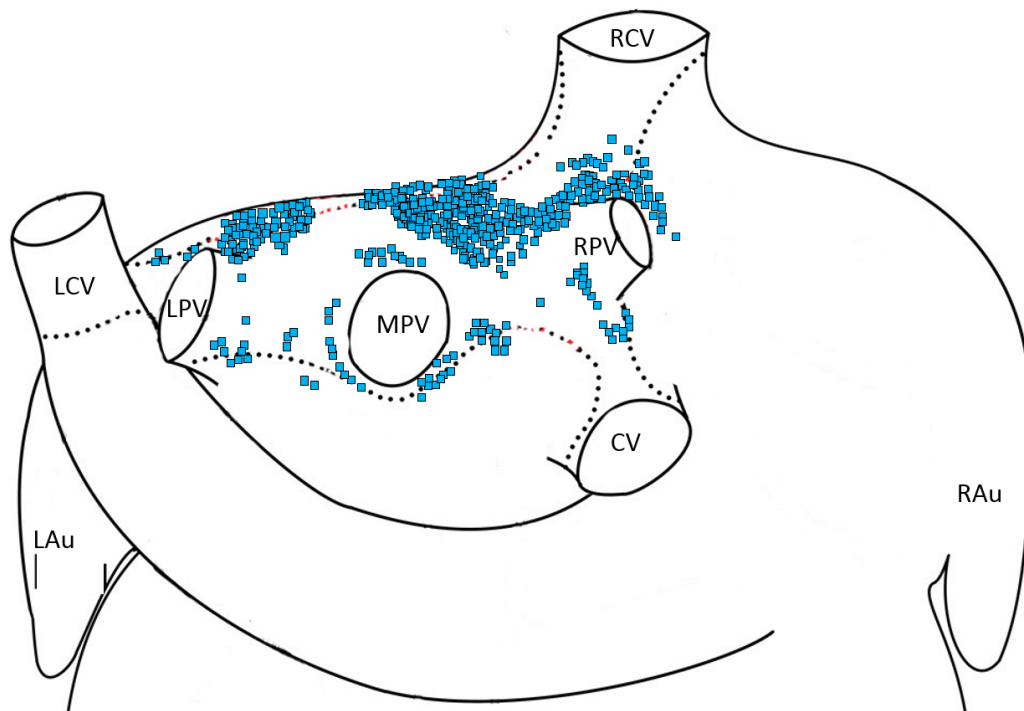


Figure 4.1. Summary of the morphological pattern of distinct intrinsic cardiac ganglia from 11 rabbit hearts. Clusters of intrinsic cardiac neurons (indicated in blue) visible on the dorsal view of the heart. Abbreviations: CV, caudal vein; Lau, left auricle; LCV, left cranial vein; LPV, left pulmonary vein; MPV, middle pulmonary vein; Rau, right auricle; RCV, right cranial vein; RPV, right pulmonary vein.

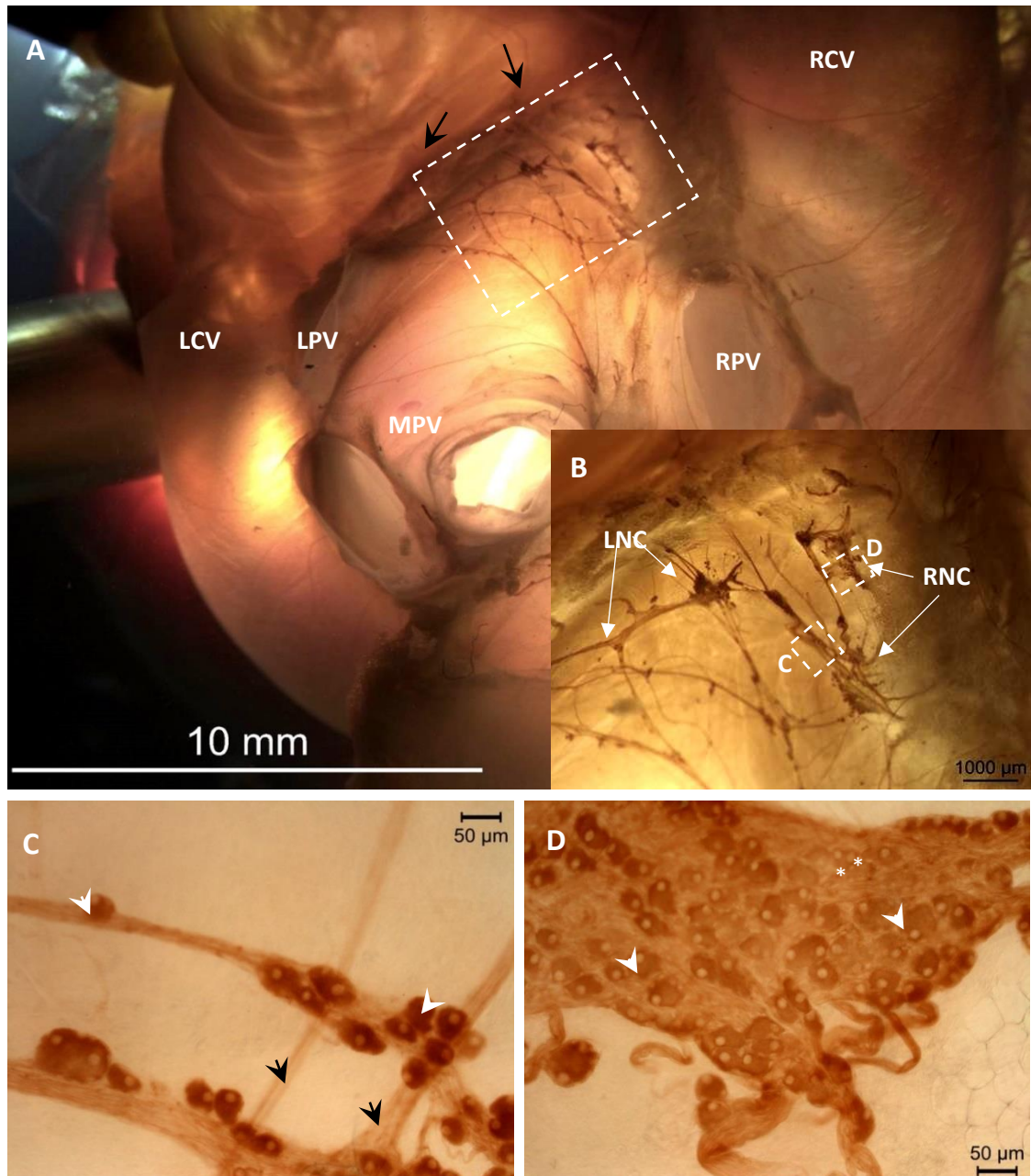


Figure 4.2. Macrographs of the rabbit heart illustrating the location of the intrinsic cardiac nerve plexus in control animals. The boxed area on the rabbit heart in **A** is enlarged in **B**. Images **C** and **D** demonstrate examples of ganglia from the right neuronal cluster. Black arrows indicate extrinsic nerves accessing the nerve plexus on the heart hilum in **A** and **B**. White arrowheads indicate examples of intrinsic cardiac neurons with black arrowheads showing interconnecting commissural nerves. Asterisks in **D** indicate examples of SIF cells located within larger ganglia. Abbreviations: LCV, left cranial vein; LNC, left neuronal cluster; LPV, left pulmonary vein; MPV, middle pulmonary vein; RCV, right cranial vein; RNC, right neuronal cluster; RPV, right pulmonary vein.

Smaller ganglia were also identified at the region of the sinus node, at the root of the right pulmonary vein, ventral to the middle pulmonary veins and on the dorsal aspect of the inferior caudal vein (i.e. the inferior vena cava) (figure 4.1). Solitary neuronal somata and small ganglia were identified at the root of the pulmonary trunk on the conus arteriosus in 7 out of 11 hearts. Numerous intrinsic cardiac nerves extended from these ganglia into the anterior walls of the left and right ventricles.

Thinner commissural nerves connected both ganglia within these clusters as well as behaving as interconnecting nerves between spatially separated ganglia (figure 4.2). These nerves connected the two larger LNC and RNCs, as well as linking smaller epicardial ganglia to these larger ganglia in 100% of hearts.

4.2.2 Heart failure and the overall distribution of intrinsic cardiac neurons in the whole rabbit heart

Remodelling of the ICNS has previously been shown in larger mammal experimental models (Singh *et al.*, 2013, Rajendran *et al.*, 2016). With the aim of determining the morphological changes to the rabbit ICNS during heart failure, whole heart AChE staining experiments were repeated using animals from a coronary artery ligation model. Experiments were repeated in a further 11 animals (7 from the heart failure group and 4 from the sham operated group).

Ventricular innervation in control animals arises from nerves accessing the arterial part of the heart hilum (Saburkina *et al.*, 2014). These nerves spread across the ventricles, branching into numerous subplexuses and extend onto both the left and right ventricles. Following myocardial infarction, studies have shown evidence of significant denervation adjacent to and at the region of infarcted tissue (Lorentz *et al.*, 2013) therefore the neuronal innervation of the ventricles in the rabbit heart failure group were examined epicardially. Extensive scar tissue was evident in all hearts from the heart failure group at the region of the left coronary artery ligation as well as peri-infarct. A complete loss of neuronal innervation was evident within the scar region yet when hearts from the HF group were compared to the sham operated and control groups, an observable increase in the number and density of visibly stained nerves was evident.

Small ganglia and individual ventricular neuronal somata were identified at the region of the conus arteriosus in sham operated and HF groups, with ganglia size ranging from 0 – 115 and 0 – 129 cells respectively.

The overall topography and distribution of ganglia was compared within the control, sham operated and heart failure groups. In 100% of hearts, neuronal somata were distributed epicardially; primarily on the heart hilum and at the roots of the pulmonary veins. A large number of neuronal somata were grouped into two clusters in both the sham and HF groups, as was seen in the control group, again termed the left and right neuronal clusters. There was no distinct difference in the overall spatial distribution of cardiac nerves and ganglia between all 3 groups.

4.2.2.1 Quantification of rabbit intrinsic cardiac ganglia and the effect of heart failure

A breakdown of the distribution of intrinsic cardiac neurons within distinct regions of the rabbit heart is detailed in table 4.1. Control rabbit hearts were studied and overall there were on average 1632 ± 216 neuronal somata per heart ranging from 1194 to 2229. In hearts from the control group, the majority of intrinsic cardiac neuronal somata were found on the atria; particularly on the heart hilum and around the roots of the pulmonary veins. Ventricular ganglia were identified in 7 out of the 11 hearts examined with a significantly ($P < 0.0001$) smaller number of neurons being found compared to the ganglia found on the atria (table 4.1). On average there were 19 ± 14 neurons present on the conus arteriosus, yet this number varied between hearts and ranged from being completely absent on the ventricles in 4/11 hearts up to 153 somata suggesting that ventricular innervation does not solely arise from ventricular ganglia. The total number of ganglia ranged from 37-91 with the smallest ganglia consisting of just 3 cells compared to the largest ganglia containing 199 neurons. Ganglia were predominantly smaller in size with fewer large ganglia containing more than 100 cells per heart.

| | Control | Sham | Heart failure |
|------------------------------------|----------------|--------------|----------------------|
| | (n=11) | (n=4) | (n=7) |
| Body weight (kg) | 2.4 ± 0.2 | 3.8 ± 0.1 | 3.9 ± 0.1 |
| Number of somata per heart | 1632 ± 216 | 1760 ± 133 | 1159 ± 101**** |
| Number of ganglia per heart | 63 ± 7 | 89 ± 25 | 58 ± 8 |
| Atrial neurons | 1603 ± 197 | 1744 ± 141 | 1146 ± 110**** |
| Ventricular neurons | 19 ± 14 | 19 ± 17 | 14 ± 9 |
| Singular neurons | 28 ± 11 | 26 ± 11 | 10 ± 4 |
| Pairs of neurons | 19 ± 5 | 15 ± 4 | 8 ± 2 |

Table 4.1. Cell numbers showing the overall distribution of intrinsic neuronal somata in the whole rabbit heart in animals from the control, sham operated and heart failure groups. Table showing the average number of somata on hearts from hearts from each of the three groups investigated. This was divided into the total number of atrial and ventricular neurons per heart. The total number of singular and paired neurons was also noted. Data is presented as mean ± SEM. Statistical analysis performed with repeated measures two-way ANOVA to compare conventional vs HF and sham vs HF, *** $p < 0.001$ and **** $p < 0.0001$.

It has been shown previously that remodelling occurs within the ICNS following heart failure (Rajendran *et al.*, 2016), with cells undergoing morphological and phenotypic changes. Therefore, in order to investigate in more detail whether heart failure leads to an alteration in the topography of the rabbit ICNS, the distribution and quantification of intrinsic cardiac neurons was compared between conventional rabbits, rabbits from the HF group and rabbits from the sham operated group.

Animals in the heart failure group were significantly heavier in comparison to control animals. Because of this, data from sham operated animals was used to determine whether changes in the topography of the rabbit ICNS were down to the development of heart disease or simply the differences in rabbit age and weight. There was no significant difference between the average numbers of neuronal somata from the control group when compared to the sham operated group. In comparison, the average number of cells per heart was significantly lower in the HF group than both the control and the sham operated group (HF: 1159 ± 101 (954 – 1401)) (table 4.1). This difference was primarily noticed with a significant reduction of neuronal somata found on the atrial region of hearts in the HF group (CN: 1603 ± 197 vs SHM: 1744 ± 141 vs HF: 1146 ± 110) ($P < 0.0001$). Conversely, there was little difference in the number of somata found on the conus arteriosus region, where nerves are known to extend solely to the ventricles (table 4.1).

Variation in cell size and area was evident on the hearts of the control animals, with ganglia containing relatively smaller cells being noted (figure 4.2D). This correlates with previous reports detailing clusters of small intensely fluorescent cells (Rysevaite *et al.*, 2011b). The location of groups of SIF cells showed no particular pattern between hearts, however on observation all small clusters of SIF cells were found within larger ganglia.

Overall, the average cell area (μm^2) in control animals was 601 ± 45 ranging from $366\mu\text{m}^2$ to $775\mu\text{m}^2$. The heart was divided into four regions known to contain specific ganglia based on the topographical map previously produced by Saburkina *et al.* (2014) and described in chapter 5 and the average cell area determined for each group. In control animals there was no significant difference between the average cell areas between all 4 of the spatially distinct regions (figure 4.4B).

In all hearts examined from the HF group, there was significant neuronal enlargement (figure 4.3), with the overall average cell area being significantly larger in comparison to both the control ($P < 0.0001$) and sham operated groups ($P < 0.001$) (figure 4.4A). There was no significant difference in the overall cell area between control animals and sham operated animals, ($601 \pm 45 \mu\text{m}^2$ vs $564 \pm 50 \mu\text{m}^2$ respectively) indicating changes in cell size were as a result of the prior coronary artery ligation and heart failure.

| | Control | Sham | Heart failure |
|---|----------------|----------------|----------------------|
| | (n=11) | (n=4) | (n=7) |
| Cell area (μm^2) | 601 \pm 45 | 564 \pm 50 | 1035 \pm 63**** |
| Cell long axis (μm) | 29.1 \pm 1.4 | 30.2 \pm 2.1 | 42.0 \pm 1.8**** |
| Cell short axis (μm) | 24.3 \pm 0.9 | 24.7 \pm 1.7 | 34.7 \pm 1.7*** |

Table 4.2: The size of neurons from rabbit hearts stained histochemically for AChE from animals from the control, sham operated and heart failure groups. The average cell area per heart was compared between all three groups with significant enlargement of neurons from hearts within the heart failure group being evident. In addition the average long and short axis of all cells on the heart were compared with evidence of significant enlargement in the heart failure group being noted.

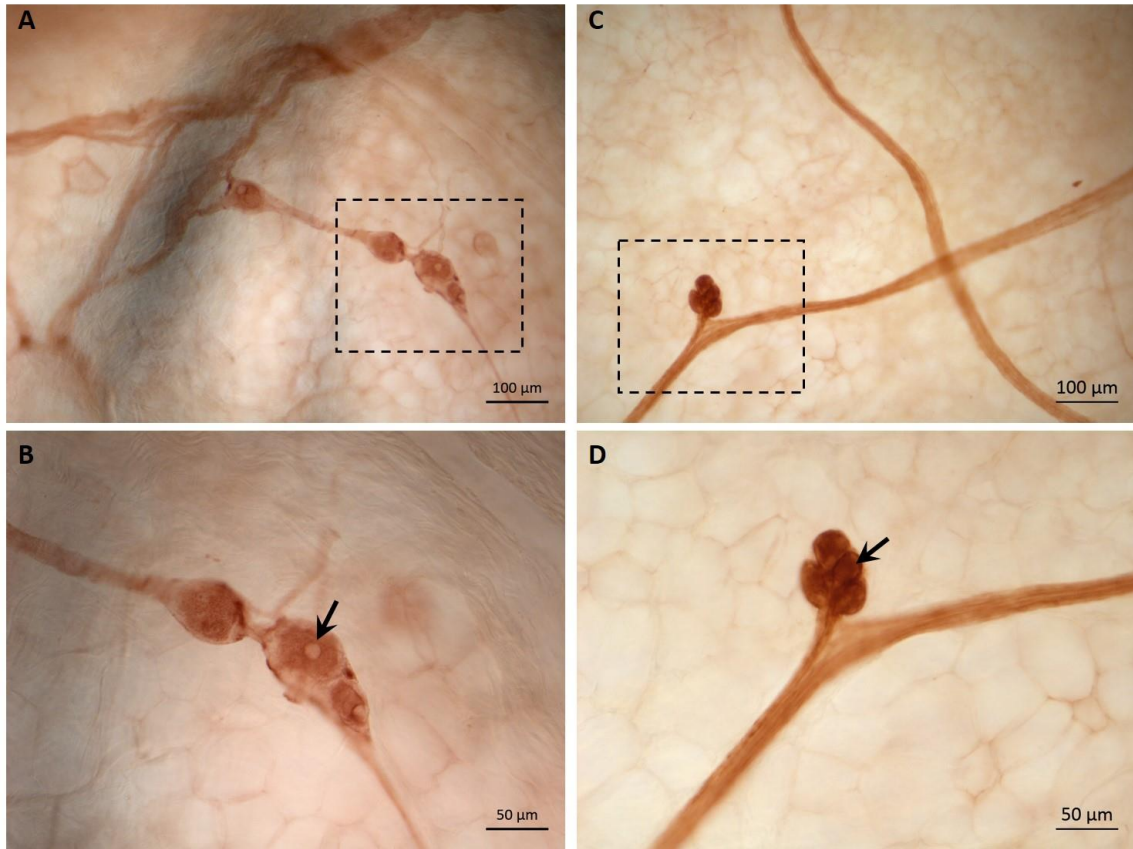


Figure 4.3. Macrographs illustrating the neuronal enlargement of somata in heart failure. Evidence of neuronal enlargement seen in the heart failure group (A and B) when compared to the control group (C and D). B and D illustrate the boxed regions in A and C with black arrows identifying individual neuronal somata. Images show ganglia within the right neuronal cluster regions from representative hearts in the heart failure (A and B) and control (C and D) groups.

Despite neuronal enlargement being observed within all regions, the level of enlargement was spatially diverse. The most significant difference seen in the HF group when compared to the control and sham operated groups was within the region of the heart hilum (CN: $632 \pm 60\mu\text{m}^2$ vs SHM: $652 \pm 50\mu\text{m}^2$ vs HF: $1185 \pm 31\mu\text{m}^2$) (figure 4.4B), with a similar level of enlargement observed at the conus arteriosus (CN: $627 \pm 50\mu\text{m}^2$ vs SHM: $521 \pm 30\mu\text{m}^2$ vs HF: $1143 \pm 109\mu\text{m}^2$). In comparison, neuronal somata measured from the right atrial region of hearts from the HF group showed no significant enlargement when compared to both the control and sham groups (CN: $567 \pm 68\mu\text{m}^2$ vs SHM: $496 \pm 32\mu\text{m}^2$ vs HF: $752 \pm 132\mu\text{m}^2$) (figure 4.4B). This suggests that neuronal enlargement of cells following heart failure occurs within regions where ganglia exert preferential influence over the site of injury, in agreement with previous morphological studies (Rajendran *et al.*, 2016, Nakamura *et al.*, 2016).

In addition to measuring the cell area, the length of both the short and long axis of all individual cells was measured (figure 4.5). There was no significant difference in both the average length of short and long axis between the control and sham operated groups (figure 4.5A). The average short axis of all cells within the heart failure group was significantly larger than that of both the control and sham operated groups (CN: $24.3 \pm 0.9\mu\text{m}$ vs SHM: $24.7 \pm 1.7\mu\text{m}$ vs HF: $34.7 \pm 1.7\mu\text{m}$). The overall average long axis was also significantly increased in the HF group when compared to both the control and sham operated groups (CN: $29.1 \pm 1.4\mu\text{m}$ vs SHM: $30.2 \pm 2.1\mu\text{m}$ vs HF: $42.0 \pm 1.8\mu\text{m}$) (table 4.2).

When neurons from 4 different regions known to contain ganglia were compared in the control and sham operated groups, there was no significant difference in the length of short and long axis between all 4 regions. The average short and long axis of cells within these 4 regions was then compared within the HF group. There was no significant difference between the lengths of the short and long axis of cells found on the heart hilum, conus arteriosus region and the region ventral to the pulmonary veins however there were significant differences between the cell lengths of the hilum, CA and ventral PV region when compared to the right atrial region (figure 4.5B), corresponding to the data shown for the average cell area within these regions.

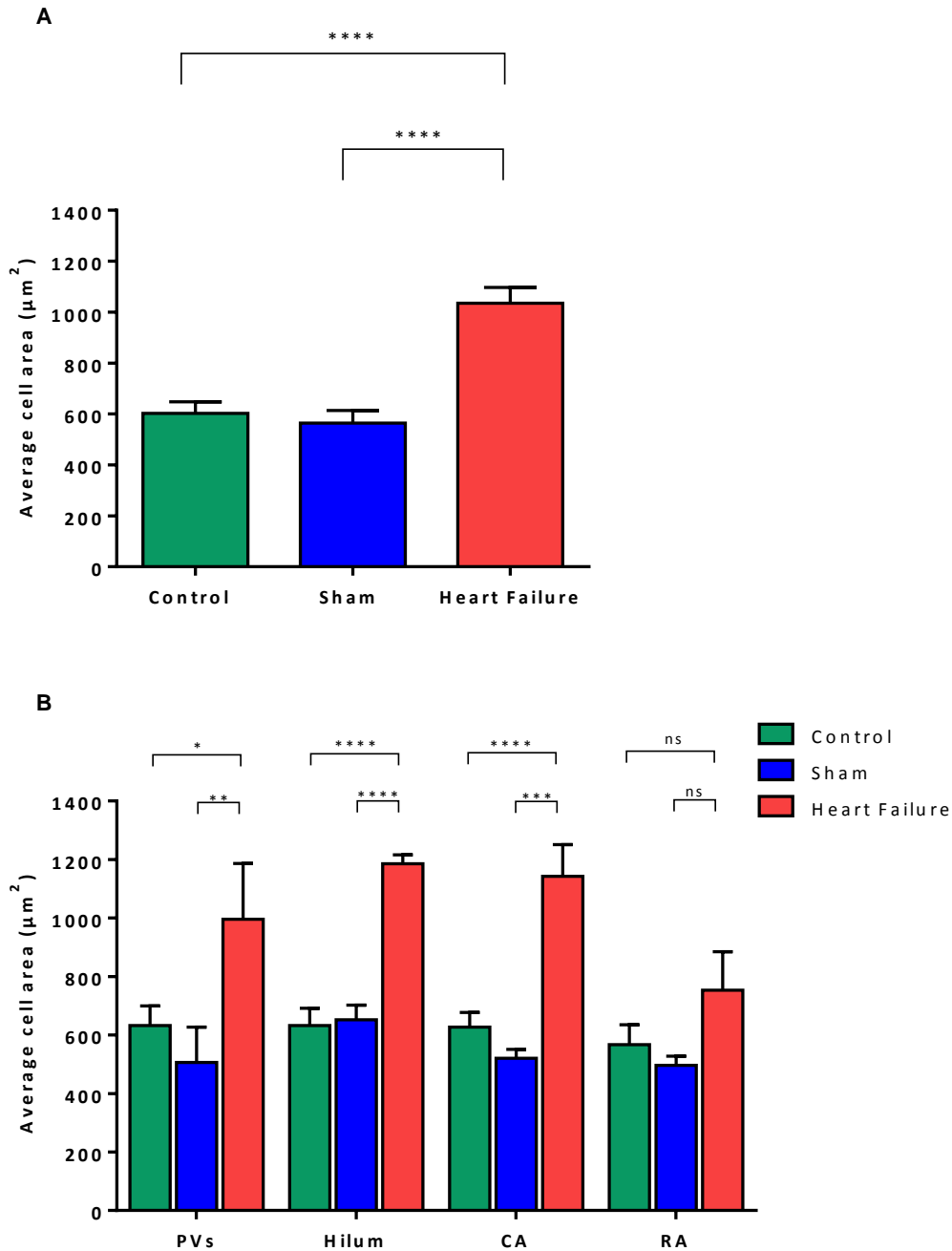


Figure 4.4. MI induces morphological changes in neuronal somata within the rabbit ICNS. The average overall cell area was quantified and compared between hearts from control, sham operated and heart failure animals (**A**). The average cell area was increased significantly in all regions examined apart from the region of the right atrial ganglionated plexus (**B**). Data are represented as mean \pm SEM. Statistical analysis performed with repeated measures two-way ANOVA, ns = no significance, * $p < 0.05$, ** $p < 0.01$, *** $p < 0.001$, **** $p < 0.0001$.

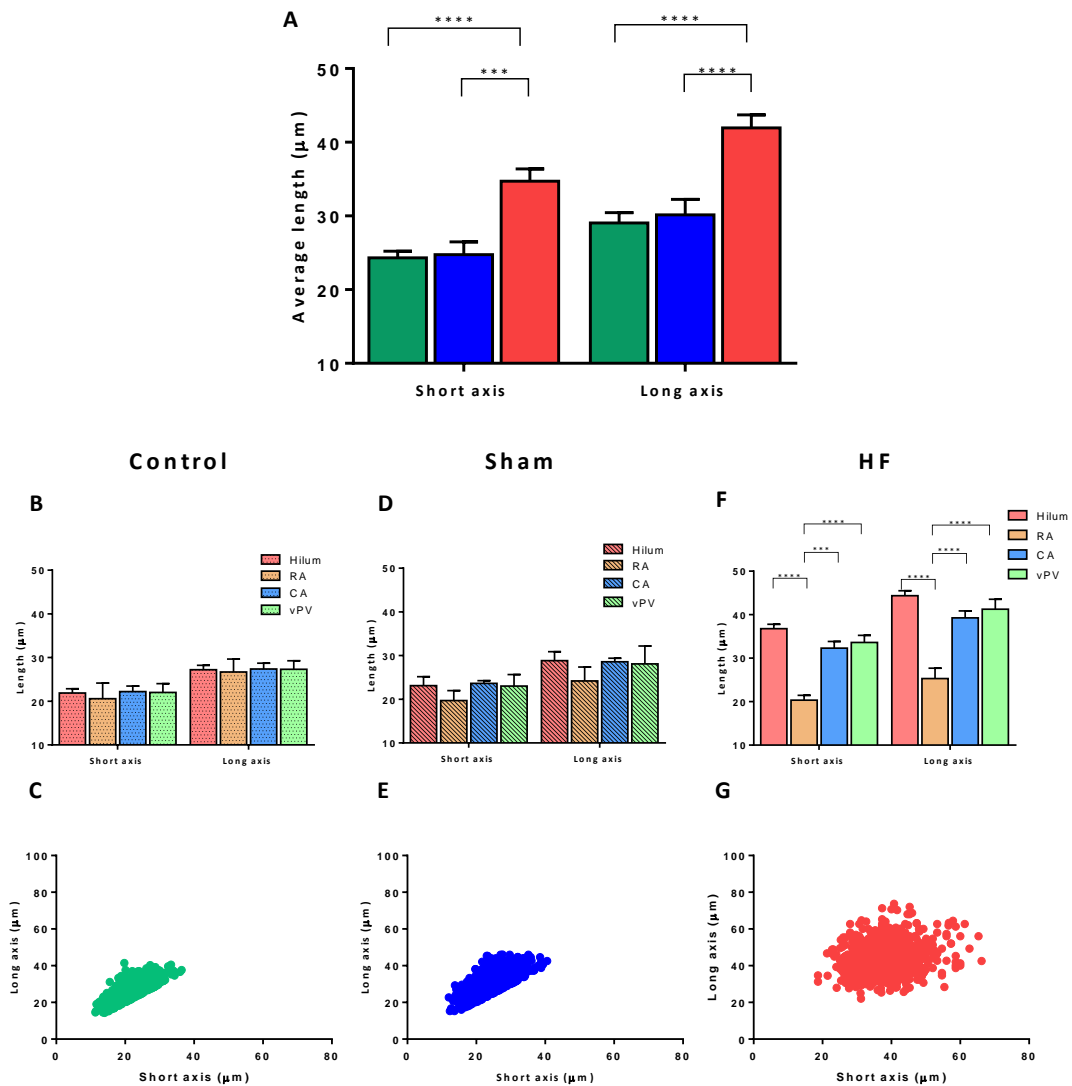


Figure 4.5. MI induced morphological changes in cell size. **A** illustrates the increase in overall average cell size within the HF group (red bars) when compared to hearts from both control (green bars) and sham operated groups (blue bars). The lengths of the short and long axis were compared within regions of the heart in all groups (**B, D and E**). There was no significant difference in the lengths of the short and long axes between all regions in the control (**B**) and sham groups (**D**). The lack of neuronal enlargement within the right atrial region in the HF group is demonstrated in **F**. Representations of the distribution of cell size are shown in **C** (control), **E** (sham operated) and **G** (HF group) showing the increased neuronal size in the HF group.

4.2.3 Distribution of immunohistochemically distinct intrinsic cardiac ganglia and neurons

In order to provide a more detailed and comprehensive map of the intrinsic cardiac ganglia in the rabbit, the distribution of cholinergic and adrenergic neurons was studied. The neurochemical profile of the ICNS was investigated solely in conventional animals and not in those that had undergone coronary artery ligation due to time constraints within this study. Using the technique of whole mount atrial preparation and carefully selected combinations of primary antibodies, immunohistochemistry was performed. Cholinergic structures were identified using antibodies to ChAT and TH for adrenergic structures.

The immunohistochemistry of the rabbit ICNS was investigated in a total of 16 control animals (1.5-2.5kg). The location of ganglionic cells positive for ChAT and/or TH and/or nNOS was reproducible from animal to animal with ganglia and cell size varying between hearts for all antibodies tested. Neurons immunoreactive for purely ChAT, TH or nNOS were consistently located on the heart hilum, at the root of the pulmonary veins and at the root of the right caudal vein, corresponding to the neurons identified previously using histological staining for AChE. ChAT immunoreactive neurons were significantly more abundant than all other phenotypes studied, with an average of 1946 ± 668 neuronal somata per heart ($59 \pm 5\%$ of neurons per heart) (table 4.3). ChAT-IR somata formed a large proportion of 2 large clusters previously identified as the LNC and RNC as well as significant proportions of smaller ganglia (figure 4.6). Neurons IR for TH only ($10 \pm 3\%$ of neurons per heart) were often found dispersed throughout larger ganglia containing numerous cell phenotypes (figure 4.6).

In addition to singularly labelled cells (i.e. ChAT only, TH only or nNOS only), numerous ganglia contained neuronal somata that were biphenotypic (figures. 4.6 and 4.7). Neurons positive for both ChAT and TH made up $18 \pm 2\%$ of all neurons, with ChAT and nNOS positive neurons making up $6 \pm 2\%$ compared to just $3 \pm 1\%$ of neurons being positive for both TH and nNOS. Neuronal somata of differing phenotype were examined in more detail with all cells being measured to determine cell area along with the length of both the short and long axis of each cell. Overall, there was no significant difference in the average cell area between all cell types studied. This was further confirmed by no

significant difference between both the length of the short and long axis between all groups.

The results obtained previously using the pan neuronal marker were compared with those obtained using whole atrial immunohistochemistry. The overall cell area of AChE stained neuronal somata showed no significant difference to all immunohistochemically stained somata suggesting a correlation between both methods.

Larger ChAT-IR and TH-IR nerve fibres passed epicardially over the venous portion of the heart hilum, extending to numerous ganglia. In all preparations examined for ChAT and TH immunoreactivity, larger bundles of nerves were present where ChAT-IR axons would extend in parallel to TH-IR axons. The majority of large nerve bundles however contained primarily TH-IR fibres (figure 4.8). These bundles ran adjacent to large ganglia containing not only TH-IR somata but where the majority of somata were IR for ChAT (figure 4.8). Thinner commissural nerves reactive for ChAT, TH and nNOS were present around ganglia present on the heart hilum and at the roots of the pulmonary veins and extended between individual ganglia (figure 4.8), synapsing onto somata.

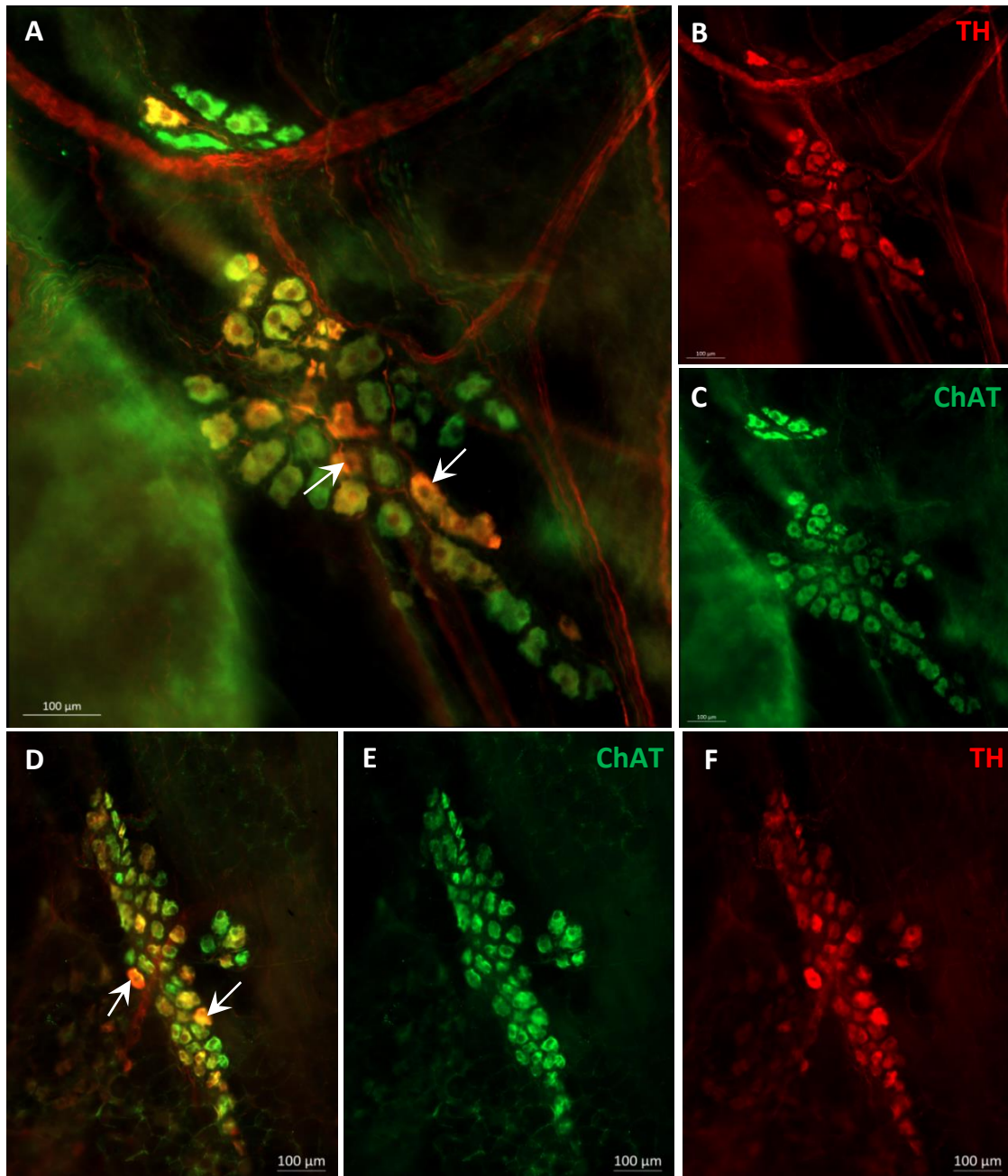


Figure 4.6. Intrinsic cardiac neurons demonstrate cholinergic or adrenergic or biphenotypic phenotypes. Images of ganglia double labelled to show ChAT (C and E) and TH (B and F). Neuronal cell bodies were predominantly IR for ChAT however evidence of possible colocalisation is apparent (white arrows). Scales bars represent 100 μ m in all images.

| | ChAT n = 9 | TH n = 10 | nNOS n = 9 |
|---|--------------------------------|----------------------------------|--------------------------------|
| Average number of somata per heart | 1946 ± 668 | 326 ± 106 | 111 ± 20 |
| Average number of somata per heart (range) | 1014 - 3240 | 35 - 854 | 54 - 193 |
| Area of neurons (µm²) | 557 ± 31 | 507 ± 35 | 478 ± 32 |
| Short axis (µm) | 25.0 ± 0.9 | 22.6 ± 1.1 | 23.1 ± 1.3 |
| Long axis (µm) | 32.2 ± 1.4 | 29.4 ± 1.6 | 29.6 ± 1.7 |
| | ChAT/TH n = 4 | ChAT/nNOS n = 3 | TH/nNOS n = 5 |
| Average number of somata per heart | 616 ± 161 | 203 ± 58 | 112 ± 36 |
| Average number of somata per heart (range) | 340 - 899 | 107 - 308 | 22 - 211 |
| Area of neurons (µm²) | 515 ± 30 | 600 ± 48 | 519 ± 45 |
| Short axis (µm) | 23.2 ± 0.4 | 25.9 ± 1.7 | 22.6 ± 1.1 |
| Long axis (µm) | 31.0 ± 1.0 | 32.2 ± 2.7 | 29.6 ± 1.6 |

Table 4.3. The average number of neurons of specific neurochemical phenotypes seen in the whole atrial preparation. Data is represented as mean ± SEM and range.

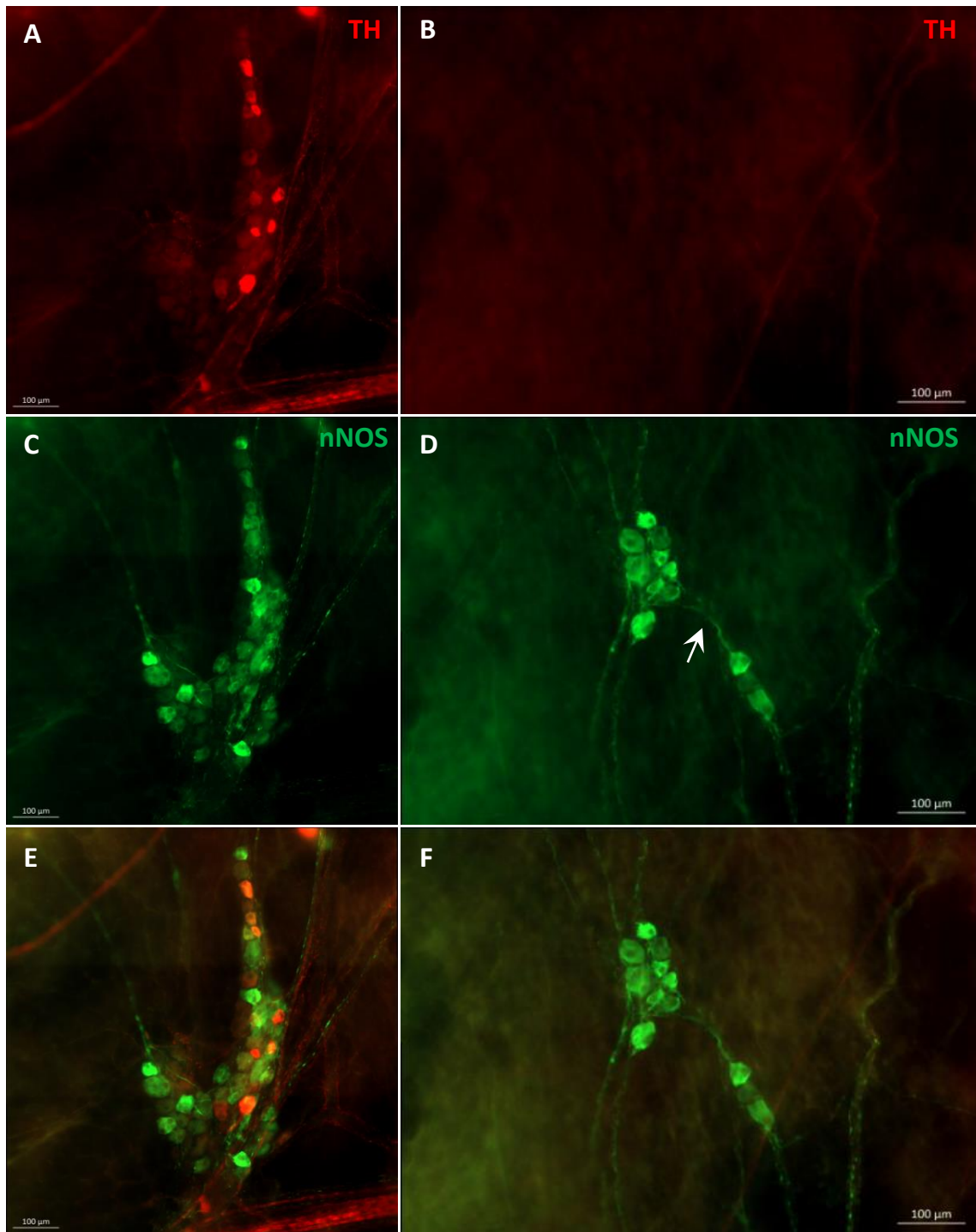


Figure 4.7. Microphotographs illustrating intrinsic cardiac neurons IR for nNOS and, TH as well as biphenotypic neurons. A, C and E: Images illustrating the presence of both TH-IR and nNOS-IR neurons on the root of the right cranial vena cava. **B, D and F:** An illustration of a smaller ganglion located in close proximity to the ganglia shown in A, C and E containing solely nNOS positive neurons and the absence of TH-IR neural structures shown in B. Panels E and F illustrate dual labelling where evident. Ganglia purely IR for nNOS were connected by thin commissural neurons (white arrows). Scale bars represent 100 μ m in all images.

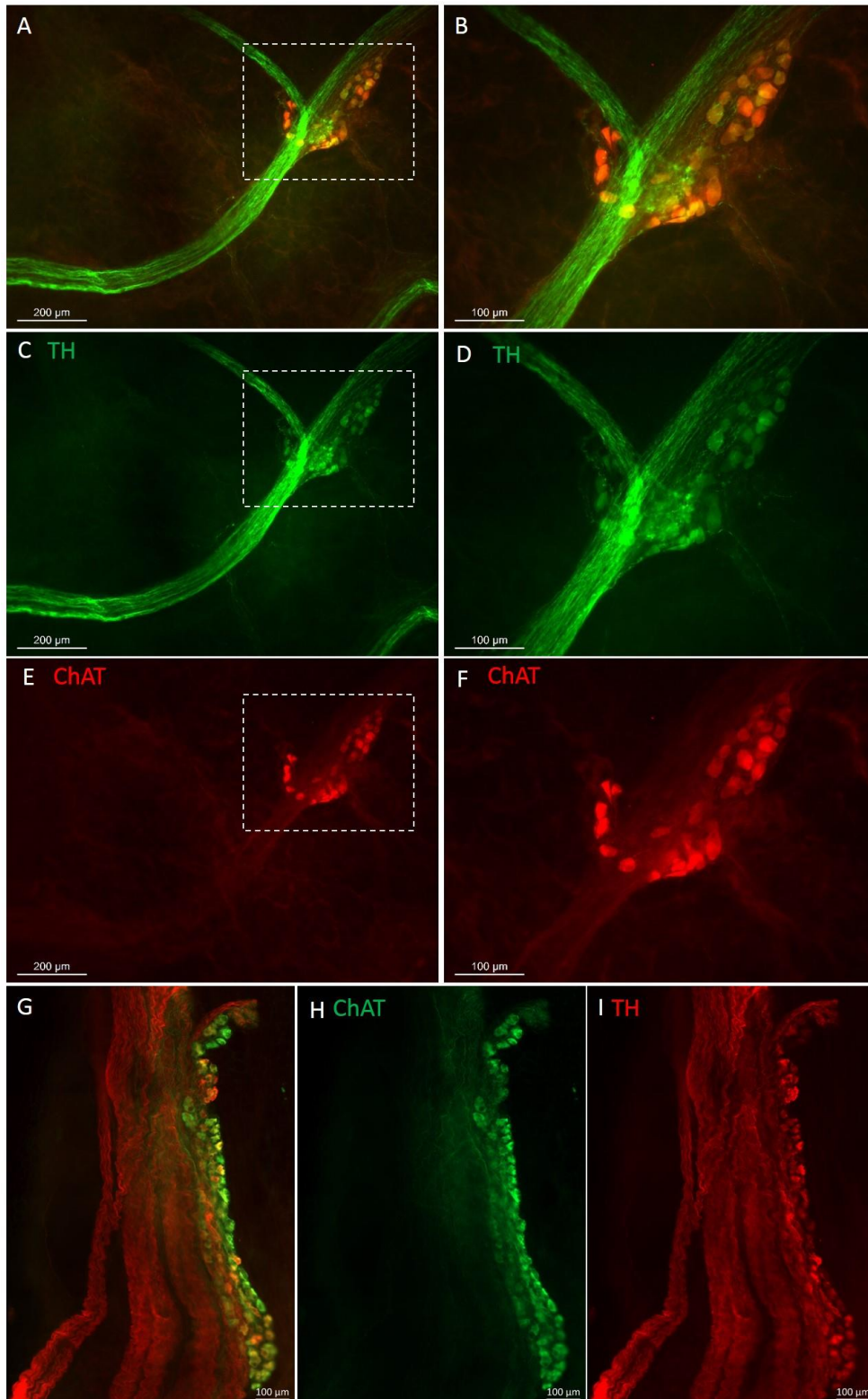


Figure 4.8. Microphotographs illustrating the predominance of TH fibres throughout the rabbit ICNS. A-F: Large TH-IR nerve bundles run adjacent to ganglia containing not only TH-IR neuronal somata, but also ChAT-IR somata. **G-I:** Microphotographs illustrating nerves accessing the heart on the medial side of the right cranial vein orifice, where TH-IR nerves fibres predominate. Scale bars represent 100µm.

4.3 Discussion

Understanding the anatomy and morphology of the ICNS is vital if future research is not only going to determine its functional capacity but also the ability of the ICNS to function during diseases such as heart failure. The work detailed in this chapter provides further insight into the overall anatomy and morphology of the ICNS in the rabbit; a model commonly used to study cardiac electrophysiology.

4.3.1 Distribution of intrinsic cardiac neurons in the whole rabbit heart

The morphological pattern of the intrinsic cardiac nervous system was revealed in whole heart preparations using histological AChE staining. Some investigators consider histological staining for AChE a method specific to visualising cholinergic (parasympathetic) neural structures only (Crick *et al.*, 1996, Crick *et al.*, 1999, Hoover *et al.*, 2004). Earlier findings by Koelle and colleagues (Koelle *et al.*, 1987) however, demonstrated staining according to Karnovsky and Roots (1964) stains both adrenergic and cholinergic neurons and nerves, including SIF cells. Nonetheless, sympathetic neural structures have less AChE activity than cholinergic fibres (Koelle *et al.*, 1987, Saburkina *et al.*, 2010). The majority of research conducted prior to the last decade examined individual ganglia such as the right atrial ganglionated plexus (Hoover *et al.*, 2009) and ganglia within the posterior atrial region (Hopkins *et al.*, 2000). More recently it has become increasingly important that the topography of the ICNS in its entirety is understood. The recent evidence of possible remodelling within the ICNS during cardiac disease (Rajendran *et al.*, 2016) and the functional role that regions of the ICNS is thought to play in arrhythmias including atrial fibrillation (Zhao *et al.*, 2015) suggests that the ICNS is significantly involved in disease. In order to understand how this system changes, if at all, with disease, a comprehensive understanding of the anatomy and topography of the ICNS is needed. Utilisation of the whole heart preparation in this study allowed the overall topography of neural structures to be examined without the damage that other techniques such as cryostat sectioning may cause.

It was shown in this chapter that despite interindividual variability in the overall morphology of the rabbit ICNS, neuronal somata lie epicardially with the majority of ganglia being distributed on the cardiac hilum. Ganglia were also commonly found

located around the roots of the pulmonary veins; a finding comparable to previously published work in other species including mice, rats and guinea pigs (Batulevicius *et al.*, 2003, Rysevaite *et al.*, 2011a, Leger *et al.*, 1999) as well as data in the rabbit (Saburkina *et al.* 2014). Despite the overall number of neurons appearing to be species specific (with larger mammals tending to exhibit larger numbers of neurons), the overall distribution of the ICNS in the hearts of smaller mammals such as mice and rats (Batulevicius *et al.*, 2003, Rysevaite *et al.*, 2011a) are comparatively similar to that of larger mammals (Saburkina *et al.*, 2010, Yuan *et al.*, 1994). This correlates with the data shown within this chapter where the topography of the rabbit ICNS appears comparative to other mammalian species.

The presence of larger nerves accessing both the arterial and venous portions of the intrinsic cardiac nervous system correlates with previous studies suggesting that the ICNS is not an isolated neuronal loop but part of the complex neuronal hierarchy including intrathoracic extracardiac ganglia (Kember *et al.*, 2011). Thinner commissural nerves linked between and appeared to connect individual ganglia, suggesting intrinsic cardiac ganglia may have the ability to generate complex feedback loops dependent upon not only the sensory inputs but also cardiac efferent signals. As well as these thinner connecting nerves, larger nerves extended from ganglia and larger neuronal clusters to innervate specific cardiac regions. These neural pathways, previously described as subplexal routes (Batulevicius *et al.*, 2008, Saburkina *et al.*, 2014) are known to be similar in several mammalian species, including the rabbit as demonstrated within this study.

Despite a large proportion of neurons being concentrated within the heart hilum, approximately 1% of neurons were described as ventricular i.e. located at the region of the conus arteriosus. Ganglia that were identified at the region of the conus arteriosus were relatively smaller, especially when compared to the larger 'clusters' identified. These findings correlate with numerous mammalian studies where nerves extend from these ganglia onto the ventral and lateral surfaces of both the left and right ventricles emphasising the importance of the ICNS in the control of ventricular function.

The study by Saburkina *et al.* (2014) reported there to be on average 2200 intrinsic cardiac neurons, yet the number estimated for within this study was slightly lower with

there being approximately 1000-2000 intrinsic cardiac neurons within the rabbit nerve plexus. Slight discrepancies in these values however may be a reflection of differences in experimental and analytical techniques. Neurons histologically stained within some neuronal clusters are arranged into compact ganglia with individual cells sometimes not being fully discernible. As a result of this and to avoid over-estimation, some neurons may not have been counted leading to an underestimation of cell numbers.

Overall, the data presented here with regards to the morphology of the rabbit intrinsic cardiac nervous system corresponds with that shown in a previous study (Saburkina *et al.*, 2014) suggesting that the rabbit ICNS is comparative to that seen in humans and can therefore be used to investigate clinically important defects and diseases including heart failure.

4.3.2 The effects of heart failure on the morphology of the rabbit ICNS

This is the first study to investigate the effect of myocardial infarction and heart failure on the gross morphology of the rabbit ICNS. Examination of the overall topography of the rabbit ICNS during heart failure was compared with that of a control group and an older (age matched) sham operated group. Overall, the distribution of ganglia showed no obvious differences. Neuronal somata, as seen in the control and sham operated groups, lay on the epicardial surface of the heart. Somata were commonly grouped into ganglia (containing 3 or more neurons) with these ganglia primarily residing on the heart hilum and at the roots of the pulmonary veins.

Despite this similarity in the overall distribution of the intrinsic cardiac nervous system in animals with heart failure as a result of myocardial infarction, notable differences were evident. It is well recognised that myocardial infarction and heart failure lead to a disruption in cardiac autonomic control at the peripheral/extrinsic level. Compromised cardiac contractility during heart failure leads to neurohumoral activation in an attempt to stabilise cardiac output. During the acute phase of heart failure there is an increase in the overall sympathetic drive and a reduction in parasympathetic tone (Triposkiadis *et al.*, 2009b, Schwarts and Ferrari, 2011). To date however, relatively little is known as to whether changes in the intrinsic cardiac nervous system contribute to this.

Morphological changes within the ICNS were quantified in response to heart failure, with remodelling in the functioning network of neurons and ganglia post-MI being demonstrated. Heart failure resulted in a significant reduction in the overall number of neuronal somata. The extent to which this remodelling occurred was spatially diverse and dependent upon the site of injury. The reduction in neuronal somata described was evident solely within the atrial regions, particularly on the heart hilum and at the roots of the pulmonary veins, yet not at the region of the conus arteriosus. Several studies investigating the effects of myocardial infarction have concentrated on specific ganglia and not the ICNS as a whole (Rajendran *et al.*, 2016, Nakamura *et al.*, 2016, Hopkins *et al.*, 2000). Utilising the whole heart preparation allows for direct comparison between the overall morphology of the ICNS of control vs heart failure animal groups.

The development of heart failure resulted in the enlargement of neuronal somata within regions known to contain ganglia providing preferential innervation of the ventricles; therefore reflecting the site of infarction. Neuronal enlargement was shown in cells within all regions examined, except for the region of the right atrial GP. This trend was further reiterated with data illustrating the significantly increased length of both the short and long axis of individual somata in all regions when compared to the region of the right atrial GP. Originally, it was thought that the right atrial GP was solely responsible for innervation of the atria and more importantly the sinoatrial node. More recently it has been determined that this is not the case and the right atrial GP plays an integral role in neuronal communication with numerous other GPs (Hou *et al.*, 2007a). Despite this, neuronal somata found within the right atrial GP remain visually unaffected during heart failure in terms of cell size therefore suggesting that this GP remains relatively isolated from the injured region of the heart.

The adaptations and changes shown within the rabbit ICNS appear to be reflex adaptations in response to pathological insult in the infarcted ventricle. Following acute myocardial infarction, Hardwick *et al.* (2014) demonstrated a consequential death of myocytes and neural degeneration. The developing injury caused as a result of ischemic insult leads to chronic neuronal signalling and the transduction of afferent signals to increased sympathetic motor control. Excessive neuronal activation of ganglia involved in the transduction of signals from the infarcted region of the ventricle may result in the

neuronal enlargement and remodelling within the ICNS itself. The cardiac injury, along with chronic neuronal signalling as a result of MI, has been linked to an elevation in the concentration of transcardiac nerve growth factor (NGF) (Singh *et al.*, 2013, Zhou *et al.*, 2004) resulting in the hypertrophy observed in neuronal somata. In addition, NGF has also been linked to an involvement in the neural remodelling of ventricular innervation following myocardial infarction (Singh *et al.*, 2013), with increased protein levels of NGF noted at the peri-ischemic region.

Previous studies, as well as the data shown within this study, show that ventricular innervation extends from numerous ganglia located not only at the ventricular region of the conus arteriosus but also from ganglia located on the venous portion of the heart hilum and at the roots of the pulmonary veins (Saburkina *et al.*, 2014, Batulevicius *et al.*, 2008, Pauza *et al.*, 2002b). Nerves extend epicardially from these ganglia via numerous routes including by the arterial part of the heart hilum and between the roots of the aorta and pulmonary trunk as well as via dorsal routes extending from larger ganglia on the venous portion of the heart. Extensive scar tissue was clearly visible following myocardial infarction. This scar formation extended from the region of the original coronary artery ligation at the left coronary artery, creating a peri-infarct region. Neuronal denervation was noted within this region, similar to data shown by Lorentz *et al.* (2013), where denervation occurred adjacent to and at the region of the original insult. This was accompanied with an observable increase in the number and density of visibly stained nerves on the remainder of the ventricular epicardium.

Intrinsic cardiac ganglia containing afferent neurons transduce sensory inputs arising from diverse regions of the heart. The sensory transduction of chronically infarcted ventricular tissue is likely to be responsible for a large proportion of pathological changes including the apparent hyperinnervation of the remaining ventricular nerve fibres in an attempt to compensate for the neuronal loss as a result of scar formation.

The only differing factor between animals in the sham-operated group and the heart failure group was the coronary artery ligation during surgery, resulting in the observable scar formation. It can therefore be assumed that the structural or function changes noted within the ICNS are as a result of MI. Older and heavier animals survived coronary artery ligation surgery more readily, therefore sham operated animals were used to

further ensure that any variation in results was due to MI and HF. One key factor to take into account is the local damage likely to be caused to nerves spanning the ventricles during the ligation of the coronary artery. This damage, which would not exist in the sham operated group, is unfortunately unavoidable when using this heart failure model. Further modification is therefore required to eliminate such damage, possibly with the utilisation of microspheres or polystyrene beads (Sabbah *et al.*, 1991).

Comparison of the anatomy of the ICNS along with quantification of intrinsic neuronal somata in the rabbit whole-mount preparation between the conventional and sham-operated group showed there to be little or no modulation of the ICNS due to age, weight or the experience of surgery. This data is supported by a previous study done by Saburkina *et al.* (2014), where a comparison was made of the intrinsic nerve plexus between juvenile (ranging from 2-6 months old and weighing $2.6 \pm 0.4\text{kg}$) and aged rabbits (ranging from 3-4 years old and weighing $4.9 \pm 0.2\text{kg}$).

4.3.3 The immunohistochemical profile of the rabbit ICNS in healthy rabbits

The ICNS is a crucial part of the cardiac neuroaxis which functions to control cardiac electrical and mechanical function. In order to maintain this control, a balance between stimulatory sympathetic and inhibitory parasympathetic is crucial. Despite the histological staining method used in this study producing an overall map of the intrinsic cardiac nervous system, the AChE stain is not suitable to determine in greater detail the full phenotype of the ICNS. In order to delve deeper into the makeup of the ICNS, more reliable and more specific markers were used including immunohistochemical labels for ChAT, TH and nNOS.

The data within this chapter describes and characterises the distribution of cholinergic and adrenergic intrinsic neurons of the rabbit heart of control animals, as well as the distribution of the neuromodulator nNOS. Neurons immunoreactive for ChAT were significantly more abundant compared to those immunoreactive for both TH and nNOS. Choline acetyltransferase is the enzyme involved in the biosynthesis of acetylcholine, primarily at nerve terminals. Cholinergic neurons express ChAT making anti-ChAT antibodies useful in the specific targeting of such neurons. Studies in various mammalian species show that between 60 and 100% of cardiac neurons are ChAT immunoreactive.

These ChAT-IR neuronal somata are often accompanied by an abundance of cholinergic nerve fibres, particularly around the sinoatrial and atrioventricular nodal regions (Inokaitis *et al.*, 2016, Hoover *et al.*, 2009). These studies, along with the data presented within this study supports the idea that the majority of neuronal somata within the ICNS play a role in the inhibitory control of cardiac function, computing downstream neuronal inputs from the cardiac vagus.

Intrinsic cardiac ganglia consisted of numerous phenotypically distinct neurons, as seen in previous studies (Rysevaite *et al.*, 2011b, Hoover *et al.*, 2009). This confirms the ever-increasing complexity of the ICNS and further demonstrates that the ICNS is not merely a parasympathetic relay station for efferent postganglionic neurons. Numerous neuronal somata IR for TH have been illustrated in this study. Tyrosine hydroxylase, the rate limiting enzyme involved in the biosynthesis of catecholamines including noradrenaline and dopamine, symbolising a sympathetic role. Generally, neuronal somata immunoreactive for TH exist as principal neurons, inter and intra-ganglionic nerves and SIF cells (Rysevaite *et al.*, 2011b). SIF cells, identified within this study to be involved in the rabbit ICNS, were found to be located within larger ganglia or grouped into small clusters. As their name suggests, SIF cells were recognisable by their more intense staining, however in comparison these neurons were much smaller compared to all other cell phenotypes (cell lengths of approximately 10µm). Despite these cells being identified previously within the ICNS of other mammalian species and it being hypothesised that these neurons act as interneurons within ganglia, their precise function still remains unknown. Relatively larger neuronal somata expressing TH were described in this study suggesting a sympathetic adrenergic role within the ICNS and the possibility of the involvement of these ganglia in the functional effects of sympathetic activation.

It is likely that the ChAT positive neurons within this study are innervated by efferent vagal fibres, however the problem of understanding role and innervation of TH-positive neurons remains unresolved. A study by Rysevaite *et al.* (2011a) reported for the first time the presence of a population of intrinsic neurons exclusively positive for TH in the mouse heart. Although it is possible that TH expressing neurons could function in a similar manner to those within the intrathoracic ganglia including the stellate ganglia,

this is still an area under some debate. Fukuda *et al.* (2015) described the innervation of sympathetic efferent neurons within the ICNS as coming from postganglionic efferent nerve fibres originating from either the T1-T4 region of the spinal cord directly or via the sympathetic efferent neurons within extracardiac intrathoracic ganglia such as the stellate and middle cervical ganglia suggesting that such neurons within the ICNS do play a role in sympathetic control of the heart. In contrast to the presence of TH within intrinsic neurons, Hoard *et al.* (2007) suggested that TH is made but not exported to terminal varicosities, hence the observation that many TH-positive neurons within intrinsic cardiac ganglia stained more intensely than noradrenergic neurons of the stellate ganglia.

Data presented in this study also illustrate the presence of neurons IR for nNOS. Neuronal nitric oxide synthase is known to be localised in intrinsic cardiac vagal neurons (Habecker *et al.*, 2016). Parasympathetic control of the heart implemented by the cardiac vagus nerve is hypothesised to be associated with neurons with the ICNS (Lo *et al.*, 2013). NO has been shown to facilitate the release of acetylcholine and induce bradycardia during activation of the vagus nerve (Herring and Paterson, 2001) via a cGMP pathway (Herring *et al.*, 2001). The abundant presence of ChAT within the ICNS and the idea that the innervation from the vagus nerves is transmitted via the ICNS would therefore imply that nNOS and NO would be expressed alongside these ganglia.

It is now well known that the ICNS does not solely consist of cholinergic and adrenergic neurons and nerve fibres. Over recent years it has been shown using immunohistochemical techniques that an increasing number of neurochemicals are presented within the ICNS. As well as the 3 neurochemicals investigated throughout this chapter, studies have shown the presence of sensory neurons reactive for substance P, CGRP, NPY and VIP.

Unfortunately, due to time constraints, study of the immunohistochemical profile of the rabbit ICNS during heart failure was not possible. In terms of the neurochemical profile of the ICNS following myocardial infarction and heart failure, very little is known. Of the few studies to have investigated the morphological remodelling of neurons within the ICNS, little has been determined about the overall change in phenotype. Based on studies where differentiation of the neurochemical phenotype has been examined

within intrinsic cardiac ganglia (Rajendran *et al.*, 2016) and cardiac neurons (Olivas *et al.*, 2016), significant alterations and differences would be expected throughout the ICNS following MI. Following MI, there is a transient increase in the cardiac acetylcholine content (Olivas *et al.*, 2016). This is due to an increase in the acetylcholine released from transdifferentiated cardiac sympathetic neurons which prior to injury were primarily involved in the release of noradrenaline and functioned in a sympathetic manner.

These findings suggest a significant role of the ICNS during heart failure in the aim of counteracting the centrally mediated parasympathetic withdrawal, however it is also feasible that this mechanism is spatially divergent and dependent upon the regions of intrinsic cardiac ganglia directly affected by myocardial infarct. MI has also been shown to induce a decrease in the cholinergic phenotype of ganglia within the ventral interventricular GP (VIV GP) (Rajendran *et al.*, 2016) along with regional increases in adrenergic sensitivity and nNOS expression (Hardwick *et al.*, 2014). Despite evidence suggesting increased nNOS expression occurs following MI, this is not the case in the right atrial GP (Dawson *et al.*, 2008), correlating with the regional effects of heart failure demonstrated within this study.

Heart failure also results in changes in the presence of VIP, known to be a modulator of cardiac function and involved in the vasodilation of cardiac vasculature. The study by Parsons *et al.* (2006) demonstrated that fibres immunoreactive for VIP were present in approximately 70% of ganglia in the guinea pig. Significant increases in the expression of VIP independent of ganglia positioning within the ICNS has been described as a result of myocardial infarction (Rajendran *et al.*, 2016); a likely consequence of the reduced ability of the heart to maintain cardiac output and blood pressure.

Overall, it can therefore be hypothesised that the ICNS is highly involved in cardiac autonomic adaptation to preserve cardiac function and counteract the damage caused by myocardial infarction and heart failure. In order to fully determine the role of the ICNS, further study is required into the phenotypical divergence of intrinsic cardiac ganglia during heart failure as well as any phenotypic changes of nerve fibres innervating the ventricles.

Chapter 5: The functional role of intrinsic cardiac ganglia in the rabbit

5.1 Introduction

Until recently, very little research had been conducted into the functional capability of the ICNS in terms of the cardiac control of electrophysiology. With the increased interest in the ICNS over the past decade and the development of comprehensive morphological maps, more and more studies have been aimed at determining the functional role of individual ganglia as well as the way in which specific ganglia interact to produce both local and remote cardiac changes (Cardinal *et al.*, 2009, Butler *et al.*, 1990, Hou *et al.*, 2007a).

The ICNS is thought to be the final stage of control of cardiac function involving the processing of sensory inputs as well as parasympathetic and sympathetic efferent inputs (Armour, 2004). Historically, it was believed that the right atrial GP was solely responsible for chronotropic regulation and the inferior vena cava-inferior left atrial GP solely involved in dromotropic regulation. More recently however, studies have demonstrated an increased level of complexity with ganglia within all regions of the ICNS demonstrating some chronotropic and dromotropic regulatory capacity (Cardinal *et al.*, 2009).

Heart failure induces morphological changes to neurons within the ICNS (Nakamura *et al.*, 2016, Rajendran *et al.*, 2016). Limited information regarding how these changes affect the ability of the ICNS to control cardiac indices is currently available. During heart failure, the ability of the heart and the ICNS to transduce afferent signals displays increased levels of heterogeneity with afferent signals from the injury site becoming attenuated in comparison to neurons at the border or away from the infarcted region (Rajendran *et al.*, 2016). This reduction in the functional connectivity of the ICNS following MI, along with the centrally mediated parasympathetic withdrawal evident within the ICNS neurons, leads to an increased propensity for the induction of cardiac arrhythmias including ventricular tachyarrhythmia.

Understanding the various aspects of the cardiac neuronal hierarchy, right down to the precise roles of the intrinsic cardiac ganglia in altering cardiac electrophysiology, enables the potential development of neuromodulation therapies for cardiac diseases including

ventricular tachyarrhythmia and atrial fibrillation. The stimulation or ablation of ganglia within the ICNS could aid in the potential treatment of cardiac diseases including heart failure where autonomic imbalance plays a significant role in the development of potentially lethal arrhythmias.

To date, little or no investigation has been aimed at determining the influences of spatially divergent ganglionic plexuses within the ICNS on cardiac electrophysiology in the rabbit, despite the rabbit often being used to investigate such factors. The primary aim of this chapter was therefore to determine the functional capabilities of specific ganglia within the rabbit ICNS using electrical stimulation, therefore activating both parasympathetic and sympathetic neurons when present. Following on from this, the effects of MI and heart failure on the ability of the ICNS to function in response to electrical stimulation were investigated utilising the coronary artery ligation model in the rabbit described previously.

5.2 Results

The interaction between ganglia within the ICNS is complex and involves numerous feedback loops. The following experiments were conducted with the aim of quantifying the functional capability of these ganglia in a rabbit model.

The Langendorff whole heart preparation was used to investigate the effect of electrical stimulation of intrinsic cardiac neurons on numerous electrophysiological parameters including heart rate and atrioventricular delay. In brief, ganglia were stimulated at 50% of the cardiac pacing threshold in either sinus rhythm or under constant atrial pacing. Changes in heart rate, left ventricular pressure, MAP duration (MAPD) and atrioventricular delay were recorded at each site. In order to allow for specific stimulation at the sites indicated in figure 5.1 and to limit the spread of electrical stimulation, small current strengths were used at a very short pulse duration of 0.1ms.

5.2.1 The effects of electrical stimulation of cardiac intrinsic ganglionated plexuses

The effect of electrical stimulation of intrinsic cardiac ganglia was examined in 14 animals (weighing 2 – 2.5kg). Ganglionated plexuses were stimulated within the regions shown in figure 5.1 with the RNC, located medially to the root of the RCV and dorsally to the root of the RPV being examined in all 14 animals. Intrinsic ganglia located within the LNC, right atrial GP and PVCV regions were investigated in fewer animals (8/14, 9/14 and 8/14 respectively).

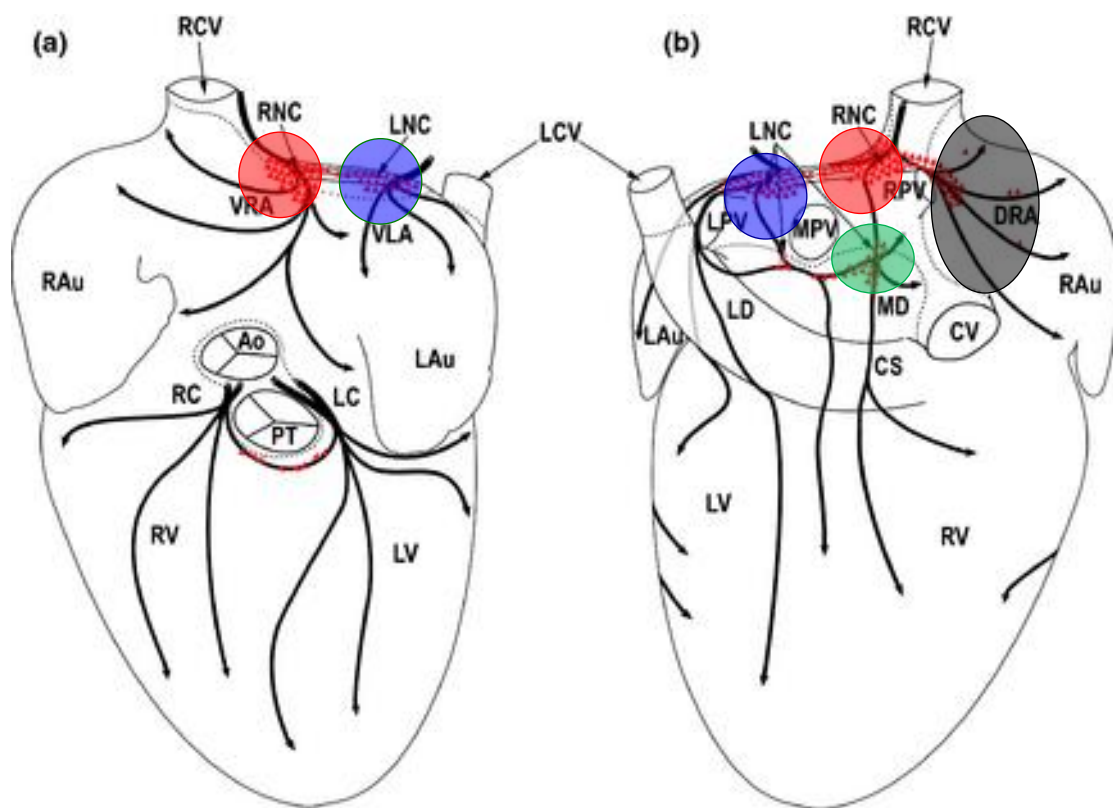


Figure 5.1. Ventral (a) and dorsal (b) view of the heart indicating the regions for electrical stimulation of the intrinsic cardiac ganglia. Abbreviations: Ao, aorta; CS, coronary sinus; CV, caudal vein; DRA, dorsal right atrial subplexus; LAu, left auricle; LC, left coronary subplexus; LCV, left cranial vein; LD, left dorsal subplexus; LNC, left neuronal cluster; LPV, left pulmonary vein; LV, left ventricle; MD, middle dorsal subplexus; MPV, middle pulmonary vein; PT; pulmonary trunk; RAu, right auricle; RC, right coronary subplexus; RNC, right neuronal cluster; RPV, right pulmonary vein; RV, right ventricle; VLA, ventral left atrial subplexus; VRA, ventral right atrial subplexus.

5.2.1.1 Chronotropic responses to electrical stimulation of intrinsic cardiac ganglia

The effects of electrical stimulation of intrinsic cardiac ganglia on heart rate during sinus rhythm were examined at a total of 56 sites. Three specific types of response were noted; i) bradycardia alone, ii) tachycardia alone and iii) bradycardia followed by tachycardia (figure 5.2). The development of tachycardia occurred on average ~5s post-stimulation commencement compared to bradycardia responses which occurred almost instantly (figure 5.2). Significant heart rate changes were evoked in 2 out of the 4 regions when the frequency of stimulation was 20Hz or more: the RA and the RNC (figure 5.3). Stimulation of plexuses within the LNC and PVCV regions at all frequencies up to 50Hz resulted in only small reductions in heart rate (-6 ± 11 bpm and -11 ± 7 bpm respectively). Overall, electrical stimulation induced tachycardia alone at 5% of sites tested (3/14 animals), all at sites within the RA region around the root of the right pulmonary vein. On the other hand, bradycardia responses were produced by electrical stimulation in all regions examined (figure 5.4). The most pronounced bradycardia responses during stimulation at 50Hz were produced in response to stimulation of the hilum region of the RNC (figure 5.4) and the RA region, with the change in heart rate (bpm) ranging from 0 to -110bpm and 0 to -101bpm respectively (average change $-25.5 \pm 4.2\%$ and $-21 \pm 12.0\%$ respectively). Bradycardia followed by tachycardia was recorded in one animal and only at 1 loci; within the RNC (155 to 145 to 160 bpm during stimulation at 10Hz). At all loci where a heart rate response was recorded during electrical stimulation, the level of heart rate change, whether a bradycardia or tachycardia, altered in a frequency dependent manner (figure 5.4). The average change in bradycardic heart rate responses increased progressively as the frequency of electrical stimulation applied to all regions increased up to 50Hz. There was no significant difference in the average change in all regions at when stimulated at 10Hz. The average reduction in heart rate during electrical stimulation at the RNC was significantly different at 20Hz ($p < 0.01$), 30Hz ($p < 0.01$), 40Hz ($p < 0.001$) and 50Hz ($p < 0.0001$) and at the RA region at 20Hz, 30Hz, 40Hz ($p < 0.05$) and 50Hz ($p < 0.01$). In comparison, despite small reductions in heart rate being noted, no statistically significant changes in HR were observed at the LNC and PVCV regions when stimulation occurred between 10 and 50 Hz.

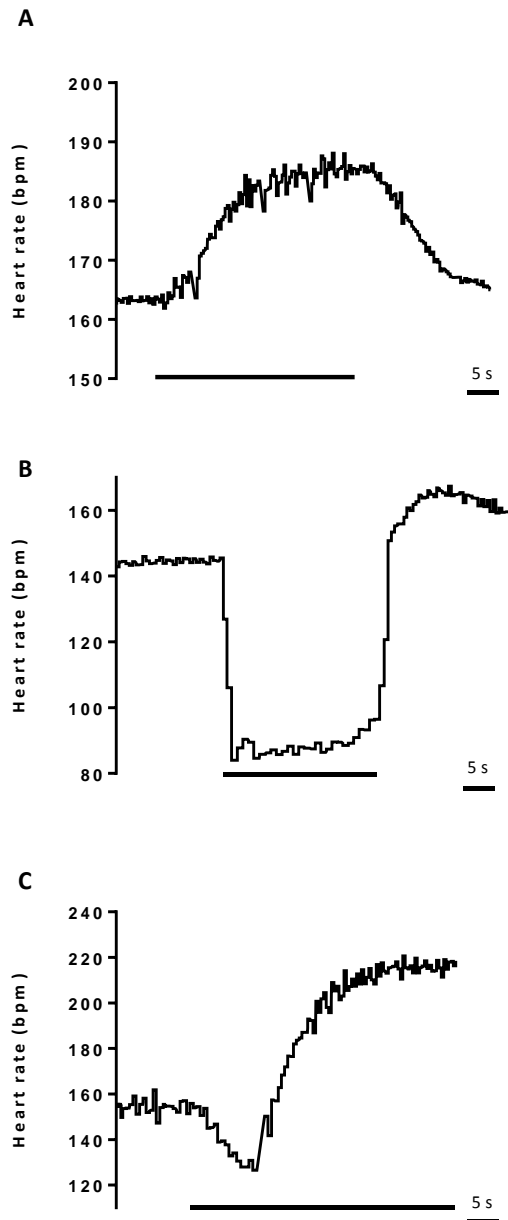


Figure 5.2. Electrical stimulation induced heart rate responses. Example raw heart rate traces illustrating the effects of electrical stimulation on individual ganglia. Stimulation of ganglia within the RA region occasionally resulted in a sympathetic increase in heart rate (**A**) with the majority of responses (particular within the RNC region as illustrated) resulting in a parasympathetic decrease (**B**). The heart was given a period without stimulation in order to allow the sympathetic ‘rebound increase’ seen following the cessation of electrical stimulation resulting in a bradycardia response. Episodes of bradycardia followed by tachycardia (**C**) occurred entirely during stimulation and not as an after effect, within the RNC region.

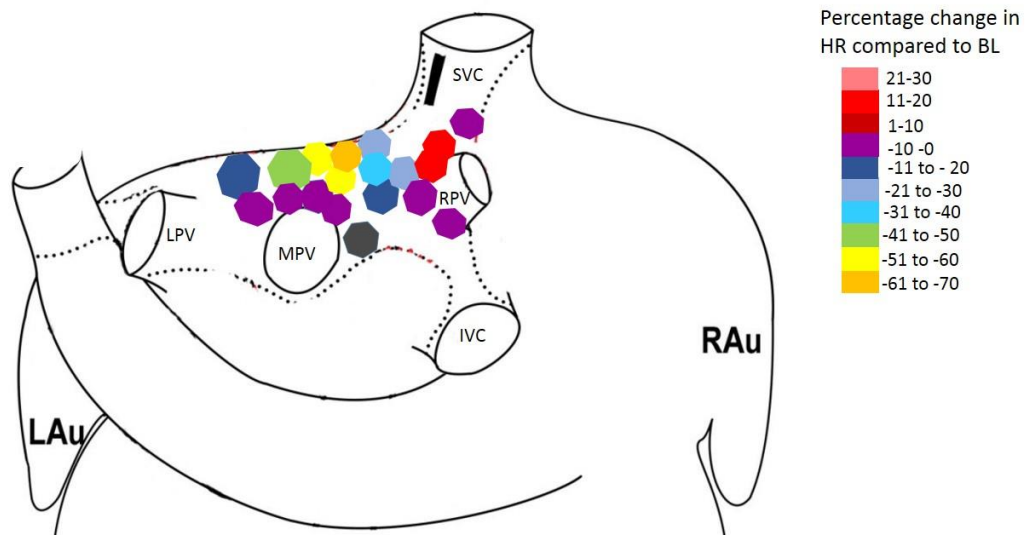


Figure 5.3. A map of the dorsal view of the heart illustrating the percentage change in heart rate from baseline during electrical stimulation of regions within the rabbit ICNS. BL, baseline; IVC, inferior vena cava; LAu, left auricle; LPV; left pulmonary vein; MPV, middle pulmonary vein; RAu, right auricle; RPV, right pulmonary vein; SVC, superior vena cava.

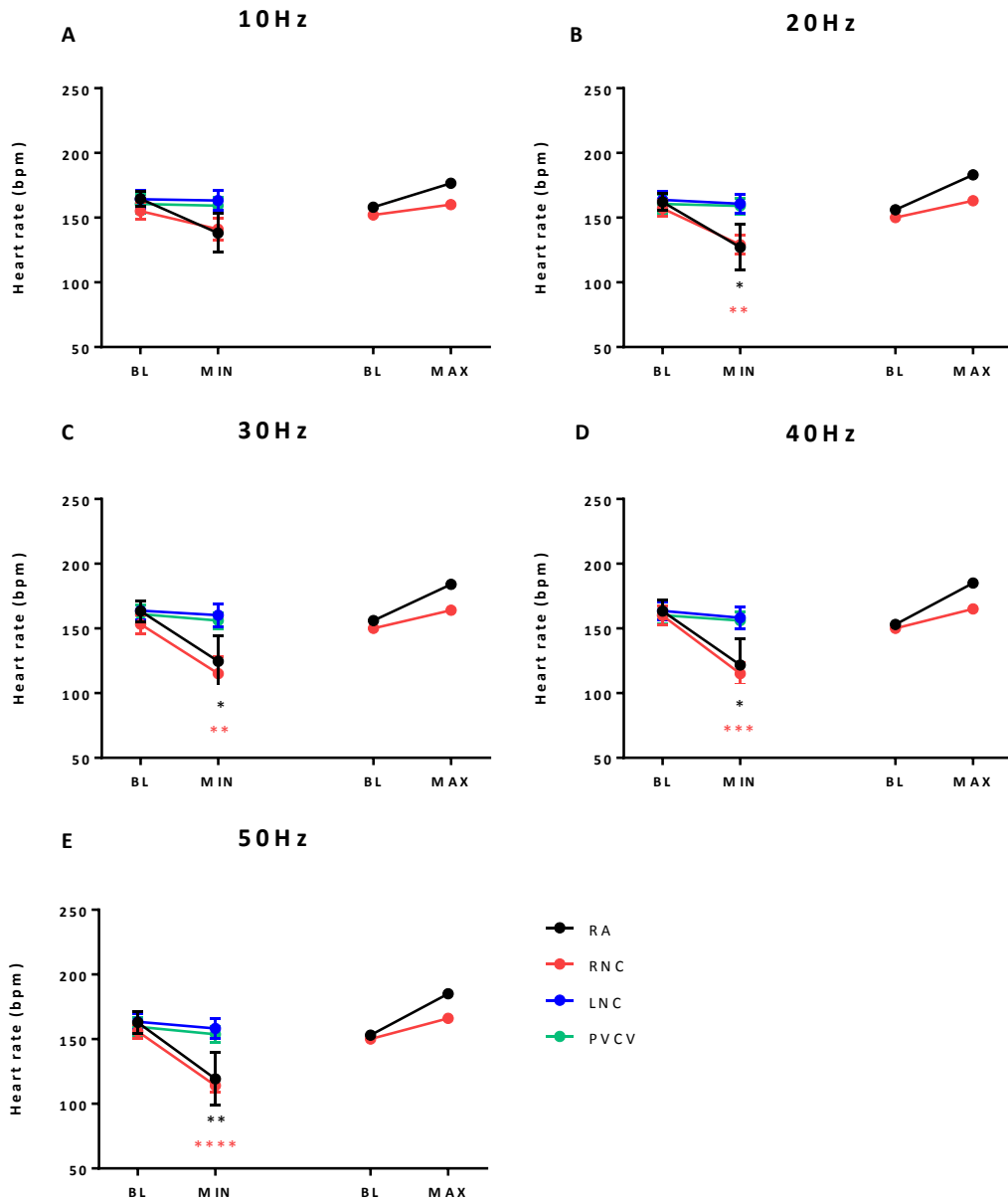


Figure 5.4. Heart rate responses induced by electrical stimulation at sites in RA, RNC, LNC and PVCV in control animals. At all sites where electrical stimulation of intrinsic cardiac ganglia produced a bradycardic response, the average reduction in heart rate hearts was compared to the average baseline heart rate. At sites where electrical stimulation produced a tachycardic response, the average baseline heart rate prior to stimulation of these loci was also compared with the average increase in heart rate. Mean data is shown at 10Hz (A), 20Hz (B), 30Hz (C), 40Hz (D) and 50Hz (E). Data represents mean \pm SEM. BL = baseline. N= 56 (14 animals). Two-way ANOVA was used to compare baseline with minimum and maximum values. * $p < 0.05$, ** $p < 0.01$, *** $p < 0.001$, **** $p < 0.0001$.

5.2.1.2 Left ventricular pressure and monophasic action potential duration changes

Mean data illustrating baseline and peak left ventricular pressure (LVP) during sinus rhythm are shown in figure 5.5A along with the mean percentage change in LVP from baseline (figure 5.5B). There was no significant difference in mean LVP during electrical stimulation when compared to baseline between each of the 4 regions tested as well as no significant difference in the percentage change in LVP when each group was compared. There was no significant difference in LVP response during stimulation of sites that induced a bradycardia when compared to sites where a tachycardia response was noted.

Monophasic action potential duration (MAPD) was recorded in all experiments. No significant difference in the percentage change in MAPD from baseline was seen in any loci stimulated even when significant changes in heart rate were noted (figure 5.5C and D).

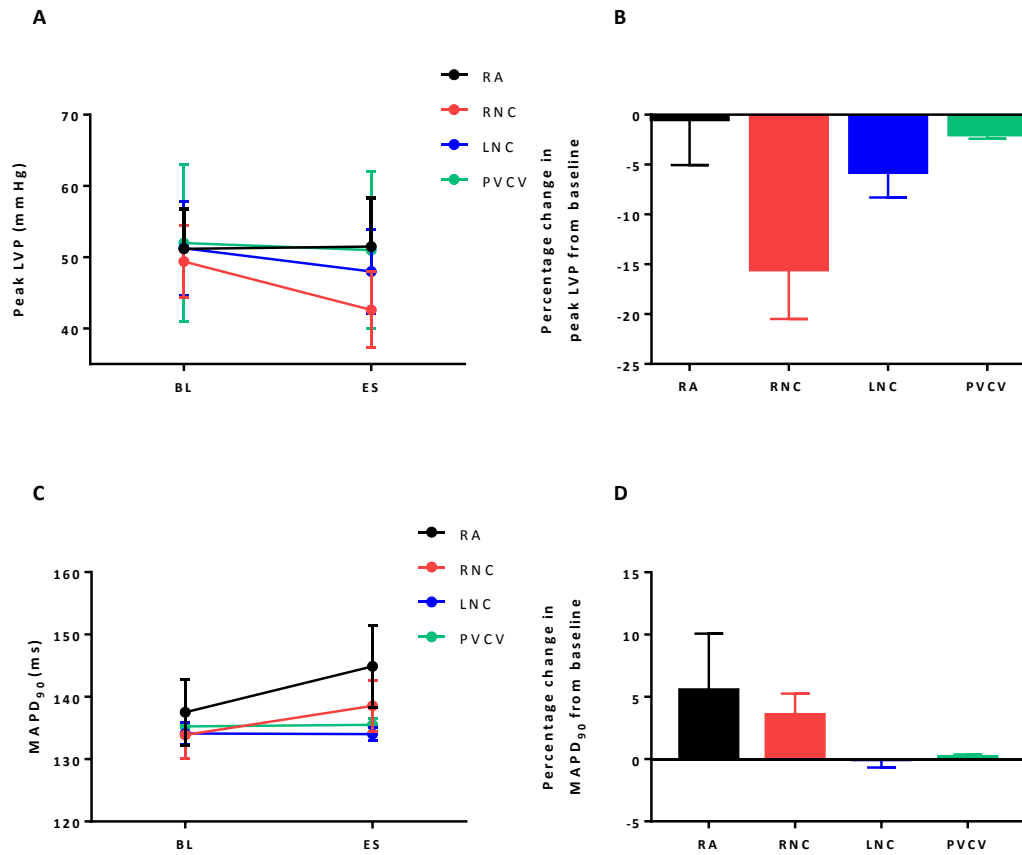


Figure 5.5. LVP and MAPD responses during electrical stimulation at sites in RA, RNC, LNC and PVCV. The effects of electrical stimulation of intrinsic cardiac ganglia on the average peak left ventricular pressure (**A**) and percentage change from baseline (**B**) where no significant change was recorded. Electrical stimulation on intrinsic cardiac ganglia resulted in no significant change in MAPD₉₀ compared to baseline (**C**) with no significant difference in the percentage change in MAPD₉₀ from baseline when compared between all four regions investigated (**D**). n = 47 (10 animals).

5.3 The functional role of the ICNS following MI

The data presented in the previous chapter along with data from previous studies demonstrates that chronic myocardial infarction induces neuronal remodelling. The true extent with which this morphological alteration occurs in a rabbit model of heart failure was discussed previously but understanding the effects of this change on cardiac electrophysiology could provide a crucial insight into understanding clinical implications following an incidence of MI.

5.3.1 Chronotropic responses to electrical stimulation of intrinsic cardiac ganglia following MI

Following on from the results obtained in the control group of animals, experiments were repeated in a further 11 animals; 7 that had undergone coronary artery ligation surgery (3.9 ± 0.3 kg) and 4 from the sham operated group (3.8 ± 0.1 kg). The effects of electrical stimulation were again examined at the 4 regions shown in figure 5.1 at frequencies ranging from 10 - 50Hz. Chronotropic responses to electrical stimulation altered in frequency dependent manner in both the sham operated (figure 5.6) and heart failure groups (figure 5.7).

Only small reductions in heart rate (1-6 bpm) were noted at all frequencies when ganglia were stimulated within the LNC and at the PVCV region in the sham operated group, correlating with the changes evident in the control group. During electrical stimulation, tachycardia responses were noted in just 1 out of the 4 sham operated animals (25%) compared to 3 out of 14 control animals (21%). There was no significant between the average increase in the heart rate during stimulation within all regions in both the control and sham operated groups.

No significant difference being noted in either the average heart rate change or the percentage change in HR between all 3 groups examined (control, sham and heart failure). As with the sham operated group, only small reductions in heart rate (1-6bpm) were noted at all frequencies when ganglia were stimulated within the LNC and PVCV region in the heart failure group. During electrical stimulation, tachycardia responses

were noted in 3 out of the 7 (43%) animals that had undergone coronary artery ligation surgery compared to just 25% previously described in the sham operated group. As with the control animals, episodes of bradycardia followed by tachycardia were recorded at one loci in an animal from the heart failure group as well as one animal from the sham operated group, both within the RNC.

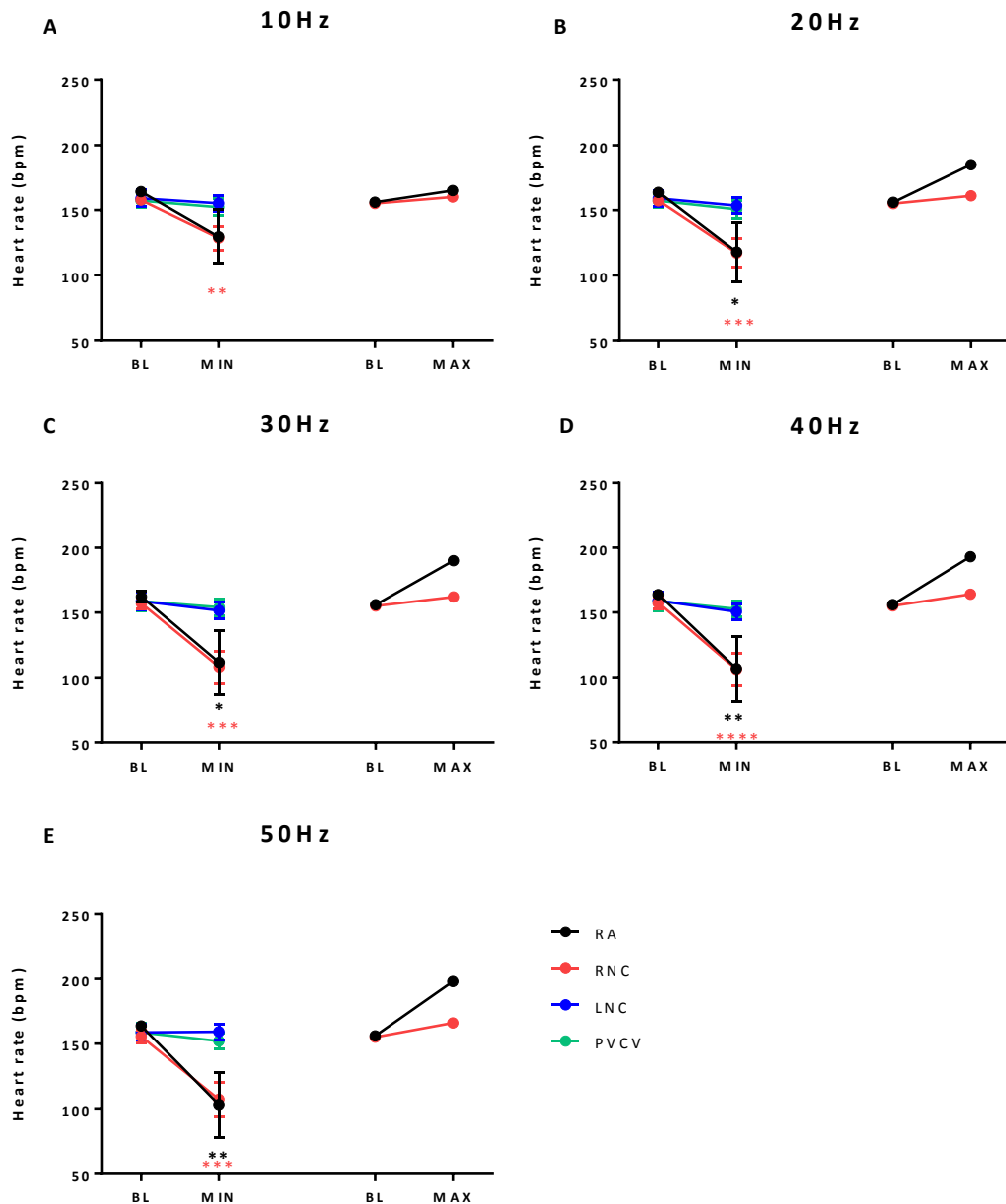


Figure 5.6. Heart rate responses induced by electrical stimulation at sites in RA, RNC, LNC and PVCV in the sham operated group. At all sites where electrical stimulation of intrinsic cardiac ganglia produced a bradycardic response, the average reduction in heart rate hearts was compared to the average baseline heart rate. At sites where electrical stimulation produced a tachycardic response, the average baseline heart rate prior to stimulation of these loci was also compared with the average increase in heart rate. Mean data is shown at 10Hz (A), 20Hz (B), 30Hz (C), 40Hz (D) and 50Hz (E). Data represents mean \pm SEM. BL = baseline. N = 22 (4 animals). Two - way ANOVA was used to compare baseline with minimum and maximum values. * $p < 0.05$, ** $p < 0.01$, *** $p < 0.001$, **** $p < 0.0001$.

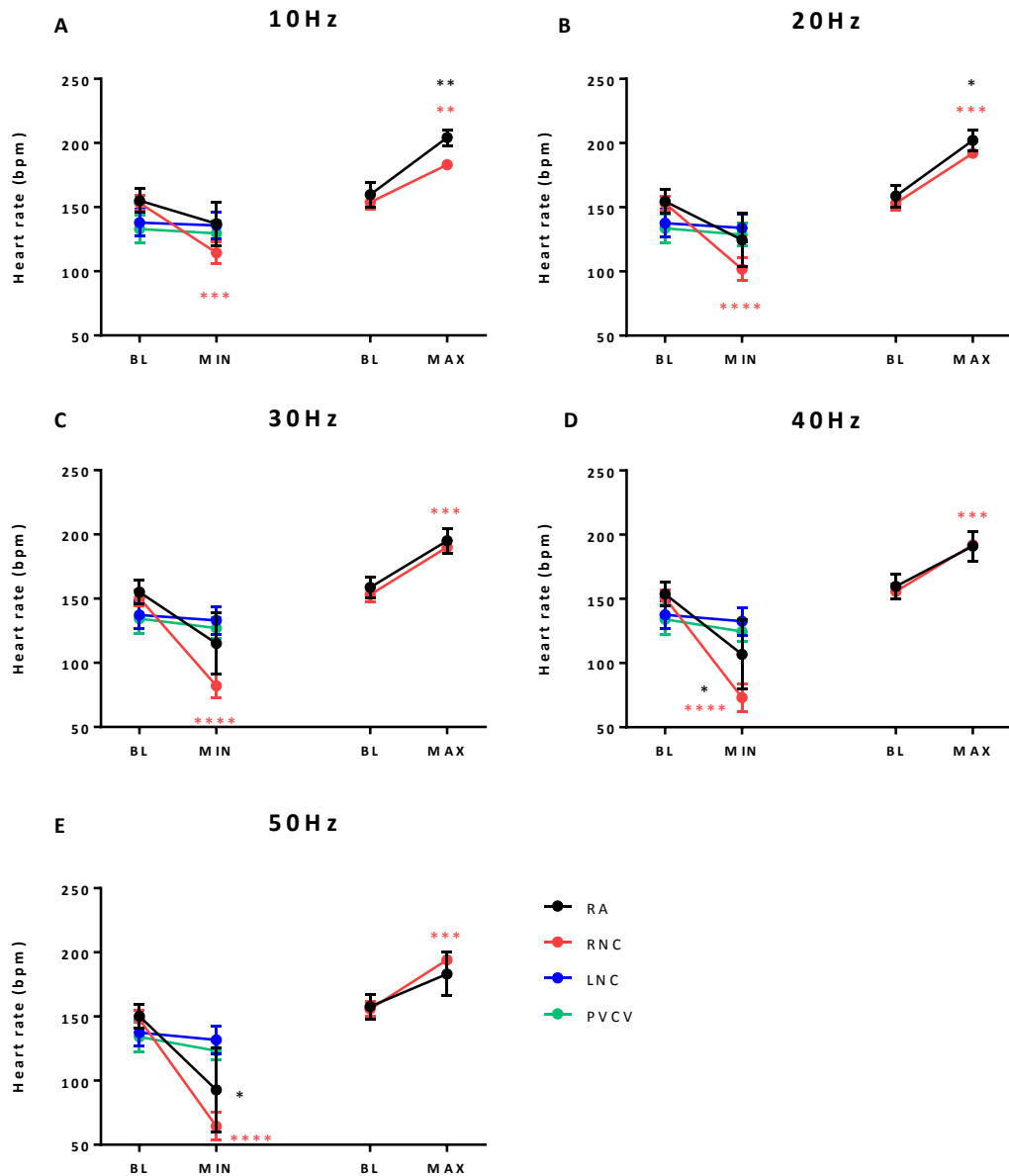


Figure 5.7. Heart rate responses induced by electrical stimulation at sites in RA, RNC, LNC and PVCV in the heart failure group. At all sites where electrical stimulation of intrinsic cardiac ganglia produced a bradycardic response, the average reduction in heart rate hearts was compared to the average baseline heart rate. At sites where electrical stimulation produced a tachycardic response, the average baseline heart rate prior to stimulation of these loci was also compared with the average increase in heart rate. Mean data is shown at 10Hz (A), 20Hz (B), 30Hz (C), 40Hz (D) and 50Hz (E). Data represents mean \pm SEM. BL = baseline. N = 44 (7 animals). Two-way ANOVA was used to compare baseline with minimum and maximum values. * $p < 0.05$, ** $p < 0.01$, *** $p < 0.001$, **** $p < 0.0001$.

The average bradycardic response was larger in animals from the heart failure group at all frequencies examined compared with the sham operated group, when ganglia within the RNC were stimulated. Significant differences in the average heart rate increase were noted in both the RA region (at 10Hz, $p < 0.05$) and within the RNC (at all frequencies tested) (figure 5.7) of the HF group compared to the sham operated group.

The percentage change in heart rate was calculated for each loci tested for both bradycardic and tachycardic responses. The average percentage change (presented as mean \pm SEM) within each of the 4 regions (RA, RNC, LNC and PVCV) was compared between the control, sham operated and heart failure groups. There was no significant difference in the percentage heart rate change within all regions when the control group was compared with the sham operated group. This was also the case when the results produced during electrical stimulation of the LNC and PVCV regions were compared between all three groups investigated, with no significant difference being evident.

Conversely, changes in heart rate as a result of stimulation at RNC and RA were significantly different in hearts from the heart failure group when compared to both the control and sham operated groups. The largest difference seen following myocardial infarction in the effects of electrical stimulation on intrinsic cardiac ganglia was recorded at loci within the RNC. The average percentage decrease in heart rate was noticeably larger in the heart failure group and at frequencies between 20 – 50Hz this decrease was significantly different when compared to both the control and sham-operated groups (figure 5.8).

A larger increase in heart rate during stimulation of particular loci within the RA and primarily the RNC regions was seen in the heart failure group when compared to both the controls and sham operated groups.. Tachycardia as a result of electrical stimulation within the RNC was significantly increased at all frequencies and the average change in heart rate was significantly different to that of the control and sham operated group (figure 5.8). Conversely, tachycardic responses as a result of stimulation of loci within the RA of hearts within the heart failure group showed a decrease with increasing frequency of stimulation, reiterating the overall complexity of the rabbit ICNS and the functional capability of the neurons within it.

5.3.2 Left ventricular pressure and monophasic action potential duration changes in the heart failure and sham operated groups

As with the control group, the left ventricular pressure and the MAPD were measured in sinus rhythm during electrical stimulation of ganglia. There was no significant difference in the average maximum LVP measurements between the control and sham operated groups (51.0 ± 0.6 mmHg vs 53.8 ± 0.9 mmHg respectively). When compared to the results from the heart failure group, there was a significant difference in the average maximum LVP (HF: 37.9 ± 7.0) ($p < 0.05$). Despite this difference, there was no significant difference in the average LVP during baseline when compared to the average LVP during electrical stimulation at loci within all regions tested.

The previous data regarding changes in MAPD during electrical stimulation was compared to data from both the sham operated and heart failure groups, with results from both groups showing no evidence of a significant change in MAPD during electrical stimulation at all frequencies investigated (10 – 50Hz).

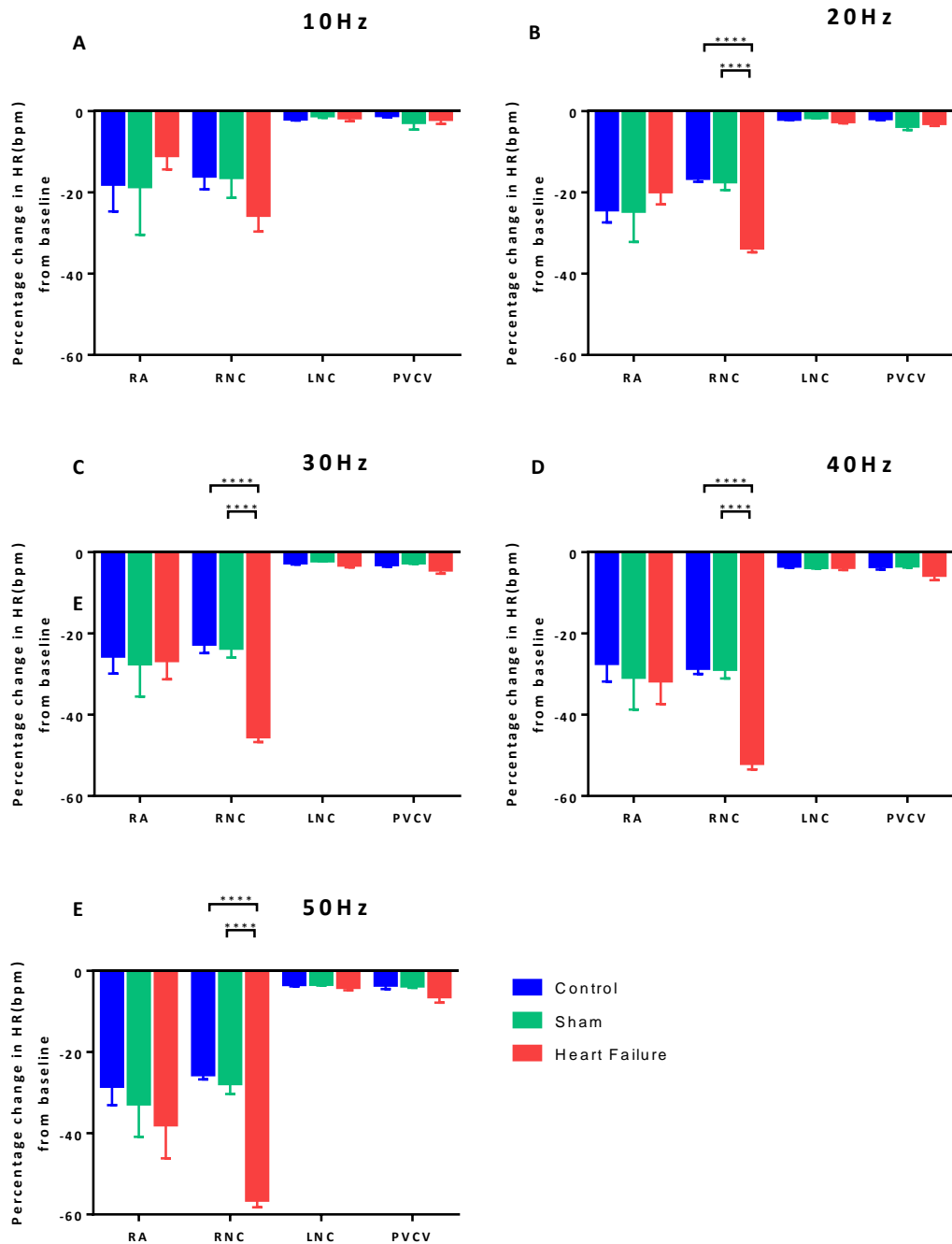


Figure 5.8. The percentage change in HR reductions during electrical stimulation of intrinsic cardiac ganglia. Mean data showing the average percentage change in bradycardic HR responses during electrical stimulation within all regions at 10Hz (A), 20Hz (B), 30Hz (C), 40Hz (D) and 50Hz (E). Data represents mean \pm SEM. Two-way ANOVA was used to compare data between control, sham and HF groups. * $p < 0.05$, ** $p < 0.01$, *** $p < 0.001$, **** $p < 0.0001$.

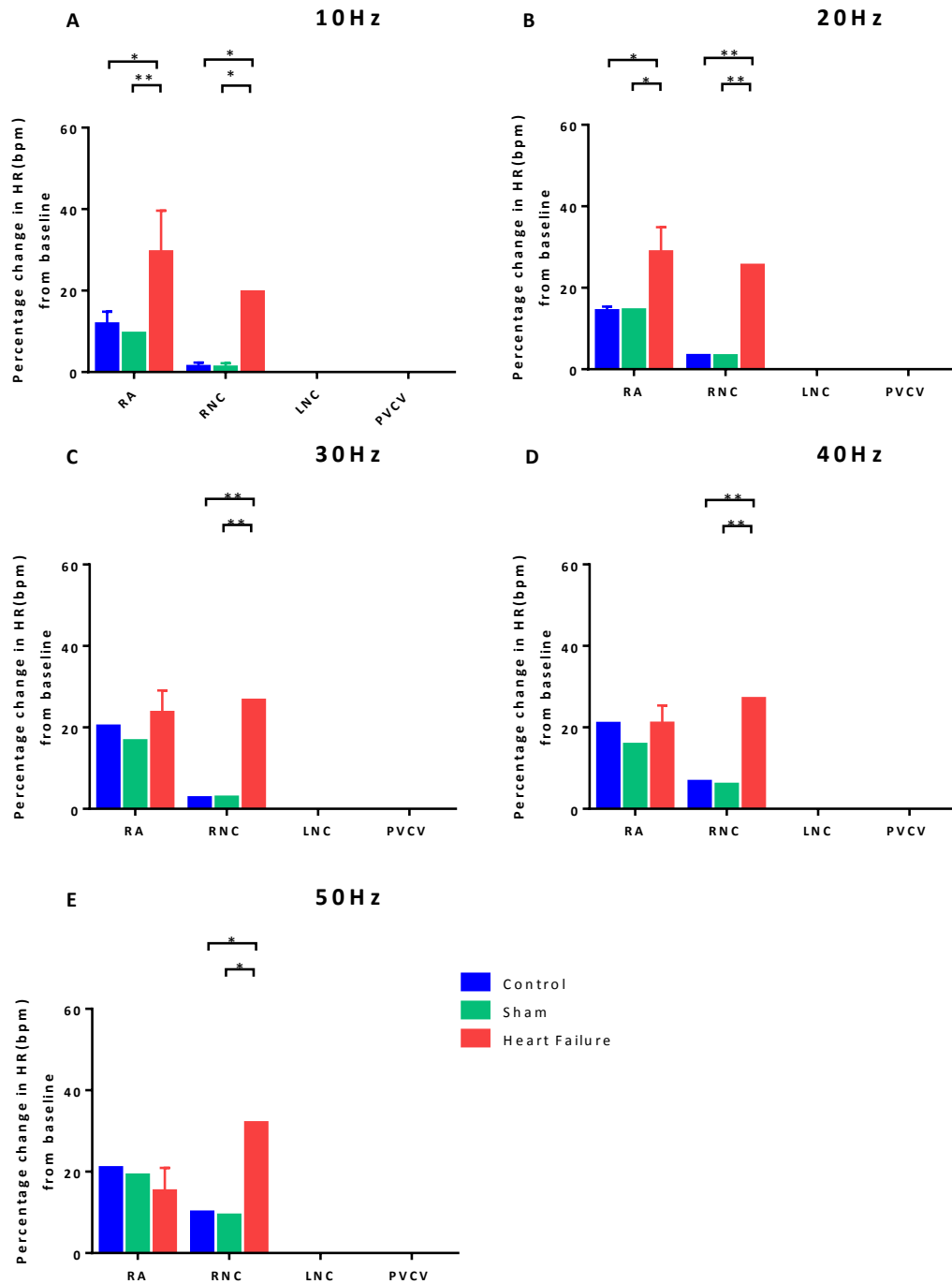


Figure 5.9. The percentage change in tachycardic HR responses during electrical stimulation of intrinsic cardiac ganglia. Mean data showing the average percentage change in tachycardic HR responses during electrical stimulation within all regions at 10Hz (A), 20Hz (B), 30Hz (C), 40Hz (D) and 50Hz (E). Data represents mean \pm SEM. Two - way ANOVA was used to compare data between control, sham and HF groups. * $p < 0.05$, ** $p < 0.01$, *** $p < 0.001$, **** $p < 0.0001$.

5.4 Dromotropic responses to electrical stimulation of intrinsic cardiac ganglia

Atrioventricular conduction was measured during constant atrial pacing by measuring the interval between the pacing stimulus and the ventricular monophasic action potential recorded from the left ventricle. In order to account for increases in HR during electrical stimulation, the heart was constantly paced at a cycle length of 300ms corresponding to a heart rate of 200bpm.

Significant AV prolongation (an example of which is illustrated in figure 5.10) occurred during electrical stimulation of at least one site within 3 out of the 4 regions examined, with only stimulation within the LNC eliciting no significant AVC changes at any of the sites tested. Changes in AV conduction were measured during electrical stimulation at 54 sites. At 45/54 sites, no significant change in AVC was measured, with the level of prolongation during stimulation at the remaining 9 sites ranging from 15ms to AVB. The most significant changes in AV conduction occurred within the RNC; the only region where electrical stimulation elicited atrioventricular block (AVB) (6/27 sites). Significant prolongation also occurred within the PVCV region (2/9 sites) (figure 5.11).

Atrial tachyarrhythmia/fibrillation was elicited following electrical stimulation of neurons within the LNC-MPV region in only one instance.

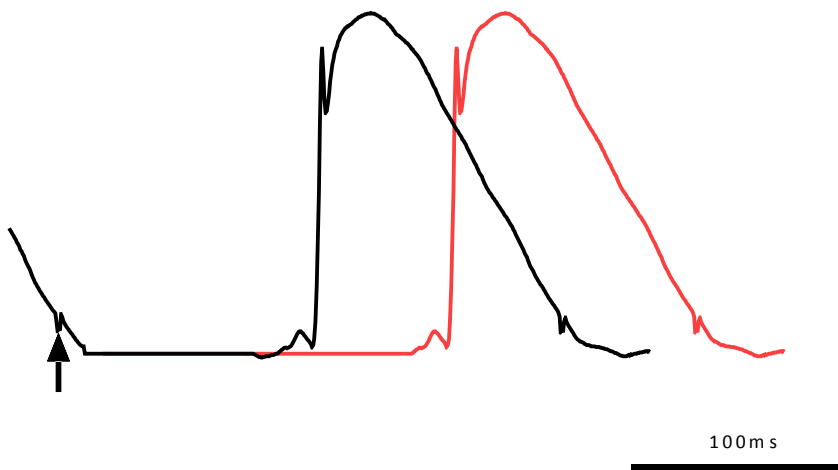


Figure 5.10. Electrical stimulation induced effects on atrioventricular conduction. Example monophasic action potential recordings illustrating the effect of electrical stimulation of intrinsic cardiac ganglia on atrioventricular delay during constant atrial pacing (the arrow illustrating the constant pacing trigger).

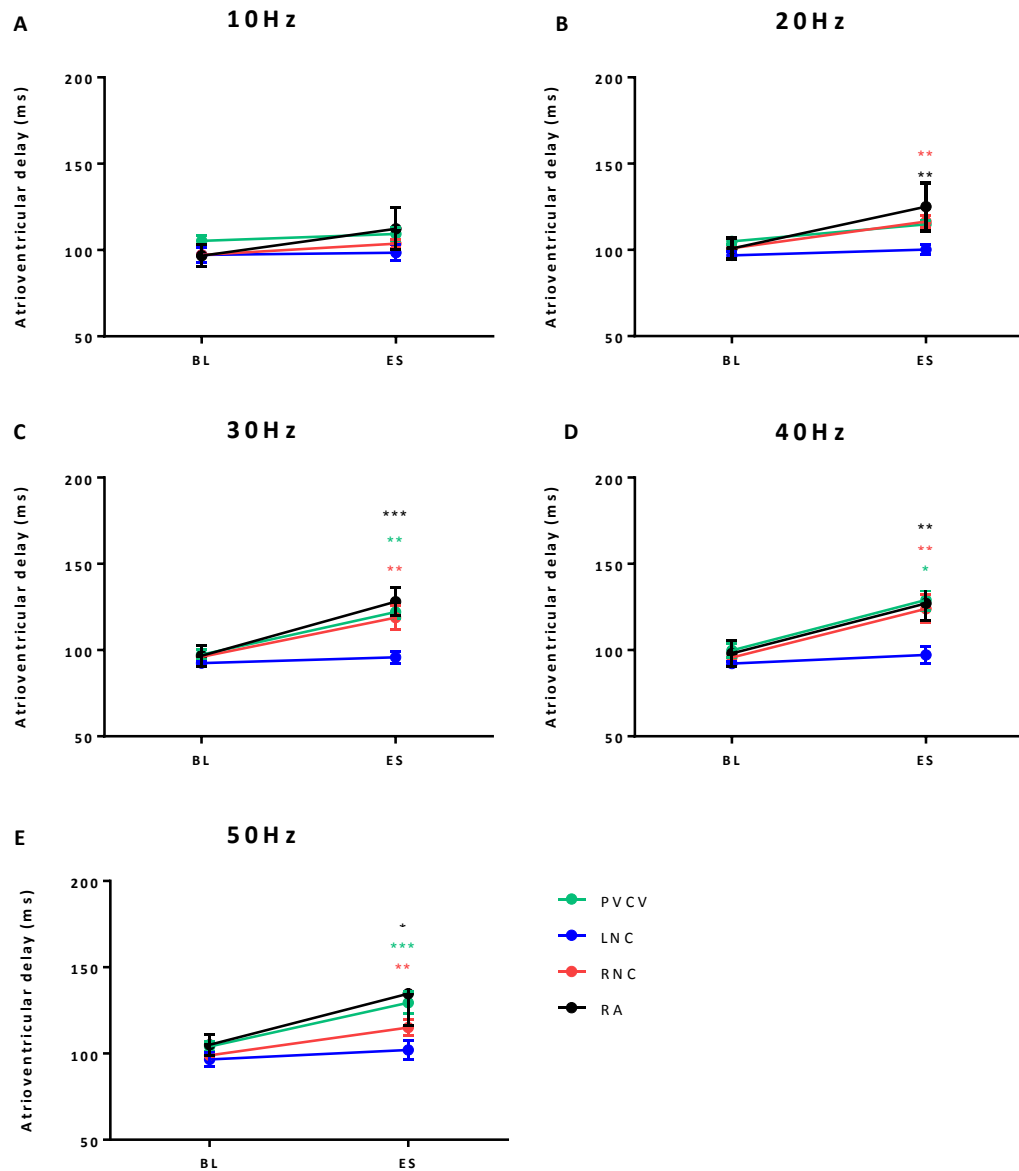


Figure 5.11. The effects of electrical stimulation on atrioventricular conduction in the control group. Mean data representing the average changes in AV delay during electrical stimulation in the control group at 10Hz (A), 20Hz (B), 30Hz (C), 40Hz (D) and 50Hz (E). Data represents mean \pm SEM. BL = baseline, ES = electrical stimulation. N = 54 (7 animals). Two-way ANOVA was used to compare baseline with values during electrical stimulation. * $p < 0.05$, ** $p < 0.01$, *** $p < 0.001$.

5.5 The effects of heart failure on dromotropic responses to electrical stimulation of intrinsic cardiac ganglia

The effects of heart failure on cardiac dromotropy during electrical stimulation were investigated. Atrioventricular delay was determined at a further 39 sites: 15 within the sham operated group (3.8 ± 0.1 kg) and 24 within the heart failure group (3.9 ± 0.3 kg). Stimulation of intrinsic cardiac ganglia within hearts from the heart failure group appeared to produce a markedly different effect on cardiac dromotropy and atrioventricular delay (figure 5.12) when compared with the control and sham operated groups (figure 5.13)

Slight AV delay prolongation was evident during stimulation of loci within the PVCV region (figure 5.12) in the heart failure group. This prolongation however, was not significant. Electrical stimulation of loci in the RA, RNC and LNC regions also resulted in no significant AV delay prolongation at all frequencies tested (figure 5.12). Further evidence of the reduced capacity of the ICNS to alter cardiac dromotropy included the complete lack of incidences of AV block during stimulation of ganglia within the heart failure group compared with AV block seen during stimulation of 12% and 18% of sites within the control and sham operated groups respectively.

On comparing the average percentage change in AV delay (from baseline) within the 3 groups (control, HF and sham), the level of prolongation was significantly reduced in both the RA and RNC regions in the heart failure group (at 10, 20 and 30Hz) (figure 5.14). However, the average change in AV delay prolongation appeared to be increased when loci within the PVCV region of hearts from the HF group were stimulated (figure 5.14) at all frequencies (10 - 50Hz) when compared to the control and sham operated groups.

No significant difference in atrioventricular delay was evident between the control and sham operated groups, with this data being reinforced when the average percentage change in AV delay within all regions was compared (figure 5.14). Atrioventricular block occurred during stimulation of 3/15 sites within the sham operated group, all within the RNC similar to the data shown from the control group.

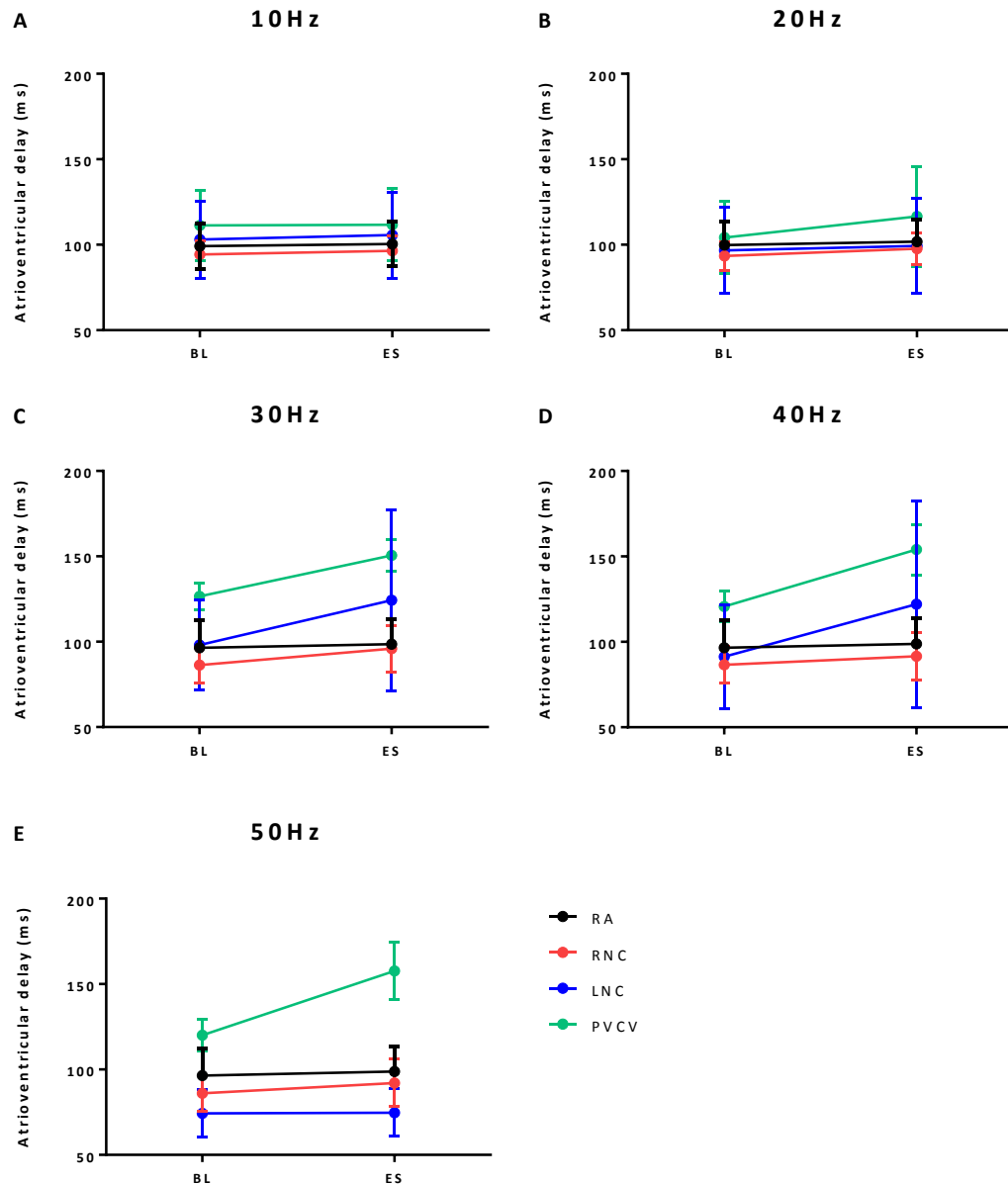


Figure 5.12. The effects of electrical stimulation on atrioventricular conduction in the heart failure group. Mean data representing the average changes in AV delay during electrical stimulation at 10Hz (A), 20Hz (B), 30Hz (C), 40Hz (D) and 50Hz (E). Data represents mean \pm SEM. BL = baseline, ES = electrical stimulation. N = 22 (7 animals). Two-way ANOVA was used to compare baseline with values during electrical stimulation, with no changes in AV delay showing significance.

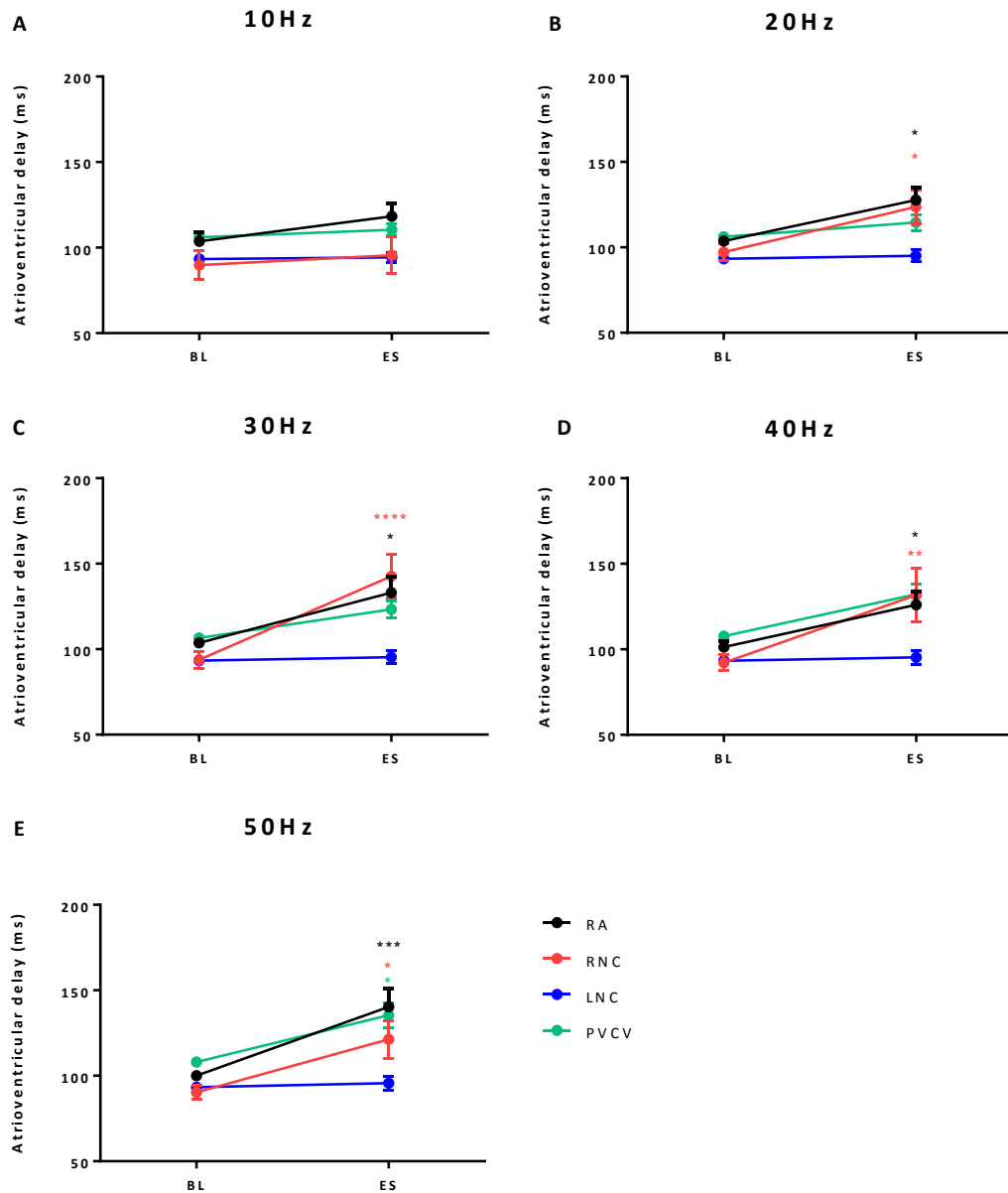


Figure 5.13. The effects of electrical stimulation on atrioventricular conduction in the sham operated group. Mean data representing the average changes in AV delay during electrical stimulation at 10Hz (A), 20Hz (B), 30Hz (C), 40Hz (D) and 50Hz (E). Data represents mean \pm SEM. BL = baseline, ES = electrical stimulation. N = 14 (4 animals). Two - way ANOVA was used to compare baseline with values during electrical stimulation. * $p < 0.05$, ** $p < 0.01$, *** $p < 0.001$, **** $p < 0.0001$.

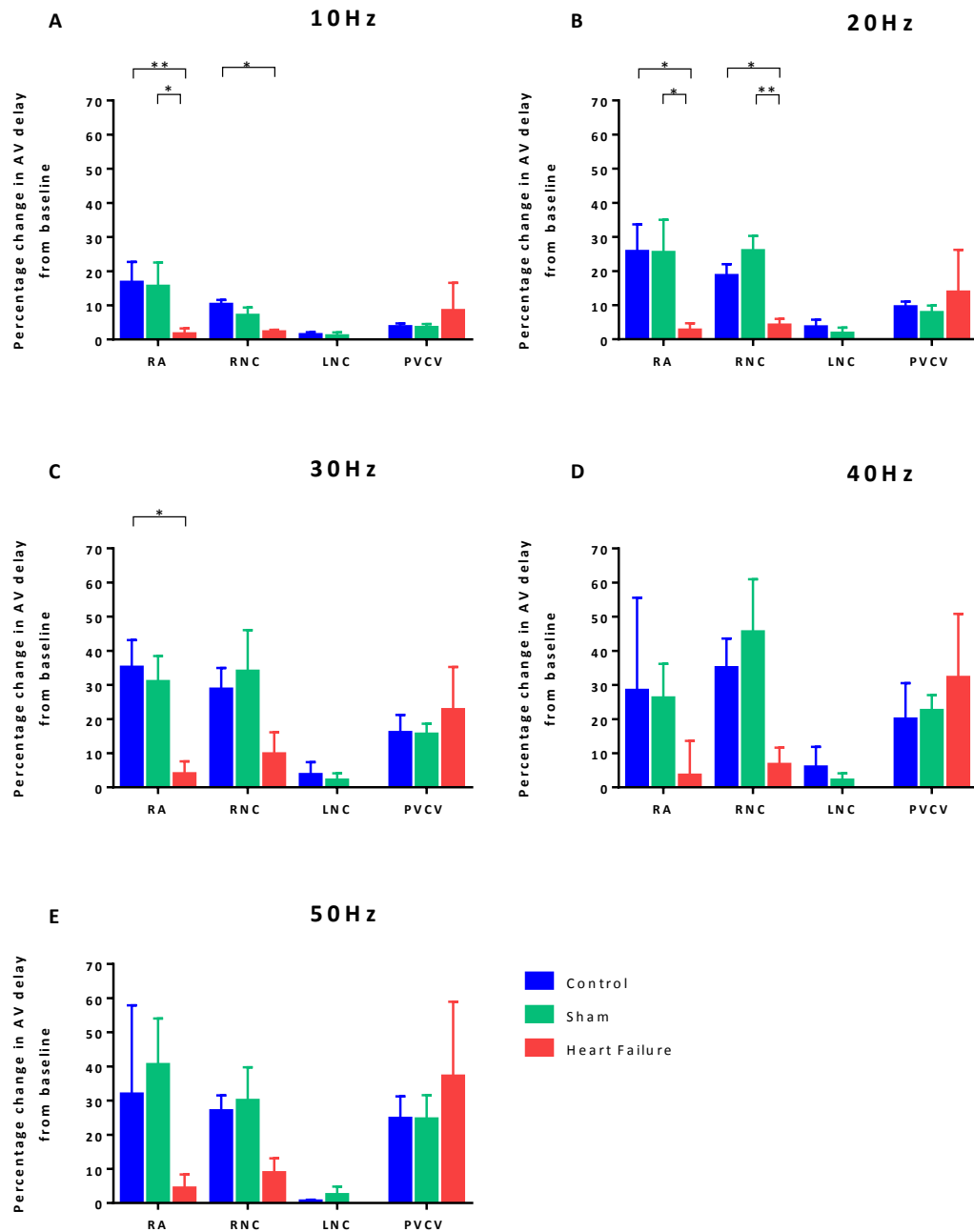


Figure 5.14. Comparison of the percentage change in atrioventricular conduction between the control, heart failure and sham operated groups. Mean data showing the average percentage change in AV delay during electrical stimulation within all regions at 10Hz (A), 20Hz (B), 30Hz (C), 40Hz (D) and 50Hz (E). Data represents mean \pm SEM. Two-way ANOVA was used to compare data between control, sham and HF groups. * $p < 0.05$, ** $p < 0.01$.

5.6 The effects of pharmacological agents on cardiac responses of electrical stimulation of intrinsic cardiac ganglia

To determine the types of autonomic receptors involved in the development of both the chronotropic and dromotropic responses to electrical stimulation of intrinsic cardiac ganglia, protocols were repeated in the presence of the autonomic ganglionic blocker hexamethonium and atropine (a muscarinic (M_2) receptor antagonist) or metoprolol (a β -adrenergic receptor blocker) in all three groups (conventional, sham operated and heart failure).

The effects of pharmacological blockers were investigated at a total of 98 sites (33 in the control group, 21 in the sham operated group and 44 in the heart failure group). Previous data within this chapter showed that significant chronotropic changes occurred at 20Hz or more, therefore all stimulation of intrinsic cardiac ganglia during the investigation of pharmacological blockers was done at 20Hz. All heart rate responses (both bradycardic and tachycardic responses) to electrical stimulation were abolished by hexamethonium (figure 5.15).

Atropine abolished all reductions in heart rate (figure 5.15) during electrical stimulation of ganglia. In the presence of atropine, no significant difference was noted in the induction of tachycardic responses evoked by electrical stimulation within the RA and RNC when heart rate responses were compared to control. Increases in heart rate evident during electrical stimulation of ganglia within the RA and RNC regions were eliminated in the presence of the metoprolol (figure 5.15 A and B).

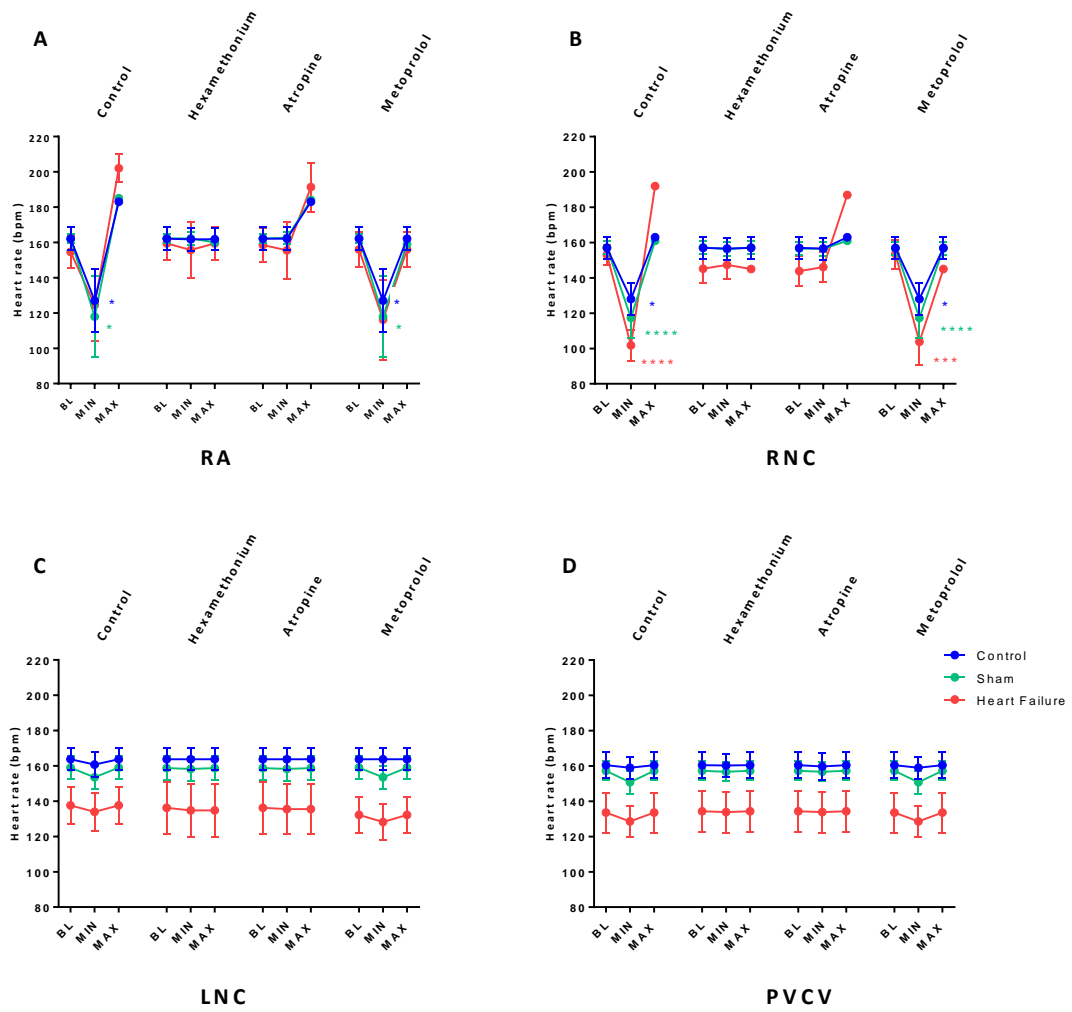


Figure 5.15. The effects of pharmacological blockers on heart rate responses to electrical stimulation. Mean data comparing heart rate changes in control conditions as well as in the presence of hexamethonium, atropine and metoprolol in all 4 regions examined; A) RA, B) RNC, C) LNC, D) PVCV. BL = baseline. Comparisons between control (n=33), sham (n=21) and HF groups (n=44) were made using two-way ANOVA. * $p < 0.05$, *** $p < 0.001$ and **** $p < 0.0001$.

5.7 Discussion

Despite the increasing appreciation amongst scientists that the intrinsic cardiac nervous system plays a crucial role in the control of cardiac function and electrophysiology, data investigating this role is limited. The aim of this chapter was therefore to investigate the functional role of intrinsic cardiac ganglia in a rabbit model, using electrical stimulation.

5.7.1. The effects of electrical stimulation of intrinsic cardiac ganglia on cardiac function

To date, this is the first study to investigate the functional role of the ganglia within the ICNS in the rabbit. Electrical stimulation resulted in spatially diverse changes in both cardiac chronotropy and dromotropy. Utilising the anatomical data shown in chapter 4, allowed for a directed approach of electrical stimulation at regions known to commonly contain intrinsic cardiac ganglia. Stimulation of these regions primarily resulted in bradycardic changes in heart rate, yet despite this, incidences of tachycardia were recorded. In addition to pure bradycardic and tachycardic responses, stimulation of loci also resulted in biphasic responses which were characterised as a bradycardia followed by a tachycardia during the period of stimulation. The incidence of biphasic effects is unsurprising since stimuli were applied to ganglia in which networks of connected neurons are present and have been demonstrated using histological study (see chapter 4). In the particular environment being investigated, the spread of electrical current from a bipolar electrode would be difficult to restrict. It is therefore not entirely possible to accurately determine whether these biphasic responses were due to the stimulation of multiple ganglia or a result of the stimulation of isolated ganglia containing numerous neuronal phenotypes.

Bradycardic responses occurred almost instantaneously following the initiation of electrical stimulation. In comparison, tachycardia responses demonstrated a longer lag time following the commencement of stimulation before the development of the heart rate change. These findings correlate with data shown by Ng *et al.* (2001) who attributed this gradual increase in heart rate during sympathetic stimulation to the slow release of noradrenaline from nerve terminals. Conversely, the almost instantaneous parasympathetic response comes as a result of rapid muscarinic receptor activation by

acetylcholine (Levy and Martin, 1996). One interesting observation was the slower initiation and development of the bradycardic change during biphasic heart rate responses. One explanation for the delay in this parasympathetic response, could be the concurrent activation of sympathetic neurons although further investigation would be required to determine the molecular reasons for such a phenomenon.

Reductions in heart rate as a response to electrical stimulation of intrinsic cardiac ganglia altered in a frequency dependent manner with increasing frequency of stimulation resulting in a greater bradycardia. This was also the case for episodes of tachycardia; with an increase in the frequency of stimulation leading to a more pronounced tachycardia. In contrast, when a biphasic response was noted, an increase in the frequency of stimulation resulted in a greater decrease in heart rate during the bradycardic phase, accompanied by a reduction in the tachycardia response.

One plausible reason for such frequency dependent behaviour during a biphasic response to electrical stimulation is the known combination of both cholinergic and adrenergic neurons within ganglia of the ICNS. As shown previously, the neurochemical composition of intrinsic cardiac ganglia demonstrates the presence of both parasympathetic neurons (immunoreactive for the cholinergic marker ChAT) as well as neurons immunoreactive for the adrenergic marker tyrosine hydroxylase. The functional capacity of these TH positive neurons is under constant debate, however it is becoming increasingly likely that these neurons do indeed function in a sympathetic manner and therefore are involved in increases in sinus rate.

In healthy control animals, the most significant changes in heart rate came as a result of electrical stimulation of ganglia within the RNC, followed closely by stimulation of ganglia within the RA. Conversely, stimulation of sites within the regions of the PVCV and LNC appeared to produce very little change in heart rate when stimulated. This apparent lack of response during stimulation of these regions does not necessarily mean that the animals where a response was not recorded were unable to elicit such a response, more that the neuronal population may not have been electrically stimulated. Anatomical studies show that intrinsic cardiac ganglia are often located on the heart hilum and around the pulmonary veins. There is however notable variation in the overall distribution of neurons and ganglia between individual hearts, making electrical

stimulation of precise ganglia difficult to achieve. Butler *et al.* (1990) previously demonstrated the absence of detectable cardiac changes during electrical stimulation at regions shown to contain intrinsic cardiac ganglia. This could therefore imply the need for differential stimulation of specific ganglia dependent upon the role and function they play in cardiac control and show that even though no change in heart rate was observed, the ganglia being stimulated may still play a significant role in the control of differing cardiac indices.

The findings reported herein demonstrate a predominant control of heart rate from ganglia within the RNC and the RA regions. Past hypotheses proposed a selective role of individual ganglia in specific cardiac indices, with the right atrial GP being solely linked to regulation of SA nodal function (Lazzara *et al.*, 1973). More recently however, it has been demonstrated in canines that GPs act to integrate autonomic innervation, with multiple GPs communicating as part of a neuronal network to fine tune cardiac responses (Hou *et al.*, 2007a). Despite ganglia within such studies demonstrating predominant roles in either chronotropic or dromotropic regulation, it is becoming increasingly obvious that all ganglia within the ICNS act in a cardiac regulatory capacity. The similarity of the present data would appear to strengthen previous conclusions made in anaesthetised dogs (Cardinal *et al.*, 2009, Zarzoso *et al.*, 2013). Electrical current activates not only nearby neuronal somata and dendrites but also afferent and efferent axons traversing the ganglia. This data was therefore compared to previous unpublished data from our group where the action of nicotine, a postsynaptic receptor stimulant, was tested. Both nicotine and electrical stimulation applied at discrete sites of the ICNS in the rabbit evoked similar kinds of cardiac effects such as increases in heart rate alone, decreases in heart rate alone or a biphasic response as well as decreases in atrioventricular conduction. It therefore appears likely that the effects of electrical stimulation on cardiac activity were caused by the activation of ICNS neurons rather than extrinsic nerve terminals. This predominance of certain ganglia in the control of specific cardiac indices is consistent with evidence for the presence of topographically distinct groups of chronotropic and dromotropic parasympathetic preganglionic neurons in the nucleus ambiguus (Gatti *et al.*, 1996).

This study demonstrates the involvement of ganglia within the majority of regions (minus those within the LNC) in the control of atrioventricular conduction. Significant prolongation in atrioventricular delay during constant atrial pacing occurred during electrical stimulation of ganglia within the RA, RNC and PVCV regions. In contrast, no significant changes in AV conduction were identified during stimulation of the LNC. Two to one atrioventricular block occurred only during stimulation of loci within the RNC.

The innervation of the atrioventricular node is thought to be primarily via the inferior right GP (Hou *et al.*, 2007a) also documented as the inferior vena cava- inferior atrial GP (Yuan *et al.*, 1994). Ablation of this GP, located at the origin of the inferior vena cava (IVC) and documented mainly in canines (Yuan *et al.*, 1994, Hou *et al.*, 2007a) has been shown to significantly reduce the effect of vagal nerve stimulation on cardiac ventricular rate. However, it is important to understand that this GP alone (or corresponding GPs located around the root of the IVC in other species) is not solely responsible in the selective innervation of the AV node. This GP rather, acts more as an integration centre for extrinsic cardiac neural inputs and an intricate intrinsic neural pathway involving numerous other ganglia such as those at the anterior right atrial and superior left atrial regions (Hou *et al.*, 2007a).

In comparison to the effects of stimulation of IC ganglia on cardiac chronotropy, one noteworthy difference was the influence of ganglia within the PVCV region on atrioventricular conduction with significant AV prolongation within this region (commonly around the origin of the inferior vena cava) being evident in the rabbit. This suggests, along with the lack of change in heart rate during stimulation of this region, that these ganglia play a dominant role in AV nodal innervation and not SA nodal control. Despite this, changes in heart rate were evident at the PVCV region, albeit relatively smaller than those seen in other regions. This correlates with the data described previously (Hou *et al.*, 2007a) and indicates that neuronal innervation occurs via communication between numerous ganglia to alter cardiac function.

Previous investigation into the functional effects of intrinsic cardiac ganglia has shown the ganglia to be capable of influencing both sinus rate and atrioventricular conduction (Moss *et al.*, 2013, Cardinal *et al.*, 2009, Hou *et al.*, 2007a), correlating with data shown

within this study. Based on this study, electrical stimulation applied to the ganglia within the RNC appears to show a predominant influence on both heart rate and atrioventricular conduction when compared to other regions investigated. This is partly supported by anatomical data from studies completed in the rabbit identifying nerves extending from the RNC and innervating the region of the SAN (Saburkina *et al.*, 2014, Inokaitis *et al.*, 2016, Zarzoso *et al.*, 2013). During investigation of the innervation of sinoatrial nodal cells in the rabbit, Inokaitis *et al.* (2016) concluded that the innervation of the SA node is extremely complex, even in comparison to that of the atrioventricular node. The potential influence of ganglia within the RA, RNC and PVCV regions shown within this study however, suggests that the innervation of the AV node is equally as complex.

The synaptic interaction and junctional receptor transmission involved in cardiac responses to electrical stimulation were tested. The effects of electrical stimulation were dependent on cholinergic nicotinic ganglion transmission. The abolition of responses to electrical stimulation with atropine and metoprolol further indicates the involvement of both cholinergic muscarinic receptors and postganglionic beta adrenoreceptor sites in the mediation of bradycardic and tachycardic effects respectively. The data from this study further confirms the notion that ganglia located at a distance to structures such as the SA and AV nodes have a significant effect on cardiac electrophysiology and highlight the importance of intrinsic cardiac ganglia in the functional control of cardiac indices. Studies investigating the modification of neuronal activity within the ICNS with either electrical stimulation or pharmacological intervention (Thompson *et al.*, 2000, Butler *et al.*, 1990, Cardinal *et al.*, 2009, Armour *et al.*, 1993) further demonstrate the complexity of the neuronal hierarchy involved in coordinating responses. However, this study has not taken into account the involvement of central and peripheral neuronal inputs, which add further complexity and in turn, further questions as to the complete mechanisms involved in neuronal cardiac control.

5.7.2. The effects of heart failure on the functional role of the ICNS

There is limited information currently available regarding the functional capacity of the ICNS following myocardial infarction. Significant neuronal morphological and phenotypic remodelling occurs as a result of the injury caused by MI therefore one of

the aims of this study was to determine the effect of this remodelling on the interaction and function of ganglia during electrical stimulation.

As indicated in chapter 4, sham operated animals were used similarly to controls and to ensure that the differences, if any, in the functional capabilities within the ICNS were as a result of coronary artery ligation and the subsequent myocardial infarction and not a consequence of the stresses of the initial surgery. No differences were observed between the sham-operated group and the control group therefore suggesting differences observed within the heart failure group could be attributable to heart failure and damage due to myocardial infarct. Heart failure results in an increase in beat to beat heart rate variation, which is under the tonic influence of the vagal control of the SA node. It is likely that heart rate variability due to alterations in autonomic modulation of the heart could therefore explain the variability in baseline heart rate shown in figure 5.12 when compared to control.

Little change in heart rate was evident during electrical stimulation of ganglia within the regions of the LNC and PVCV, similar to that in control animals. As described previously, this is likely to be due to a non-dominant role of ganglia within this regions in the control of cardiac chronotropy. The average bradycardic response to stimulation of ganglia within the RNC however, was greater at all frequencies investigated. This was accompanied by a significant increase in tachycardia responses during stimulation of ganglia within both the RA and the RNC.

The reduced blood supply to regions of the ventricular myocardium has a direct effect on the neuronal innervation in that area. Ganglia within the ICNS transduce this information, with neuronal remodelling occurring to counteract the damage and potentially to alter cardiac function in order to maintain cardiac output. As mentioned previously, heart failure results in an increase in sympathetic drive and a parasympathetic withdrawal. As well as an increase in the bradycardic response to ganglia stimulation, the overall percentage of sites where tachycardia was noted increased in comparison to that seen in control and sham operated animals. This increase is likely to be associated with the central increase in sympathetic tone. The data shown within this study suggests that the intrinsic cardiac nervous system plays two different roles in the control of cardiac function in heart failure: 1) increasing

sympathetic activity to counteract the failing of the heart and the overall deleterious effects on cardiac output and 2) trying to compensate for these central autonomic changes by increasing the level of parasympathetic activity. This hypothesis correlates with data shown by Rajendran *et al.* (2016) who demonstrated an MI-induced decrease in the cholinergic phenotype of neurons within the ventral interventricular GP (VIV-GP), a ganglionic region known to innervate the ventricles and therefore linked to the infarcted ventricular region. This decrease in cholinergic phenotype along with excessive and chronic activation of intrinsic cardiac neurons involved in the transduction of afferent signals from damaged myocardium (Huang *et al.*, 1993, Arora *et al.*, 2003) contributes further to the dysregulation of cardiac control and further suggests a role of the ICNS in the contribution to the increase in sympathetic drive.

Alongside the differences observed in the control of heart rate of from the ICNS following MI, significant differences in atrioventricular conduction were noted compared to healthy control animals. Out of all loci stimulated, the only ganglia to induce a change in AV delay were located within the PVCV region. This alteration in the control of atrioventricular conduction coincides with the morphological remodelling seen as a result of MI and although speculative, could suggest a protective adaptation with the neuronal connections linking ganglia around the PVCV, the region primarily involved in AV-delay prolongation, with ganglia located elsewhere within the ICNS being altered.

Subpopulations of neurons within the ICNS termed local circuit neurons receive both afferent and efferent inputs. These neurons integrate and process information even in the heart failure state (Rajendran *et al.*, 2016) indicating the capacity of the ICNS to continue processing information during MI. Significant changes in the level of afferent neuronal inputs not only targets ganglia innervating the regions of infarcted tissue but multiple populations of intrinsic cardiac neurons (Arora and Armour, 2003) therefore stimulating remodelling throughout a large proportion of the ICNS.

There is an increase in the percentage of neurons that receive efferent sympathetic and parasympathetic inputs following MI (Rajendran *et al.*, 2016). It has been described that the main priority of the central autonomic nervous system following MI is the processing of central demands for blood flow and cardiac output. The increase in efferent

communication alongside the intricate neuronal remodelling that occurs within the ICNS provides a platform for the ICNS to provide a level of protection against the central neuronal alterations and the increasing susceptibility to the development of cardiac arrhythmias.

Ganglia within the ICNS play a role in the initiation and maintenance of arrhythmias such as atrial fibrillation (Zhou *et al.*, 2007) with selective ablation of ganglia being shown to reduce any predisposition to such arrhythmias. The effects of GP stimulation of ventricular electrophysiology however, have not been studied here and remains unknown amongst scientists. He *et al.* (2013) showed that GP stimulation can prolong ventricular ERP and significantly decrease the slope of the ventricular APD restitution curve, suggesting that stimulation of intrinsic cardiac ganglia may provide a level of protection against ventricular arrhythmia, however further study is need to determine the true extent of this protection in the rabbit and during heart failure.

Despite the data from this study clearly showing the individual capabilities and overlap of specific regions of ganglia on spatially divergent regions, it is important to acknowledge the need for further investigation to fully determine the precise connections between ganglia and singular sites.

Chapter 6: The interaction between peripheral neuronal inputs and the ICNS

6.1 Introduction

Autonomic cardiac innervation involves a complex interaction between both the extrinsic cardiac neuronal inputs and the intrinsic cardiac nervous system. Relatively few studies have delved into the precise interactions between these extrinsic inputs including the vagus nerves and central sympathetic inputs and the network of ganglionated plexi that reside at the level of the heart itself.

It is well known that parasympathetic vagal stimulation exerts a negative chronotropic and dromotropic effect on the heart. Preganglionic vagal efferent fibres synapse with postganglionic fibres at the level of the heart and, upon stimulation, rapid muscarinic receptor activation via the release of acetylcholine results in changes in cardiac electrophysiology. Previous work by our group further characterised the effects of vagal nerve stimulation in the dual innervated heart preparation (Ng *et al.*, 2001, Brack *et al.*, 2004), noting that stimulation of the right vagus nerve produces a greater change in heart rate when compared to the left vagus nerve. On the other hand, stimulation of the left vagus nerve produces greater effects on AV conduction than the right. These difference have been attributed to the selective distribution of vagal fibres to both the AV and SA nodes.

GPs have been shown to be regions of neuronal integration with vagal neuronal innervation travelling through multiple plexuses before accessing the sinoatrial and atrioventricular nodes and modulating sinus rate and atrioventricular conduction (Hou *et al.*, 2007b). The GP located between the superior vena cava and the aorta has been described as the primary region of interaction between the extrinsic and intrinsic cardiac nervous systems and that ablation of this GP region results in the elimination of the effects of vagus nerve stimulation. This suggests therefore, that vagus nerve stimulation of the SA node requires an interaction with the GPs of the ICNS.

Previous investigation has demonstrated the involvement of both the peripheral neuronal inputs such as the vagosympathetic trunk and the intrinsic cardiac ganglia in the initiation and development of atrial fibrillation. Understanding these complex

interactions if therefore crucial in order to understand the development of cardiac disease.

The majority of studies to date that have investigated the interactions between the extrinsic and intrinsic cardiac nervous system have been conducted in larger mammals, primarily canines (Lo *et al.*, 2013, Hou *et al.*, 2007b). The objective of this study was therefore to conduct preliminary investigations into the interactions between part of the extrinsic cardiac nervous system (the vagus nerves) and the ICNS in a rabbit model by examining the effects of electrical stimulation on heart rate and atrioventricular conduction.

6.2 Results

The functional interaction between the vagal nerves and the intrinsic cardiac ganglia was investigated using the dual innervated perfused heart preparation. Experiments were completed using adult male New Zealand white rabbits ($n= 7$, $2.3 \pm 0.1\text{kg}$). To determine the interaction between the vagal nerves and intrinsic cardiac ganglia, ganglia were stimulated at 50% of the cardiac pacing threshold either in the presence of background vagus nerve stimulation (described throughout this chapter as VS_GP) or prior to the addition of vagus nerve stimulation (GP_VS). Changes in heart rate and atrioventricular delay were recorded for each site investigated.

6.2.1 Heart rate response characteristics of vagal nerve stimulation

Prior to examining the interaction between both the left and right vagus nerves and the intrinsic cardiac ganglia, the effects of vagal nerve stimulation on heart rate were investigated. To determine the stimulation parameters for vagal stimulation during GP and vagal interaction protocols, the effect of changing stimulus strength at a fixed frequency was examined followed by the effect of changing frequency at a fixed voltage in a total of 7 preparations. Vagal nerve stimulation caused an instantaneous reduction in heart rate which reached a steady-state plateau. This steady state was maintained and the heart rate value used for determining the effects of stimulation on heart rate. Following nerve stimulation, the heart was allowed to recover and heart rate allowed to return to a stable baseline.

Vagal nerve stimulation at increasing voltages at a fixed frequency of 5Hz resulted in a reduction in heart rate from a baseline value of $160 \pm 8.6\text{bpm}$ to $99 \pm 10.8\text{bpm}$ (RVS) and $98 \pm 6.3\text{bpm}$ (LVS) at 20V. Significant heart rate changes during VNS when compared to baseline occurred at 3 – 20V. The voltage-dependent reduction in heart rate plateaued on average at around 5V during stimulation of the RVS and 10V with LVS stimulation (figure 6.1A). Frequency dependent responses were examined at the voltage that produced a heart rate equivalent to 80% of the maximal response of stimulation of the right and left vagi ($6 \pm 1\text{V}$ and $7 \pm 1\text{V}$ respectively).

There were progressively greater reductions in heart rate with increasing frequencies up to 10Hz (figure 6.1B). Previous studies have demonstrated stimulation at frequencies

higher than 10Hz can trigger sinus arrest (Ng *et al.*, 2001) hence the maximum frequency investigated was 10Hz. Heart rate reductions were greater with RVS compared to LVS however this difference was not significant. The average frequencies of stimulation that produced heart rates between 70 and 100bpm were $8 \pm 1\text{Hz}$ (RVS) and $8 \pm 1\text{Hz}$ (LVS).

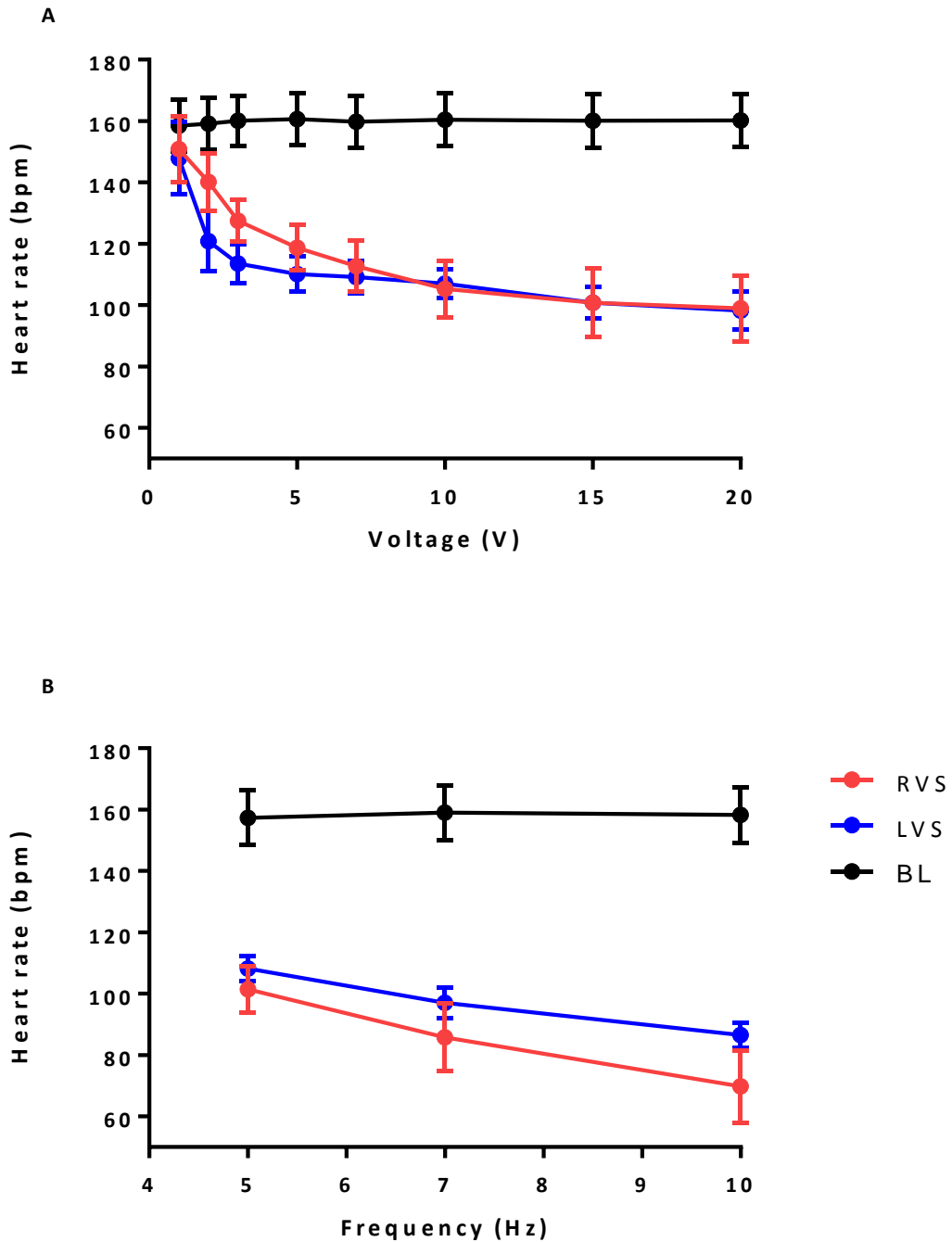


Figure 6.1: Voltage and frequency dependent changes in heart rate during vagus nerve stimulation. A. Graph showing mean heart rate data with left and right vagal nerve stimulation relative to baseline at various voltages at a constant frequency (n=7). B. Graph showing mean heart rate data during left and right vagus nerve stimulation compared to baseline at various stimulation frequencies at a constant voltage (n=7).

6.2.2 The effects of peripheral and intrinsic cardiac stimulation on cardiac chronotropy

Due to the nature of the preparation, all intrinsic cardiac ganglia that were electrically stimulated during this part of the study were located within the RNC. The interaction between intrinsic cardiac ganglia within the RNC and the left vagus was investigated at a total of 13 sites and the right vagus at 7 sites. Data shown previously (see chapter 5) demonstrated that the majority of responses induced during stimulation of loci within the RNC were bradycardic with only one incidence of bradycardia followed by a tachycardia being noted. Electrical stimulation of intrinsic cardiac ganglia resulted in a reduction in heart rate (ranging from -21 to -85bpm) in all incidences.

Dependent upon the protocol being used, stimulation (of either a GP or the left or right vagus) was initiated until the heart rate reached a steady state, after which the second stimulation was commenced. Figure 6.2E illustrates a typical heart rate response to background RVS with the addition of GP stimulation alongside as well as stimulation of a GP followed by the addition of vagal stimulation. In order to compare the effects of left and right vagal stimulation and the interaction with intrinsic cardiac ganglia, experiments were conducted with the aim of investigating both the left and right vagi at the same intrinsic loci, however this was only possible at 7 sites.

Stimulation of either the left vagus, right vagus or GP alone resulted in significant heart reductions in heart rate ($152 \pm 5\text{bpm}$ vs $98 \pm 4\text{bpm}$, $135 \pm 4\text{bpm}$ vs $89 \pm 5\text{bpm}$ and $144 \pm 5\text{bpm}$ vs $95 \pm 6\text{bpm}$ respectively). The reduction in heart rate seen with background left or right vagal stimulation was further decreased with the addition of GP stimulation. This was also the case when left or right vagal stimulation was added to background GP stimulation (figures 6.2A and B). Stimulation of both the left vagus and intrinsic GPs (irrespective of order of stimulation) resulted in significant heart rate reductions when compared to LVS or GP stimulation only. Conversely the greater bradycardia response evident when investigating the interaction of the right vagus with GPs was not significant (figure 6.2B).

The mean percentage change in heart rate was compared between all stimulation protocols (figures 6.2C and D). Dual stimulation (with both left and right vagus protocols) resulted in greater percentage changes however these were not significant when

investigating the right vagus. Stimulation of the LVS alongside GP stimulation however, produced significant increases in the average percentage change in HR. The effects of left vagus interaction with GPs were compared with those of the right vagus with no significant difference between all protocols being evident.

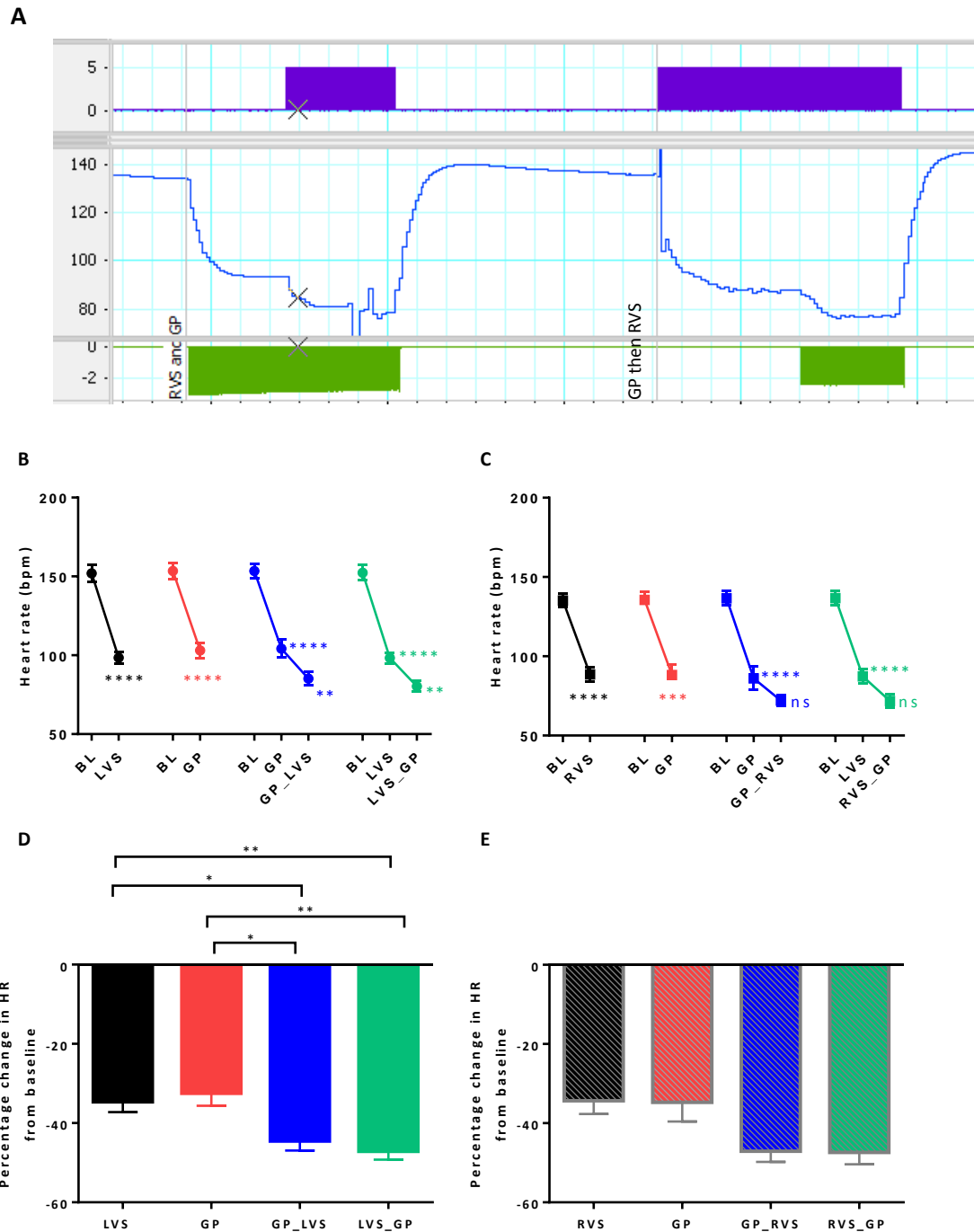


Figure 6.2. The effects of vagus nerve stimulation and electrical stimulation of intrinsic cardiac ganglia on heart rate. A raw heart rate trace (A) illustrating the effect of RVS (green block) either stimulated prior to the addition of RVS or added to background GP stimulation (purple block). B represents the changes in heart rate during stimulation of the left vagus, intrinsic cardiac ganglia, GP stimulation with added LVS (GP_LVS) and LVS stimulation with added GP stimulation (LVS_GP). C represents the average HR during stimulation of protocols involving the right vagus nerve. Statistical analysis performed to determine any significant difference in HR when compared to BL and then whether additional stimulation resulted in a further significant change. D and E represent that average percentage change in HR with all stimulation protocols. All data is represented as mean \pm SEM. Statistical analysis performed with one-way ANOVA and unpaired two-tailed t-test (* $p < 0.05$, ** $p < 0.01$, *** $p < 0.001$ and **** $p < 0.0001$).

6.2.3 The effects of peripheral and intrinsic cardiac stimulation on cardiac dromotropy

The effects of left vagus nerve and GP stimulation on atrioventricular conduction were examined in 7 hearts at a total of 10 sites with the interaction with the right vagus being examined at 6 sites. Atrioventricular conduction was measured during constant atrial pacing at a cycle length of 300ms (heart rate of 200bpm).

Significant AV-delay prolongation occurred during stimulation of the left vagus nerve ($121 \pm 7\text{ms}$ vs $152 \pm 6\text{ms}$) yet RVS did prolong AV delay but this prolongation was not significant ($133 \pm 8\text{ms}$ vs $146 \pm 6\text{ms}$). Slight AV-delay prolongation was also noted during stimulation of all intrinsic loci. The addition of GP stimulation to both left and right vagal stimulation as well as the addition of left and right vagal stimulation to background GP stimulation resulted in further AV-delay prolongation (figure 6.3) although this increase in prolongation was relatively small.

The effects of dual stimulation were greater during stimulation of the LVS and ICG when compared to those seen in with the RVS and ICG. In contrast to the similar heart rate changes seen when all left and right vagal protocols were compared, there were significant differences in the interaction between the left and right vagus nerves with the ganglia within the RNC (LVS vs RVS ($p < 0.01$), GP_LVS vs GP_RVS ($p < 0.01$) and LVS_GP vs RVS_GP ($p < 0.01$).

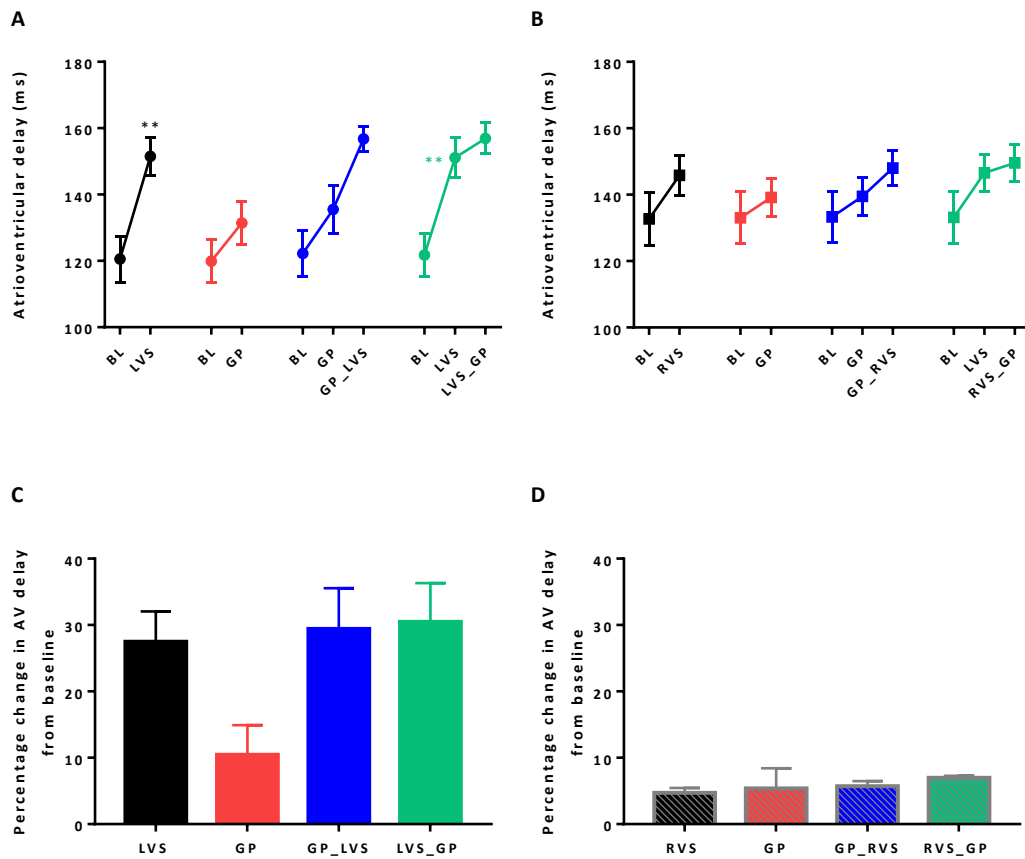


Figure 6.3: The effects of vagus nerve stimulation and electrical stimulation of intrinsic cardiac ganglia on atrioventricular conduction. A represents the changes in atrioventricular conduction during stimulation of the left vagus, intrinsic cardiac ganglia, GP stimulation with added LVS (GP_LVS) and LVS stimulation with added GP stimulation (LVS_GP). B represents the average atrioventricular delay during stimulation of protocols involving the right vagus nerve. C and D represent that average percentage change in AV delay with all stimulation protocols. All data is represented as mean \pm SEM. Stastical analysis performed with one- way ANOVA and unpaired two-tailed t-test (** $p < 0.01$).

6.2.4 Pharmacological blockade of vagal and ICNS responses to electrical stimulation

Figures 6.4 and 6.5 summarise the data obtained during pharmacological blockade using hexamethonium (LVS; n = 9 and RVS; n = 5) and atropine (LVS; n = 7 and RVS; n = 5). Hexamethonium abolished both GP and vagally mediated effects on heart rate (figure 6.4) and atrioventricular delay (figure 6.5) without affecting baseline values in unstimulated conditions. Ganglionic inhibition with hexamethonium significantly reduced the average percentage heart rate change during all stimulation parameters (figures 6.4C and D) (using 2-way ANOVA and comparing the average percentage change in HR between control vs hexamethonium). For example, the mean percentage change in heart rate during LVS_GP stimulation decreased from $-47.1 \pm 2.1\%$ to $-0.3 \pm 0.4\%$ as well as RVS_GP stimulation changing from $-47.0 \pm 2.6\%$ to $-0.1 \pm 0.2\%$. This suggests that intrinsic cardiac ganglia play a role in the integration between the extrinsic and intrinsic cardiac nervous system and that the vagus nerves act through GPs.

Muscarinic receptor blockade with atropine also resulted in eradication of all changes in heart rate irrespective of which vagus nerve or intrinsic cardiac ganglia was involved in stimulation. This was also the case with all changes in atrioventricular delay being abolished with atropine (figure 6.5). Significant reductions in the average percentage change in atrioventricular delay occurred with all stimulation protocols excluding during GP stimulation when investigating the interaction with the left vagus.

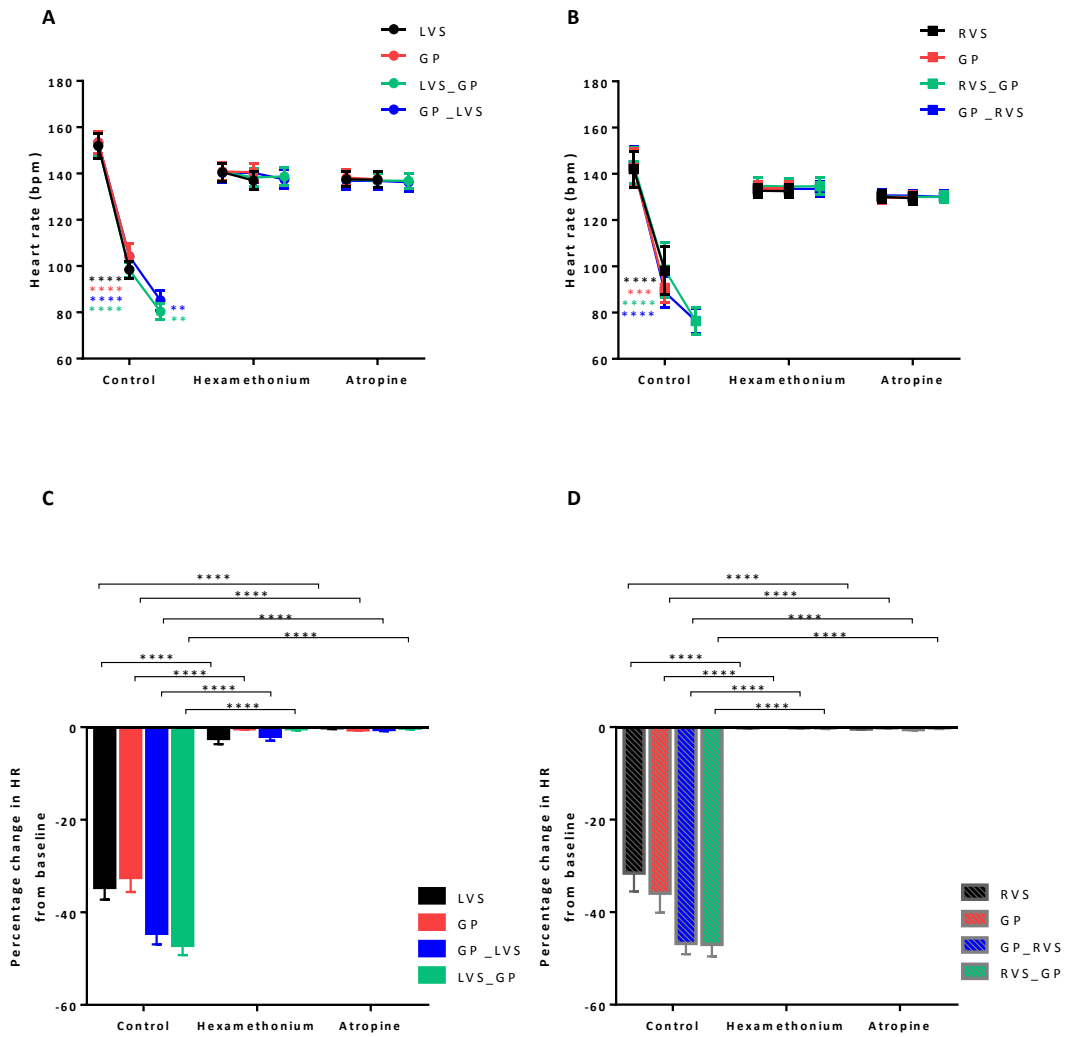


Figure 6.4: Pharmacological autonomic blockade of heart rate responses to vagus nerve and intrinsic cardiac ganglia stimulation. Data representing the average heart rate changes during stimulation protocols during control, hexamethonium and atropine protocols (A and B). Data presented as mean \pm SEM. Statistics performed using one-way ANOVA to compare heart rate during stimulation to baseline heart rate as well as compare background stimulation to dual stimulation. C and D show the average percentage change in heart rate from baseline during all stimulation protocols in conditions of control, hexamethonium and atropine. A and C indicate the effects of left vagus stimulation with B and D illustrating the effects of right vagus stimulation. Statistics to compare control protocols with each pharmacological blocker were performed using two-way ANOVA. (** $p < 0.01$ and **** $p < 0.0001$).

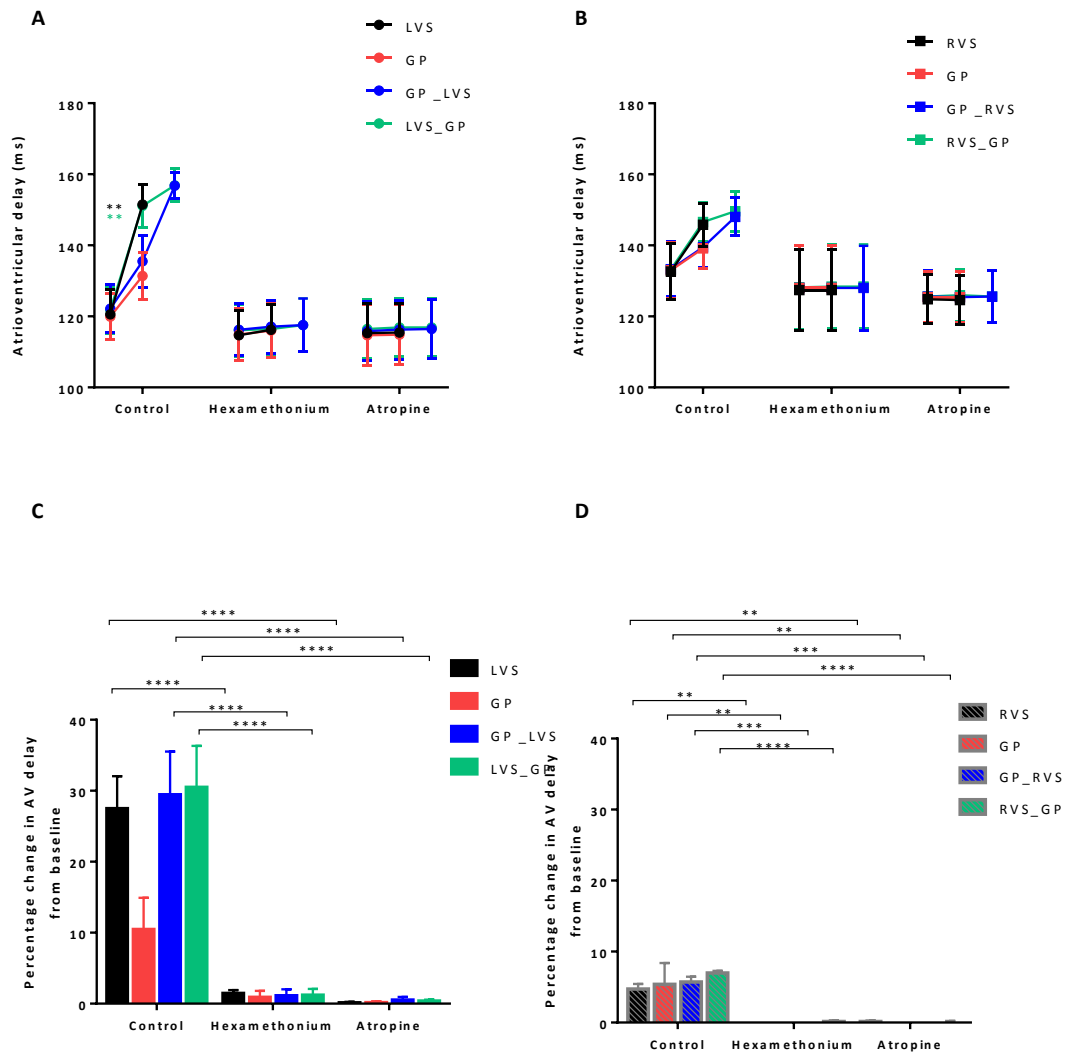


Figure 6.5: Pharmacological autonomic blockade of dromotropic responses to vagus nerve and intrinsic cardiac ganglia stimulation. Data representing the average change in atrioventricular delay during stimulation protocols in control, hexamethonium and atropine (A and B). Data presented as mean \pm SEM. Statistics performed using one-way ANOVA to compare AV delay during stimulation to baseline heart rate as well as compare background stimulation to dual stimulation. C and D show the average percentage change in AV delay from baseline during all stimulation protocols in conditions of control, hexamethonium and atropine. A and C indicate the effects of left vagus stimulation with B and D illustrating the effects of right vagus stimulation. Statistics to compare control protocols with each pharmacological blocker were performed using two-way ANOVA. (** $p < 0.01$, *** $p < 0.001$ and **** $p < 0.0001$).

6.3 Discussion

In this study, the interactions between peripheral autonomic nerves and the intrinsic cardiac nervous system and the role they play in the modulation of heart rate and atrioventricular conduction were investigated.

It has previously been shown that the use of the isolated perfused rabbit heart with intact dual autonomic innervation allows the study of the effects of the extrinsic cardiac nerves on cardiac electrophysiology (Ng *et al.*, 2001). This preparation was therefore used to characterise the effects of these neuronal inputs with those now known to reside at the level of the heart within the ICNS itself.

Stimulation of the vagus nerves at varying voltages and frequencies was completed to determine the level of stimulation required to produce comparatively similar changes in heart rate between all experiments. Electrical stimulation of both the left and right vagus nerves was shown to produce both a voltage and frequency dependent reduction in heart rate. The abrupt changes in heart rate during stimulation come about as a result of the rapid activation of muscarinic receptors by acetylcholine (Levy *et al.*, 1993), which is quickly broken down following the cessation of stimulation by acetylcholinesterase. In this study, greater decreases in heart rate were observed during stimulation of the right vagus nerve when compared to that of the left, during stimulation at higher frequencies. This correlates with previous data shown by Ng *et al.* (2001) and has been attributed to the predominance of the right vagus nerve at the sinoatrial node (Ardell and Randall, 1986).

This study investigated the interaction of the vagus nerves with the ganglia within the right neuronal cluster only. The right neuronal cluster is a collection of neurons and ganglia known to be located at the cranial aspect of the interatrial groove, extending to the root of the superior vena cava and right pulmonary vein (Saburkina *et al.*, 2014). Stimulation at all loci within the RNC in this instance resulted in a bradycardic change in heart rate. It has previously been reported (chapter 5) that stimulation of the ganglia within the RNC can result in a biphasic response, however, this was not evident during this study. Despite this absence of sympathetic response, it is likely still that ganglia

within the ICNS of these animals are capable of producing such a response, however, in this instance, the specific ganglia necessary to do so were not stimulated.

The data within this study demonstrates that the bradycardic response seen as a result of electrical stimulation of intrinsic cardiac ganglia is greater in the presence of either left or right vagal nerve stimulation, independent of the order of stimulation. This suggests that postganglionic vagal nerve fibres potentially synapse with neurons within the intrinsic cardiac ganglia, which act as a gating centres to determine the level of output and therefore innervation of the sinoatrial node.

Stimulation of the left vagus in addition to GP stimulation resulted in greater reductions in heart rate when compared to those seen during stimulation of the right vagus. Based on the understanding that the right vagus is predominant in the control of heart rate via the SA node, this result is contrary to what is currently known. The most likely explanation for this difference in heart rate change between the left and right vagi regards the involvement of specific ganglia within the ICNS. Experiments were completed with the aim of investigating the stimulation of both vagus nerves with the same intrinsic cardiac loci. Unfortunately due to experimental issues such as nerve damage or the movement of the stimulating electrode prior to the completion of stimulation protocols, this was not always possible. It could therefore be plausible that the ganglia examined in collaboration with the right vagus nerve played a slightly different role in cardiac control compared to those stimulated alongside the left vagus. One noteworthy point to mention is the variation in the baseline heart rate when comparing the effects of stimulation of either the left vagus, right vagus or GP alone. Unfortunately a direct comparison between all methods of stimulation within the same preparations could not be made due to technical difficulties in electrode placement and nerve damage. This could also explain why although similar heart rate effects were seen when the left and right vagus nerves alongside GP stimulation were compared (figure 6.2), the data when examining the right vagus stimulation was not statistically significant.

Stimulation of all loci examined resulted in prolongation of atrioventricular delay. As shown with heart rate, this effect was further increased with the addition of vagus nerve stimulation. Stimulation of the left vagus resulted in a significantly larger delay in

atrioventricular conduction when compared to the right vagus, correlating with previous data demonstrating the left vagus plays a predominant role in the innervation of the atrioventricular node (Ng *et al.*, 2001).

Classically it was thought that efferent vagal innervation was concentrated at both the sinoatrial and atrioventricular nodes (Herring and Paterson, 2009) and that the ICNS acted purely as a parasympathetic relay station. This has been shown to not be the case however, with the ICNS now being documented as the third tier of neuronal circuitry alongside the spinal cord and medulla and extracardiac neurons such as the stellate ganglia (Armour, 2007). Ganglia within the ICNS, which is capable of functioning as an independent neuronal circuit (Armour *et al.*, 1998, Murphy *et al.*, 2000), communicate to co-ordinate peripheral reflex function. This correlates with the data shown throughout this chapter illustrating a significant level of crosstalk between vagal efferent nerves and the intrinsic cardiac ganglia.

Study in larger mammals shows that ablation of the ganglia located between the superior vena cava and the aorta, corresponding to the location of the RNC in the rabbit, results in the acute elimination of the effects of vagal stimulation (Chiou *et al.*, 1997). It was proposed that this GP was the 'head station' between the extrinsic and intrinsic cardiac nervous systems (Lo *et al.*, 2013), playing a crucial role in cardiac function and more importantly, the initiation of autonomic arrhythmias. Previous studies have demonstrated that individual ganglia do not necessarily have select functions in cardiac control but instead initiate complex central and local reflexes via the recruitment of cholinergic and adrenergic efferent postganglionic neurons (Armour, 2011). It is because of this interaction between ganglionic plexuses and central neuronal command centres, as well as with neuronal somata within other ganglia of the ICNS (Armour, 2011), that all ganglia must be examined together in order to understand the true effects of vagal nerve stimulation on the ICNS.

The data shown herein demonstrates that the induction of both cardiac bradycardia and AV delay prolongation during combined electrical stimulation of the vagus nerves and intrinsic cardiac ganglia within the RNC is abolished in the presence of both hexamethonium and atropine. This data correlates with that shown previously where vagal nerve stimulation was abolished in the presence of both atropine and

hexamethonium (Cardinal *et al.*, 2009, Ng *et al.*, 2001, Brack *et al.*, 2011), without altering cardiac function in unstimulated conditions and suggests that vagus nerve stimulation activates subpopulations of intrinsic cardiac neurons thereby modulating vagal input to both the sinoatrial and atrioventricular nodes.

Nicotinic blockade using hexamethonium leads to compromised synaptic efficacy within the ICNS, which has previously been shown to reduce cardiac susceptibility to arrhythmia during episodes of autonomic dysfunction (Gibbons *et al.*, 2012). The intricacy of the ICNS was further confirmed by Lo *et al.* (2013) who found that ablation of the GP located between the superior vena cava and aorta increased susceptibility to atrial fibrillation, suggested that activity of the extrinsic cardiac nerves including the vagi may tonically inhibit rather than stimulate the activity of the ICNS.

Despite the data shown here demonstrating a significant interaction between the vagal nerves and the intrinsic cardiac nervous system, the precise influence of the intrinsic cardiac ganglia on extrinsic autonomic postganglionic nerve terminal still requires clarification. Although the isolated innervated heart preparation enables the study of extrinsic innervation, it does not necessarily provide the ideal platform for investigating the full ICNS. Traditional Langendorff perfusion via the aorta allows for dissection down to the level of the heart known to contain the intrinsic cardiac ganglia (Saburkina *et al.*, 2014, Yuan *et al.*, 1994, Pauza *et al.*, 2002a). Due to the orientation of the heart within the preparation and connections via the ascending aorta, precise stimulation of intrinsic cardiac ganglia was difficult to achieve, hence stimulation at only the RNC region being achievable. Future study would therefore require modification of this preparation to allow access to the intrinsic cardiac nervous system via the dorsal region of the thorax.

A limiting factor in determining the functional role of the intrinsic cardiac nervous system using electrical stimulation, is determining the precise positioning of the stimulating electrode and understanding specifically which ganglia are involved in the production of the cardiac responses seen. In order to develop a thorough and complete understanding of the complex involvement of the ICNS in cardiac control, it is vital that further investigation be done not only to identify the connections between individual ganglia but also at a more central level, to determine the complete interaction of all

levels of neuronal hierarchy from the central command of the brainstem and spinal cord right down to individual ganglia within the ICNS.

Chapter 7: Concluding remarks

Over the past two decades, there has been increasing recognition for the functional role of the intrinsic cardiac nervous system in the autonomic control of cardiac function. The location of the ICNS in the rabbit at the level of the heart hilum and at the roots of the pulmonary veins, correlating with that of the ICNS in humans, suggests that this network may act as a final stage in the regulation of cardiac control. Previously, only one study has been aimed at determining the anatomical distribution of the rabbit ICNS (Saburkina *et al.*, 2014), the data of which correlates with the data from that in this thesis. By replicating and modifying the methods used in the study from 2014, the effects of myocardial infarction and heart failure could be investigated.

This is the first study to investigate the functional effects of activating sites within ganglia of the ICNS in rabbit hearts. Unlike previous *in vivo* studies conducted in dogs, the tests carried out in this study were performed on a Langendorff perfused heart preparation to avoid the influence of extrinsic autonomic nerves and circulatory factors and therefore demonstrating the functional independence of the nerves and ganglia within the rabbit ICNS. This study shows that the electrical effects observed were dependent on cholinergic nicotinic ganglion transmission and that bradycardiac effects were mediated by cholinergic muscarinic receptors whilst tachycardiac effects were mediated via postganglionic beta adrenoreceptor sites, correlating with immunohistochemical data showing the wide phenotypic complexity of the ICNS. Of particular importance are the clear demonstration of neurons immunoreactive solely for nNOS, with nerve fibres synapsing with neurons in connecting ganglia. Earlier studies in isolated innervated rabbit heart preparations showed that stimulation of the cervical vagus nerve produced an anti-arrhythmic effect on ventricular contraction dependent solely upon nitrergic postganglionic fibres (Brack *et al.*, 2011, Coote, 2013). This study provides histological support for this concept and exploration of the physiology of these neurons is required.

The intrinsic cardiac ganglia act not as singular entities, but as part of a larger neuronal network providing constant finely tuned feedback in the control of cardiac function (figure 7.1). The continued growing interest of the functional complexity of the ICNS and the interaction of the ICNS with the remainder of the autonomic neuronal hierarchy,

provides numerous avenues for further investigation and the possible utilisation of this interaction in reversing the damage and dysfunction caused by cardiac disease.

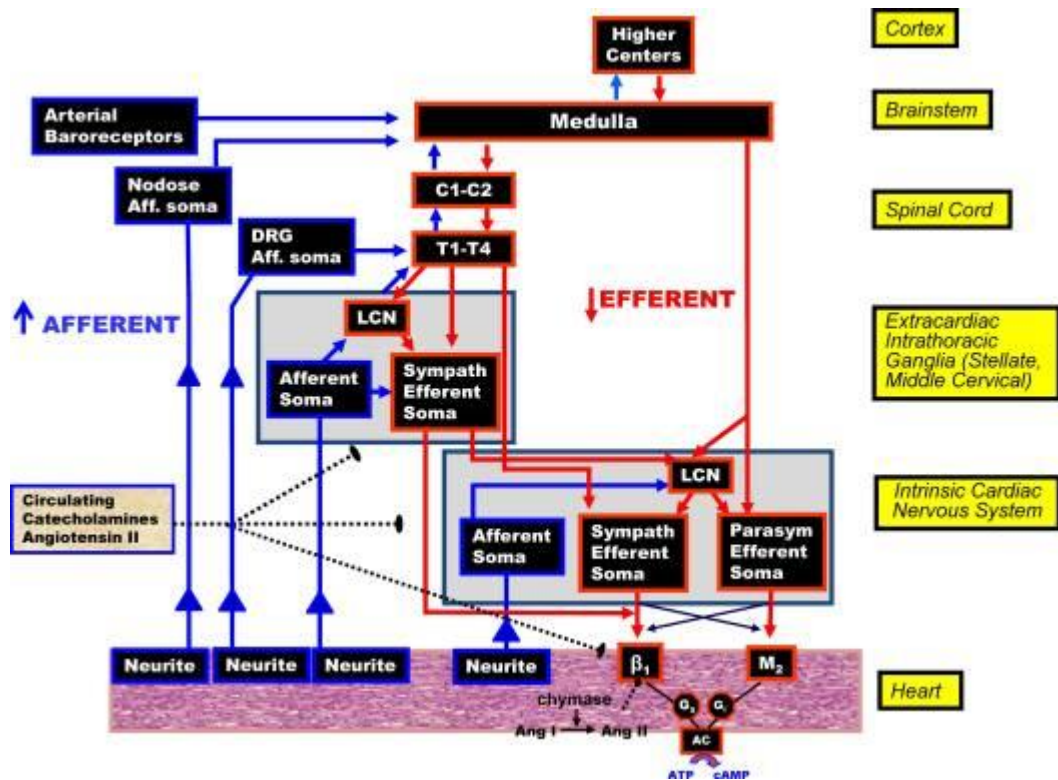


Figure 7.1: The organisation of the neural innervation of the heart. The heart is innervated by numerous tiers of neural circuits from the higher centres to the complex interactions within the ICNS itself. This figure by (Fukuda *et al.*, 2015), illustrates the basic framework for understanding cardiac innervation, correlating with the data shown within this thesis. Abbreviations: Aff, afferent; Ang, angiotensin; C, cervical; DRG, dorsal root ganglia; LCN, local circuit neuron; T, thoracic.

Since the discovery of the ICNS, studies have implicated the involvement of this neuronal network in not only normal physiology but also in the development of disease pathology. Heightened sympathetic tone, a recognised pro-arrhythmic marker, along with an increase in parasympathetic withdrawal indicates a significant involvement of the autonomic nervous system in heart failure. The significant structural and functional remodelling of the ICNS also seen as a consequence of MI suggests that one function of this network is to protect the heart against central neuronal dysregulation and to reduce the susceptibility of the heart to the development of potentially lethal arrhythmias. Based on these findings and current literature, the ICNS could be a significant potential therapeutic target for cardiac diseases with a known involvement of the autonomic nervous system.

The induction of alterations in the neurochemical phenotype of neurons as a result of MI is regionally diverse. Recent literature has failed to investigate this alteration within the ICNS in its entirety. In order to fully understand the significance and link between these changes in phenotype and the resultant changes in functional capabilities, a complete phenotypic map of the ICNS in a heart failure needs to be developed. Using the immunohistochemical techniques detailed within this study with the inclusion of additional neurochemical markers, in animals that have undergone coronary artery ligation, would provide an insight into the adaptation and remodelling that occurs within the ICNS in order to counteract the overall failing of the heart seen in heart failure.

This study has examined the basic functional capabilities of individual ganglionic plexuses, yet literature suggests this is far from the complete story. In order to determine the precise interactions between spatially divergent ganglia, further investigation using pharmacological activation as well as ablation of specific ganglia is necessary.

The experiments shown in this study also demonstrate an interaction between the neurons within the intrinsic cardiac nervous system and peripheral neuronal inputs to the heart. To date, this is the first study to investigate the interactions between the vagus nerve and the ICNS in the rabbit using a novel modification of the dual innervated heart preparation. As with the Langendorff preparation, this model allows for the investigation of this important neural interaction, whilst eliminating the effects of

circulatory hormonal factors. The evidence shown herein suggesting that postganglionic vagal fibres synapse with intrinsic cardiac neurons, supports previous *in vivo* findings and highlights the importance of this study. Understanding this important neural interaction improves our knowledge of cardiac innervation and neural control, with further investigation being necessary to understand the functional role of the autonomic nervous system in cardiac diseases including in heart failure and lethal arrhythmias.

One significant difficulty in determining the precise interaction between the spatially and functionally diverse intrinsic cardiac ganglia and the peripheral nerves was the accessibility and visualisation of the region of the heart known to contain the ICNS. This experimental drawback came as a result of the orientation of the heart within the dual innervated heart preparation. Further investigation into the precise interaction between specific individual ganglia and the extrinsic neuronal hierarchy would therefore require modification of the preparation and potentially the development of an alternative experimental setup to enable access to the region of the heart hilum.

In conclusion, based upon currently available literature and the findings shown within this study, the ICNS plays a vital role in the control and regulation of cardiac function. However, in order to fully elucidate the precise involvement of the ICNS in autonomic control, further research is needed.

Chapter 8: Bibliography

ACCILI, E. A., PROENZA, C., BARUSCOTTI, M. & DIFRANCESCO, D. 2002. From funny current to HCN channels: 20 years of excitation. *News Physiol Sci*, 17, 32-7.

ARDELL, J. L. 1994. Structure and function of mammalian intrinsic cardiac neurons *In: ARMOUR, J. A. & ARDELL, J. L. (eds.) Neurocardiology*. New York: Oxford University Press.

ARDELL, J. L. & ARMOUR, J. A. 2016. Neurocardiology: Structure-Based Function. *Compr Physiol*, 6, 1635-1653.

ARDELL, J. L., RAJENDRAN, P. S., NIER, H. A., KENKNIGHT, B. H. & ARMOUR, J. A. 2015. Central-peripheral neural network interactions evoked by vagus nerve stimulation: functional consequences on control of cardiac function. *Am J Physiol Heart Circ Physiol*, 309, H1740-52.

ARDELL, J. L. & RANDALL, W. C. 1986. Selective vagal innervation of sinoatrial and atrioventricular nodes in canine heart. *Am J Physiol*, 251, H764-73.

ARMOUR, J. A. 1991. Anatomy and function of the intrathoracic neurons regulating the mammalian heart. *In: ZUCKER, I. H. & GILMORE, J. (eds.) Reflex Control of the Circulation*. Boca Raton, FL: CRC Press.

ARMOUR, J. A. 2004. Cardiac neuronal hierarchy in health and disease. *Am J Physiol Regul Integr Comp Physiol*, 287, R262-71.

ARMOUR, J. A. 2007. The little brain on the heart *Cleveland Clinic Journal of Medicine* 74, S48-51.

ARMOUR, J. A. 2008. Potential clinical relevance of the 'little brain' on the mammalian heart. *Exp Physiol*, 93, 165-76.

ARMOUR, J. A. 2011. Physiology of the intrinsic cardiac nervous system. *Heart Rhythm*, 8, 739.

ARMOUR, J. A., COLLIER, K., KEMBER, G. & ARDELL, J. L. 1998. Differential selectivity of cardiac neurons in separate intrathoracic autonomic ganglia. *Am J Physiol*, 274, R939-49.

ARMOUR, J. A. & HOPKINS, D. A. 1981. Localization of sympathetic postganglionic neurons of physiologically identified cardiac nerves in the dog. *J. Comp. Neurol*, 169-184.

ARMOUR, J. A., HUANG, M. H. & SMITH, F. M. 1993. Peptidergic modulation of in situ canine intrinsic cardiac neurons. *Peptides*, 14, 191-202.

- ARMOUR, J. A., MURPHY, D. A., YUAN, B. X., MACDONALD, S. & HOPKINS, D. A. 1997. Gross and microscopic anatomy of the human intrinsic cardiac nervous system. *Anat Rec*, 247, 289-87.
- ARORA, R. C. & ARMOUR, J. A. 2003. Adenosine A1 receptor activation reduces myocardial reperfusion effects on intrinsic cardiac nervous system. *Am J Physiol Regul Integr Comp Physiol*, 284, R1314-21.
- ARORA, R. C., CARDINAL, R., SMITH, F. M., ARDELL, J. L., DELL'ITALIA, L. J. & ARMOUR, J. A. 2003. Intrinsic cardiac nervous system in tachycardia induced heart failure. *Am J Physiol Regul Integr Comp Physiol*, 285, R1212-23.
- AZEVEDO, E. R. & PARKER, J. D. 1999. Parasympathetic control of cardiac sympathetic activity: normal ventricular function versus congestive heart failure. *Circulation*, 100, 274-9.
- BALUK, P. & GABELLA, G. 1990. Some parasympathetic neurons in the guinea-pig heart express aspects of the catecholaminergic phenotype in vivo. *Cell Tissue Res*, 261, 275-85.
- BATTER, C., VEIGEL, C., HOMSHER, E. & SELLERS, J. R. 2014. To understand muscle you must take it apart. *Front Physiol*, 11, 90.
- BATULEVICIUS, D., PAUZIENE, N. & PAUZA, D. H. 2003. Topographic morphology and age-related analysis of the neuronal number of the rat intracardiac nerve plexus. *Ann Anat*, 185, 449-59.
- BATULEVICIUS, D., PAUZIENE, N. & PAUZA, D. H. 2005. Architecture and age-related analysis of the neuronal number of the guinea pig intrinsic cardiac nerve plexus. *Ann Anat*, 187, 225-43.
- BATULEVICIUS, D., SKRIPKA, V., PAUZIENE, N. & PAUZA, D. H. 2008. Topography of the porcine epicardiac nerve plexus as revealed by histochemistry for acetylcholinesterase. *Auton Neurosci*, 138, 64-75.
- BEAUMONT, E., SALAVATIAN, S., SOUTHERLAND, E. M., VINET, A., JACQUEMET, V., ARMOUR, J. & ARDELL, J. L. 2013. Network interactions within the canine intrinsic cardiac nervous system: implications for reflex control of regional cardiac function. *J Physiol*, 591, 4515-33.
- BEAUMONT, E., WRIGHT, G. L., SOUTHERLAND, E. M., LI, Y., CHUI, R., KENKNIGHT, B. H., ARMOUR, J. A. & ARDELL, J. L. 2016. Vagus nerve stimulation mitigates intrinsic cardiac neuronal remodelling and cardiac hypertrophy induced by chronic pressure overload in guinea pig. *Am J Physiol Heart Circ Physiol*, 310, H1349-59.

- BERS, D. M. 2001. *Excitation-contraction coupling and cardiac contractile force*, London, Kluwer Academic.
- BERS, D. M. 2006. Altered cardiac myocyte Ca regulation in heart failure. *Physiology (Bethesda)*, 21, 380-387.
- BIBEVSKI, S. & DUNLAP, M. E. 2011. Evidence for impaired vagus nerve activity in heart failure. *Heart Fail Rev*, 16, 129-35.
- BRACK, K. E., COOTE, J. H. & NG, G. A. 2004. Interaction between direct sympathetic and vagus nerve stimulation on heart rate in the isolated rabbit heart. *Exp Physiol*, 89, 128-39.
- BRACK, K. E., COOTE, J. H. & NG, G. A. 2011. Vagus nerve stimulation protects against ventricular fibrillation independent of muscarinic receptor activation. *Cardiovasc Res*, 91, 437-46.
- BRACK, K. E., PATEL, V. H., COOTE, J. H. & NG, G. A. 2007. Nitric oxide mediates the vagal protective effect on ventricular fibrillation via effects on action potential duration restitution in the rabbit heart. *J Physiol*, 583, 695-704.
- BRACK, K. E., WINTER, J. & NG, G. A. 2013. Mechanisms underlying the autonomic modulation of ventricular fibrillation initiation--tentative prophylactic properties of vagus nerve stimulation on malignant arrhythmias in heart failure. *Heart Fail Rev*, 18, 389-408.
- BRODDE, O.-E. & MICHEL, M. C. 1999. Adrenergic and muscarinic receptors in the human heart. *Pharmacological Reviews*, 51, 651-690.
- BROWN, H. F., DIFRANCESCO, D. & NOBLE, S. J. 1979. How does adrenaline accelerate the heart? *Nature*, 280, 235-236.
- BUCCHI, A., BARUSCOTTI, M., ROBINSON, R. B. & DIFRANCESCO, D. 2007. Modulation of rate by autonomic agonists in SAN cells involves changes in diastolic depolarization and the pacemaker current. *J Mol Cell Cardiol*, 43, 39-48.
- BUTLER, C. K., SMITH, F. M., CARDINAL, R., MURPHY, D. A., HOPKINS, D. A. & ARMOUR, J. A. 1990. Cardiac responses to electrical stimulation of discrete loci in canine atrial and ventricular ganglionated plexi. *Am J Physiol* 259, H1365-H1373.
- CARDINAL, R., PAGE, P., VERMEULEN, M., ARDELL, J. L. & ARMOUR, J. A. 2009. Spatially divergent cardiac responses to nicotinic stimulation of ganglionated plexus neurons in the canine heart. *Auton Neurosci*, 145, 55-62.

- CHANG, H. Y., LO, L. W., LIN, Y. J., LEE, S. H., CHIOU, C. W. & CHEN, S. A. 2014. Relationship between intrinsic cardiac autonomic ganglionated plexi and the atrial fibrillation nest. . *Circ J*, 78, 922-8.
- CHENG, Z. & POWLEY, T. L. 2000. Nucleus ambiguus projections to cardiac ganglia of rat atria: an anterograde tracing study. . *J Comp Neurol*, 424, 588-606.
- CHENG, Z., POWLEY, T. L., SCHWABER, J. S. & DOYLE, F. J. R. 1999. Projections of the dorsal motor nucleus of the vagus to cardiac ganglia in rat atria: an anterograde tracing study. . *J Comp Neurol*, 410, 320-41.
- CHIN, S. H. 2017. *Autonomic modulation in a rabbit model of heart failure* Doctor of Philosophy, University of Leicester.
- CHIOU, C. W., EBLE, J. N. & ZIPES, D. P. 1997. Efferent vagal innervation of the canine atria and sinus and atrioventricular nodes. The third fat pad. . *Circulation*, 95, 2573-84.
- CHOATE, J. K., DANSON, E. J., MORRIS, J. F. & PATERSON, D. J. 2001. Peripheral vagal control of heart rate is impaired in neuronal NOS knockout mice. *Am J Physiol Heart Circ Physiol*, 281, H2310-H2317.
- CHOATE, J. K. & PATERSON, D. J. 1999. Nitric oxide inhibits the positive chronotropic and inotropic responses to sympathetic nerve stimulation in the isolated guinea-pig atria. . *J Auton Nerv Syst*, 75, 100-108.
- COHN, J. N., FERRARI, R. & SHARPE, N. 2000. Cardiac remodeling - concepts and clinical implications: a consensus paper from an international forum on cardiac remodeling. . *J Am Coll Cardiol*, 35, 569-82.
- COOTE, J. H. 2013. Myths and realities of the cardiac vagus. *J Physiol*, 591, 4073-85.
- COOTE, J. H. & CHAUHAN, R. A. 2016. The sympathetic innervation of the heart: Important new insights. *Autonomic Neuroscience*, 199, 17-23.
- CRICK, S. J., SHEPPARD, M. N., ANDERSON, R. H., POLAK, J. M. & WHARTON, J. 1996. A quantitative study of nerve distribution in the conduction system of the guinea pig heart. *J Anat*, 188, 403-16.
- CRICK, S. J., SHEPPARD, M. N., HO, S. Y. & ANDERSON, R. H. 1999. Localisation and quantitation of autonomic innervation in the porcine heart 1: conduction system. . *J Anat*, 195 (pt3), 341-57.
- DAWSON, T. A., LI, D., WOODWARD, T., BARBER, Z., WANG, L. & PATERSON, D. J. 2008. Cardiac cholinergic NO-cGMP signalling following acute myocardial infarction and nNOS gene transfer. *Am J Physiol Heart Circ Physiol*, 295, H990-998.

- DEHLIN, H. M. & LEVICK, S. P. 2014. Substance P in heart failure: the good and the bad. *Int J Cardiol*, 170, 270-7.
- DENNINGER, J. W. & MARLETTA, M. A. 1999. Guanylate cylcase and the NO/cGMP signalling pathway *Biochim Biophys Acta*, 1411, 334-350.
- DIFRANCESCO, D. 2010. The role of the funny current in pacemaker activity. *Circ Res*, 106, 434-46.
- DIFRANCESCO, D. & TROMBA, C. 1988. Muscarinic control of the hyperpolarization-activated current (if) in rabbit sino-atrial node myocytes. *J Physiol*, 405, 493-510.
- DUNLAP, M. E., BIBEVSKI, S., ROSENBERRY, T. L. & ERNSBERGER, P. 2003. Mechanisms of altered vagal control in heart failure: influence of muscarinic receptors and acetylcholinesterase activity. *Am J Physiol* 285, H1632-H1640.
- EDLER, I. & HERTZ, C. H. 1954. The use of ultrasonic reflectoscope for the continuous recording of the movements of heart walls. *Clinical Physiology and Functional Imaging* 24, 118-136.
- EINBRODT 1859. Ueber Herzeizung und ihr Verhaeltnis zum Blutdruck. *Akad. Wiss. Sitzungsber*, 38, 345-359.
- FEHER, J. 2012. The cardiac action potential *Quantitative Human Physiology* Elsevier
- FRYATT, A. G., VIAL, C., MULHERAN, M., GUNTHORPE, M. J. & GRUBB, B. D. 2009. Voltage-gated sodium channel expression in rat spiral ganglion neurons *Molecular and Cellular Neuroscience* 42, 399-407.
- FUKUDA, K., KANAZAWA, H., AIZAWA, Y., ARDELL, J. L. & SHIVKUMAR, K. 2015. Cardiac innervation and sudden cardiac death. *Circ Res*, 116, 2005-19.
- GAGLIARDI, M., RANDALL, W. C., BIEGER, D., WURSTER, R. D., HOPKINS, D. A. & ARMOUR, J. A. 1988. Activity of in vivo canine cardiac plexus neurons. *Am J Physiol*, 255, H789-800.
- GATTI, P. J., JOHNSON, T. A. & MASSARI, V. J. 1996. Can neurons in the nucleus ambiguus selectively regulate cardiac rate and atrio-ventricular conduction? *J Auton Nerv Syst*, 57, 123-7.
- GIBBONS, D. D., SOUTHERLAND, E. M., HOOVER, D. B., BEAUMONT, E., ARMOUR, J. A. & ARDELL, J. L. 2012. Neuromodulation targets intrinsic cardiac neurons to attenuate neuronally mediated atrial arrhythmias. *Am J Physiol Regul Integr Comp Physiol*, 302, R357-64.

GRAY, A. L., JOHNSON, T. A., ARDELL, J. L. & MASSARI, V. J. 2004. Parasympathetic control of the heart. II. A novel interganglionic intrinsic cardiac circuit mediates neural control of heart rate. *J Appl Physiol* (1985), 96, 2273-8

HABECKER, B. A., ANDERSON, M. E., BIRREN, S. J., FUKUDA, K., HERRING, N., HOOVER, D. B., KANAZAWA, H., PATERSON, D. J. & RIPPLINGER, C. M. 2016. Molecular and cellular neurocardiology: development and cellular and molecular adaptations to heart disease. *J Physiol*, 594, 3853-75.

HAMRELL, B. B. & ALPERT, N. R. 1986. Cellular basis of the mechanical properties of hypertrophied myocardium. *In: FOZZARD, H. A., HABER, E., JENNINGS, R. B., KATZ, A. M. & MORGAN, H. E. (eds.) The heart and cardiovascular system* New York (NY): Raven Press.

HARDWICK, J. C., RYAN, S. E., BEAUMONT, E., ARDELL, J. L. & SOUTHERLAND, E. M. 2014. Dynamic remodeling of the guinea pig intrinsic cardiac plexus induced by chronic myocardial infarction. *Auton Neurosci*, 181, 4-12.

HAUPTMAN, P. J., SCHWARTZ, P. J., GOLD, M. R., BORGGREFE, M., VAN VELDHUISEN, D. J., STARLING, R. C. & MANN, D. L. 2012. Rationale and study design of the increase of vagal tone in heart failure study: INOVATE-HF. *Am Heart J*, 163, 954-962 e1.

HE, B., LU, Z., HE, W., WU, L., CUI, B., HU, X., YU, L., HUANG, C. & JIANG, H. 2013. Effects of ganglionated plexi ablation on ventricular electrophysiological properties in normal hearts and after acute myocardial ischemia. *Int J Cardiol*, 168, 86-93.

HENNING, R. J. & SAWMILLER, D. R. 2001. Vasoactive intestinal peptide: cardiovascular effects. *Cardiovasc Res*, 49, 27-37.

HERRING, N. 2015. Autonomic control of the heart: going beyond the classical neurotransmitters. *Exp Physiol*, 100, 354-8.

HERRING, N., CRANLEY, J., LOKALE, M. N., LI, D., SHANKS, J., ALSTON, E. N., GIRARD, B. M., CARTER, E., PARSONS, R. L., HABECKER, B. A. & PATERSON, D. J. 2012. The cardiac sympathetic co-transmitter galanin reduces acetylcholine release and vagal bradycardia: implications for neural control of cardiac excitability. *J Mol Cell Cardiol*, 52, 667-76.

HERRING, N., DANSON, E. J. & PATERSON, D. J. 2002. Cholinergic control of heart rate by nitric oxide is site specific. *News Physiol Sci*, 17, 202-6.

HERRING, N., LOKALE, M. N., DANSON, E. J., HEATON, D. A. & PATERSON, D. J. 2008. Neuropeptide Y reduces acetylcholine release and vagal bradycardia via a Y2 receptor-mediated, protein kinase C-dependent pathway. *J Mol Cell Cardiol*, 44, 477-85.

- HERRING, N. & PATERSON, D. J. 2001. Nitric oxide-cGMP pathway facilitates acetylcholine release and bradycardia during vagal nerve stimulation in the guinea-pig in vitro. *J Physiol*, 535, 507-18.
- HERRING, N. & PATERSON, D. J. 2009. Neuromodulators of peripheral cardiac sympatho-vagal balance. *Exp Physiol*, 94, 46-53.
- HERRING, N., ZAMAN, J. A. & PATERSON, D. J. 2001. Natriuretic peptides like NO facilitate cardiac vagal neurotransmission and bradycardia via a cGMP pathway. *Am J Physiol Heart Circ Physiol*, 281, H2318-27.
- HERSHBERGER, R. E., ANDERSON, F. L. & BRISTOW, M. R. 1988. The vasoactive intestinal peptide receptor in failing human ventricular myocardium exhibits increased affinity and decreased density. *Circ Res*, 65, 283-94.
- HOARD, J. L., HOOVER, D. B. & WONDERGEM, R. 2007. Phenotypic properties of adult mouse intrinsic cardiac neurons maintained in culture. *Am J Physiol Cell Physiol*, 293, C1875-83.
- HOOVER, D. B. 1990. Effects of substance P on rate and perfusion pressure in the isolated guinea pig heart. *J Pharmacol Exp Ther*, 252, 179-84.
- HOOVER, D. B., GANOTE, C. E., FERGUSON, S. M., BLAKELY, R. D. & PARSONS, R. L. 2004. Localization of cholinergic innervation in guinea pig heart by immunohistochemistry for high-affinity choline transporters. *Cardiovasc Res*, 62, 112-21.
- HOOVER, D. B. & HANCOCK, J. C. 1988. Distribution of substance P binding sites in guinea-pig heart and pharmacological effects of substance P. *J Auton Nerv Syst*, 23, 189-97.
- HOOVER, D. B., ISAACS, E. R., JACQUES, F., HOARD, J. L., PAGE, P. & ARMOUR, J. A. 2009. Localization of multiple neurotransmitters in surgically derived specimens of human atrial ganglia. *Neuroscience*, 164, 1170-9.
- HOOVER, D. B., SHEPHERD, A. V., SOUTHERLAND, E. M., ARMOUR, J. A. & ARDELL, J. L. 2008. Neurochemical diversity of afferent neurons that transduce sensory signals from dog ventricular myocardium. *Auton Neurosci*, 141, 38-45.
- HOPKINS, D. A. & ARMOUR, J. A. 1984. Localization of sympathetic postganglionic and parasympathetic preganglionic neurons which innervate different regions of the dog heart. *J Comp Neurol*, 229, 186-98.
- HOPKINS, D. A. & ARMOUR, J. A. 1989. Ganglionic distribution of afferent neurons innervating the canine heart and cardiopulmonary nerves. *J Auton Nerv Syst*, 26, 213-22.

- HOPKINS, D. A., MACDONALD, S. E., MURPHY, D. A. & ARMOUR, J. A. 2000. Pathology of intrinsic cardiac neurons from ischemic human hearts. *Anat Rec*, 259, 424-36.
- HORACKOVA, M., SLAVIKOVA, J. & BYCZKO, Z. 2000. Postnatal development of the rat intrinsic cardiac nervous system: a confocal laser scanning microscopy study in whole-mount atria. *Tissue Cell*, 32, 377-88.
- HOU, Y., SCHERLAG, B. J., LIN, J., ZHOU, J., SONG, J., ZHANG, Y., PATTERSON, E., LAZZARA, R., JACKMAN, W. M. & PO, S. S. 2007a. Interactive atrial neural network: Determining the connections between ganglionated plexi. *Heart Rhythm*, 4, 56-63.
- HOU, Y., SCHERLAG, B. J., LIN, J., ZHOU, J., SONG, J., ZHANG, Y., PATTERSON, E., LAZZARA, R., JACKMAN, W. M. & PO, S. S. 2007b. Interactive atrial neural network: Determining the connections between ganglionated plexi. *Heart Rhythm*, 4, 56-63.
- HUANG, M. H., ARDELL, J. L., HANNA, B. D., WOLF, S. G. & ARMOUR, J. A. 1993. Effects of transient coronary artery occlusion on canine intrinsic cardiac neuronal activity. *Integr Physiol Behav Sci*, 28, 5-21.
- IMAIZUMI, S., MAZGALEV, T., DREIFUS, L. S., MICHELSON, E. L., MIYAGAWA, A., BHARATI, S. & LEV, M. 1990. Morphological and electrophysiological correlates of atrioventricular nodal response to increased vagal activity. *Circulation*, 82, 951-64.
- INOKAITIS, H., PAUZIENE, N., RYSEVAITE-KYGUOLIENE, K. & PAUZA, D. H. 2016. Innervation of sinoatrial nodal cells in the rabbit. *Ann Anat*, 205, 113-21.
- KALLA, M., CHOTALIA, M., COUGHLAN, C., HAO, G., CRABTREE, M. J., TOMEK, J., BUB, G., PATERSON, D. J. & HERRING, N. 2016. Protection against ventricular fibrillation via cholinergic receptor stimulation and the generation of nitric oxide. *J Physiol*, 594, 3981-3992.
- KARNOVSKY, M. J. & ROOTS, L. 1964. A "Direct-Coloring" Thiocholine Method for Cholinesterases. *J Histochem Cytochem*, 12, 219-21.
- KAWASHIMA, T. 2005. The autonomic nervous system of the human heart with special reference to its origin, course and peripheral distribution. *Anat. Emybryol*, 425-438.
- KEMBER, G., ARMOUR, J. A. & ZAMIR, M. 2011. Neural control of heart rate: the role of neuronal networking. *J Theor Biol*, 277, 41-7.
- KLIMASCHEWSKI, L., KUMMER, W., MAYER, B., COURAUD, J. Y., PREISLER, U., PHILIPPIN, B. & HEYM, C. 1992. Nitric oxide synthase in cardiac nerve fibers and neurons of rat and guinea pig heart. *Circ Res*, 71, 1533-7.

KOELLE, G. B., MASSOULIE, J., EUGENE, D., MELONE, M. A. & BOULLA, G. 1987. Distributions of molecular forms of acetylcholinesterase and butyrylcholinesterase in nervous tissue of the cat. . *Proc Natl Acad Sci U S A*, 84, 7749-52.

KOUMI, S., BACKER, C. L. & ARENTZEN, C. E. 1995. Characterization of Inwardly Rectifying K⁺ Channel in Human Cardiac Myocytes. Alterations in channel behaviour in myocytes isolated from patients with idiopathic dilated cardiomyopathy. . *Circulation*, 92, 164-74.

KUNCOVA, J., SLAVIKOVA, J. & REISCHIG, J. 2003. Distribution of vasoactive intestinal polypeptide in the rat heart: effect of guanethidine and capsaicin. *Ann Anat*, 185, 153-61.

KUROTOBI, T., SHIMADA, S., KINO, N., ITO, K., TONOMURA, D., YANO, K., TANAKA, C., YOSHIDA, M., TSUCHIDA, M. & FUKUMOTO, H. 2015. Features of intrinsic ganglionated plexi in both atria after extensive pulmonary isolation and their clinical significance after catheter ablation in patients with atrial fibrillation. *Heart Rhythm*, 12, 470-6.

LA ROVERE, M. T., BIGGER JR, J. T., MARCUS, F. I., MORTARA, A. & SCHWARTZ, P. J. 1998. Baroreflex sensitivity and heart rate variability in prediction of total cardiac mortality after myocardial infarction. *Lancet*, 351, 478-484.

LANGLEY, G. 1921. *The Autonomic Nervous System* Cambridge, UK., Cambridge University Press

LAZZARA, R., SCHERLAG, B. J., ROBINSON, M. J. & SAMET, P. 1973. Selective in situ parasympathetic control of the canine sinoatrial and atrioventricular nodes. *Circ Res*, 32, 393-401.

LEDERER, W. J., BERLIN, J. R., COHEN, N. M., HADLEY, R. W., BERS, D. M. & CANNELL, M. B. 1990. Excitation-contraction coupling in heart cells. Roles of the sodium-calcium exchange, the calcium current, and the sarcoplasmic reticulum. *Ann N Y Acad Sci*, 588, 190-206.

LEVY, M. N. & MARTIN, P. J. 1996. Autonomic control of cardiac conduction and automaticity. *In*: SHEPHERD, J. T. & VATNER, S. F. (eds.) *Nervous Control of the Heart*. Amsterdam: Harwood Academic Publishers.

LEVY, M. N., YANG, T. & WALLICK, D. W. 1993. Assessment of beat-by-beat control of heart rate by the autonomic nervous system: molecular biology technique are necessary, but not sufficient. *J Cardiovasc Electrophysiol*, 4, 183-193.

LI, L., HATCHER, J. T., HOOVER, D. B., GU, H., WURSTER, R. D. & CHENG, Z. J. 2014. Distribution and morphology of calcitonin gene-related peptide and substance P immunoreactive axons in the whole-mount atria of mice. *Auton Neurosci*, 181, 37-48.

- LIAO, K., YU, L., ZHOU, X., SAREN, G., WANG, S., WANG, Z., HUANG, B., YANG, K. & JIANG, H. 2015. Low-level baroreceptor stimulation suppresses atrial fibrillation by inhibiting ganglionated plexus activity. *Can J Cardiol*, 31, 767-74.
- LO, L. W., SCHERLAG, B. J., CHANG, H. Y., LIN, Y. J., CHEN, S. A. & PO, S. S. 2013. Paradoxical long-term proarrhythmic effects after ablating the "head station" ganglionated plexi of the vagal innervation to the heart. *Heart Rhythm*, 10, 751-7.
- LORENTZ, C. U., PARRISH, D. C., ALSTON, E. N., PELLEGRINO, M. J., WOODWARD, W. R., HEMPSTEAD, B. L. & HABECKER, B. A. 2013. Sympathetic denervation of peri-infarct myocardium requires the p75 neurotrophin receptor. *Exp Neurol*, 249, 111-119.
- LOSCALZO, J. & VITA, J. A. 2000. Nitric Oxide and the Cardiovascular System *Humana Press*.
- LUNDBERG, J. M., FRANCO-CERECEDA, A., LACROIX, J. S. & PERNOW, J. 1991. Release of vasoactive peptides from autonomic and sensory nerves. *Blood Vessels*, 28, 27-34.
- MARX, S. O., REIKEN, S., HISAMATSU, Y., JAYARAMAN, T., BURKHOFF, D., ROSEMBLIT, N. & MARKS, A. R. 2000. PKA phosphorylation dissociates FKBP12.6 from the calcium release channel (ryanodine receptor): defective regulation in failing hearts. *Cell* 101, 365-76.
- MONGILLO, M., TOCCHETTI, C. G., TERRIN, A., LISSANDRON, V., CHEUNG, Y. F., DOSTMANN, W. R., POZZAN, T., KASS, D. A., PAOLOCCI, N., HOUSLAY, M. D. & ZACCOLO, M. 2006. Compartmentalized phosphodiesterase-2 activity blunts beta-adrenergic cardiac inotropy via an NO/cGMP-dependent pathway. *Circ Res*, 98, 226-234.
- MOSS, E., CARDINAL, R., YIN, Y. & PAGE, P. 2013. Bilateral atrial ganglionated plexus involvement in atrial responses to left-sided plexus stimulation in canines. *Cardiovasc Res*, 99, 194-202.
- MURPHY, D. A., THOMPSON, G. W., ARDELL, J. L., MCCRATY, R., STEVENSON, R. S., SANGALANG, V. E., CARDINAL, R., WILKINSON, M., CRAIG, S., SMITH, F. M., KINGMA, J. G. & ARMOUR, J. A. 2000. The heart reinnervates after transplantation. *Ann Thorac Surg*, 69, 1769-81.
- MURRAY, K. J. 1990. Cyclic AMP and mechanisms of vasodilation. *Pharmacol Ther*, 47, 329-45.
- NAKAMURA, K., AJIJOLA, O. A., ALIOTTA, E., ARMOUR, J. A., ARDELL, J. L. & SHIVKUMAR, K. 2016. Pathological effects of chronic myocardial infarction on peripheral neurons mediating cardiac neurotransmission. *Auton Neurosci*, 197, 34-40.

NERBONNE, J. M. & KASS, R. S. 2005. Molecular Physiology of Cardiac Repolarization. *Physiol Rev*, 85, 1205-1253.

NG, G. A. 2016. Neuro-cardiac interaction in malignant ventricular arrhythmia and sudden cardiac death. *Auton Neurosci*, 199, 66-79.

NG, G. A., BRACK, K. E. & COOTE, J. H. 2001. Effects of direct sympathetic and vagus nerve stimulation on the physiology of the whole heart - a novel model of isolated Langendorff perfused rabbit heart with intact dual autonomic innervation. *Exp Physiol*, 86, 319-29.

NG, G. A., BRACK, K. E., PATEL, V. H. & COOTE, J. H. 2007. Autonomic modulation of electrical restitution, alternans and ventricular fibrillation initiation in the isolated heart. *Cardiovasc Res*, 73, 750-60.

NG, G. A., COBBE, S. M. & SMITH, G. L. 1998. Non-uniform prolongation of intracellular Ca^{2+} transients recorded from the epicardial surface of isolated hearts from rabbits with heart failure *Cardiovasc Res*, 37, 489-502.

NOLAN, J., BATIN, P. D., ANDREWS, R., LINDSAY, S. J., BROOKSBY, P., MULLEN, M., BAIG, W., FLAPAN, A. D., COWLEY, A., PRESCOTT, R. J., NEILSON, J. M. & FOX, K. A. 1998. Prospective study of heart rate variability and mortality in chronic heart failure: results of the United Kingdom heart failure evaluation and assessment of risk trial (UK-heart). *Circulation*, 98, 1510-6.

NORRIS, J. E., LIPPINCOTT, D. & WURSTER, R. D. 1977. Responses of canine endocardium to stimulation of the upper thoracic roots. *Am J Physiol*, 233, H655-9.

OLIVAS, A., GARDNER, R. T., WANG, L., RIPPLINGER, C. M., WOODWARD, W. R. & HABECKER, B. A. 2016. Myocardial infarction causes transient cholinergic transdifferentiation of cardiac sympathetic nerves via gp130. *J Neurosci*, 36, 479-88.

OPIE, L. H. 2004. *Heart physiology: from cell to circulation*, Lippincott Williams and Wilkins.

OSMAN, F., KUNDU, S., TUAN, J., JEILAN, M., STAFFORD, P. J. & NG, G. A. 2010. Ganglionic plexus ablation during pulmonary vein isolation - predisposing to ventricular arrhythmias? *Indian Pacing Electrophysiol J*, 10, 104-107.

PAPKA, R. E. & URBAN, L. 1987. Distribution, origina and sensitivity to capcaicin of primary afferent substance P-immunoreactive nerves in the heart. *Acta Physiol Hung*, 69, 459-68.

PARSONS, R. L., LOCKNAR, S. A., YOUNG, B. A., HOARD, J. L. & HOOVER, D. B. 2006. Presence and co-localization of vasoactive intestinal polypeptide with neuronal nitric

oxide synthase in cells and nerve fibers within guinea pig intrinsic cardiac ganglia and cardiac tissue. *Cell Tissue Res*, 323, 197-209.

PAUZA, D. H., PAUZIENE, N., PAKELTYTE, G. & STROPUS, R. 2002a. Comparative quantitative study of the intrinsic cardiac ganglia and neurons in the rat, guinea pig, dog and human as revealed by histochemical staining for acetylcholinesterase. *Ann Anat*, 184, 125-36.

PAUZA, D. H., RYSEVAITE-KYGUOLIENE, K., VISMANTAITE, J., BRACK, K. E., INOKAITIS, H., PAUZA, A. G., RIMASAUSKAITE-PETRAITIENE, V., PAUZAITE, J. I. & PAUZIENE, N. 2014. A combined acetylcholinesterase and immunohistochemical method for precise anatomical analysis of intrinsic cardiac neural structures. *Ann Anat*, 196, 430-40.

PAUZA, D. H., SABURKINA, I., RYSEVAITE, K., INOKAITIS, H., JOKUBAUSKAS, M., JALIFE, J. & PAUZIENE, N. 2013. Neuroanatomy of the murine cardiac conduction system: a combined stereomicroscopic and fluorescence immunohistochemical study. *Auton Neurosci*, 176, 32-47.

PAUZA, D. H., SKRIPKA, V. & PAUZIENE, N. 2002b. Morphology of the intrinsic cardiac nervous system in the dog: a whole-mount study employing histochemical staining with acetylcholinesterase. *Cells Tissues Organs*, 172, 297-320.

PAUZA, D. H., SKRIPKA, V., PAUZIENE, N. & STROPUS, R. 2000. Morphology, distribution, and variability of the epicardiac neural ganglionated subplexuses in the human heart. *Anat Rec*, 259, 353-82.

PAUZIENE, N., ALABURDA, P., RYSEVAITE-KYGUOLIENE, K., PAUZA, A. G., INOKAITIS, H., MASAITYTE, A., RUDOKAITE, G., SABURKINA, I., PLISIENE, J. & PAUZA, D. H. 2016. Innervation of the rabbit cardiac ventricles. *J Anat*, 228, 26-46.

POOLE-WILSON, P. A. 1993. Heart failure. Unfinished business - a possible role for vasodilators. *Int J Cardiol*, 40, 1-6.

PRIOLA, D. V., SPURGEON, H. A. & GEIS, W. P. 1977. The intrinsic innervation of the canine heart: a functional study. *Circ Res*, 40, 50-56.

PYE, M. P., BLACK, M. & COBBE, S. M. 1996. Comparison of in vivo and in vitro haemodynamic function in experimental heart failure: use of echocardiography. *Cardiovasc Res* 31, 873-81.

RAJENDRAN, P. S., NAKAMURA, K., AJIJOLA, O. A., VASEGHI, M., ARMOUR, J. A., ARDELL, J. L. & SHIVKUMAR, K. 2016. Myocardial infarction induces structural and functional remodeling of the intrinsic cardiac nervous system. *J Physiol*, 594 (2), 321-341.

- RANDALL, D. C., BROWN, D. R., LI, S. G., OLMSTEAD, M. E., KILGORE, J. M., SPRINKLE, A. G., RANDALL, W. C. & ARDELL, J. L. 1998. Ablation of posterior atrial ganglionated plexus potentiates sympathetic tachycardia to behavioral stress. *Am J Physiol*, 275, R779-87.
- RANDALL, D. C., BROWN, D. R., MCGUIRT, A. S., THOMPSON, G. W., ARMOUR, J. A. & ARDELL, J. L. 2003. Interactions within the intrinsic cardiac nervous system contribute to chronotropic regulation. *Am J Physiol Integr Comp Physiol*, 285, 1066-75.
- RANDALL, D. C., RANDALL, W. C., BROWN, D. R., YINGLING, J. D. & RAISCH, R. M. 1992. Heart rate control in awake dog after selective SA-nodal parasympathectomy. *Am J Physiol*, 262, H1128-35.
- RANDALL, W. C. 1977. Sympathetic Control of the Heart. In: RANDALL, W. C. (ed.) *Neural Regulation of the Heart* New York: Oxford University Press.
- RANDALL, W. C., ARDELL, J. L. & BECKER, D. M. 1985. Differential responses accompanying sequential stimulation and ablation of vagal branches to dog heart. *Am J Physiol*, 249, H133-40.
- RANDALL, W. C., WURSTER, R. D., RANDALL, D. C. & XI-MOY, S. X. 1996. From cardioaccelerator and inhibitory nerves to a heart brain: an evolution of concepts. In: J.T., S. & VAINER, S. F. (eds.) *Nervous Control of the Heart* Amsterdam: Hardwood Academic Publishers.
- RICHARDSON, R. J., GRKOVIC, I. & ANDERSON, C. R. 2003. Immunohistochemical analysis of intracardiac ganglia of the rat heart. *Cell Tissue Res*, 314, 337-50.
- RYSEVAITE, K., SABURKINA, I., PAUZIENE, N., NOUJAIM, S. F., JALIFE, J. & PAUZA, D. H. 2011a. Morphologic pattern of the intrinsic ganglionated nerve plexus in mouse heart. *Heart Rhythm*, 8, 448-54.
- RYSEVAITE, K., SABURKINA, I., PAUZIENE, N., VAITKEVICIUS, R., NOUJAIM, S. F., JALIFE, J. & PAUZA, D. H. 2011b. Immunohistochemical characterization of the intrinsic cardiac neural plexus in whole-mount mouse heart preparations. *Heart Rhythm*, 8, 731-8.
- SABBAH, H. N., STEIN, P. D., KONO, T., GHEORGHIAD, M., LEVINE, T. B., JAFRI, S., HAWKINS, E. T. & GOLDSTEIN, S. 1991. A canine model of chronic heart failure produced by multiple sequential coronary microembolizations. *Am J Physiol Heart Circ Physiol*, 260, H1379-1384.
- SABURKINA, I., GUKAUSKIENE, L., RYSEVAITE, K., BRACK, K. E., PAUZA, A. G., PAUZIENE, N. & PAUZA, D. H. 2014. Morphological pattern of intrinsic nerve plexus distributed on the rabbit heart and interatrial septum. *J Anat*, 224, 583-93.

SABURKINA, I., RYSEVAITE, K., PAUZIENE, N., MISCHKE, K., SCHAUERTE, P., JALIFE, J. & PAUZA, D. H. 2010. Epicardial neural ganglionated plexus of ovine heart: anatomic basis for experimental cardiac electrophysiology and nerve protective cardiac surgery. *Heart Rhythm*, 7, 942-50.

SCHERLAG, B. J. & PO, S. 2006. The intrinsic cardiac nervous system and atrial fibrillation. *Curr Opin Cardiol*, 21, 51-4.

SCHRODER, F., HANDROCK, R., BEUCKELMANN, D. J., HIRT, S., HULLIN, R., PRIEBE, L., SCHWINGER, R. H., WEIL, J. & HERZIG, S. 1998. Increased availability and open probability of single L-type calcium channels from failing compared with nonfailing human ventricle. *Circulation*, 98, 969-76.

SCHWARTS, P. J. & FERRARI, G. M. 2011. Sympathetic-parasympathetic interaction in health and disease: abnormalities and relevance in heart failure. *Heart Fail Rev*, 16, 101-107.

SEKI, A., GREEN, H. R., LEE, T. D., HONG, L., TAN, J., VINTERS, H. V., CHEN, P. S. & FISHBEIN, M. C. 2014. Sympathetic nerve fibers in human cervical and thoracic vagus nerves. *Heart Rhythm*, 11, 1411-7.

SERONE, A. P. & ANGUS, J. A. 1999. Neuropeptide Y is a prejunctional inhibitor of vagal but not sympathetic inotropic responses in guinea-pig isolated left atria. *Br J Pharmacol*, 127, 383-90.

SHEN, M. J. & ZIPES, D. P. 2014. Role of the autonomic nervous system in modulating cardiac arrhythmias. *Circ Res*, 114, 1004-1021.

SINGH, S., JOHNSON, P. I., LEE, R. E., ORFEI, E., LONCHYNA, V. A., SULLIVAN, H. J., MONTROYA, A., TRAN, H., WEHRMACHER, W. H. & WURSTER, R. D. 1996. Topography of cardiac ganglia in the adult human heart. *J Thorac Cardiovasc Surg*, 112, 943-53.

SINGH, S., SAYERS, S., WALTER, J. S., THOMAS, D., DIETER, R. S., NEE, L. M. & WURSTER, R. D. 2013. Hypertrophy of neurons within cardiac ganglia in human, canine, and rat heart failure: the potential role of nerve growth factor. *J Am Heart Assoc*, 2, e000210.

SLAVIKOVA, J., KUNCOVA, J., REISCHIG, J. & DVORAKOVA, M. 2003. Catecholaminergic neurons in the rat intrinsic cardiac nervous system. *Neurochem Res*, 28, 593-8.

SMITH, F. M. 1999. Extrinsic inputs to intrinsic neurons in the porcine heart in vitro. *Am J Physiol* 276, R455-R467.

STEELE, P. A., GIBBINS, I. L. & MORRIS, J. L. 1996. Projections of intrinsic cardiac neurons to different targets in the guinea-pig heart. *J Auton Nerv Syst*, 56, 191-200.

- STEELE, P. A., GIBBINS, I. L., MORRIS, J. L. & MAYER, B. 1994. Multiple populations of neuropeptide-containing intrinsic neurons in the guinea-pig heart. *Neuroscience*, 62, 241-50.
- THOMPSON, G. W., COLLIER, K., ARDELL, J. L., KEMBER, G. & ARMOUR, J. A. 2000. Functional interdependence of neurons in a single canine intrinsic cardiac ganglionated plexus. *J Physiol*, 528, 561-71.
- TRIPOSKIADIS, F., KARAYANNIS, G., GIAMOUZIS, G., SKOULARIGIS, J., LOURIDAS, G. & BUTLER, J. 2009a. The sympathetic nervous system in heart failure physiology, pathophysiology, and clinical implications. *J Am Coll Cardiol*, 54, 1747-62.
- TRIPOSKIADIS, F., KARAYANNIS, G., GIAMOUZIS, G., SKOULARIGIS, J., LOURIDAS, G. & BUTLER, J. 2009b. The sympathetic nervous system in heart failure: physiology, pathophysiology and clinical implications. *J Am Coll Cardiol*, 54, 1747-1762.
- VAITKEVICIUS, R., SABURKINA, I., RYSEVAITE, K., VAITKEVICIENE, I., PAUZIENE, N., ZALIUNAS, R., SCHAUERTE, P., JALIFE, J. & PAUZA, D. H. 2009. Nerve supply of the human pulmonary veins: an anatomical study. *Heart Rhythm*, 6, 221-8.
- VERRIER, R. L., THOMPSON, P. L. & LOWN, B. 1974. Ventricular vulnerability during sympathetic stimulation: role of heart rate and blood pressure *Cardiovasc Res*, 8, 602-610.
- WAKE, E. & BRACK, K. 2016. Characterization of the intrinsic cardiac nervous system *Auton Neurosci*, 199, 3-16.
- WANG, L., LI, D., PLESTED, C. P., DAWSON, T. D., TESCHEMACHER, A. & PATERSON, D. J. 2006. Noradrenergic neuron-specific overexpression of nNOS in cardiac sympathetic nerves decreases neurotransmission. *J Mol Cell Cardiol*, 41, 364-370.
- WANG, Z., FENG, J., SHI, H., POND, A., NERBONNE, J. M. & NATTEL, S. 1999. Potential molecular basis of different physiological properties of transient outward K⁺ current in rabbit and human atrial myocytes. *Circ Res*, 84, 551-61.
- WEIHE, E. & REINECKE, M. 1981. Peptidergic innervation of the mammalian sinus nodes: vasoactive intestinal peptide, neurotensin, substance P. *Neurosc Lett*, 26, 283-288.
- WINTER, J., TANKO, A. S., BRACK, K. E., COOTE, J. H. & NG, G. A. 2012. Differential cardiac responses to unilateral sympathetic nerve stimulation in the isolated innervated rabbit heart. *Auton Neurosci*, 166, 4-14.
- WOROBIEW, W. P. 1925. Die Nerven des menschlichen und tierischen Herzens. *Deutsche Medizin Wochenschrift*, 36, 1509-1535.

- XU, Z. J. & ADAMS, D. J. 1993. Alpha-adrenergic modulation of ionic currents in cultured parasympathetic neurons from rat intracardiac ganglia. *J Neurophysiol*, 69, 1060-70.
- YANG, T. & LEVY, M. N. 1984. The phase-dependency of the cardiac chronotropic responses to vagal stimulation as a factor in sympathetic-vagal interactions. *Circ Res*, 54, 703-10.
- YANG, T. & LEVY, M. N. 1992. Sequence of excitation as a factor in sympathetic - parasympathetic interactions in the heart. *Circ Res*, 71, 898-905.
- YU, Y., LIU, L., JIANG, J. Y., QU, X. F. & YU, G. 2012. Parasympathetic and substance P-immunoreactive nerve denervation in atrial fibrillation models. *Cardiovasc Pathol*, 21, 39-45.
- YUAN, B. X., ARDELL, J. L., HOPKINS, D. A., LOSIER, A. M. & ARMOUR, J. A. 1994. Gross and microscopic anatomy of the canine intrinsic cardiac nervous system. *Anat Rec* 239, 75-87.
- ZARZOSO, M., RYSEVAITE, K., MILSTEIN, M. L., CALVO, C. J., KEAN, A. C., ATIENZA, F., PAUZA, D. H., JALIFE, J. & NOUJAIM, S. F. 2013. Nerves projecting from the intrinsic cardiac ganglia of the pulmonary veins modulate sinoatrial node pacemaker function. *Cardiovasc Res*, 99, 566-75.
- ZHAO, Q., DENG, H. J., X., DAI, Z., WANG, X., WANG, X., GUO, Z., HU, W., YU, S., YANG, B., TANG, Y. & HUANG, C. 2015. Effects of intrinsic and extrinsic cardiac nerves on atrial arrhythmia in experimental pulmonary artery hypertension. *Hypertension*, 66, 1042-9.
- ZHOU, J., SCHERLAG, B. J., EDWARDS, J., JACKMAN, W. M., LAZZARA, R. & PO, S. S. 2007. Gradients of atrial refractoriness and inducibility of atrial fibrillation due to stimulation of ganglionated plexi. *J Cardiovasc Electrophysiol*, 18, 83-90.
- ZHOU, S., CHEN, L. S., MIYAUCHI, Y., MIYAUCHI, M., KAR, S., KANGAVARI, S., FISHBEIN, M. C., SHARIFI, B. & CHEN, P. S. 2004. Mechanisms of cardiac nerve sprouting after myocardial infarction in dogs. *Circ Res*, 95, 76-83.
- ZUCKER, I. H., SCHULTZ, H. D., PATEL, K. P., WANG, W. & GAO, L. 2009. Regulation of central angiotensin type 1 receptors and sympathetic outflow in heart failure. *Am J Physiol Heart Circ Physiol*, 297, H1557-66.